

**Advanced Wireless Local Area  
Networks in the Unlicensed  
Sub-1 GHz ISM-bands**



# **Advanced Wireless Local Area Networks in the Unlicensed Sub-1 GHz ISM-bands**

Proefschrift

ter verkrijging van de graad van doctor  
aan de Technische Universiteit Delft,  
op gezag van de Rector Magnificus prof. ir. K.C.A.M. Luyben,  
voorzitter van het College voor Promoties,  
in het openbaar te verdedigen op woensdag 15 oktober 2014 om 12.30 uur  
door

Stefan Herbert AUST

Diplom-Ingenieur (Dipl.-Ing.)  
van Universiteit Bremen, Duitsland  
geboren te Delmenhorst, Duitsland.

Dit proefschrift is goedgekeurd door de promotor:

Prof. dr. ir. I.G.M.M. Niemegeers

Copromotor: Dr. R.R. Venkatesha Prasad

Samenstelling promotiecommissie:

Rector Magnificus,	voorzitter
Prof. dr. ir. I.G.M.M. Niemegeers,	Technische Universiteit Delft, promotor
Dr. R.R. Venkatesha Prasad,	Technische Universiteit Delft, copromotor
Prof. dr. ir. S.M. Heemstra de Groot,	Technische Universiteit Eindhoven
Prof. dr. K. Moessner,	Universiteit van Surrey, Verenigd Koninkrijk
Prof. K.V.S. Hari,	Indian Institute of Science, Bangalore, India
Prof. dr. D. Dahlhaus,	Universiteit van Kassel, Duitsland
Dr. ir. F.A. Kuipers,	Technische Universiteit Delft

Copyright © 2014 by S.H. Aust

All rights reserved. No part of the material protected by this copyright notice may be reproduced or utilized in any form or by any means, electronic or mechanical, including photocopying, recording or by any information storage and retrieval system, without the prior permission of the author.

ISBN 978-94-6259-364-0

Front & back cover: S.H. Aust, 30 June 2014.  
Printed in the Netherlands by Ipskamp Drukkers.

Typeset by the author with the L<sup>A</sup>T<sub>E</sub>X documentation system. An electronic version of this dissertation is available at <http://repository.tudelft.nl/>

Author email: [stefanaust@ieee.org](mailto:stefanaust@ieee.org)

# Abstract

This dissertation addresses the challenges of wireless local area networks (WLANs) that operate in the unlicensed sub-1 GHz industrial, scientific, and medical (ISM) band. Frequencies in the 900 MHz spectrum enable a wider coverage due to the longer propagation characteristics of the radio waves. To utilize globally available sub-1 GHz (S1G) ISM-bands, the IEEE 802.11ah Task Group started to standardize a new WLAN protocol in 2010. The IEEE 802.11ah WLAN protocol enables moderate data rates over a wider coverage area. However, this introduces newer challenges that need to be addressed in such a system. They are, reduction of energy consumption and the network performance in high density WLANs. Additionally, the presence of short-range wireless personal networks (WPANs) in the S1G ISM radio-band is of paramount importance. Coexistence problems between WLANs and WPANs compromise the data transmission performance in both networks due to numerous data retransmissions. However, the fact that no IEEE 802.11ah WLAN currently exists limits the discussion on potential system improvements. Therefore, a novel wireless prototype is proposed in this thesis that enables the testing of S1G WLANs.

This dissertation is organized into two parts. The first part outlines the motivation for S1G WLANs (Chapter 1) and introduces the emerging IEEE 802.11ah WLAN protocol amendment (Chapter 2). It includes the fundamentals of the S1G physical layer (PHY) and media access control (MAC) strategies, followed by an introduction of the IEEE 802.11ah WLAN protocol functions.

The second part includes the building of such a network and testing it on a testbed. To obtain over-the-air evaluation results of the new S1G WLAN, a novel narrow-band multiple-input multiple-output (MIMO) IEEE 802.11ah WLAN prototype is proposed (Chapter 3). This prototype consists of software-defined radio (SDR) hardware and software components operating at 900 MHz. In general, the prototype allows first-hand experiments using carrier frequencies in the license-exempt 915 to 930 MHz ISM-band in Japan. The motivation is to obtain performance results of data transmission under controlled environmental conditions and to evaluate the findings, including the signal characteristics, upper bound of throughput, and coexistence issues. The prototype utilizes the 802.11ah PHY and MAC scheme along with the limited channel bandwidth of 1 MHz. Additionally, a novel

SDR-based spectral-time sensor is developed to observe the spectral characteristics of the wireless signals in the 920 MHz radio-band in real-time and in batch mode.

To increase the wireless coverage range, MIMO modifications are proposed to exploit precoding features (Chapter 4). The proposed modifications include the use of modified Preparata codes, including the *Grassmannian* and *Kerdock* manifold. The obtained precoding performance is compared with numerical results. The results indicate that the proposed codebook modifications can provide significant coding gains with reduced computational complexity. Additionally, findings on wireless beamforming in S1G WLANs, which is an important signal transmission technique to mitigate wireless interference in long-range outdoor scenarios, are presented and discussed. Multi-flow scenarios are evaluated, in which observed performance gains suggest that further optimization would be beneficial, e.g., for device-to-device (D2D) communication systems. Single-input single-output (SISO) performance evaluations indicate the upper throughput boundaries of the S1G WLANs, whereas MIMO evaluation results provide insights on the transmission performance of concurrent flows when beamforming is used.

Next, the energy consumption of Wi-Fi modules is evaluated and energy consumption reduction strategies are proposed which are beneficial for the deployment of so called *Wi-Fi sensors* in the S1G ISM-band. More specifically, to reduce the energy consumption of Wi-Fi sensors, a novel multi-antenna switching algorithm is proposed (Chapter 5). The evaluation results indicate significant energy consumption reduction for multi-antenna Wi-Fi sensors.

Of paramount importance are the interference challenges in WLANs when wireless personal body area networks (WPANs) coexist in the same radio-band. Packet collisions between WLANs and WPANs are evaluated with the help of the proposed IEEE 802.11ah WLAN prototype (Chapter 6). The spectral-time observation results of the WPAN-to-WLAN packet collisions are illustrated, and the collision patterns are presented. The problems with management frame collisions in highly dense WLANs are discussed, and a radio resource monitoring and management (RRMM) scheme for long-range S1G WLANs is proposed (Chapter 7). To minimize packet collisions in largely dense WLANs the orthogonal sectorization of the S1G WLANs is proposed and is studied analytically. The results indicate that the proposed sectorization is beneficial to reduce collisions of WLAN management frames. Finally, findings are summarized and a detailed view of potential future research for S1G WLANs is provided (Chapter 8).

Stefan Herbert Aust

# Samenvatting

Dit proefschrift richt zich op draadloze lokale netwerken (WLANs) die gebruik maken van de sub-1 GHz (S1G) industriële, wetenschappelijke en medische frequentieband (ISM-band). De ISM frequenties in het 900 MHz spectrum zijn aantrekkelijk omdat ze, wegens de goede propagatie van de radiogolven, communicatie over grotere afstanden mogelijk maken. IEEE heeft om die reden in 2010 de Task Group IEEE 802.11ah opgericht, met als opdracht een standaard te maken voor een nieuw WLAN protocol voor de S1G ISM-band. IEEE 802.11ah richt zich op WLANs die een groot gebied bestrijken en moderate data transfer snelheden mogelijk maken. Er zijn echter een aantal technische uitdagingen te wijten aan de grotere oppervlakte die bestreken wordt, de noodzaak om het energieverbruik te beperken en de mogelijke grote dichtheid van communicerende apparaten in het WLAN. Bovendien is er mogelijke interferentie met korte-afstand personal networks (WPANs) die eveneens gebruik maken van de S1G ISM-band. Dit kan de prestaties van beide soorten netwerken, WLAN en WPAN, negatief beïnvloeden door het ontstaan van een groot aantal retransmissies. Het feit dat er vooralsnog geen IEEE 802.11ah WLANs bestaan, bemoeilijkt de discussie over de wenselijke ontwerpverbeteringen. Om die reden hebben we, in dit proefschrift, een nieuw prototype voorgesteld dat het mogelijk maakt S1G WLANs te testen.

Het proefschrift bestaat uit twee onderdelen. Het eerste deel geeft de motivatie voor S1G WLANs (Hoofdstuk 1) en beschrijft het in ontwikkeling zijnde amendement van de IEEE802.11ah standaard (Hoofdstuk 2). Het omvat de strategie van de S1G physical layer (PHY) en media access control (MAC), en een discussie van de protocol functies.

Het tweede deel bevat de originele contributies van dit proefschrift. Om een experimentele evaluatie van het nieuwe S1G WLAN mogelijk te maken wordt, in Hoofdstuk 3, een nieuw smalbandig multiple-input multiple-output (MIMO) IEEE 802.11ah WLAN prototype voorgesteld. Dit prototype is gebaseerd op software-defined radio (SDR) hardware en op software componenten voor 900 MHz radio. Met dit prototype kunnen experimenten in de, in Japan licentievrije, 915 tot 930 MHz ISM-band gedaan worden. De bedoeling is om in een “controlled environment” data transmissie prestatiemetingen te verrichten en deze te gebruiken om onderzoek

te doen naar o.a. de signaal kenmerken, de throughput grenzen, en coëxistentie problemen met andere systemen die in dezelfde frequentieband werken. Het prototype gebruikt de 802.11ah PHY en MAC en een kanaal bandbreedte van 1 MHz. We hebben ook een nieuwe SDR spectral-time sensor ontwikkeld om de spectrale eigenschappen van draadloze signalen in de 920 MHz radio-band in real-time en in batch mode te observeren.

Om het bereik van de S1G WLANs te vergroten wordt een gewijzigde MIMO techniek voorgesteld die gebruik maakt van precoding (Hoofdstuk 4). Hierbij maken we gebruik van gemodificeerde Preparata codes, waaronder Grassmannian en Kerdock manifolds. De prestaties hiervan worden vergeleken met numerieke resultaten. Hieruit blijkt dat deze codeboek wijzigingen een significante coding gain opleveren en een reductie van de complexiteit. We onderzoeken eveneens beamforming technieken om interferentie tegen te gaan in lange-afstand scenario's. Onze analyse van multi-flow scenario's laat een prestatiewinst zien en suggereert dat een verdere optimalisatie nog meer verbetering kan opleveren, bij voorbeeld voor device-to-device (D2D) communicatie. De prestatieanalyse van single-input single-output (SISO) levert een indicatie op van de bovengrenzen van de throughput van S1G WLANs. De MIMO evaluatie geeft inzicht in de prestaties van WLANs wanneer parallele data stromen en beamforming gebruikt worden.

Vervolgens wordt het energieverbruik van Wi-Fi modules onderzocht, en worden strategieën ontwikkeld om het verbruik te beperken wanneer het netwerk bedoeld is voor Wi-Fi sensors in the S1G ISM-band. Hiervoor hebben we een nieuw multi-antenne switching algoritme ontwikkeld (Hoofdstuk 5). We laten zien dat dit een significante reductie van het energieverbruik oplevert.

Van bijzonder belang is de interferentie tussen WLANs en WPANs in de S1G ISM-band. We onderzoeken daarom de botsingen die optreden tussen frames van deze twee systemen. We doen dit o.a. aan de hand van ons voorgesteld IEEE 802.11ah WLAN prototype (Hoofdstuk 6). We observeren hiervoor het spectrum-tijd beeld van de botsingen en de botsingspatronen.

In het bijzonder kijken we naar de problemen die optreden bij management-frame botsingen in scenario's waar de dichtheid van apparaten en sensoren groot is. Als oplossing stellen we een radio-resource monitoring and management (RRMM) systeem voor (Hoofdstuk 7). Om het aantal botsingen in dicht bezette WLANs te minimaliseren, gebruiken we orthogonale sectorvorming en evalueren deze oplossing. We komen tot de constatactie dat deze sectorvorming inderdaad de botsingen tussen management-frames gevoelig vermindert. We sluiten het proefschrift af met een samenvatting van onze resultaten en geven een gedetailleerd beeld van welk onderzoek, in onze visie, in de toekomst nodig is om het potentieel van S1G WLANs in de toekomst ten volle te benutten (Hoofdstuk 8).

Stefan Herbert Aust



# Contents

<b>Abstract</b>	<b>i</b>
<b>Samenvatting</b>	<b>iii</b>
<b>1 Introduction</b>	<b>1</b>
1.1 Challenging the S1G radio-band: “A new platform for innovation” .	4
1.1.1 The push: Technological developments . . . . .	4
1.1.2 The pull: Applications, markets and business opportunities .	6
1.1.3 System challenges and opportunities for S1G WLANs . . . . .	7
1.2 Selected system boundaries of the thesis . . . . .	10
1.3 Research objectives . . . . .	11
1.4 Contributions . . . . .	13
1.5 Organization . . . . .	14
<b>2 S1G WLAN PHY and MAC fundamentals</b>	<b>17</b>
2.1 Design implications on S1G WLAN PHY . . . . .	17
2.1.1 Signal propagation and path loss . . . . .	18
2.1.2 Sub-1 GHz WLAN path loss models . . . . .	20
2.2 Global S1G ISM-bands . . . . .	21
2.2.1 United States . . . . .	23
2.2.2 Europe . . . . .	24
2.2.3 Japan . . . . .	25
2.2.4 China . . . . .	26
2.2.5 South Korea . . . . .	26
2.3 Spectrum masks requirements . . . . .	26
2.4 Modulation . . . . .	27
2.5 Modulation schemes and energy consumption . . . . .	28
2.6 Link budget . . . . .	30
2.7 Multi-antenna systems . . . . .	30
2.7.1 SISO channel capacity . . . . .	31
2.7.2 2×2 MIMO channel capacity . . . . .	32
2.8 Beamforming . . . . .	33

2.8.1	Phased array beamforming: 2-dipole antenna array . . . . .	34
2.8.2	MIMO beamforming: Eigenvalue based beamforming (EBB) . . . . .	37
2.8.3	Multi-antenna configuration model . . . . .	40
2.9	The IEEE 802.11ah PHY design . . . . .	41
2.10	The IEEE 802.11ah MAC design . . . . .	42
2.10.1	Enhanced distributed channel access (EDCA) . . . . .	44
2.10.2	(Periodic) restricted access window ((P)RAW) . . . . .	44
2.10.3	Sectorized spatial access . . . . .	45
2.11	Bibliographical notes . . . . .	45
2.12	Discussion and summary . . . . .	48
2.12.1	Discussions . . . . .	48
2.12.2	Summary of the chapter . . . . .	49
<b>3</b>	<b>IEEE 802.11ah prototype</b> . . . . .	<b>51</b>
3.0.3	Purpose . . . . .	51
3.0.4	Design issues . . . . .	52
3.0.5	Hardware architecture . . . . .	53
3.0.6	Software architecture . . . . .	55
3.0.7	Required modifications . . . . .	57
3.0.8	Link setup . . . . .	58
3.1	Alternative testbeds and prototypes . . . . .	58
3.2	The test site . . . . .	60
3.2.1	Anechoic chamber . . . . .	61
3.2.2	Shielded tent . . . . .	61
3.2.3	Shielded room . . . . .	63
3.3	Test site measurement configuration . . . . .	66
3.3.1	Setup A: Anechoic chamber with ground plane . . . . .	66
3.3.2	Setup B: Shielded room . . . . .	69
3.3.3	Setup C: Shielded tent . . . . .	70
3.4	Other used equipment . . . . .	71
3.4.1	Used 900 MHz & 2.4 GHz WPAN devices . . . . .	71
3.4.2	Spectrum analyzer . . . . .	71
3.4.3	S1G spectral-time sensor (COTS-SDR) . . . . .	72
3.5	Signal assessment . . . . .	73
3.6	Bibliographical notes . . . . .	83
3.7	Discussion and summary . . . . .	84
3.7.1	Discussions . . . . .	84
3.7.2	Summary of the chapter . . . . .	85
<b>4</b>	<b>Coverage enhancement</b> . . . . .	<b>87</b>
4.1	Precoding . . . . .	89
4.1.1	Alamouti precoding . . . . .	90
4.1.2	Codeword generation . . . . .	91
4.1.3	Codeword selection strategies . . . . .	93

4.2	Codebooks for coverage enhancement . . . . .	93
4.2.1	Grassmannian codebook . . . . .	94
4.2.2	Kerdock codebook . . . . .	94
4.2.3	Modified Kerdock codebook . . . . .	95
4.3	Evaluation on precoding performance . . . . .	95
4.3.1	Grassmannian and Kerdock (simulation) . . . . .	95
4.3.2	Modified Kerdock (simulation) . . . . .	96
4.3.3	Experimental evaluation of modified codebooks . . . . .	98
4.4	Precoding performance evaluation of rotating codebooks . . . . .	100
4.5	Experimental 2×2 beamform evaluation . . . . .	109
4.5.1	Multi-flow: 2-flow configuration . . . . .	110
4.6	SISO and MIMO single flow performance . . . . .	120
4.7	Bibliographical notes . . . . .	125
4.8	Discussion and summary . . . . .	127
4.8.1	Discussions . . . . .	127
4.8.2	Summary of the chapter . . . . .	127
<b>5</b>	<b>Energy consumption reduction</b> . . . . .	<b>129</b>
5.1	Energy consumption reduction strategies . . . . .	130
5.2	Problem formulation . . . . .	130
5.3	Proposal: Selective multi-antenna RFCC . . . . .	131
5.3.1	RF chain control energy consumption reduction . . . . .	132
5.3.2	Multi-antenna energy consumption model . . . . .	132
5.3.3	Analysis of the proposed RFCC scheme . . . . .	133
5.4	Bibliographical notes . . . . .	138
5.5	Discussion and summary . . . . .	139
5.5.1	Discussions . . . . .	139
5.5.2	Summary of the chapter . . . . .	141
<b>6</b>	<b>Wireless coexistence</b> . . . . .	<b>143</b>
6.1	Interference in S1G ISM radio-bands . . . . .	144
6.1.1	S1G WLAN to WPAN coexistence . . . . .	144
6.1.2	S1G WLAN to UHF-RFID coexistence . . . . .	146
6.2	Packet collisions and collision patterns . . . . .	146
6.3	WLAN/WPAN coexistence in the S1G ISM-band . . . . .	147
6.3.1	Spectrum characteristic of S1G WLAN signal . . . . .	147
6.3.2	Spectrum characteristic of S1G WPAN-DATA signal . . . . .	148
6.3.3	WLAN-DATA to WPAN-DATA collision pattern . . . . .	150
6.3.4	WPAN-DATA to WLAN-ACK frame collision pattern . . . . .	151
6.3.5	Observed collision patterns . . . . .	152
6.3.6	Packet collision and collision detection . . . . .	153
6.4	Proposed coexistence mitigation strategies . . . . .	157
6.4.1	Cognitive radio architecture . . . . .	158
6.4.2	Proposal I: S1G collision detection unit (S1G-CDU) . . . . .	159

6.4.3	Proposal II: Dynamic RAW (D-RAW) . . . . .	161
6.4.4	Proposal III: Location-based clear channel access (LB-CCA) . . . . .	162
6.4.5	Proposal IV: Centralized clear channel access (C-CCA) . . . . .	162
6.5	Bibliographical notes . . . . .	162
6.6	Discussion and summary . . . . .	164
6.6.1	Discussions . . . . .	164
6.6.2	Summary of the chapter . . . . .	166
<b>7</b>	<b>High-density media access</b>	<b>167</b>
7.1	Problem formulation: Media access in highly dense WLANs . . . . .	167
7.1.1	Definition of massive access in WLANs . . . . .	167
7.2	Proposal: Sector-based RTS/CTS media access scheme . . . . .	171
7.2.1	Problem formulation . . . . .	171
7.2.2	Optimized media access scheme . . . . .	173
7.2.3	Discussion of simulation results . . . . .	177
7.3	Radio resource monitoring and management (RRMM) framework . . . . .	180
7.4	Bibliographical notes . . . . .	184
7.5	Discussion and summary . . . . .	184
7.5.1	Discussions . . . . .	184
7.5.2	Summary of the chapter . . . . .	185
<b>8</b>	<b>Conclusions</b>	<b>187</b>
8.1	Recapitulation of research objectives . . . . .	188
8.2	Recapitulation of research contributions . . . . .	190
8.3	Future research topics . . . . .	192
8.4	Epilogue . . . . .	193
<b>A</b>	<b>IEEE 802.11n, 802.11ac, 802.11ah PHY/MAC parameter list</b>	<b>195</b>
<b>B</b>	<b>Standard contributions by the author</b>	<b>199</b>
	<b>Symbols</b>	<b>203</b>
	<b>Abbreviations</b>	<b>205</b>
	<b>Bibliography</b>	<b>211</b>
	<b>Publications by the author</b>	<b>231</b>
	<b>Acknowledgments</b>	<b>235</b>
	<b>Curriculum vitae</b>	<b>237</b>

# Chapter 1

## Introduction

With a long range and easy penetration of obstacles, radio-frequencies below 1 GHz offer a new value to wireless local area networks (WLAN)-based communication systems. Because of the easy penetration, the wireless *coverage*<sup>1</sup> of a so called sub-1 GHz (S1G) WLAN increases significantly. Additionally, narrow-band wireless channels, which are typical in the S1G radio-bands, are less affected by frequency fading; thus, increasing the potential wireless coverage. Fig 1.1 depicts the advantages of using carrier frequencies below 1 GHz and emphasizes the shortcomings of higher frequencies because of the reduced coverage. The figure illustrates the throughput performance, which decays as the distance between sender and receiver increases, when the *link budget* calculation for different carrier frequencies and transmission power  $P_{tx} = 30$  dBm is applied. In particular, Fig. 1.1 illustrates that the S1G radio-band is very useful for wireless communication in outdoor locations. This is similar to other research findings regarding the enhanced outdoor range and services that require a larger coverage area [1].

In addition to the technological advances of the new S1G WLANs, the user market penetration of WLAN technologies has experienced tremendous success since the beginning of the first standardization of WLAN in 1997. More than 300 million WLAN devices were shipped in 2007, and it is expected that more than one billion Wi-Fi devices will be shipped every year during this decade [3]. The widespread penetration of Wi-Fi devices, e.g., to install office and private WLANs for wireless Internet access, has led to the realization of ubiquitous access by *everyone* and *everywhere*. High throughput (HT) has been achieved by utilizing orthogonal frequency division multiplexing (OFDM) and by a wider channel bandwidth<sup>2</sup> in higher radio-bands, e.g., to allow high speed downloads of high definition (HD) content. Recently, a new movement in the wireless domain has been observed, starting with the idea of widespread wireless access of *smart things*, including all facets of sensors

---

<sup>1</sup>Coverage is defined as the maximum range at which a wireless link provides a required signal to noise (SNR) ratio with minimum outage probability.

<sup>2</sup>In this dissertation *bandwidth* refers to the *coherence bandwidth* of a wireless system.

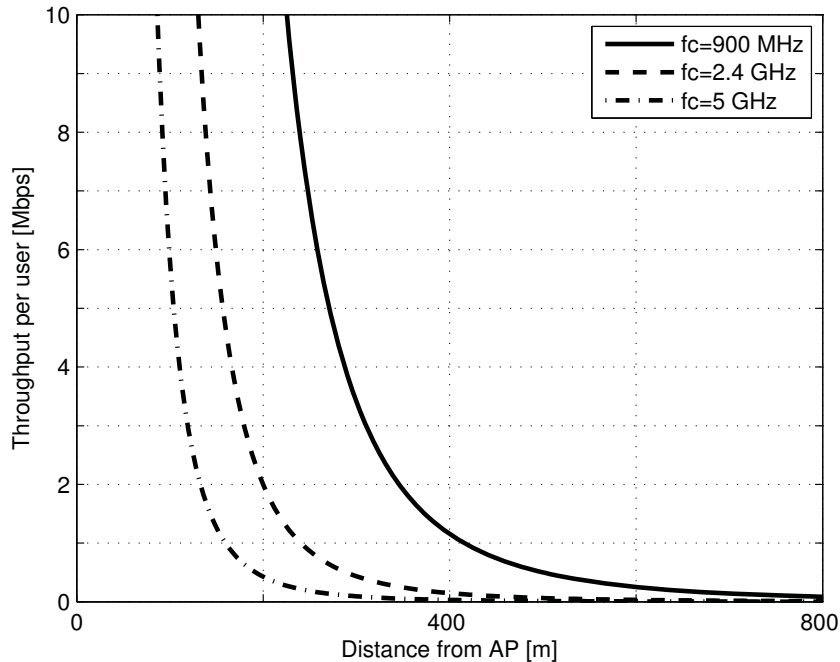


**Figure 1.1** – Basic throughput performance vs. coverage at different frequencies, transmission power  $P_{tx} = 30$  dBm, bit rate = 200 kbps, antenna gain (tx & rx antenna) = 3 dB, antenna height (WLAN AP) = 15 m; cf. estimation of achievable data rate as a function of communication distance and carrier frequency by Johannson [1]. The link budget calculation by Porat [2] is applied.

and meter devices. Ubiquitous wireless access in combination with a wide coverage range are the new trends for short burst data transmission in narrow-bands to build cost-efficient, license-exempt wireless access for the Internet of things (IoT), machine-to-machine (M2M), and smart grids. Using the alternative S1G radio-bands would prevent congested wireless access in the 2.4/5 GHz radio-bands<sup>1</sup>. The use of carrier frequencies below 1 GHz motivated the IEEE 802.11 standards committee to launch a new project that aims to utilize radio frequencies in the S1G industrial, scientific, and medical (ISM) band<sup>2</sup>. Although the use of 900 MHz carrier frequencies for proprietary WLAN has already been utilized, a global standard

<sup>1</sup>The use of the 60 GHz for very high throughput (VHT) that allows transmission rates in the Gigabit regime is standardized in IEEE 802.11ad [4].

<sup>2</sup>The ISM-bands are the preferred choice, but other alternative unlicensed bands are also in the scope of IEEE 802.11 standards.

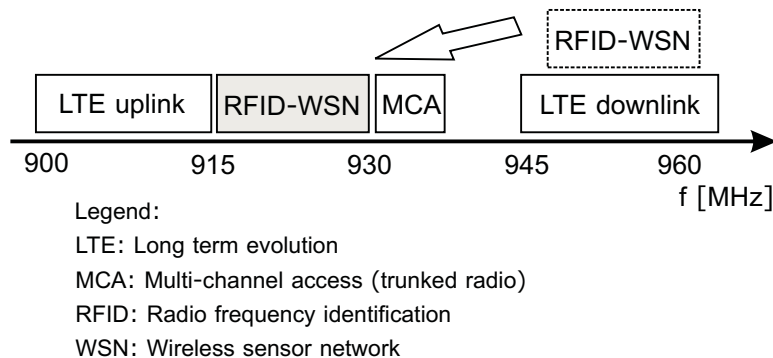


**Figure 1.2** – Rebanding of candidate spectrum (RFID-WSN) in the Japanese S1G radio-band for S1G WLANs.

is yet to come. The IEEE 802.11 LAN/MAN standards committee started the development of the enhancement of physical layer (PHY) and media access control (MAC) for license-exempt operation in the S1G radio-band with a new working group IEEE 802.11ah in 2011 [5, 6]. The IEEE 802.11ah standardization project began with only a few attendees who participated in the working group. However, this dramatically changed when the M2M, IoT, and smart grid use cases attained increased popularity in 2012. New opportunities for novel WLAN services with long-range, short-burst traffic attracted important global players, such as Qualcomm, Broadcom, Intel, Nokia, Huawei and NEC to contribute on the standardization of a global S1G WLAN protocol.

During the same time period various regulators started to modify the frequency spectrum assignments. Fig. 1.2 depicts the candidate spectrum for the S1G WLANs in the Japanese S1G radio-band. The figure illustrates the rebanding of the radio frequency identifier and wireless sensor networks (RFID-WSN), which was completed in 2012. Current WLANs achieve PHY data rates of up to 6 Gbps, e.g., with IEEE 802.11ad [4]. New PHY and MAC schemes have been developed, which allow a high-speed data rate, even when this is only achievable at very short distances between the sender and receiver device. The trend was to develop higher data rates and to utilize new modulation techniques and multi-antenna systems, such as multiple-input multiple-output (MIMO), larger channel bandwidths up to hundreds of MHz, and channel state information (CSI) feedback. S1G WLANs will be based on similar high-speed data PHY and MAC transmission schemes but with a significantly limited channel bandwidth, e.g., 1 MHz in the Japanese S1G ISM-band. In addition, because of the increased penetration of lower frequencies, interference challenges become prominent. Additionally, S1G WLANs will share the spectrum with other IEEE 801.15.4 sensor devices [7], competing for concurrent wireless access in the same wireless channel. This dissertation addresses these relevant challenges of S1G WLANs.

## 1.1 Challenging the S1G radio-band: “A new platform for innovation”

Google Inc. published a statement in August 2013 that calls for the *unrestricted* use of the license-exempt ISM-band at 902 to 928 MHz in the United States because “... the 802.11ah standard enjoys widespread support from the Wi-Fi industry and holds the potential to unlock a new wave of mobile-to-mobile communication in this band” [8]. Additionally, Google Inc. underlines its intention because it has focused its activities “on an unlicensed spectrum as a platform for innovation” [8]. The petition<sup>1</sup> by Google Inc. refers to a list of publications, including the published paper<sup>2</sup> *IEEE 802.11ah: Advantages in standards and further challenges for S1G Wi-Fi* [9] with the intention to advertise these potential opportunities. With this petition, Google Inc. requests that the U.S. Federal Communications Commission (FCC) should guarantee the *unrestricted access* for any potential user, e.g., IEEE 802.11ah-based communication systems, in the 902 to 928 MHz ISM-band<sup>3</sup>. Service providers need the guarantee that the ISM-band access techniques allow the unrestricted use of well-defined portions of the radio-bands. It underlines the fact that the S1G radio-band has a huge economic value for service providers, e.g., to realize *cost-efficient* wireless services.

### 1.1.1 The push: Technological developments

The development of a globally standardized S1G WLAN was mainly driven by the fact that unused wireless channel resources were identified in the S1G band, which might be useful in designing an outdoor long-range WLAN. The IEEE 802.11 S1G study group (SG) provided a platform for these ideas and designed a project authorization project (PAR), which aimed to utilize global ISM-band S1G frequencies. The new standard aimed to provide the same user experiences for S1G WLANs similar to the 2.4/5 GHz WLANs. The IEEE 802.11ah project was approved in the late 2010. In parallel, the IEEE 802.11ac standard was still in progress. Other WLAN standards, such as IEEE 802.11ad WLAN protocol that utilizes larger channel bandwidths at 60 GHz, led the discussion on enhancing the IEEE 802.11n throughput performance, introducing high data rate quadrature amplitude modulation (QAM) schemes, frame aggregation and multi-user (MU) MIMO. The new PHY and MAC layers of the IEEE 802.11ac standard have caused the industry to ship IEEE 802.11ac high data rate devices to the mass market. The reuse of the

---

<sup>1</sup>Reply comments of Google Inc. - in support of petitions for reconsideration. In the matter of request by Progeny LMS, LLC, for waiver of certain multilateration location and monitoring service rules - before the Federal Communications Commission, Washington, D.C. 20554, WT docket No. 11-49, pp. 1-10 [8].

<sup>2</sup>The cited publication is part of the thesis.

<sup>3</sup>This has been motivated through the presence of licensed commercial service operations of location and monitoring services applications in the 902-928 MHz ISM-band by a single license holder. More details about the FCC petition are given in [8].



IEEE 802.11ac features for the IEEE 802.11ah WLAN protocol amendment would be beneficial, e.g., to reuse the WLAN chip design and to provide triple-band or quadruple-band WLAN devices in the near future that will enable WLAN communication using carrier frequencies at 900 MHz, 2.4 GHz, 5 GHz, and 60 GHz.

In addition to the development of WLANs, another important development on so called wireless personal area networks (WPANs) happened. The objective for WPANs was to standardize low-rate, low-energy, and cost-efficient communication systems for the mass market. IEEE 802.15.4 [7] was developed as this system and was enhanced by IEEE 802.15.4g [10], IEEE 802.15.4e [11], and IEEE 802.15.4k [12] to allow improved modulation schemes, including OFDM. With the ever-increasing computational power of communication devices, the use of high data rate modulations and pre-coding schemes, such as space time block coding (STBC), are applicable. Fig. 1.3 illustrates the development of both, IEEE 802.11 and IEEE 802.15.4. Although IEEE 802.15.4-based hardware allows the setup of *large-scale*

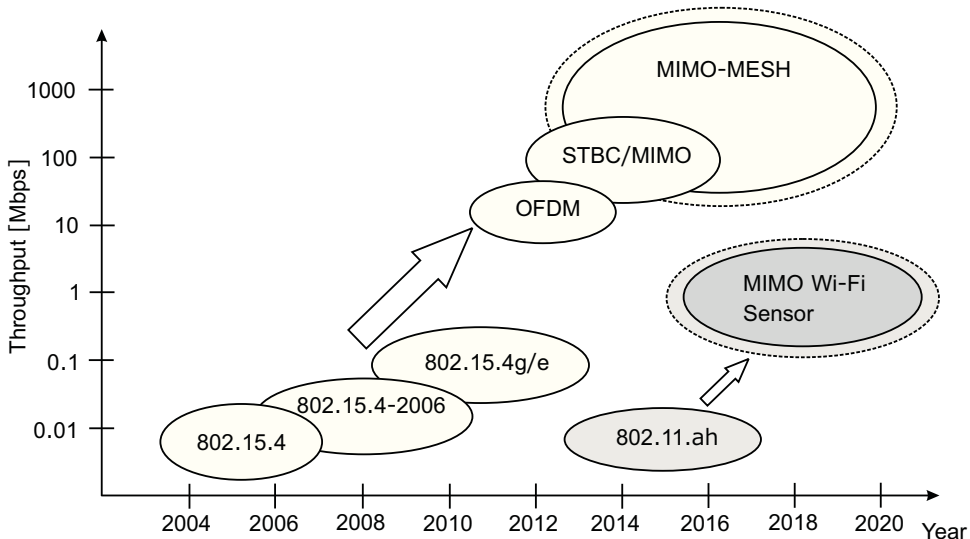


**Figure 1.3** – Evolution of wireless sensor networks to higher throughput with the help of applied advanced communication technologies.

*sensor networks*, IEEE 802.11-based hardware targets the high throughput regime for mass communication devices. However, with the pushing IEEE 802.11ah, a potential disruptor to IEEE 802.15 has been initiated, leveraging the deployment of WLAN-based sensor networks in the near future. It is well understood that IEEE 802.15.4 provides energy-efficient communication in the short-range. Battery power saving strategies, such as wake-up and sleep cycles, are crucial for IEEE 802.15.4 to provide a long-lasting battery lifetime, e.g., > 10 years. If IEEE 802.11ah is to succeed as a new WLAN protocol, it must adopt similar system characteristics as

in IEEE 802.15.4 systems. Hence, IEEE 802.11ah PHY and MAC schemes need to support energy savings, long-range coverage and interference mitigation strategies.

### 1.1.2 The pull: Applications, markets and business opportunities

An S1G WLAN would provide a wide variety of new applications and services. The following main areas of potential applications for the S1G WLAN have been identified:

1. *Smart spaces*: Smart spaces<sup>1</sup> refer to all types of smart environments, including the smart grid, smart communities, smart cities, and smart world. The vision is that the environment becomes more aware of human activities by means of sensors and contributes helpful information for human needs. Because of user experiences and the wide deployment of WLANs, S1G will add to the deployment, e.g., to build up S1G WLAN networks.
2. *Internet of things (IoT)*: In May 2011, the ITU-T IoT-GSI was created to consolidate the study on beyond next generation networks (NGN). The ITU-T agreed to an IoT definition that describes a global infrastructure, which enables new services by linking physical and virtual things and to exploit further information that is helpful for the information society [13]. The IoT would surely benefit from S1G WLANs because of its cost-efficient and simple to use characteristics.
3. *Machine-to-machine (M2M)*: This new communication type aims for the optimization of non-human communication among machines and software modules, e.g., to exchange sensor data and system states. M2M communication can be within a system (I/O interfaces) or external via wired or wireless connections. S1G WLAN would be a candidate system for supporting the M2M paradigm.
4. *Device-to-device (D2D)*: The idea of a simple data exchange among devices in close proximity has led to the development of D2D systems. It is envisioned that D2D systems will allow wireless communication systems to improve their reliability during system outages when resilient communication is essential, e.g., to rescue humans during earthquakes (disaster networks) and to support humans in dangerous and difficult-to-reach areas. Another D2D example is the direct exchange of data among users, e.g., between smart phones in vehicles.
5. *Mobile broadband services in rural areas*: Recently, telecom operators have engaged in S1G spectrum auctions worldwide. Spectrum auctions in New Zealand in October 2013 achieved 163.65 million USD for the Government of New Zealand. Telecom (37% market share), Vodafone (42% market share),

---

<sup>1</sup>Smart spaces are also defined as locations, such as libraries, conference centers, exhibitions.

and 2degree (20 % market share) bid on three  $2 \times 15$  MHz spectrum slots. The monetary spending ratio is 1.818 million USD per 1 MHz spectrum or 406.893 USD per 1 MHz/user (4.468 million inhabitants, density  $16.5/\text{km}^2$ ). This auction was successful for the Government of New Zealand, entering the fourth generation of mobile services [14]. The termination of analog services in the *licensed* S1G band has offered new business models for long-term evolution (LTE) services, such as offering mobile broadband access in rural areas. In addition, the wider coverage is cost-efficient because a smaller number of base stations need to be deployed.

### 1.1.3 System challenges and opportunities for S1G WLANs

High data rate WLANs have been realized by using carrier frequencies in higher radio-bands, including 2.4 GHz, 5 GHz, and 60 GHz, where more channel bandwidth is available for high rate modulation schemes. Because high data rates achieve several Gbps, the coverage for these WLANs is very limited. By using assigned S1G radio-bands, a new trend emerged for wider coverage but with significant throughput limitations. Thus, the S1G system challenges are twofold. First, the increase in throughput would be essential to attract new customers for S1G WLANs. Second, the coverage needs to be carefully increased, combined with a reduced interference on other systems. A wider coverage could further reduce the system costs by deploying a smaller number of S1G WLAN access points (APs). Fig. 1.4 illustrates the challenges of WLANs, which have evolved into high data rate regimes but have shown significant coverage range limitations. The figure depicts the *economical parameters* (throughput versus coverage range) as a *production possibility frontier* (PPF) graph. In contrast, the IEEE 802.11ah WLAN protocol amendment will provide a moderate data rate at a longer coverage range. Additionally, increasing the S1G WLAN boundaries to a greater throughput performance and wider coverage would attract additional service providers in the future. However, the wider range of S1G WLANs will result in overlapping basic service sets (OBSS) in indoor and outdoor environments. System limitations may arise from the presence of indoor S1G WLANs, which may interfere with outdoor long-range S1G WLANs.

To optimize the performance of S1G WLANs, a proper management of the limited system resources is essential because of the new system constraints (longer range, energy efficiency, coexistence, number of WLAN stations (WLAN STAs)). Therefore, the required radio resource management (RRM) in wireless communication systems can be divided into sub-groups, including transmission power management, energy management, interference management, and high-density media access management. The following optimization challenges are the research target of the thesis, which are:

1. Transmission power:

The first concern in long-range WLANs is the coverage. This is different from indoor WLANs, where the data rate is the first concern. With the demand for

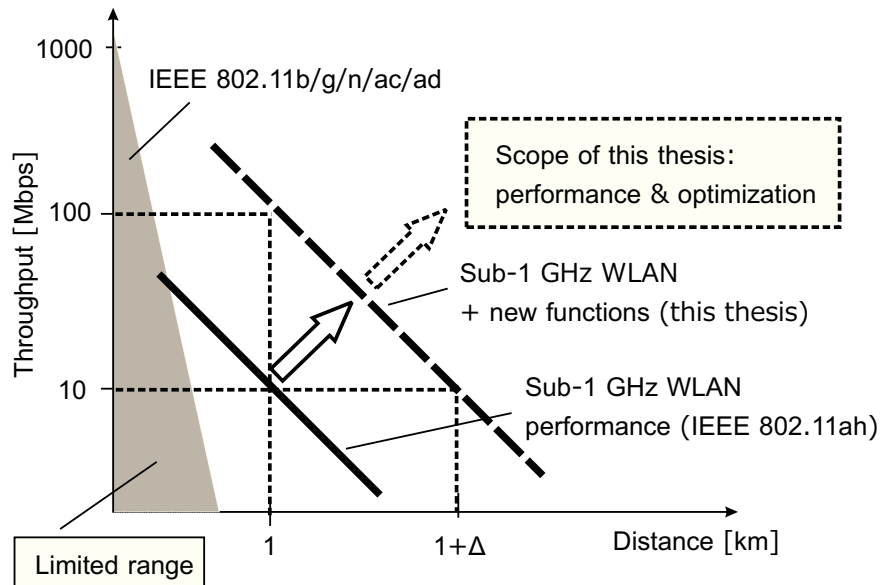


**Figure 1.4** – S1G WLAN performance evaluation and improvement as identified target of this dissertation.

a long-range system, higher transmission power and reliability is important to avoid data retransmissions. Several diversity mechanisms are relevant, which includes multi-antenna diversity and code-diversity. The proposed diversity mechanisms and their performance are investigated in this dissertation.

2. Energy consumption reduction:

The reduction of energy consumption in wireless communication systems attained significant attention during the last several years, starting with the energy consumption reduction in wireless handsets and cellular base stations. This trend has also motivated the industry to develop and promote energy saving measures in their WLANs. Moreover, for the deployment of smart grids, the WLAN must reduce its energy consumption so that the battery lifetime can be prolonged [15].

3. High-density media access:

The use of S1G WLANs in highly dense urban environments leads to the presence of hundreds or thousands of WLAN stations (WLAN STAs) in the coverage of a single WLAN access point (WLAN AP). It is required to evaluate whether the standardized media access schemes can support these new communication types. The massive and concurrent access may lead to transmission challenges in the upper regimes, which may lead to system instabilities. Even the use of prioritized access schemes may lead to the collision of

WLAN management frames if hundreds of similar messages are sent inside a single WLAN coverage. Packet collision probabilities need to be investigated and remedies need to be developed to mitigate the probability of packet collisions so that data loss can be mitigated.

#### 4. Wireless coexistence:

The IEEE 802.15.4 wireless communication systems will play an important role as a purely measurement data transmission system rather than as a communication system in regimes up to 100 kbps with minimum or no IP support. In contrast, an IEEE 802.11ah-based *Wi-Fi sensor*<sup>1</sup> inherits IP support and would allow new application scenarios at higher data rate regimes up to several Mbps, allowing a combined system of sensors and communication applications. Entirely, a new application would surely be possible, which is not solely bound to the metering data.

In the first deployment phase, the IEEE 802.15.4 and IEEE 802.11ah networks would coexist. From this coexistence, new challenges would appear because of the use of S1G ISM radio-bands for concurrent data transmission. The carrier detection of both systems would only provide very limited detection schemes, which would lead to packet collisions and severe data losses. As a result, batteries would drain faster because of the frequent data packet retransmissions.

To mitigate the negative effects of the WLAN/WPAN coexistence, it is important to evaluate the effects of the coexistence between IEEE 802.15.4 and IEEE 802.11 S1G systems, which operate in the same proximity and at the same carrier frequencies. Instead of equipping smart meter devices with the IEEE 802.15.4 communication technology, the IEEE 802.11ah WLAN protocol could be a candidate instead. The scenario that there is a widespread use of mobile devices, such as smart phones that are already equipped with Wi-Fi sensors, is promising. Thus, the S1G WLAN fills the gap between the limited IEEE 802.15.4-based sensor networks and the widespread use of WLANs. Fig. 1.5 illustrates the use of the IEEE 802.15.4 sensor networks, which also utilize the ZigBee<sup>TM</sup> protocol stack. Additionally, to harmonize the sensor networks, the IEEE 802.11ah standard serves as a global standard opportunity, which mitigates the design of proprietary system solutions. Moreover, compared to other wireless communication standards for sensor networks, IEEE 802.11ah enables IP-connectivity, similar to other legacy WLANs.

The standardization of WLANs operating in the S1G radio-band allows a simple way to contribute new protocol features because no legacy S1G WLANs exists. This is an opportunity to design and contribute protocol enhancements to the S1G WLAN protocol amendment. In particular, the long range and dense number of the WLAN STAs require solutions that do not need to follow existing standards. However, there

---

<sup>1</sup>In this thesis, the term *Wi-Fi sensor* defines a narrow-band WLAN device that is optimized for short-burst of sensor data transmission at moderate data rate and reduced energy consumption.

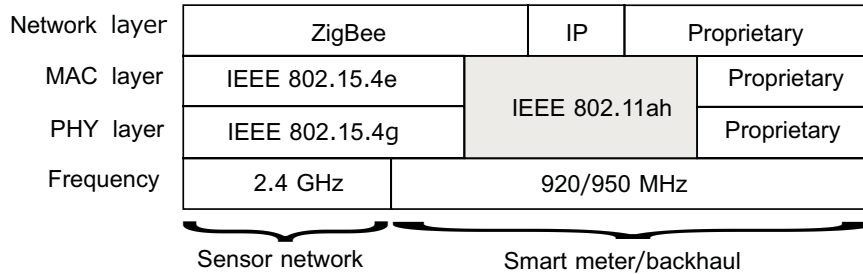


**Figure 1.5** – Protocol stack of different wireless sensor networks.

is a demand from WLAN vendors to keep the protocol design concise. Therefore, the IEEE 802.11ah WLAN protocol amendment is based on the latest WLAN standards, including high-speed WLAN protocol architectures, such as IEEE 802.11ac [16].

## 1.2 Selected system boundaries of the thesis

In this dissertation, an IEEE 802.11ah WLAN prototype is designed that operates in the license-exempt<sup>1</sup> radio-band. Other light-licensed or licensed WLANs are out of the scope for this dissertation. The selected system boundaries are:

1. *Frequency spectrum*: 920 MHz to 930 MHz Japanese ISM-band because the proposed IEEE 802.11ah WLAN prototype is located in a Japanese research laboratory.
2. *One-hop WLAN scenario*: Multi-hop and mesh-type networks are not considered.
3. *MIMO-OFDM*: Higher order modulation schemes based on IEEE 802.11ac [16] and IEEE 802.11n [17] are considered because they are state-of-the-art in modern WLANs.
4. *2×2 multi-antenna system*: The reason for selecting a 2×2 antenna system is motivated by the selected hardware setup of the S1G WLAN prototype. The selection of a universal software radio peripheral (USRP) as a software-defined radio (SDR) platform provides a simple setup that allows the synchronized use of two USRP daughterboards without the need for an external clock, e.g., to synchronize a MIMO system with two *spatial streams* (SD). In addition, a 2×2 WLAN configuration is highly considered as a practical system setting by the industry. Higher-order antenna systems would lead to increased energy consumption at the AP and STA. In particular, any additional increase of

<sup>1</sup>Note that license-exempt does not mean that the user can apply any type of device. The communication devices need to be licensed since it must be capable of operating under the compliance of the regulator.

energy consumption at the STA (Wi-Fi sensor) is seen as critical to the battery lifetime.

5. *Line-of-sight (LOS) and short-distance*: These limitations arise from the fact that no test frequency is available, e.g., for field testing in large outdoor environments. Instead, field tests have been conducted in shielded locations, mainly to avoid the emission of non-certified radio communication.
6. *2-user, 2-flow scenarios*: This is mainly due to hardware cost restrictions.
7. *Coexistence*: Wireless coexistence is considered between the IEEE 802.15 and IEEE 802.11ah systems. Other systems, such as RFID or LTE, are not considered.
8. *Energy reduction schemes*: The evaluation of energy reduction schemes is conducted under real-world conditions. However, it is restricted to the use of MIMO systems in the 2.4 GHz band (IEEE 802.11n [18]) because no *certified* IEEE 802.11ah WLAN hardware product is available on the market yet.

### 1.3 Research objectives

The objective of this dissertation is to motivate the use of S1G WLANs as a new type of wireless system in future network deployments. However, little or no experience has been reported in the literature on how to setup and maintain these new WLANs. Therefore, the research objective is to find answers to the relevant questions related to future S1G WLANs. Additionally, the hardware and software settings of the S1G WLANs offer a large variety of configurations that include:

1. Radio configurations, including the channel bandwidth, carrier frequency, sending power, and signal detection levels.
2. Transmission characteristics, including the throughput selection (low/high), number of transmit/receive antennas, SISO, MIMO, and beamforming.
3. Media access configuration, including centralized/distributed MAC access, signal protection, interference mitigation, synchronization, and prioritization.

The configuration of the S1G WLAN properties is addressed in this dissertation. The following research questions have been identified as the most relevant and are discussed in five chapters of this dissertation:

1. *“How does a real-world S1G WLAN operate?”*: WLANs at 2.4/5.2 GHz are well investigated. However, with the use of lower frequencies, new system challenges arise, including a limited channel bandwidth and MIMO-OFDM operation in narrow-bands. It is essential to have first-hand experiences with real-world hardware for a new potential WLAN. Upper throughput performances should be known, e.g., to make realistic predictions of the network

throughput characteristics. In this dissertation, an S1G WLAN hardware (HW) prototype is proposed. In particular, the design steps and selection process of relevant hardware components are discussed. Information is provided on which hardware is used and on which software extensions are essential to build the IEEE 802.11ah WLAN prototype.

2. “*What are the performance boundaries of the S1G WLANs?*”: The S1G ISM-bands have significant channel bandwidth limitations. For instance, in Japan only a 1 MHz channel bandwidth in the 915 to 930 MHz band is allowed. Applying MIMO-OFDM in these limited channel bandwidths, e.g., for short data burst transmissions, is a new paradigm in wireless sensor communication. Cellular technologies use MIMO-OFDM, such as the LTE in the 700 or 800 MHz band but with larger bandwidths. Thus, it is important to obtain a deeper understanding of the performance of the MIMO-OFDM scheme in narrow-bands, e.g., to estimate the upper transmission boundaries. This dissertation presents the very first insight into the *over-the-air* S1G WLAN performance in field measurements.
3. “*What are the problems with coexistence in S1G WLANs?*”: Similar to the coexistence of wireless systems in the 2.4 GHz radio-band, e.g., among WLANs, Bluetooth, ZigBee, IEEE 802.11, and IEEE 802.15, there is the potential threat of coexistence problems when utilizing S1G WLANs. Using the proposed S1G WLAN prototype, a first-hand study regarding coexistence problems among WLANs and IEEE 802.15.4 WPANs is conducted to monitor coexistence problems. The packet collisions of WLAN and WPAN data frames are classified to answer the question of whether energy detection methods work to guarantee a fair media access.
4. “*How to address the demand for an energy-efficient S1G WLAN?*”: Energy efficiency in WLANs has become an important research topic, e.g., to reduce the energy consumption of WLAN APs. In this dissertation, the energy consumption of the IEEE 802.11n WLAN module is evaluated because there is no IEEE 802.11ah WLAN module available yet. A multi-antenna MIMO-OFDM is proposed for S1G WLANs, and a potential solution for reducing the energy consumption when switching among active multi-antenna radio frequency (RF)-chains is presented. This dissertation contains a thorough evaluation of the RF-chain control (RFCC) proposal. In addition, a helpful analytical model is proposed to verify the experimental results.
5. “*How to maintain a highly dense WLAN because of wider coverage?*”: A wider coverage range allows more WLAN STAs to associate with a single WLAN AP. This *massive access* of WLAN STAs is a new challenge in future long-range WLANs. Massive access can be seen as a new communication type and as such needs further evaluation, e.g., which media access scheme would be appropriate to serve hundreds or thousands of WLAN STAs at one single WLAN AP concurrently.



Hence, the research objectives in this thesis are categorized into the following tasks:

1. IEEE 802.11ah WLAN prototype design and implementation based on the IEEE 802.11ah WLAN protocol amendment.
2. Wireless coverage enhancement.
3. Energy consumption reduction strategies.
4. Coexistence among IEEE 802.15.4 and IEEE 802.11 (S1G WLAN prototype).
5. Media access in high-density WLANs.

All of the proposed solutions in this dissertation can coexist and have been implemented or tested in the proposed S1G WLAN prototype under real-world conditions. In the next section, all contributions of this dissertation are listed and each of them is explained.

## 1.4 Contributions

There are two main concepts included in this dissertation. The first concept is the realization of a *long-range* S1G WLAN prototype. The second concept is the proposal of a more *energy efficient* S1G WLAN. These protocol advancements have been tested in the proposed IEEE 802.11ah WLAN prototype. Developing an IEEE 802.11ah WLAN prototype has many advantages. It starts with that a prototype is highly flexible, which means that at any time during the IEEE 802.11ah standard development, it can be easily modified. In case of a software-based WLAN prototype, the software modules can be easily modified, compared to integrated Wi-Fi solutions, which only provide a static solution.

Additionally, the experience of using an SDR-based prototype is beneficial to design new spectrum sensing devices, e.g., to examine the signal characteristics in a particular radio-band. In addition, other spectral events can be monitored, such as packet collisions. The development of a so called *spectral-time sensor* is advantageous for the development of advanced WLAN coexistence schemes. To achieve new knowledge and insight from this new long-range and energy-efficient WLAN, the design of the novel and first implementation of an S1G WLAN prototype is the target of this dissertation. The main contributions of this dissertation are listed as follows:

1. *IEEE 802.11ah (S1G) WLAN prototype*: A  $2 \times 2$  MIMO-OFDM SDR-based S1G WLAN prototype is presented. The design requirement is that the S1G WLAN prototype follows the PHY and MAC operations as defined in the IEEE 802.11ah draft<sup>1</sup>. Four S1G WLAN nodes are realized to conduct the multi-node evaluations in the S1G ISM-band.

---

<sup>1</sup>IEEE 802.11ah specification framework protocol conformance [19] and IEEE 802.11ah draft version 2.0 [5].

2. *Transmission power:* An evaluation of the upper performance boundaries of the S1G WLAN prototype. The target spectrum is the Japanese ISM 915 to 930 MHz radio-band, as defined in ARIB STD-T108 version 1.0 [20]. WLAN transmissions are emitted at  $f_c = 923$  MHz. Precoding schemes are implemented and modified to enhance the wireless coverage, including the *Grassmannian* and *Kerdock* manifold.
3. *Energy consumption reduction strategies:* A proposed energy-aware wireless communication scheme for multi-antenna MIMO systems is realized. The proposed RF-chain control scheme reduces the energy consumption in low data rate regimes.
4. *Wireless coexistence:* A detailed evaluation of coexistence problems among the IEEE 802.15.4 system and the IEEE 802.11ah WLAN prototype in the S1G-band. The monitoring, identification, and classification of packet collisions in the S1G radio-band are discussed and remedies are proposed. Spectral-time sensing is performed to identify spectral events, such as packet collisions among the IEEE 802.15.4 system and IEEE 802.11ah WLAN prototype.
5. *High-density media access:* A discussion of media access scenarios in highly dense WLANs. Media access limitations of legacy WLANs results in massive access scenarios of hundreds or thousands WLAN STAs. The identification of request to send (RTS) frame collisions is critical in highly dense WLANs. The proposed remedies include orthogonal space diversity mechanisms.

## 1.5 Organization

This dissertation is organized into two parts. In the first part, the background of WLANs and the implications of the S1G radio-band data transmission are outlined. In chapter 2, the basics on the physical signal transmission are presented. In particular, path loss models and link budget calculations related to the 900 MHz radio-band are included. In addition, Chapter 2 covers the media access schemes and discusses the related literature regarding the use of sector antennas to mitigate mutual wireless link interference. Fig. 1.6 illustrates the structure of the dissertation. The second part of this dissertation contains the original contributions. Chapter 3 outlines the need for an S1G WLAN prototype, which is constructed as the first real-world IEEE 802.11ah WLAN protocol implementation. Chapter 4 presents results on the coverage enhancement strategies in S1G WLANs. This chapter includes the first over-the-air measurements that are conducted with the proposed IEEE 802.11ah WLAN prototype. The SISO and MIMO measurements are conducted to identify the upper transmission performance boundaries, including the ICMP, UDP, and TCP transmissions. Additionally, the multi-flow scenarios are included to identify any potential challenges when concurrent flows are transmitted.

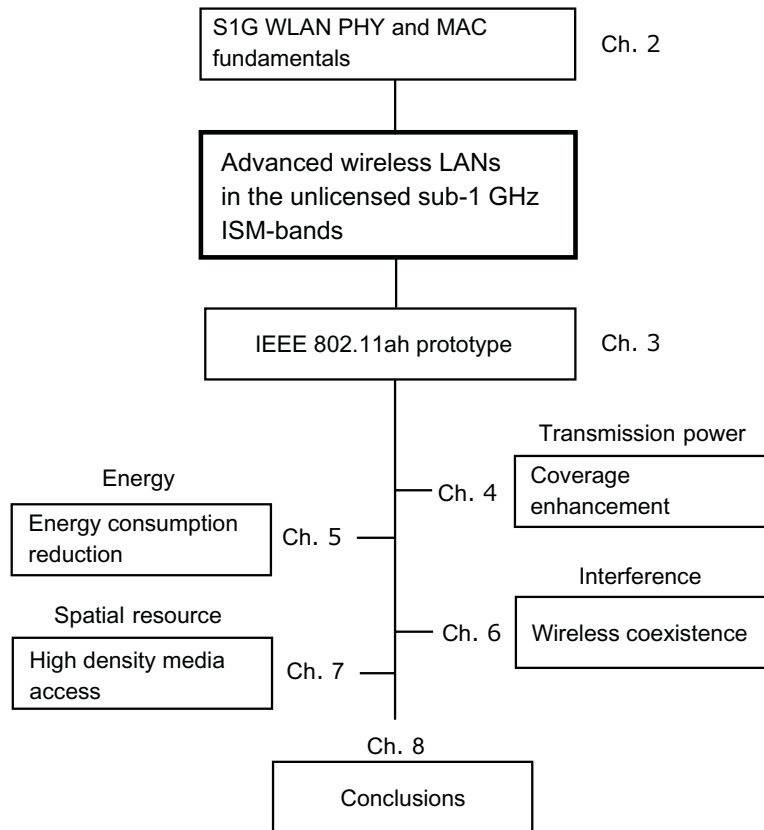


**Figure 1.6** – Organization of the thesis.

Chapter 5 discusses the energy consumption in a multi-antenna MIMO system, including a energy consumption model for wireless systems and a proposed dynamic antenna-switching scheme. In Chapter 6, the proposed S1G WLAN prototype operates at 923 MHz. At the same carrier frequency, a configured IEEE 802.15.4-based WPAN coexists and transmits data. Over-the-air data packet collisions between the S1G WLAN and the WPAN devices are demonstrated. Observed collision patterns are discussed, and remedies are proposed. Chapter 7 reports on the challenges of wireless access in highly dense S1G WLANs. A radio resource monitoring and management (RRMM) system is proposed, which aims to manage the media access in high-density S1G WLANs. Chapter 8 concludes this dissertation and outlines future research opportunities.



## Chapter 2

# S1G WLAN PHY and MAC fundamentals

The goal of this chapter is to build the framework of this thesis by presenting the fundamental sub-1 GHz channel characteristics. The objective is to identify the *effective* transmission gains, e.g., when using lower frequencies and multiple transmit antennas, which improve the *link budget*. S1G transmission gains have been utilized in the standardization effort of IEEE 802.11ah, which specifies a global S1G WLAN protocol. IEEE 802.11ah PHY and MAC features are presented, which have been discussed in the IEEE 802.11ah task group (TG). The knowledge of the IEEE 802.11ah protocol is helpful to judge the *actual* performance gains of the proposed IEEE 802.11ah WLAN prototype in Chapter 3.

### 2.1 Design implications on S1G WLAN PHY

An S1G WLAN must be designed for transmission characteristics which are unique for radio frequencies below 1 GHz. These characteristics are outlined in this section. The IEEE 802.11ah WLAN protocol amendment has to utilize the advanced transmission schemes of the latest WLAN protocol, which is the IEEE 802.11ac protocol [16] that uses multiple-input multiple-output (MIMO) orthogonal frequency division multiplexing (OFDM). Hence, the challenges of signal transmission, modulation, and the capacity of multi-antenna systems are discussed.

### 2.1.1 Signal propagation and path loss

A transmitting antenna located in free space<sup>1</sup>, follows the *Friis* equation modeled as [21]

$$\frac{P_{rx}}{P_{tx}} = G_{tx}G_{rx} \left( \frac{\lambda}{4\pi d} \right)^2, \quad (2.1)$$

where  $P_{tx}$  and  $P_{rx}$  are the transmitted and received power in [dB], respectively.  $G_{tx}$  and  $G_{rx}$  are the antenna gains in [dBi] at the transmitter and the receiver side, respectively.  $P_{rx}$  decays over the distance  $d$  [m] between transmitter and receiver. Equation 2.1 includes the well-known relationship  $\lambda = c/f_c$ , with wavelength  $\lambda$  [m],  $c$  as the propagation speed of light in vacuum in [m/s] and  $f_c$  as the carrier frequency in [Hz]. Table 2.1 lists the wavelengths of different WLANs corresponding their carrier frequencies.

**Table 2.1** – Wavelengths of different WLAN carrier frequencies

WLAN	$f_c$	$\lambda$ [m]
IEEE 802.11a	5.2 GHz	0.05
IEEE 802.11b	2.4 GHz	0.12
IEEE 802.11ah (S1G WLAN)	920 MHz	0.32

The basic path loss  $PL_{ref}$  between isotropic antennas is useful as a reference model and is defined as the increased path loss over  $d$  in [km] given by [22]

$$PL_{ref}(dB) = 32.44 + 20 \log_{10} f_{MHz} + 20 \log_{10} d_{km}. \quad (2.2)$$

To compare the path loss characteristics,  $PL_{ref}$  is calculated for three different carrier frequencies  $f_c = 900$  MHz, 2.4 GHz, and 5 GHz. Fig. 2.1 illustrates the reduced path loss at lower frequencies. An effective gain of 6 to 9 dB is the result when using carrier frequencies at 900 MHz compared to 2.4 GHz [21–23].

Next, the wave propagation characteristics at 900 MHz are analyzed in detail. In Fig. 2.2 the general received signal power based on the *two ray ground model* with  $f_c = 900$  MHz,  $P_{tx} = 30$  dBm and  $h_{tx} = h_{rx} = 3$  m, is illustrated. It demonstrates that at near distance the path loss equals the average path loss of the free-space propagation. Then the path loss model follows the two-ray ground model after the propagated signal reaches the *break point*  $d_{BP}$  at 283 m. In practice, the accuracy of a two stage path loss model supersedes the simple Friis path loss model, by considering the characteristic break point. The break point distance  $d_{BP}$  from the sender is given by [21]

$$d_{BP} = \frac{4\pi h_{tx} h_{rx}}{\lambda}, \quad (2.3)$$

<sup>1</sup>In the absence of multi-path propagation.

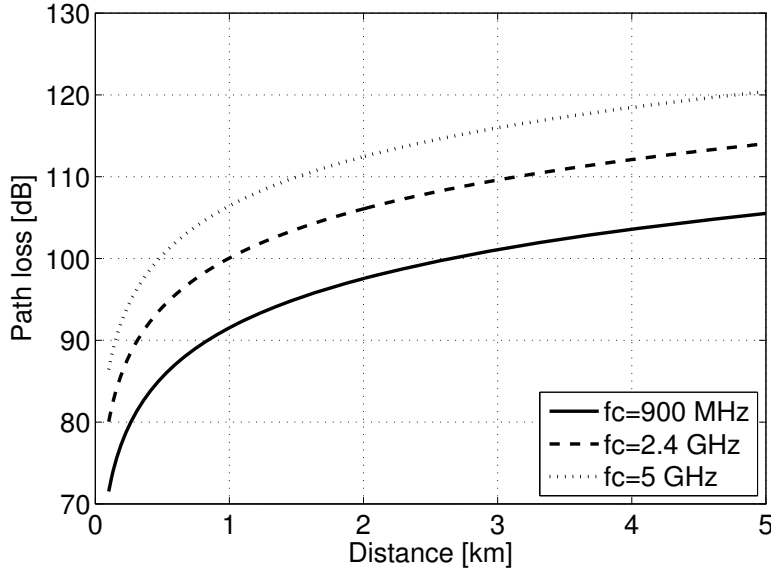


**Figure 2.1** – Numerical example of the isotropic path loss model at three different carrier frequencies  $f_c$ . It indicates a gain of  $>6$  dB, which is typical for carrier frequencies at 900 MHz compared to 2.4 GHz [21].

with  $h_{tx}$   $h_{rx}$  as the transmitter and receiver antenna height, respectively. By consequence, the path loss increases (with increased attenuation/decade cf. 2.4, 2.5) from the break point. A detailed comparison of alternative path loss models<sup>1</sup>, which would consider break point and variable antenna heights, is given in [23]. As a result, the Hata model exhibited similar path loss characteristics, but with higher flexibility, including variable antenna heights<sup>2</sup>. The general distribution of Rayleigh and Rician are utilized to model wireless fading channels [24]. Fig. 2.3 illustrates the PDF of the Rayleigh and the PDF of the Rician distribution with the Rician K-factor = 20 dB, indicating a strong line-of-sight fading channel characteristic. The figure indicates the location (x-axis) and the occurrence of the statistical distribution (y-axis). In WLANs, when WLAN driver<sup>3</sup> information is accessible, the received signal power can be extracted from the measured received signal strength indicator

<sup>1</sup>It included the IEEE 802.11ah urban path loss models, the Lee model, and the Hata model.

<sup>2</sup>The IEEE 802.11ah path loss model indicated a significant underestimated path loss with an initial attenuation, which was found at 12 dB less compared to the path loss model from the literature [23].

<sup>3</sup>The WLAN driver is a piece of software, which operates the WLAN hardware on different operating systems, e.g., *Madwifi* for Linux systems.

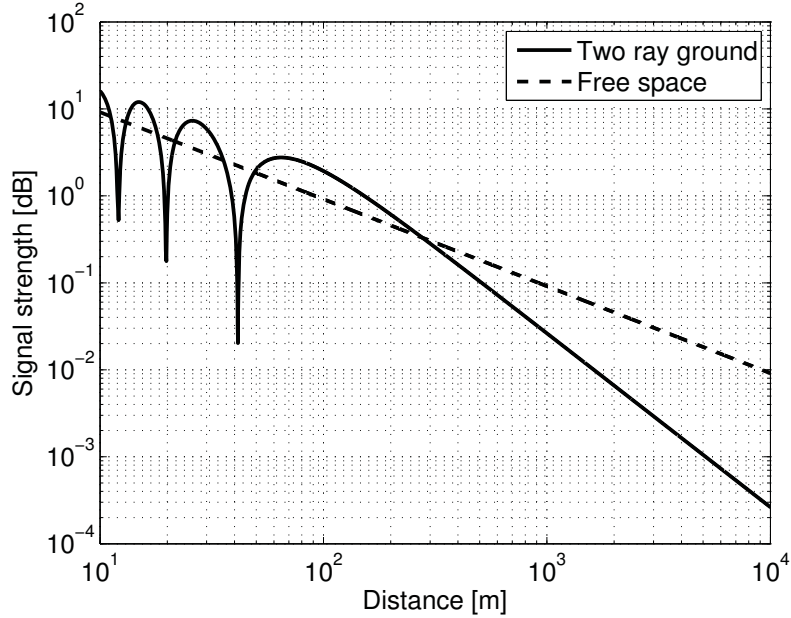


**Figure 2.2** – Illustration of two ray ground model with  $f_c = 900$  MHz,  $P_{tx} = 30$  dBm and  $h_{tx} = h_{rx} = 3$  m, with  $d_{BP} = 283$  m.

(RSSI) of the WLAN driver<sup>1</sup>, which is available as an output value in most of the WLAN drivers.

### 2.1.2 Sub-1 GHz WLAN path loss models

Sub-1 GHz path loss models are widely discussed in the literature [21,22]. Improved path loss models for sub-1 GHz WLANs are discussed, which include specific path loss models for urban environments, e.g., the *urban macro* model with WLAN antenna height  $h_t = 15$  m and the *urban pico* model with  $h_t = 2$  m. The WLAN STA<sup>2</sup> antenna height is  $h_R = 2$  m in both models. The urban macro path loss model  $L_{macro}(dB)$  is given by [25], partly referred as [26]

$$L_{macro}(dB) = 8 + 37.6 \log_{10}(d), \quad (2.4)$$

<sup>1</sup>The RSSI is implementation specific and does not always follow a linear function.

<sup>2</sup>In this thesis, STA means non-AP STA.



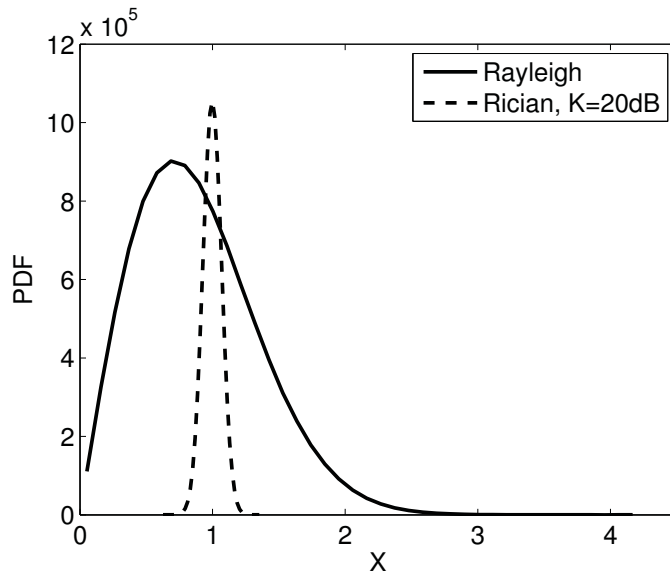


**Figure 2.3** – PDF of Rayleigh and Rician distribution (K=20 dB).

with  $d$  in [m] between WLAN AP and STA (Fig. 2.4(a)). The urban pico path loss model  $L_{pico}(dB)$  (Fig. 2.4(b)) is given by

$$L_{pico}(dB) = 23.3 + 36.7 \log_{10}(d). \quad (2.5)$$

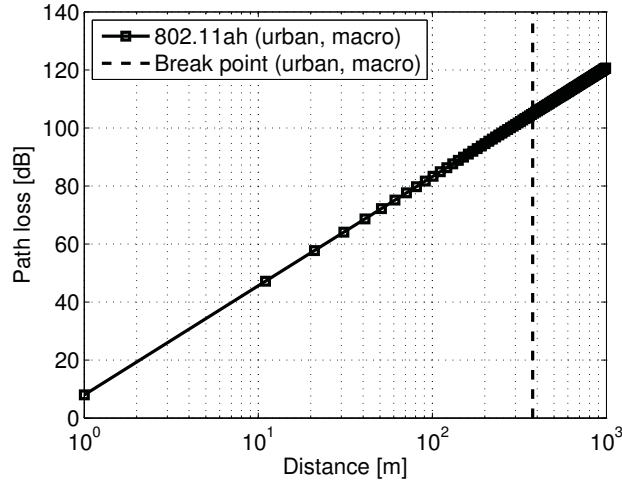
The sub-1 GHz path loss models reflect the characteristics of the following use cases as defined as in [25]: The *urban areas* with *urban micro* (UMi), *urban macro* (UMa); the *suburban areas* with *suburban macro* (SMa); the *rural areas* with *rural macro* (RMa); and *others* with *indoor hotspot* (InH), and *outdoor-to-indoor* (O-to-I).

## 2.2 Global S1G ISM-bands

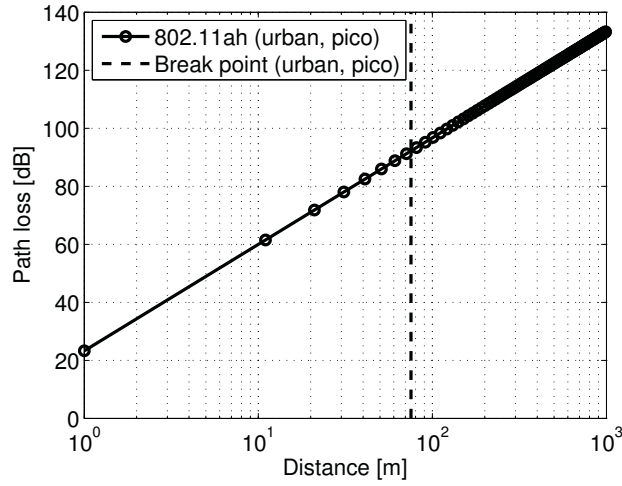
Worldwide there are several sub-1 GHz ISM-bands available<sup>1</sup>, which are applicable for wireless data transmission systems, in particular for WLANs, including the U.S., Japan, Europe, South Korea, Singapore, and Australia (Fig. 2.5). These ISM-bands only provide several MHz of channel bandwidth<sup>2</sup>, so called *narrow-bands*. In particular, Japan allows only 1 MHz bandwidth, which can be utilized for wireless data transmission, as illustrated in Fig. 2.5. Legacy IEEE 802.11 MIMO-OFDM operations have been applied to much wider channel bandwidths, e.g., 20 MHz (IEEE 802.11b/g), 40 MHz (IEEE 802.11n), 80 MHz, and 160 MHz

<sup>1</sup>Unlicensed sub-1 GHz radio-bands are available, e.g., 870 MHz and 915 MHz in Europe.

<sup>2</sup>In this thesis, channel bandwidth refers to the coherence bandwidth.



(a) IEEE 802.11ah path loss, urban macro, with break point  $d_{bp} = 376.8$  m.



(b) IEEE 802.11ah path loss, urban pico, with break point  $d_{bp} = 75.36$  m.

**Figure 2.4** – Illustration of sub-1 GHz path loss model (IEEE 802.11ah) for urban macro and urban pico. A potential break point - at the antenna heights,  $h_t = 10$  m for urban macro and  $h_t = 2$  m for urban pico, both with  $h_{rx} = 1$  m - is additionally depicted.

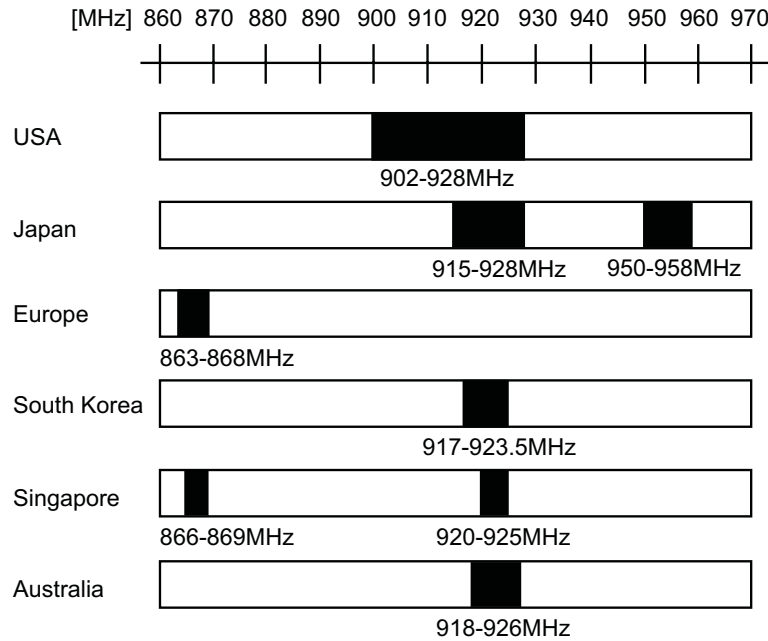


**Figure 2.5** – Overview of global sub-1 GHz ISM-bands.

(IEEE 802.11ac). Applying WLAN data transmission to narrow-bands is a new paradigm in future WLANs and the data transmission performance in narrow-bands is almost unknown<sup>1</sup>. Hence, a thorough evaluation of sub-1 GHz WLAN performance boundaries is essential, e.g., to motivate further improvements, such as increased coverage range, robust communication, higher data rate, and reduced energy consumption. Details on the authorized radio-bands of sub-1 GHz WLAN PHY are outlined in the following. The source of the channelization is the adopted IEEE 802.11ah *specification framework* [19].

### 2.2.1 United States

The U.S. channelization defines 26 of 1 MHz channels, from 902 to 928 MHz (Fig. 2.6). This channelization proposal was controversy, because the utilization of 1 MHz channels is inefficient when wider channels can be used instead, e.g., at 2, 4, 8, and 16 MHz. However, there was consensus in the IEEE 802.11ah TG to adopt a channel plan that would include 1 MHz channel bandwidth and to support the

<sup>1</sup>A proprietary WLAN card operating at 900 MHz has been released in the U.S., using 5, 10, and 20 MHz channel bandwidths, based on IEEE 802.11g protocol and Atheros<sup>TM</sup>AR5414 chipset. Card information: 32-bit mini-PCI, Type IIIa, tx power: 28 dBm, sensitivity: -95 dBm (DSSS, 1 Mbps), tx power: 28 dBm, sensitivity: -92 dBm (OFDM, 6 Mbps), data rate: 6-54 Mbps. Indoor range: 400 m, outdoor range: 50 km.

limited Japanese bandwidth regulation (Section 2.2.3). There is an advantage that 1 MHz channels would allow 26 of 1 MHz orthogonal channels, which could be useful to create multiple wireless service opportunities<sup>1</sup> (cf. Google Inc. petition as discussed in Section 1.1). The higher bandwidth channels (4-16 MHz) show an offset of 2 MHz, starting at 904 MHz to avoid potential adjacent channel interference (ACI) with wireless communication systems located at the lower frequency spectrum. The U.S. channelization allows one single 16 MHz channel bandwidth, which is a potential candidate channel for Wi-Fi off-loading applications. The maximum equivalent isotropically radiated power (EIRP) is 30 dBm for all channels, allowing the realization of an outdoor long-range WLAN.

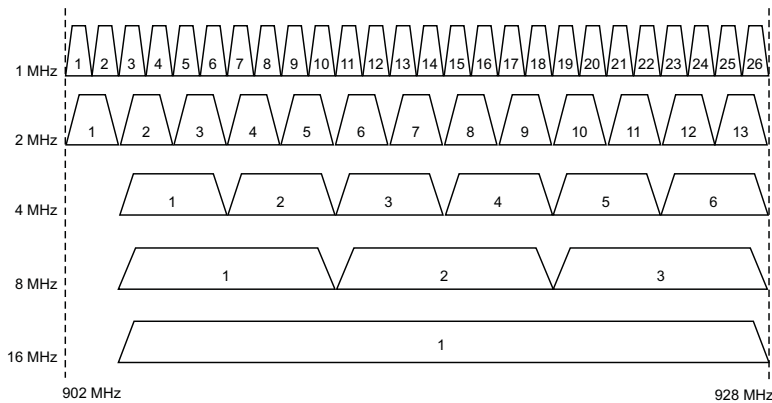


**Figure 2.6** – Potential sub-1 GHz WLAN channelization for United States.

### 2.2.2 Europe

The sub-1 GHz WLAN channelization for Europe includes 5 channels with 1 MHz and 2 channels with 2 MHz channel bandwidth between 863 MHz and 868 MHz (Fig. 2.7). Several chip vendors propose to consider a potential sub-1 GHz WLAN operating in the unlicensed 870 MHz and 915 MHz radio-bands<sup>2</sup>. A detailed EU S1G frequency plan, including the 863-870 MHz radio-band and its assigned service usage, is presented in [28, 29].

<sup>1</sup>Initial proposals suggested to consider 2, 4, 8, and 16 MHz channels in the U.S. To approach consensus - here with the Japanese channelization plan - the U.S. channelization includes 1 MHz channel bandwidth.

<sup>2</sup>Qualcomm proposed IEEE 802.11ah in this radio-bands [27]. 870 MHz would be a favorite, compared to 915 MHz where Global System for Mobile Communications - Railway (GSM-R) is a primary user.

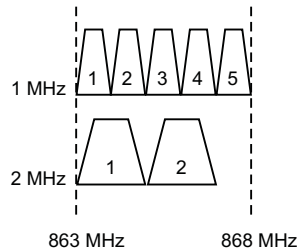


**Figure 2.7** – Potential sub-1 GHz WLAN channelization for Europe.

### 2.2.3 Japan

The Japanese sub-1 GHz WLAN channelization includes the frequencies between 916.5 MHz and 927.5 MHz (Fig. 2.8). It defines different EIRP levels, including 10 mW, 20 mW, and 250 mW, as defined in the ARIB-STD T108 standard [20]. Note that the channelization assignment by the Japanese regulator is significantly different compared to other countries. The center frequency  $f_0$  is used instead of the start frequency of a particular channel bandwidth  $BW = f_2 - f_1$  with  $f_1$  as the lower band frequency and  $f_2$  upper band frequency to define the channel band (indicated by the offset of 0.5 MHz in Fig. 2.8). Frequency regulators of other countries use the start frequency  $f_1$  to define the channel bands. The Japanese regulator defines up to 6 different spectrum masks, between 915 to 930 MHz [20]. The spectrum masks of the lower 915 MHz band are most restrictive to protect the presence of *passive* RFID systems<sup>1</sup>. Spectrum masks for 10 mW, 20 mW, and 250 mW EIRP are different. The channelization allows the bonding of maximum 5 consecutive channels of each 200 kHz with the result of 1 MHz channel bandwidth. The bonded channels require a wider spectrum mask, with same side lobe emission restriction, compared to a single 200 kHz channel. An alternative channelization could include 3 orthogonal channels allowing 250 mW EIRP, which would require *light licensing*. This would allow additional applications, such as long-range backhaul links or Wi-Fi off-loading.

Japanese cellular operators expressed their concern at the spectrum regulator about two main aspects, when deploying a sub-1 GHz WLAN. First, the presence of sub-1 GHz WLANs could be an interference source in the lower radio-bands. The suggestion is that WLAN should follow the requirements by the cellular operators. Second, a sub-1 GHz WLAN may be a potential candidate for an alternative long-range wireless communication. However, the requirement for low duty cycle ( $<1\%/h$ ) may not allow these services<sup>2</sup>.

<sup>1</sup>This could result in certified sub-1 GHz WLANs by hardware manufacturers, which most likely would try to avoid the use of lower 915 MHz channels to circumvent restrictive spectrum masks.

<sup>2</sup>Other ideas for sub-1 GHz may include social messaging services.

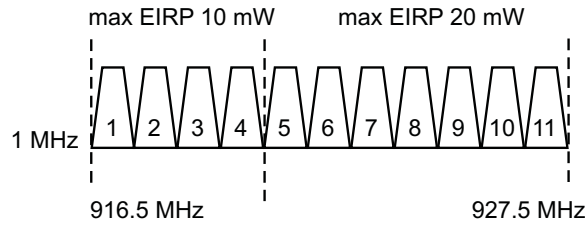


**Figure 2.8** – Potential sub-1 GHz WLAN channelization for Japan.

### 2.2.4 China

The Chinese channelization includes frequencies between 755 MHz with maximum EIRP at 5 mW and from 779 MHz to 787 MHz with maximum EIRP at 10 mW (Fig. 2.9).

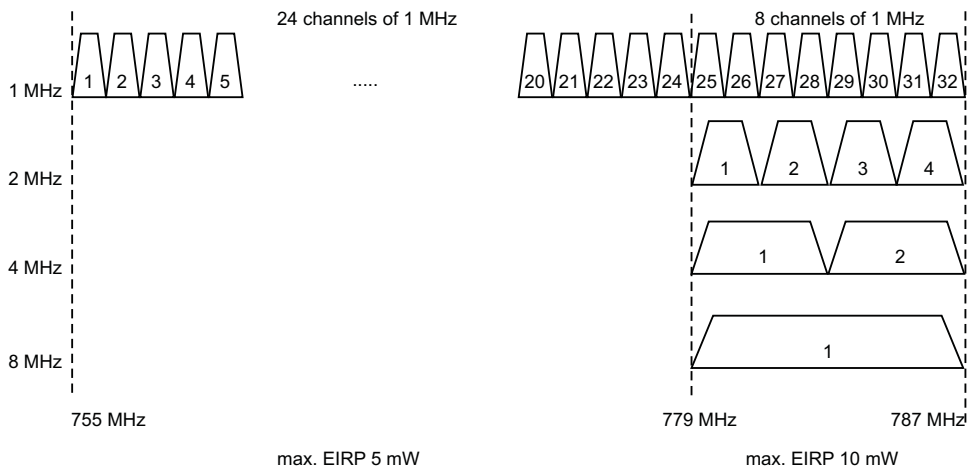


**Figure 2.9** – Potential sub-1 GHz WLAN channelization for China.

### 2.2.5 South Korea

The South Korean channelization includes 6 channels at 1 MHz, 3 channels with 2 MHz and 1 channel at 4 MHz channel bandwidth, from 917.5 to 923.5 MHz (Fig. 2.10).

## 2.3 Spectrum masks requirements

A certification of a wireless system requires the compliance of *spectrum masks*. As an example, the Japanese spectrum masks are outlined in the following, which define 6

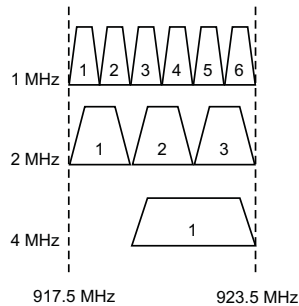


**Figure 2.10** – Potential sub-1 GHz WLAN channelization for South Korea.

different types of spectrum masks in the sub-1 GHz ISM-band between 915 MHz and 930 MHz. Hardware vendors need to comply on these spectrum requirements, e.g., to acquire a certification by the regulator for a potential new wireless communication system. In particular, the spectrum mask for *specified low tx-power radio stations* as defined in ARIB STD-T108 [20] is depicted in Fig. 2.11. The spectrum mask defines the allowed power emission between 922.3 MHz to 928.1 MHz<sup>1</sup>. This spectrum mask is used as a reference to judge the radio emission characteristics of the proposed sub-1 GHz WLAN prototype. The spectrum mask in Fig. 2.11 illustrates the maximum power of bonded 200 kHz consecutive channels, which is  $P_{tx} = 20$  mW (13 dBm). Adjacent channel leakage power is at  $\leq -15$  dBm (lower/upper sideband emission), the spurious emission strength is at  $\leq -36$  dBm/100 KHz (Fig. 2.11).

## 2.4 Modulation

The sub-1 GHz WLAN modulation schemes are somewhat similar to the specifications as for IEEE 802.11n and IEEE 802.11ac. In particular, it includes the well-known WLAN modulation and coding schemes (MCS). binary phase shift keying (BPSK), quadrature phase shift keying (QPSK), and quadrature amplitude modulation (QAM) modulation are proposed for sub-1 GHz WLANs to provide legacy support with the IEEE 802.11n and IEEE 802.11ac PHY specifications. New robust modulation schemes have been proposed in sub-1 GHz WLANs, which include the signal repetition for longer-range applications (MCS 10: BPSK with repetition [19]). Table 2.2 lists the MCS rates for SISO and MIMO (2 spatial streams), respectively for IEEE 802.11n,  $BW = 20$  MHz [31]. The limited channel bandwidth of sub-1 GHz WLANs results in reduced transmission capabilities (data rate<sup>2</sup>). Table 2.3 lists the IEEE 802.11ah PHY data rates [5].

<sup>1</sup>Prior ARIB STD-T108, the sub-1 GHz radio-band was regulated in ARIB STD-T96 [30].

<sup>2</sup>Using the Equation 2.11 the data rate for narrow-band sub-1 GHz WLANs can be approximated using the IEEE 802.11n data rates (Table 2.2), both for SISO (single stream) and MIMO (2-stream)

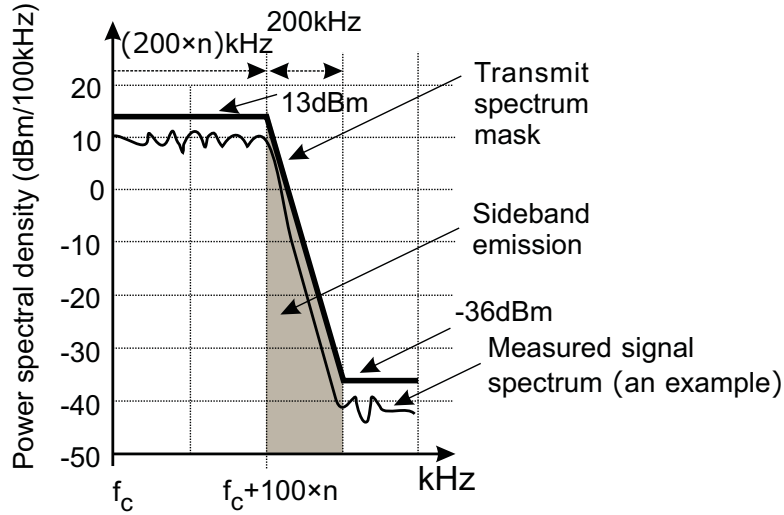


**Figure 2.11** – Illustration of the Japanese spectrum mask (upper half) as defined for the radio-band from 922.3 MHz to 928.1 MHz,  $P_{tx} = 20$  mW [20]. This spectrum mask is relevant, because the proposed sub-1 GHz WLAN prototype uses carrier frequencies in the same radio-band.

**Table 2.2** – IEEE 802.11n SISO and MIMO (2 spatial streams) MCS,  $BW = 20$  MHz [17].

MCS index	Modulation & coding	Data rate [Mbps]	Spatial stream
0 [8]	BPSK, 1/2	6.5 [13.0]	1 [2]
1 [9]	QPSK, 1/2	13.0 [26.0]	1 [2]
2 [10]	QPSK, 3/4	19.5 [39.0]	1 [2]
3 [11]	16-QAM, 1/2	26.0 [52.0]	1 [2]
4 [12]	16-QAM, 3/4	39.0 [78.0]	1 [2]
5 [13]	64-QAM, 2/3	52.0 [104.0]	1 [2]
6 [14]	64-QAM, 3/4	58.5 [117.0]	1 [2]
7 [15]	64-QAM, 5/6	65.0 [130.0]	1 [2]

## 2.5 Modulation schemes and energy consumption

Future wireless systems have to prolong battery life (e.g., Wi-Fi sensor) and to comply to ever increasing energy consumption policy restrictions. Hence, the avoidance



**Table 2.3** – IEEE 802.11ah SISO and MIMO (2 spatial streams) MCS,  $BW = 1$  MHz [5]. Note that the IEEE 802.11ah MCS index starts at zero for each different mode, compared to the IEEE 802.11n MCS index. MCS 10 is the new IEEE 802.11ah repetition mode, so called *rep-2 mode*. The short GI ( $4 \mu s$ ) enables 10% increased data rate.

MCS index	Modulation & coding	Data rate [kbps], GI= $8 \mu s$	Spatial stream
0 [0]	BPSK [BPSK], 1/2 [1/2]	300 [600]	1 [2]
1 [1]	QPSK [QPSK], 1/2 [1/2]	600 [1200]	1 [2]
2 [2]	QPSK [QPSK], 3/4 [3/4]	900 [1800]	1 [2]
3 [3]	16-QAM [16-QAM], 1/2 [1/2]	1200 [2400]	1 [2]
4 [4]	16-QAM [16-QAM], 3/4 [3/4]	1800 [3600]	1 [2]
5 [5]	64-QAM [64-QAM], 2/3 [2/3]	2400 [4800]	1 [2]
6 [6]	64-QAM [64-QAM], 3/4 [3/4]	2700 [5400]	1 [2]
7 [7]	64-QAM [64-QAM], 5/6 [5/6]	3000 [6000]	1 [2]
8 [8]	256-QAM [256-QAM], 3/4 [3/4]	3600 [7200]	1 [2]
9 [9]	256-QAM [256-QAM], 5/6 [5/6]	4000 [8000]	1 [2]
10 [-]	BPSK [-], 1/4 [-]	150 [-]	1 [-]

of any unnecessary energy consumption is essential. In WLANs, the modulation scheme has a direct impact on the energy consumption. For instance, higher modulation schemes lead to higher energy consumption of the WLAN module (processor) due to the simultaneous calculation of multiple data symbols in the base band. To analyze the energy consumption of a particular modulation scheme, an energy consumption model is needed. The energy for transmitting a single bit of information  $E_{bit}$  is given by [32]

$$E_{bit}[\text{Joule}] = \frac{E_{start}}{L} + \frac{P_{elec} + P_{RF}(M)}{R_S \cdot \log_2 M} \cdot \left(1 + \frac{H}{L}\right) \quad (2.6)$$

with packet payload size  $L$ , fixed overhead  $E_{start}$ , and the symbol rate  $R_S$  for an  $M$ -array modulation scheme.  $P_{elec}$  represents the circuit energy consumption and  $P_{RF}$  represents the power delivered by the power amplifier, which needs to go up as  $M$  increases, to maintain the same error rate and packet header size  $H$ .

Interestingly, the use of multiple-antennas has a much higher impact on the WLAN energy consumption compared to the modulation. In this thesis a detailed

evaluation on the energy consumption in a multi-antenna WLAN module is presented in Chapter 5, which will enhance the energy model given in Equation 2.6 and a new multi-antenna energy consumption reduction scheme is proposed.

## 2.6 Link budget

A wireless system and its data transmission capability can be expressed by calculating the link budget (LB). It includes all positive and negative contributions of system parameters, which may have an impact on the transmission performance, such as carrier frequency  $f_c$  [Hz], transmit power  $P_{tx}$  [dBm], antenna gains  $G_{tx}$  [dB],  $G_{rx}$  [dB], antenna heights  $h_{tx}$  [m],  $h_{rx}$  [m], path loss  $PL(d)$  [dB], shadowing standard deviation  $\sigma^2$  [dB], noise  $N_0$  [dB], bit rate (selected modulation scheme)  $s$  [kbps], implementation loss  $l_{imp}$  [dB], and multipath fading loss  $l_{multipath}$  [dB]. The link budget is modeled by

$$LB[dB] = f(f_c, PL(d), P_{tx}, G_{tx}, G_{rx}\sigma^2, N_0, s, l_{imp}, l_{multipath}). \quad (2.7)$$

Given  $f_c = 900$  MHz,  $P_{tx} = 20$  dBm,  $h_{tx} = 20$  m, the approximate *outdoor* path loss is [2]

$$LB_{outdoor} \cong 133.5 \text{ dB}, \quad (2.8)$$

with an approximated coverage range  $r_{coverage} = 1537$  m. A suggested *downlink* link budget for indoor locations, which was motivated by a home energy management system (HEMS) study, including indoor measurements in European houses, is given by [33] where

$$LB_{indoor} \cong 112 \text{ dB}, \quad (2.9)$$

with  $P_{tx} = 10$  dBm,  $PL_{indoor} = 78$  dB and a limited antenna gain  $G_{rx} = -11$  dBi due to the small form factor of a potential in-house sensor deployment. Other schemes, such as signal *pre-coding*, can positively contribute to the overall link budget. The orthogonal space time block coding (OSTBC) can add up to 6-9 dB, by transmitting the *codeword indicator*, as a form of channel state information (CSI), derived from the pre-selected *codebook* for a given  $N_{tx}$ ,  $N_{rx}$  multi-antenna wireless system, which describes the channel state. Knowing the available link budget  $LB$  and the required link budget for a certain  $E_b/N_0$ , the available *link margin*  $L_{margin}$  can be estimated by

$$L_{margin} = LB - E_b/N_0(\text{required}). \quad (2.10)$$

## 2.7 Multi-antenna systems

One of the main advantages of sub-1 GHz WLANs, compared to IEEE 802.15.4 WPAN systems, is the utilization of multi-antenna systems. Longer coverage, less outage and higher data rates can be achieved due to the efficient use of wireless

channel capacity. The channel capacity describes the theoretical amount of data, which can be transferred over the media, depending on its *channel bandwidth*<sup>1</sup> in [Hz] and signal to noise ratio (SNR) in [dB]. The Shannon-Theorem<sup>2</sup> is defining the channel capacity  $C$  given by

$$C = BW \cdot \log_2(1 + SNR) \quad [bit/s], \quad (2.11)$$

with channel bandwidth  $BW$ . This well-known formula is very useful, e.g., to compare the throughput of a given wireless transmission system at different  $BW$  or to estimate the upper bound of the throughput characteristic of a wireless channel<sup>3</sup>.

### 2.7.1 SISO channel capacity

A transmitted signal over a wireless channel can be modeled by

$$y = hx + z, \quad (2.12)$$

where  $y$  is the received signal,  $h$  is the complex channel state,  $x$  is the transmitted signal, and  $z$  is the additive white Gaussian noise with zero mean. Multiple input and output signals over different antennas are modeled by

$$\begin{pmatrix} y_1 \\ y_2 \\ \vdots \\ y_n \end{pmatrix} = \begin{pmatrix} h_{11} & h_{12} & \cdots & h_{1m} \\ h_{21} & h_{22} & & h_{2m} \\ \vdots & & \ddots & \vdots \\ h_{n1} & h_{n2} & \cdots & h_{nm} \end{pmatrix} \begin{pmatrix} x_1 \\ x_2 \\ \vdots \\ x_m \end{pmatrix} + \begin{pmatrix} z_1 \\ z_2 \\ \vdots \\ z_n \end{pmatrix}. \quad (2.13)$$

First, a SISO communication link is modeled by

$$h = h_I + jh_Q, \quad (2.14)$$

where  $h_I$  is the real part and  $h_Q$  is the imaginary part of the wireless channel. Next, channel capacity  $C$  [bits/s/Hz] of a SISO channel is given by

$$C = \log_2 \left( 1 + \frac{X}{\sigma^2} |h|^2 \right), \quad (2.15)$$

where

$$C = \log_2(1 + \gamma). \quad (2.16)$$

---

<sup>1</sup>In this thesis the *channel bandwidth* is used to describe the width of a radio-band used for data transmission,  $BW = f_2 - f_1$  where  $f_1 < f_2$ . In computer networks *bandwidth* is also used to describe the amount of data transferred per second. In this thesis *data rate* or *throughput* is more helpful to use.

<sup>2</sup>The Shannon-Hartley Theorem refers to both inventors of the channel capacity theorem.

<sup>3</sup>*Spectral efficiency* is used to judge the transmission characteristic of a given wireless communication system in [bit/s/Hz].

A helpful approximation is given by

$$C \approx \log_2 \gamma, \quad \gamma \gg 1, \quad (2.17)$$

where  $X$  is the received signal,  $\sigma^2$  is the received noise, and  $\gamma$  is the *signal to noise ratio* (SNR) of the wireless system.

### 2.7.2 $2 \times 2$ MIMO channel capacity

The  $2 \times 2$  MIMO communication system can be modeled by

$$A = \begin{bmatrix} x_1 & x_2 \\ -x_2^* & x_1^* \end{bmatrix} \text{i.i.d.}, \quad (2.18)$$

where  $*$  represents the *complex conjugate* of the transmitted symbol  $x$  of the  $2 \times 2$  *Alamouti* matrix; cf. [34]. The receiver can be modeled with inverse matrix given by

$$H^{-1} = \frac{1}{x_1 x_1^* + x_2 x_2^*} \begin{bmatrix} x_1 & x_2 \\ -x_2^* & x_1^* \end{bmatrix}. \quad (2.19)$$

The channel capacity  $C$  of a  $2 \times 2$  MIMO is given by

$$C = \log_2 \left( 1 + \frac{X}{2\sigma^2} (\lambda_1 + \lambda_2) + \left( \frac{X}{2\sigma^2} \right)^2 (\lambda_1 \lambda_2) \right), \quad (2.20)$$

where

$$\lambda_1 + \lambda_2 = |h_{11}|^2 + |h_{12}|^2 + |h_{21}|^2 + |h_{22}|^2, \quad (2.21)$$

and

$$\lambda_1 \lambda_2 = (|h_{11}|^2 + |h_{12}|^2) \cdot (|h_{21}|^2 + |h_{22}|^2). \quad (2.22)$$

A simple *closed-loop* multi-antenna wireless transmission system with feedback information is illustrated in Fig. 2.12. The figure illustrates the increased diversity gain which can be exploited with MIMO by transmitting multiple copies of the signal over multiple antennas. Highest channel capacity is reached in this example with  $N_t = N_r = 4$ .

The outage capacity of a MIMO system with unknown *channel state information* (CSI) is given by [36]:

$$\mathbf{C} = \log_2 \det \left( \mathbf{I} + \frac{P}{\sigma^2} \mathbf{H} \mathbf{H}^H \right), \quad (2.23)$$

with  $P/\sigma^2$  as the mean SNR. Fig. 2.13 illustrates the ergodic channel capacity for different antenna constellations, including sender and receiver antenna constellation.

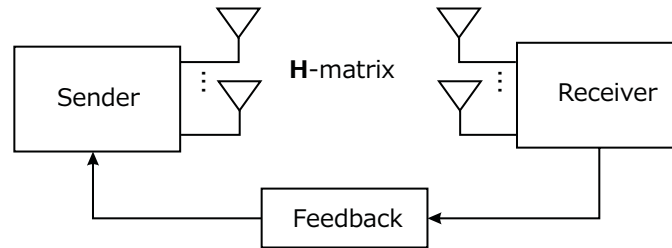


**Figure 2.12** – Closed-loop multi-antenna system with CSI feedback [35].

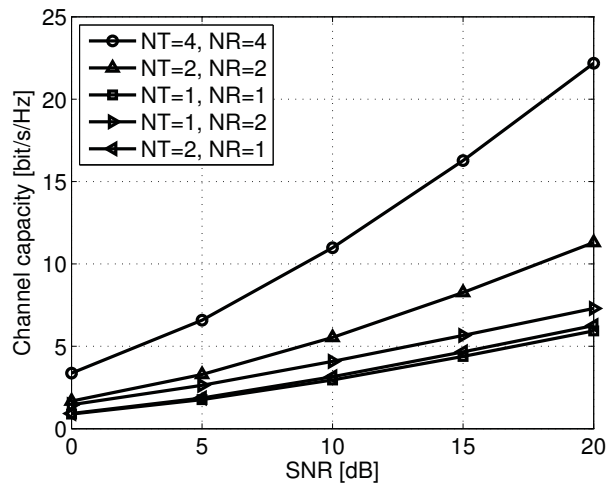


**Figure 2.13** – Illustration of ergodic channel capacity for different antenna constellations.

## 2.8 Beamforming

With the deployment of IEEE 802.11n the presence of *beamforming* in wireless systems received some level of attention. Although this technique has been applied to radio systems since the mid of the last century [37], e.g., to amplify the transmitted signal, the beamforming has become a necessity in modern wireless communication systems. IEEE 802.11n and IEEE 802.11ac provide beamforming as an optional feature, e.g., to increase the SNR level and to reduce interference. IEEE 802.11ah is going to utilize beamforming to further reduce interference, e.g., in wide-range outdoor systems. Beamforming is widely understood to beam the transmitted energy in a particular direction, e.g., to increase the received signal. In the presence of few wireless terminals this assumption may hold. However, IEEE 802.11ah aims to support hundreds or thousands of STAs associated with a single AP, and as such

simple beamforming may not be a single solution. Phased array beamforming can be used to beam the signal towards a single user. However, *side lobes* are emitted, e.g., for any kind of multi-antenna systems<sup>1</sup>. In contrast, *MIMO beamforming* is the sum of signals, which are transmitted via uncorrelated (decoupled) channels. This is somewhat different from the *phased array beamforming*, which is the sum of a signal in the far field [38].

Beamforming can be either applied at the AP, the STA or both, which would require a multi-antenna system at either at the network units (cf. 2.7.2). For instance, it would be simple but efficient to equip the AP with multiple antennas, e.g., either to beam the signal in a particular direction or to provide MU-MIMO spatial streams to each single terminal. It is envisioned that the WLAN STA - here a IEEE 802.11ah STA - may not be equipped with multiple antennas, e.g., due to cost or design restrictions. In this scenario, the AP would beamform the signal (downlink) towards the STA resulting in a higher SNR, e.g., when the STA is out of sight (NLOS).

The STA could also be equipped with multiple antennas, e.g., 2 dipole or 2 chip antennas. These antennas could be used to increase the signal reception (antenna diversity) or to beam the signal towards the AP (uplink). Instead of using beamform in the uplink, an alternative is to use the multi-antenna at the AP and to combine and amplify the highest received signals, using the *maximum ratio combining* (MRC) scheme. This would shift the computational complexity, and as such the energy consumption, from the STA towards the AP. By consequence, it would increase the STA's battery lifetime.

### 2.8.1 Phased array beamforming: 2-dipole antenna array

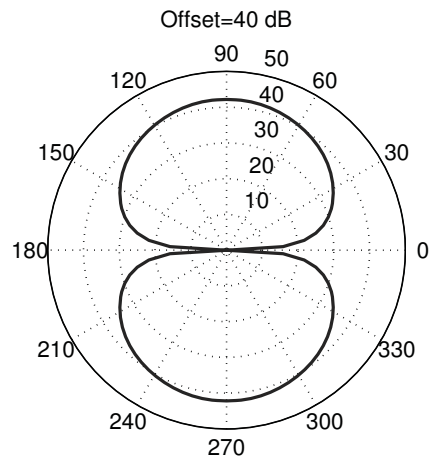
In the following, a 2-dipole antenna system is evaluated, which is applied in this thesis to operate as a multi-antenna MIMO-OFDM sub-1 GHz WLAN prototype. Most WLAN APs are shipped with multi-antenna dipole antennas. The directivity pattern of a single dipole is illustrated in Fig. 2.14, indicating the dipole elevation plane (Fig. 2.14(a)) and azimuth plane (Fig. 2.14(b)).

The illustration of an *endfire* multi-antenna array is given in Fig. 2.15. A 4-antenna array is illustrated (A1, A2, A3, A4) with antenna separation distance  $d$  and beam target in  $\theta$ .

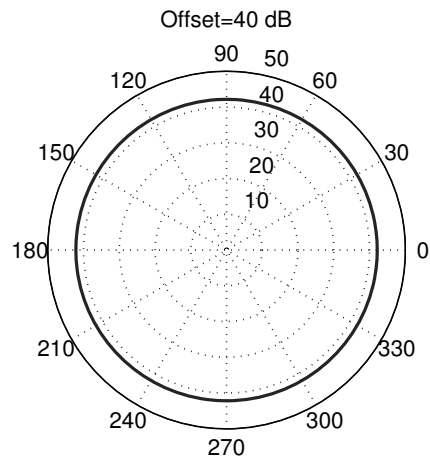
To judge the measurement results when using the sub-1 GHz WLAN prototype, the theoretical basis and evaluation of radiation pattern of sub-GHz antennas at  $f_c = 923$  MHz are outlined. The method of moments (MoM) simulation model of an ideal 2-dipole antenna array (with single feed, 1 Volt,  $f_c = 920$  MHz) is illustrated in Fig. 2.16.

---

<sup>1</sup>Smart antennas may be useful to further reduce side lobes, and as such are not considered in this thesis. However, some may claim that a combination of IEEE 802.11n/ac/ah PHY/MAC optional beamforming and smart antennas may mitigate the interference, e.g., in large outdoor deployments. Ruckus<sup>TM</sup> wireless systems provide combined smart antenna and stock IEEE 802.11 system solutions.



(a) Directivity pattern (elevation plane, y-z)



(b) Directivity pattern (azimuth plane, x-z)

**Figure 2.14** – Radiation pattern of  $\lambda/2$  900 MHz dipole at  $f_c = 923$  MHz, feed = 1 V.

The simulated antenna array of a 2-dipole setup for different dipole separation is illustrated in Figure 2.17.

The assumption is an ideal antenna array with single feed in an environment without the superposition of any reflections, e.g., from walls or ceilings, using a

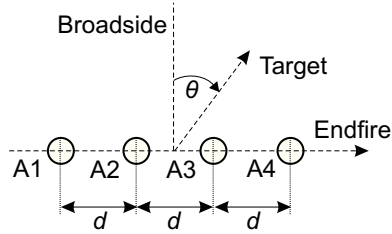


**Figure 2.15** – Multi-antenna array (endfire).

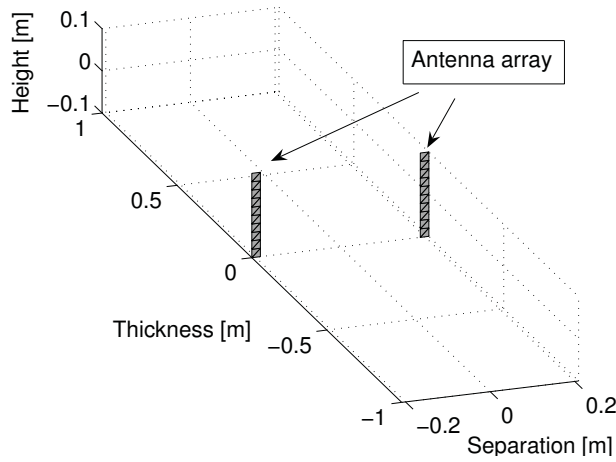


**Figure 2.16** – Simulation model of 2-dipole antenna radiation model at antenna separation distance  $d_a = 0.4$  m, antenna height  $h = 0.2$  m, and antenna thickness  $b = 1$  mm (MoM dipole micro strip antenna simulation model [39]).

sphere model. The antenna resistance, reactance, and the radiated power varies with the increased antenna distance. At 0.18 m the radiated power of the dipole array reaches its maximum at 6.4 mW, which is in the regime of the applied antenna power of 10 dBm. The evaluation of a practical 2-dipole antenna array exhibit different directivity characteristics due to the impact of the wireless surroundings and the RF system. This circumstance will be examined in the thesis by designing a multi-antenna SIG WLAN prototype.

The modeled radiation effect, when the antenna separation changes, is illustrated in Fig. 2.18. The antenna separation generates different radiation patterns with different beam widths; thus, the antenna constellation determines the RF signal at the receiver under ideal conditions. However, in Chapter 4, Section 4.5,



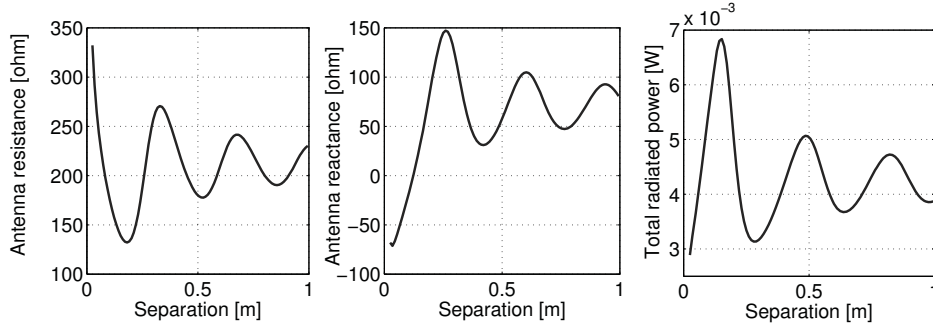


**Figure 2.17** – Simulation results of 2-dipole antenna radiation model ( $f_c = 920$  MHz, 1 Volt antenna feed) vs. antenna separation distance  $d = 0.05 - 1.0$  m, antenna height  $h = 0.2$  m, and antenna thickness  $b = 1$  mm).

beamforming is discussed under realistic wireless conditions. A significant reduction in beamforming performance can be observed when RF system conditions are sub-optimal, compared to modeled beamforming systems.

### 2.8.2 MIMO beamforming: Eigenvalue based beamforming (EBB)

To enhance the benefit of a multi-antenna MIMO system, the signal to noise ratio (SNR) can be increased by using eigenvalue based beamforming (EBB)<sup>1</sup>. These beamforming methods have been applied to the 3rd generation partnership project (3GPP) long term evolution (LTE) cellular communication systems [42]. Fig. 2.19 illustrates a beamform system, with transmit beamform and the maximum ratio combining (MRC) option at the receiver side.

The detection of symbols  $\hat{s}$  using MRC is given by [43]

$$s'_1 = \frac{1}{|h_1|^2 + |h_2|^2} (h_1^* y_1 + h_2 y_2^*), \quad (2.24)$$

$$s'_2 = \frac{1}{|h_1|^2 + |h_2|^2} (h_1^* y_2 - h_2 y_1^*). \quad (2.25)$$

The eigenvalue based two-dimensional (2D) beamformer is “optimal for systems with  $N_t = 2$  transmit antennas” [35]. Increased performance can be achieved when beamforming is combined with adaptive modulation schemes, e.g., WLAN MCS rates. Fig. 2.20 depicts a 2D-beamformer.

<sup>1</sup>Eigenvector beamforming is also referred as matched-filter beamforming [40, 41].

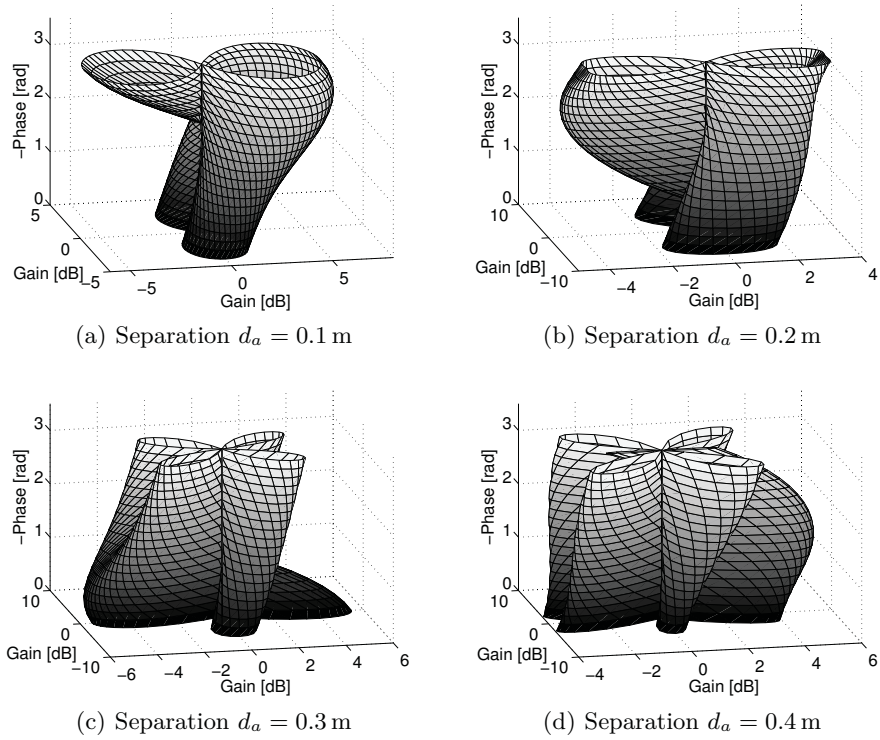


**Figure 2.18** – Simulation of  $2 \times 2$  dipole antenna radiation model ( $f_c = 920$  MHz, 1 Volt antenna feed) vs. antenna separation distance  $d_a = 0.1 - 0.4$  m, antenna height  $h = 0.2$  m, and antenna thickness  $b = 0.001$  m (MoM dipole micro strip antenna simulation model [39]).

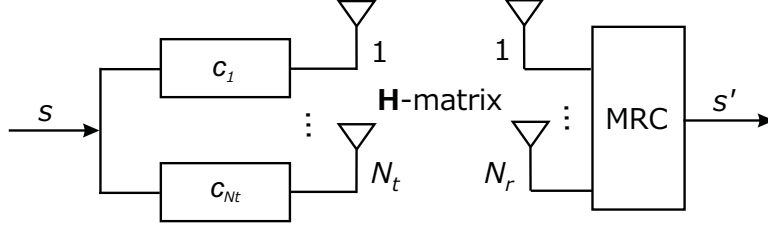


**Figure 2.19** – Illustration of a transmit beamformer and MRC receiver [35].

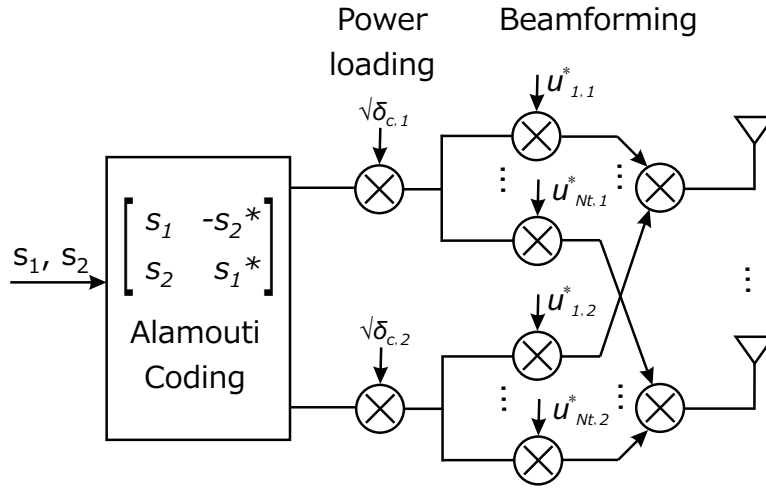


**Figure 2.20** – Illustration of a 2D-beamformer [35].

The 2D beamformer<sup>1</sup> with  $N_{tx} = 2$  is given by [35]

$$\mathbf{X} = [ \mathbf{u}_{c,1}^*, \mathbf{u}_{c,2}^* ] \begin{bmatrix} \sqrt{\delta_1} & 0 \\ 0 & \sqrt{\delta_2} \end{bmatrix} \begin{bmatrix} s_1 & -s_2^* \\ s_2 & s_1^* \end{bmatrix}, \quad (2.26)$$

with the power loading  $\sqrt{\delta_1}$ ,  $\sqrt{\delta_2}$  and the *Alamouti code* symbols  $s_1$ ,  $s_2$ . By consequence, the optimal beamform directions - if (partial) CSI is available - are given by

$$\mathbf{u}_{c,1} = \mathbf{u}_{H,1}, \quad \mathbf{u}_{c,2} = \mathbf{u}_{H,2}, \quad (2.27)$$

with the first two eigenvectors  $\mathbf{u}_{H,1}$ ,  $\mathbf{u}_{H,2}$  of  $\mathbf{H}$ . The eigenvalue based beamforming, which has a separated beamform algorithm for each sender and receiver signal, is evaluated as one of the beamforming schemes in the proposed prototype of this

<sup>1</sup>Referred as *orthogonal STBC* (OSTBC)-beamforming combination [35].

thesis. For  $2 \times 2$  MIMO<sup>1</sup> the vector creation is based on the singular value decomposition (SVD) of the transmission matrix  $\mathbf{H}$ . To obtain the capacity of user  $k$  as a function of  $\mathbf{H}_k$  and the channel fading matrix  $\mathbf{M}_k$  the formula by Liu *et al.*, can be used, which is modeled by [42]

$$C_k^{EBB} = \log 2 \left| \mathbf{I} + \frac{\mathbf{H}_k \mathbf{M}_k^{EBB} \mathbf{M}_k^{EBB \dagger} \mathbf{H}_k^\dagger}{\delta_n^2 \mathbf{I} + \sum_{i=1, i \neq k}^k \mathbf{H}_i \mathbf{M}_i^{EBB} \mathbf{M}_i^{EBB \dagger} \mathbf{H}_i^\dagger} \right|. \quad (2.28)$$

The EBB scheme increases the SNR, but does not mitigate the interference of multiple users. To mitigate the interference a zero forcing (ZF) in form of a block diagonalization (BD) algorithm can be applied<sup>2</sup>. Here, the formula by Liu *et al.*, can be used, which is given by [42]

$$C_k^{BD} = \log 2 \left| \mathbf{I} + \frac{\mathbf{H}_k \mathbf{M}_k^{BD} \mathbf{M}_k^{BD \dagger} \mathbf{H}_k^\dagger}{\delta_n^2 \mathbf{I}} \right|. \quad (2.29)$$

It has been demonstrated that by applying the BD algorithm the MU interference can be reduced. However, the BD precoding scheme also reduces the receive power<sup>3</sup> and comes with significant computational complexity (CC). To reduce the complexity of BD, a combination with the vector perturbation (VP) scheme is proposed by Chen *et al.*, [44]. The vector perturbation scheme is a generalized version of the Tomlinson-Harashima precoding (THP)<sup>4</sup> non-linear precoding scheme<sup>5</sup>. The shortcoming of the proposed BD-VP combination, which is able to completely suppress multi-user interference (MUI) in multi-user multiple-stream scenarios, is that an increase of noise occurs. Motivated by this observation, Chen *et al.*, proposed further enhancements, including a low-complexity ZF-based VP algorithm [44] with further improvements on the complexity using quantized channel feedback as proposed in [45].

### 2.8.3 Multi-antenna configuration model

To configure an efficient WLAN PHY, it is required to identify the optimal number of antennas, which would result in maximum transmission performance. The

<sup>1</sup>For MISO a simple maximal ratio transmission scheme can be applied.

<sup>2</sup>A simple yet straight-forward solution would be the precoding of the transmission matrix by (a) multiplying the transmitted signal with normalized ZF or (b) minimum mean squared error (MMSE) inverse of the channel matrix [44].

<sup>3</sup>A proposed combination of EBB and ED for MU-MIMO LTE systems is proposed by liu *et al.*, [42].

<sup>4</sup>THP is a sub-optimal structure of the dirty paper coding (DPC) scheme.

<sup>5</sup>The use of non-linear precoding schemes allows the reduction of the elevated noise level (noise enhancements) [44].

optimal number of transmit antennas is given by [46]

$$C \geq \max_{N'_{tx} \leq N_{tx}} (1 - N'_{tx} \Omega_{P,min}) E \Omega, \quad (2.30)$$

where

$$\Omega = \left[ \log_2 \det \left( \mathbf{I}_{N_{rx}} + \frac{\mathbf{H}\mathbf{H}^H}{N'_{tx}} \right) \frac{\gamma}{\left( \sqrt{1 - N'_{tx} \Omega_{P,min}} + \sqrt{N'_{tx} \Omega_{P,min}} \right)^2} \right], \quad (2.31)$$

and  $\mathbf{I}_{N_{rx}}$  as the identity matrix  $N_{rx} \times N_{rx}$ , the effective SNR  $\gamma$ , and  $\mathbf{H}$  with

$$\mathbf{H} = \begin{pmatrix} H^{1,1} & H^{2,1} & \dots & H^{N_{tx},1} \\ H^{1,2} & H^{2,2} & & H^{N_{tx},2} \\ \vdots & & \ddots & \vdots \\ H^{1,N_{rx}} & H^{N_{rx}-1,N_{rx}} & \dots & H^{N_{tx},N_{rx}} \end{pmatrix}. \quad (2.32)$$

It was argued that the optimal number  $N'_{tx}$  of transmit antennas  $N_{tx}$  and receive antennas  $N_{rx}$  should be equal to maximize the capacity of MIMO-OFDM, optimized for high SNR

$$N'_{tx} = \min \left\{ N_{tx}, N_{rx}, \frac{1}{2\Omega_{P,min}} \right\}, \quad (2.33)$$

with sampling of data frame with the minimum pilot overhead  $\Omega_{P,min}$ , in dimensions  $D_f$  (frequency) and  $D_t$  (time)

$$\Omega_{P,min} = \frac{1}{D_{f,max} D_{t,max}}. \quad (2.34)$$

To further maximize the capacity, the number of training information should be less than the half of the data frame. Further, pilot tones and data symbols should be sent with equal transmit power<sup>1</sup> [46].

## 2.9 The IEEE 802.11ah PHY design

IEEE 802.11ah PHY will support the global available sub-1 GHz ISM radio-bands, separated in 1, 2, 4, 8, and 16 MHz channel bandwidths, as discussed in previous Section 2.2. The *tone spacing*, also called as *subcarrier distance* is 31.25 kHz, which is a *down-clocked*<sup>2</sup> subtone spacing version from IEEE 802.11ac, which is 312.5 KHz. IEEE 802.11ah utilizes a down clocked bandwidth of IEEE 802.11ac 20/40/80 and

<sup>1</sup>For  $N_T = N_R = 1/2\Omega_{P,min}$ . Changing the pilot tone transmit power is known as *pilot boost*.

<sup>2</sup>Details on down-clocking and variable OFDM tone spacing is given in [47].

160 MHz [48]. Additionally, a bandwidth option is specified for 1 MHz wide channels. A 64 point IFFT at 2 MHz sampling rate is specified, with a symbol period of  $40 \mu s$ . Additionally, a 32 IFFT is specified for 1 MHz bandwidth channels. The maximum number of *spatial streams* (SS) is 4, which allows  $4 \times 4$  MIMO-OFDM. *Multi-user* (MU) MIMO-OFDM is specified. Further, *space time block codes* (STBC) and *null data packet* (NDP) *sounding* [49], which are reused padding and sounding schemes from IEEE 802.11ac, are specified for IEEE 802.11ah.

IEEE 802.11ah specifies a hybrid binary convolutional coding (BCC) scheme and low-density parity-check code (LDPC) for *zero padding* to keep the padding process similar to the IEEE 802.11ac padding schemes [50]. At the receiver side, utilizing the MRC (cf. 2.8.2) scheme can further improve the signal quality (SNR), e.g., multiple single flows from STAs received at multiple antennas at the AP [43]. An additional modulation and coding scheme *MCS0-rep2* provides an additional 6 dB gain compared to MCS0 at 64 FFT mode [48]. This repetition scheme supports a data rate of 150 Kbps at the longest range, and is applied only for a single SS operation ( $N_{ss} = 1$ , no STBC). This new MCS option would allow a wider coverage, which is essential to provide wireless access, e.g., in *gray zones*. The increase of coverage in indoor environments is 1.1 fold (Area2/Area1, cf. Fig. 2.21(a)), whereas the increase of coverage in outdoor environments is 2 fold (Area2/Area1, cf. Fig. 2.21(b)) when applying the path loss models from Section 2.1.2 [9].

## 2.10 The IEEE 802.11ah MAC design

In contrast to the IEEE 802.11ah PHY, the MAC is significantly different from the IEEE 802.11ac MAC. First, the IEEE 802.11ah use case scenarios consider sensor nodes, sensor back-haul, and outdoor hotspot deployment. To facilitate these scenarios, the MAC need to enable wireless long range, enhanced battery lifetime, large number of associated STAs and interference reduction schemes in OBSS. The most salient distinction between IEEE 802.11ah and other standardized WLANs is the use of the unlicensed sub-1 GHz ISM-band. The IEEE 802.11ah WLAN protocol amendment aims to maximize the coverage range, while minimizing the energy consumption. Further, IEEE 802.11ah utilizes OFDM as modulation scheme for narrow-band WLAN access<sup>1</sup>. It enables use cases, including indoor/outdoor smart meter device communication, health care, Wi-Fi off-loading, and WLAN AP coverage extension. A detailed discussion on IEEE 802.11ah use cases is presented in [9, 52]. Additionally, the new IEEE 802.11ah protocol specification gives the opportunity to include new features due to the fact that no legacy support needs to be considered. Restricted access window (RAW), target wake time (TWT), subchannel selective transmission (SST), and sectorized access are new MAC functions and their functionality and performance in real networks is yet unknown. Additionally,

---

<sup>1</sup>Non-OFDM use cases (IEEE 802.11b) are presented in [51], including smart home, camera remote control, smart metering, traveling salesperson, home security door and window sensors.

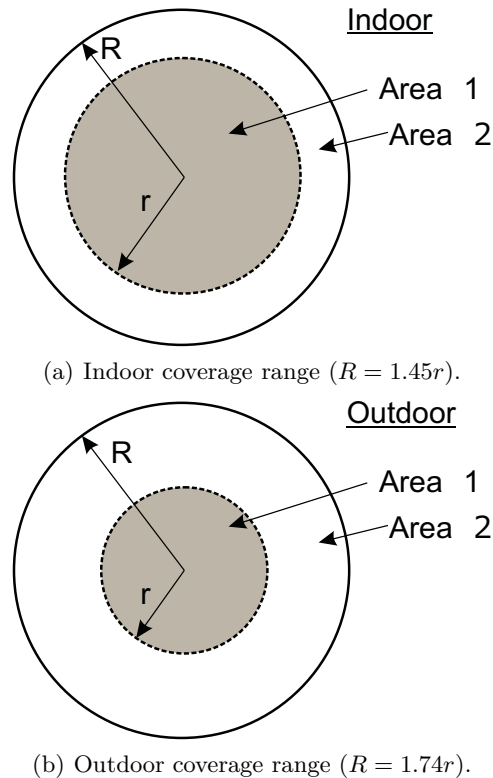


**Figure 2.21** – Illustration of the IEEE 802.11ah advanced repetition scheme.

energy consumption is a primary concern in potential IEEE 802.11ah-based communication systems. Hence, energy consumption strategies are essential to deploy Wi-Fi sensor networks. Other MAC functions include *block acknowledgment* (block ACK), enhanced *address ID* (AID) to support more than 2007 nodes<sup>1</sup>, *null data packet* sounding (NDP), *synchronization*, *speed frame* (SF) data exchange, and *sectorized spatial access*. The functions on the new IEEE 802.11ah MAC are as follows:

1. The enhanced distributed channel access (EDCA) is used in IEEE 802.11ah, which enables the prioritization of data traffic.
2. Advanced energy saving MAC strategies are incorporated, such as target wake time (TWT) to enable a long battery-lifetime.

<sup>1</sup>There is an address space limitation in [17] that only allows the addressing of  $\leq 2007$  STAs. IEEE 802.11ah use cases include long-range WLANs with 6000 STAs associated with a single AP; thus, exceeding the address space in [17].

3. Restricted access window (RAW), subchannel selective transmission (SST), and sectorized spatial access allow enhanced protocol procedures to improve coexistence WLAN STAs.

### 2.10.1 Enhanced distributed channel access (EDCA)

A combination of DCF and PCF core functions builds the foundation of the advanced hybrid coordination function (HCF) that includes the HCF Controlled Channel Access (HCCA) method [3]. An enhancement of HCF using contention-based channel access is going to be utilized in IEEE 802.11ah [5], called the enhanced distributed channel access (EDCA), which has been applied in IEEE 802.11n [17] and IEEE 802.11ac [16]. EDCA classifies content into four access categories (ACs), including *background*, *best effort*, *video*, and *voice* traffic, with increasing access priority (background  $\hat{=}$  lowest access priority, voice  $\hat{=}$  highest access priority). The four access categories allow eight different content streams [17]. For each of the ACs, an enhanced modification of DCF (EDCAF) is used that allows transmission opportunity (TXOP) operations to enable QoS [17].

### 2.10.2 (Periodic) restricted access window ((P)RAW)

The IEEE 802.11ah MAC defines a new *uplink* (STA to AP) and *downlink* (AP to STA) channel access method called restricted access window (RAW) and periodic RAW (PRAW), introduced in the IEEE 802.11ah draft [5]. The new access scheme allows the grouping of different device classes, including sensor devices and off-loading devices. RAW enables low energy consumption strategies, such as wake-up sequences. Further details on the new access schemes are:

1. *Restricted Access Window (RAW)*: The RAW-based channel access provides a time-slotted uplink channel access during the access window  $T_{RAW}$  (Fig. 2.22). Time-slots can have different slot durations  $T_S$ . A STA may wake-up at target beacon transmission time (TBTT) to identify its slot duration  $T_S$  indicated by the AP beacon with beacon interval  $T_{beacon}$  [17]. It allows the STA to stay in sleep-mode before access the assigned time-slot. STAs execute EDCA operation in case of channel access. A different TXOP rule may be applied to avoid transmission durations, which should be  $<T_S$  [5].
2. *Periodic RAW (PRAW)*: The periodic window assignment allows the channel access scheduled for a group of active polling STAs. The window is indicated for a long term period (AP long beacon frame). The AP decides the resource allocation dynamically. A PRAW group-based (group ID) scheduled STA sends data whenever it wakes up and after executing a basic CCA followed by ECDA. No channel access is allowed by STAs, which do not belong to the assigned transmission group. Grouping can be logical (AID) or physical (antenna beam, sector) assigned by the AP or optionally feedback by the STA.



Traffic indication map (TIM) STAs [17] and off-loading STAs are not allowed to access the channel during PRAWs.

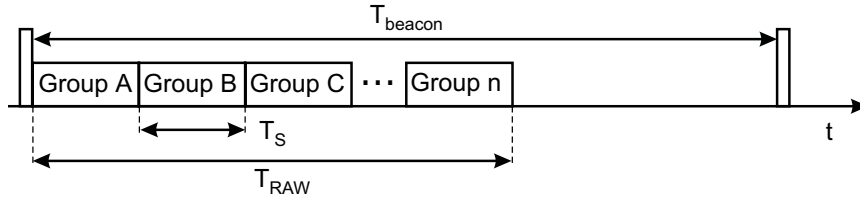


Figure 2.22 – Illustration of IEEE 802.11ah RAW operation [5].

### 2.10.3 Sectorized spatial access

Similar to the ideas in [53], the IEEE 802.11ah WLAN protocol suggests the use of sectorized antennas. It enables the control of any potential contention within an AP coverage range by dividing the BSS in sectors in which STAs operate [5]. STAs associated with at least one sector may start transmitting while STAs in other sectors remain silent to minimize contention. During *sector capabilities exchange*, STA and AP may announce their sectorized access capabilities. Two sectorization operations are supported, *group sectorization* and *TXOP-based sectorization*. During the *sector training operation*, an AP transmits training NDPs over all sectors. This enables STAs to discover the optimal sector for data transmission, e.g., based on CSI information. A *fast sector discovery* facilitates a contention reduced transmission of *sector IDs* from multiple STAs. This thesis addresses the problems of wireless contention and sectorization in Chapter 7.

## 2.11 Bibliographical notes

Significant research work on the performance evaluation of beamforming when using smart antennas in WLANs, and in particular for IEEE 802.11n WLANs, have been published in a series of contributions by Babich and Comisso *et al.*, in [54–59]. The authors evaluated the performance of beamforming for *low-rank*<sup>1</sup> WLAN channels in [54]. Four antenna radiation patterns were investigated, a *uniform linear array* (ULA), a rectangular array (URA), a uniform circular array (UCA), and finally a concentric ring array (CRA), which has somewhat similarities with the design of an *ESPAR* antenna<sup>2</sup> [60]. The results indicated that by increasing the

<sup>1</sup>If  $BW \ll 1/\Delta\tau$  AND  $\hat{\sigma}_\varphi \ll \varphi_{3dB}$ ; a channel is called *low-rank*. If  $BW > 1/\Delta\tau$  OR  $\hat{\sigma}_\varphi > \varphi_{3dB}$ ; a channel is called *high-rank*, with  $\varphi_{3dB}$  as the 3 dB beamwidth of the antenna radiation pattern and  $\hat{\sigma}_\varphi$  as the channel angular spread.  $\tau_l(\varphi) = \frac{d}{c}(l - \frac{3}{2}) \cos \varphi$ ; for 2-linear dipole array with  $l$  elements [54].

<sup>2</sup>Electrically-steerable parasitic array radiator (ESPAR) antennas enable 8 dBi gain in WLANs [60].

number of antennas and adding circular array patterns, higher performance gains can be achieved (factor 2) because of suppressed side-lobes and sharp nulls, which less interfere with other WLAN terminals in near proximity. The linear arranged antenna arrays always showed a grating lobe at  $180^\circ$  compared to the desired direction. In contrast, smart antenna arrays exhibited significant reduced side lobes with a single main lobe in the desired direction. However, these higher order antenna arrays raise many questions, such as functionality and achievable gains in practical deployment scenarios. Babich *et al.*, evaluate antenna separation effects through simulations, e.g., of a simple linear  $\lambda/2$  dipole antenna array, but not in real environments [54]. The authors speculated that other influences, such as the surrounding environment (multipath), network topology (node deployment), length of the training sequences<sup>1</sup>, the MAC protocol, and implementation of the functions in the signal processing unit, may have an impact on the achievable throughput.

Further evaluation of smart antennas in IEEE 802.11n networks have been conducted in [55] with the simulation of switched-beam antennas (SBA), directional antennas (DA), and adaptive antennas (AA) motivating a mathematical framework to evaluate the throughput performance and average packet delay. The authors concluded that by selecting the 802.11 DCF parameters carefully, a large number of STAs is manageable, e.g., with a pre-defined contention window selected as low as possible to force the network to simultaneous communications while using smart, directional antennas, which increases the spatial reuse. Babich *et al.*, also evaluated the performance of their numerical SBA and smart antenna (SA) models in simulated outdoor environments [56]. They concluded that a large number of simultaneous communication can be achieved when there is no multipath ( $\hat{\sigma}_\varphi = 0^\circ$ )<sup>2</sup> [56]. It was reported that if the spatial correlation between the received signals gets lower, a reduced number of simultaneous communications  $L_{max}$  can be observed. Further, the authors outlined the reasons for the delayed deployment of smart antennas in WLANs, arguing that the challenges of a new MAC, which need to keep backward compatibility with widely deployed IEEE 802.11 WLANs, are significant. In particular, *deafness*, *ACK suicide*, MAC and routing misconfiguration need to be addressed to achieve optimal network performance with smart antennas [56]. Coexistence problems among wireless systems, such as IEEE 802.15.4 and IEEE 802.11, have not been considered by the authors.

Enhanced media access schemes have been proposed to gain higher throughput. In [61], a comprehensive overview is given in which modified MAC schemes enable the use of smart antennas in WLANs. Due to the rapid development of *cognitive radio networks* new access schemes are possible to design. In particular, the frequent sensing of the wireless spectrum can be helpful to detect a variety of transmission

<sup>1</sup>The use of training sequences has indicated a reciprocal effect on the network throughput due to the induced network overhead [54].

<sup>2</sup>A typical outdoor channel was reported with  $5^\circ \leq \hat{\sigma}_\varphi \leq 15^\circ$ .

problems, including *performance anomalies*<sup>1</sup> and *packet collisions*. In [62], the sensing of the wireless spectrum when multiple data links are established were analyzed. The proposal is to sense packet collisions and to compare the statistics with WLAN driver parameter, such as CRC errors. It was found that by using an external spectrum sensing device both, detected packet collisions and CRC statistics indicate similar results<sup>2</sup>. This can be useful, e.g., to design a new access scheme that incorporates the *passive sensing*<sup>3</sup> of the access media, e.g., to design a *collision detection*-based media access scheme<sup>4</sup>.

Further improvements of media access and resource allocation in *Device-to-Device* (D2D) communication are proposed by Zhou *et al.*, in [63] and [64]. The authors proposed a modified CSMA/CA access scheme in which D2D devices are organized in groups and as such may share the granted media access after RTS/CTS handshake<sup>5</sup>. During the media access multiple D2D links may use the media according to a pre-defined bandwidth requirements for each D2D link, e.g., allocated by the *base station* (BS). Numerical results show a higher spectrum resource allocation efficiency. However, the limited number of orthogonal WLAN channels in the 2.4 GHz band limits the number of concurrent links.

A simultaneous polling mechanism for IEEE 802.11ah-based sensor networks using Zadoff-Chu (ZC) sequences was proposed by Kim *et al.*, [65]. When utilizing the PCF in large dense networks the large number of polling messages from the AP along with the ACKs sent by each single STA results in network inefficiency<sup>6</sup>. In the proposed multiplexing scheme, the AP sends poll messages to multiple STAs simultaneously and the ACK of each WLAN STA is sent in the same access period, which minimizes contention. The simultaneous ACK transmission is resolved in the code domain rather than the time or frequency domain, by utilizing orthogonal sequences, the *ZC sequences* that are applied in LTE, which are known for their optimal orthogonal characteristics. Hrovat *et al.*, [66] reported in their survey of radio propagation characteristics at 900 MHz for *arched* and *rectangular* tunnels and in coal mines of several kilometers length. Propagation in tunnels is significantly different compared to outdoor areas and is classified in three regions, namely, (i)

---

<sup>1</sup>So called *performance anomalies* are referred as the result of reduced network data rate during concurrent data transmission of low and high data rate frames because of the increased *airtime* of robust modulation schemes compared to high data rate modulation schemes.

<sup>2</sup>It was confirmed that packet collisions can lead to CRC errors, which in turn may not consequently result in lost data frames.

<sup>3</sup>Passive sensing is where the media is sensed for spectrum information without involving in the communication, e.g., by sending packets, whereas *active sensing* may require the sending of a data frame, e.g., to estimate the condition of a communication path, communication time, etc.

<sup>4</sup>This can result in a novel access scheme that may be called CSMA/collision detection (CSMA/CD).

<sup>5</sup>A conventional WLAN device in half duplex mode can either transmit or receive data frames, but not concurrently receive or transmit data frames. This results in an inefficient spectral utilization. Advanced MAC schemes will allow full duplex operation, which results in increased spectrum utilization.

<sup>6</sup>The PCF scheme is applied mainly in industry WLANs in which guaranteed QoS support is required.

near region with high path loss, (ii) far region where *waveguide effect* is apparent, and (iii) extreme far region where the path loss follows the free path loss propagation model for tunnels with large transverse dimensions  $x$  [m]. The *breakpoint* location is  $l_{bp} = x^2/\lambda$ , which depends on the carrier frequency, the tunnel geometry and the antenna characteristics. Scaling laws versus throughput capacity in random networks up to 1000 node population are reported in [67]. Different movement patterns (random walk, random way-point, Levy walk) versus network delay time were discussed and classified as trade-off regions.

Finally, SIG PHY characteristics are analyzed in the context of IEEE 802.11af, which defines specifications for spectrum sharing among unlicensed white space devices and incumbent user of the TV white space (TVWS) band [68]. Details on the penetration performance at lower frequencies, include brick (-1.5 to -7 dB), glass (-0.4 to 3.1 dB), plywood (-0.15 to -1.4 dB), and reinforced concrete (-23.5 dB to -30 dB) [68]. Main challenges are uncertainties in the wireless access due to the *non-guaranteed* access, required entities, including data base and location server, and limited white space availability in metropolitan areas; thus, IEEE 802.11af is more suitable in rural areas to provide medium/high data rates.

## 2.12 Discussion and summary

### 2.12.1 Discussions

A successful sub-1 GHz WLAN standard should result in a consensus among the involved regulatory domains. This would make the final standard more attractive to device manufacturers and chip vendors. In particular, the channel bandwidth is one of the most important PHY parameter (Section 2.2). Regarding a standardized sub-1 GHz WLAN the following implications can be observed:

1. Japan is leading the development of a regional wireless sub-1 GHz smart grid in the year of 2013 that consists of 920 MHz, 2.4 GHz, and 5 GHz WLAN mesh and sensor networks<sup>1</sup>. With the ratification of ARIB STD-T108 [20] in February 2012, device manufacturers offer various hardware devices, e.g., wireless sensors that operate in the 920 MHz ISM-band (partly with IEEE 802.15.4g and IEEE 802.15.4e support and Wi-SUN certified). Both, the presence of sub-1 GHz WLANs as well as sub-1 GHz WPANs will result in interference problems. Potential coexistence solutions can further strengthen Japan's leadership position in the sub-1 GHz market.
2. The U.S. market can be seen as pioneering the development of sub-1 GHz WLANs, in particular for potential Wi-Fi off-loading. However, there is a potential threat that sub-1 GHz services might be affected by the presence

---

<sup>1</sup>The sub-1 GHz ISM-band deployment consists of IEEE 802.15.4g/e certified sensor nodes.

of a *primary user* that is allowed to offer location-based services in the 902-928 MHz ISM-band<sup>1</sup>.

3. Chinese manufacturers show a strong interest in the sub-1 GHz radio-bands. However, due to the clustering of numerous frequency portions and overlapping with public broadcast services, it may be challenging to achieve a successful product placement.
4. The use of sub-1 GHz WLAN technology in Europe is developing. Only few frequencies are accessible, which would be attractive for IoT and smart grid applications. Note that during the standardization process of sub-1 GHz WLANs only few European members were engaged compared to the strong commitment by Asian (China, Japan, South Korea, Singapore, Taiwan) and U.S. contributors. No significant contributions by European participants were observed during the standardization process<sup>2</sup>.

### 2.12.2 Summary of the chapter

The standardization of sub-1 GHz WLAN facilitates the use of carrier frequencies in the 900 MHz band, which are globally available. Some countries offer sufficient channel bandwidth, e.g., to enable wireless sensing, IoT, and smart grid applications. However, some other countries, such as Japan, provide only limited access. It has been argued that the use of lower frequencies and the use of multiple antennas increase the link budget. New MAC features can be easily added, including narrow-band MIMO-OFDM, energy saving strategies, support of large number of WLAN STAs, and beamforming, because the sub-1 GHz WLAN protocol does not need to comply on any WLAN legacy support. It has been argued that beamforming enables new transmission schemes that could mitigate the contention among multiple STAs. In particular, beamforming is discussed in this thesis and evaluated in detail to identify the apparent gains of spatial diversity in WLANs. The *linear antenna array* beamforming does not provide an optimal solution to interference mitigation, but is simple to setup compared to smart antenna arrays.

Finally, beamforming would exacerbate the hidden node problem, which requires remedies and as such adds to the PHY/MAC WLAN complexity. The new IEEE 802.11ah WLAN standard may provide remedies, such as RAW, TWT, SST, and sectorized spatial access. The performance of these new MAC schemes is unknown and should be tested, e.g., with an S1G WLAN prototype. In the following chapter a novel S1G WLAN prototype is proposed that is used throughout this thesis to evaluate S1G PHY and MAC functions.

---

<sup>1</sup>Google Inc. petition for unrestricted access in the 900 MHz ISM-band [8].

<sup>2</sup>This observation can be made for Australia and New Zealand.



## Chapter 3

# IEEE 802.11ah prototype

In this chapter a sub-1 GHz WLAN transceiver (send/receive) prototype is developed to conduct wireless tests in real environments. The prototype has to enable the emission of wireless signals, which comply on the Japanese<sup>1</sup> regulatory spectrum requirements of short-range communication systems, according to ARIB STD-T108 [20]. In addition, wireless signals have to be based on advanced IEEE 802.11 PHY/MAC protocols, including IEEE 802.11n [17] and IEEE 802.11ah [5], so that multi-antenna and MIMO-OFDM techniques can be utilized. To test the sub-1 GHz WLAN prototype in real environments, the selection of a test site is needed.

### 3.0.3 Purpose

The purpose of the sub-1 GHz WLAN prototype is to accomplish several goals in this thesis. Getting first-hand knowledge about relevant sub-1 GHz PHY and MAC operations is a primary goal in this thesis. Next, wireless performance is tested, including signal characteristics, throughput, delay, and antenna settings. Further, the prototype is used to identify apparent diversity gains, e.g., antenna diversity, code diversity, and beamforming performance. Finally, the goal is to setup multiple prototypes simultaneously to evaluate the transmission performance in multi-flow scenarios. The goals are:

1. *Knowledge:* Getting first-hand knowledge about sub-1 GHz WLANs in real environments.
2. *Testing:* Testing of transmission performance metrics.
3. *Evaluation:* Performance evaluation and identification of apparent diversity gains and validation of protocol modifications (single-flow, multi-flow).

Next, the prototype design issues and potential solutions are discussed in detail.

---

<sup>1</sup>The wireless setup is located in a Japanese laboratory.

### 3.0.4 Design issues

The main challenge is that IEEE 802.11ah WLANs will not be available until 2015. Hence, no commercial-off-the-shelf (COTS) solution<sup>1</sup> is available yet. This motivates the design of a wireless prototype. Further, in this thesis, cost restrictions are high and the re-use of available hardware, e.g., hardware in the laboratory, is preferred. Hence, the potential setup costs have to be considered. Next, it is preferred that the prototype has a flexible PHY and MAC architecture to implement and test WLAN protocol modifications. Finally, the goal is to realize test scenarios with multiple wireless terminals to evaluate coexistence issues and multi-flow performance. Potential solutions are:

1. *Software-defined radio (SDR)*: A cost efficient solution is a SDR-based prototype that consists of USRP RF front-end hardware [69] and *GnuRadio* software modules [70]. SDRs are widely accepted and applicable to many wireless systems (trunk radios, peer-to-peer networks, military communication systems) [71]. A single USRP is about 1000-2000USD plus RF daughterboards, which are at 400-800 USD. The minimal design costs allow the setup of multiple prototypes. However, an SDR-based solution never perfectly utilizes the hardware components, due to additional software/hardware handshake procedures. This compromises the theoretically achievable data rates in a significant manner. However, due to the high degree of flexibility, an SDR-based solution is sufficient for signal evaluation.

The open-source software GnuRadio is selected to provide a highly flexible PHY and MAC architecture. The re-use factor (human knowledge, tested source code) is very high, when using GnuRadio. Basic wireless projects are fast to realize, in 2-6 man months. However, some expertise is required for software modifications, e.g., to attach different daughterboards. The SDR-based prototype is highly flexible and as such it is only sub-optimal in the system performance. By consequence, wireless transmission performance is limited.

2. *Field programmable gate array (FPGA)*: Alternatively, high-speed FPGA systems are preferred when realizing wireless prototypes with high data rate modulation that are spectrum agile. However, the costs are significantly high, which are at 4000-10000USD for a single FPGA system. In addition, FPGA maintenance requires expertise and significant development time up to 12-18 man months.
3. *Wi-Fi module and WLAN cards*: Wi-Fi certified modules (or Wi-Fi chip) enable high data rates in compliance with IEEE 802.11 protocols. However, these Wi-Fi modules are difficult to purchase as prototypes. Wi-Fi modules development costs are high and sensitive to design changes, e.g., due to

---

<sup>1</sup>General purpose HW.



changes in wireless protocol standards [72]. Alternatively, the use of *proprietary* COTS WLAN cards is also possible. However, these devices cannot be manipulated, e.g., changing the carrier frequencies or channel bandwidth<sup>1</sup>.

The SDR-based solution has been selected to realize the prototype because of the minimal design *costs*, highly *flexible* PHY and MAC, and the high *re-use* factor (human knowledge, written software). The prototype hardware solution and software solution are presented in the following sections.

### 3.0.5 Hardware architecture

In Section 3.0.4 the SDR-based prototype was motivated that consists of USRP and open-source software. The USRP provides the RF front-end that emits the radio signal at  $f_c = 923$  MHz with  $2 \times 2$  MIMO-OFDM with  $BW = 1$  MHz channel bandwidth, according to ARIB STD-T108 [20]. Table 3.1 presents an overview of the COTS USRP<sup>2</sup> devices (USR P 1 & USRP 2) used in the thesis. The USRP 1 comes

COTS Hardware type	Purpose	Remarks
USR P 1	SDR RF front-end, which operates at $f_c = 923$ MHz	The USRP 1 main-board supports two daughterboards; thus, a simple $2 \times 2$ MIMO setup is possible. Two SBX daughterboards ( $BW = 40$ MHz) are selected to operate at the target radio-band.
USR P 2	Spectral-time sensor RF front-end, which operates at $f_c = 923$ MHz	The USRP 2 hardware specification allows a high resolution spectrum sensing; thus, this hardware type is useful to setup a spectrum sensor that operates at the target radio-band, e.g., to capture radio signals emitted the from IEEE 802.11ah prototype.

**Table 3.1** – List of the USRP devices (USR P 1 & USRP 2) used in the thesis.

with an A/D 12 bit with a sending rate at 64 MS/s (32 MHz). The primary connector of the USRP 1 is an USB 2.0 port with a maximum sending rate at 480 Mbps. The USRP 2 comes with 14 bit A/D and a sampling rate at 100 MS/s (50 MHz). The

<sup>1</sup>Atheros X9, Wi-Fi at 920 MHz, with 5, 10, 15 MHz channel bandwidth and  $\leq 1$  W sending power, U.S. radio-band certified, proprietary WLAN [73].

<sup>2</sup>The new USRP X300 supports double mounted SBX ( $BW = 40$  MHz) and the new SBX ( $BW = 120$  MHz) daughterboards. The new USRP series was released in the final phase of the thesis.

primary connector of the USRP 2 is Ethernet (GbE) with a maximum sending rate at 1000 Mbps. To emit the radio signal in the 900 MHz assigned radio-band, the SBX daughterboard is applied, which enables the emission of radio signals up to  $P_{tx} \leq 100$  mW between  $f_c = [400, \dots, 4400]$  MHz. It supports MIMO with  $\leq 40$  MHz channel bandwidth [69]. The SBX board uses a wideband synthesizer with integrated voltage controlled oscillator (VCO) (AD 4350<sup>1</sup> [74]).

The SBX provides many advantages compared to other SDR hardware, which offer a limited output power that would require external power amplifier, e.g., for long-range tests<sup>2</sup>. Further, the USRP 1 is selected, because its main board enables the use of two SBX daughterboards, which facilitates concurrent transmission using two antennas (Fig. 3.1). It does not need any external reference signal (clock), such as USRP 2, to enable synchronized signal transmission among two antennas. The USRP 1 is connected via USB 2.0 port to an external host PC that runs the necessary software applications (Section 3.0.6). The USRP 1 is equipped with two VERT 900 omni-directional vertical antennas with 3 dBi gain (Fig. 3.1). As a dual-band antenna it includes the two radio-bands 824-960 MHz and 1710-1990 MHz [69]. The antenna height<sup>3</sup> is 236.5 mm. A 2×2 multi-antenna constellation is sufficient to test MIMO-OFDM features. Using more antennas would significantly add to the complexity of the prototype, e.g., a high number of spatial streams (SS) support requires additional computational power. The prototype details are:

1. Carrier frequency  $f_c = 923$  MHz.
2. Channel bandwidth  $BW = 1$  MHz, in compliance with ARIB STD-T108 [20].
3. 2 SBX 900 MHz daughterboards [77].
4. Driver modifications to support SBX (the 2.4 GHz XCVR daughterboard is supported by default [78]).
5. 2×2 MIMO-OFDM, according to IEEE 802.11 protocols [17].
6. Multi-antenna setup to test beamforming.

The hardware solution<sup>4</sup> has been introduced in [34] and [31]. The following section gives further details on the software solution.

<sup>1</sup>Minimum RF output power  $P_{tx}(min) = -4$  dBm, maximum RF output power  $P_{tx}(max)^{AD4350} = 5$  dBm plus power amplifier on the SBX daughterboard with maximum output power  $P_{tx}(max)^{SBX} = 20$  dBm output power.

<sup>2</sup>Maveriq<sup>TM</sup>SDR, AD 9361 [75],  $P_{tx}(max) = 5$  dBm,  $f_c = [70, \dots, 6000]$  MHz, modulation accuracy (EVM) = -42 dB (19.2 MHz reference clock at  $f_c = 800$  MHz) [76].

<sup>3</sup>900 MHz Wi-SUN certified modules use chip antennas with 1 cm length. Alternatively, small form factor *meta-material* antennas are proposed.

<sup>4</sup>The SDR-based WLAN prototype solution has not been certified by a regulator and as such can only be used in isolated environments.

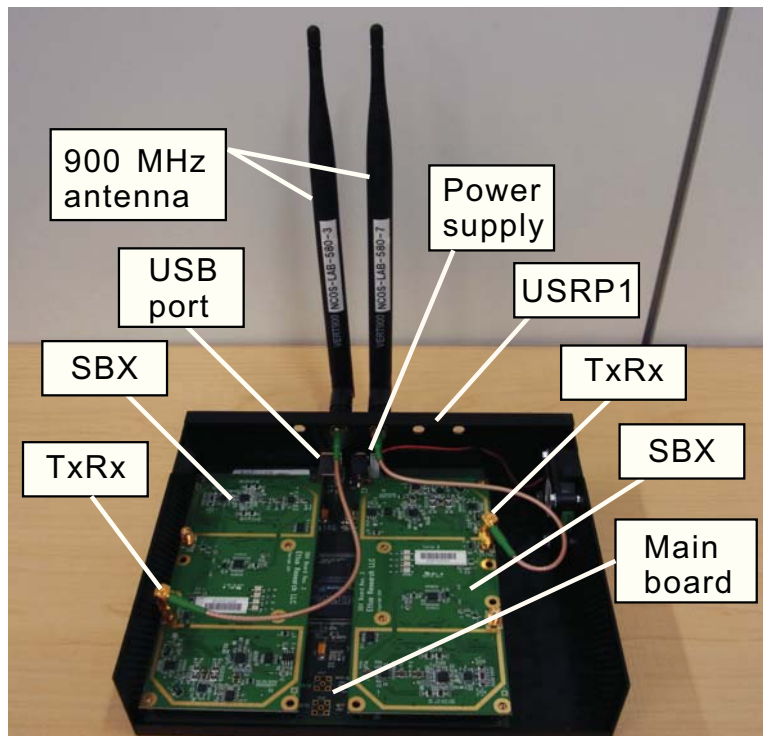


**Figure 3.1** – Illustration of the USRP1 hardware setup. It shows two VERT 900 antennas attached to the Tx/Rx SBX ports. In addition, it illustrates two SBX daughterboards attached to the USRP1 main board, the USB 2.0 port, and power supply.

### 3.0.6 Software architecture

For the sub-1 GHz platform open-source software is applied to design a generic platform that enables a variable carrier frequency  $f_c$  setting in the sub-1 GHz assigned radio-band. In addition, it must facilitate MIMO-OFDM operations with a limited channel bandwidth  $BW = 1$  MHz. Further, a flexible and open-source PHY and MAC implementation is preferred to modify and test new WLAN protocol features. A combination of two independent software projects, called *GnuRadio* [70] and *Hydra* [79, 80] provides the basic software solution. Table 3.2 presents an overview of the software modules (GnuRadio, Hydra, and required software modifications) used in the thesis. In Fig. 3.2 the sub-1 GHz WLAN prototype software architecture is illustrated, as published in [34]. GnuRadio provides the required software framework to control the USRP1 hardware from a host PC via USB 2.0 at 8 MS/s

Software	Purpose	Remarks
GnuRadio	Generic PHY and MAC SDR software libraries, which are essential to realize an USRP-based SDR, including modulation/demodulation, encapsulation/de-encapsulation, USRP interface libraries.	GnuRadio only supports generic modulation function. To realize a IEEE 802.11 compliant SDR, additional software is required.
Hydra	SDR software that utilizes GnuRadio and USRP1 to provide IEEE 802.11n WLAN protocol operations at 2.4 GHz	Hydra only provides generic IEEE 802.11n WLAN operations. It supports USRP1 devices; thus, it is helpful to realize an IEEE 802.11ah WLAN prototype.
Modified GnuRadio & Hydra	Required software modifications to support multiple SBX daughterboards to realize an SDR that operates at $f_c = 923$ MHz.	Realization of an IEEE 802.11ah WLAN prototype that operates as $2 \times 2$ MIMO-OFDM WLAN at $f_c = 923$ MHz. Modifications on USRP hardware driver (UHD) and Hydra software modules, including PHY (down-clocking, OFDM subcarrier settings) and MAC (inter frame spacing time, CSMA/CA) operations.

**Table 3.2** – List of the SDR modules used in the thesis.

(Fig. 3.2). GnuRadio is used to enable the basic PHY and MAC operations when using USRP.

In addition, advanced IEEE 802.11n PHY/MAC protocol support is needed to enable multi-antenna support to transmit MIMO-OFDM signals. The software project *Hydra* does this job and enables the emission of data frames in the 2.4 GHz assigned radio-band using XCVR daughterboards [78]. Hydra is an open-source software application, written in C++ and Python that allows the assessment of encode/decoded data frames in real-time and uses advanced WLAN protocols, such as IEEE 802.11n for multi-antenna MIMO-OFDM transmission. Hydra does this by providing a *virtual* tunnel device (TUN) to route IP data traffic (IP address) to the radio (MAC address). In addition, it enables the visualization of PHY/MAC

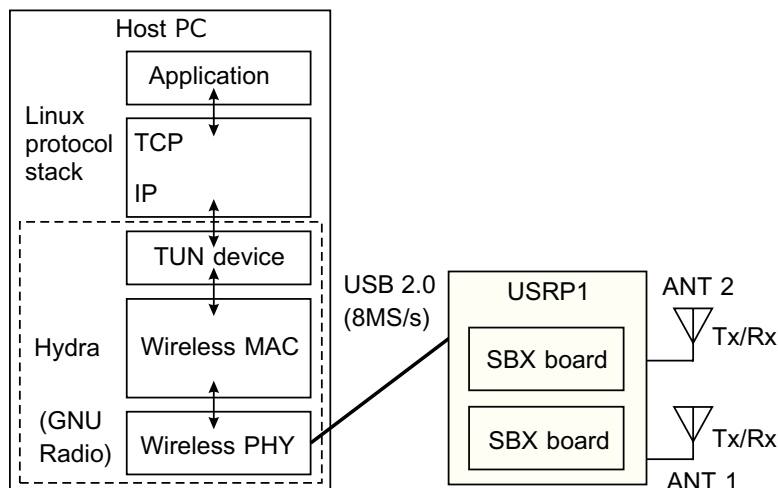


**Figure 3.2** – Illustration of S1G WLAN prototype HW/SW architecture.

performance metrics, such as bit error rate (BER), in-phase/quadrature (I/Q) signal constellation, CSI information, channel gain, and H-matrix parameter. It supports 2-way communication and allows the development of optional features, including *data framing* and *block ACKs*. It includes software libraries with IEEE 802.11n core functions. Hydra utilizes multiple USRPs to support MIMO features. Hydra was selected to provide a flexible PHY and MAC that supports IEEE 802.11n protocol features. Further, it allows the modifications of PHY and MAC features, which can be easily added and tested.

### 3.0.7 Required modifications

The USRP 1 is connected to a host PC via USB 2.0 interface to send/receive data from the application running at the PC. The USRP 1 USB connection is known for its critical sending rate limitation of 8MS/s (Fig. 3.2). The host PC is a 3.2 GHz high performance Linux PC with Ubuntu distribution. It hosts the GnuRadio software for USRP control and the modified Hydra software to enable WLAN traffic based on IEEE 802.11 core functions. Modifications have been published as part of this thesis in [31] and [34]. The required changes are:

1. *Software modification*: Hydra supports 2.4 GHz XCVR daughterboards, which is Hydra's default radio-band. Hence, modifications are required to enable Hydra to use SBX daughterboards at different carrier frequencies, e.g.,  $f_c = 923$  MHz. Fig. 3.3 illustrates the function call procedure among the relevant software modules. It is divided in PHY (IEEE80211-mimo), the MAC (gr-hydra, gr-mimo), and RF front-end (GnuRadio, USRP 1/SBX). In Tx mode, data arrive at the MAC, which are forwarded to the PHY via *trvector*. The

PHY returns the I/Q signals, which are forwarded as input signal to the USRP1. In the Rx mode, the incoming signal is received by the USRP1, which is forwarded as I/Q signal to the MAC (gr-hydra). Hydra information is removed and the I/Q signal is forwarded to the PHY, which decodes the signal into a txvector forwarded to the MAC (gr-mimo).

To solve the problem of controlling the SBX hardware, differences in the hardware architecture of XCVR [78] and SBX [77] need to be identified [31]. The required software modifications are written as part of a new USRP hardware driver (UHD).

2. *Multiple SBX daughterboard support:* To enable the use of multiple SBX daughterboards, software modifications are required, which allow the concurrent emission of data frames. In particular, so called *overrun* and *underrun* error messages because of the use of multiple SBX daughterboards, are managed by additional driver modifications.
3. *IEEE 801.11ah:* To comply to the emerging IEEE 802.11ah protocol, WLAN protocol modifications are necessary in Hydra. In particular, changes on the physical layer convergence protocol (PLCP) are required, including length of the *short training field* (STF), *long training field* (LTF) and signal field. In addition, IEEE 802.11ah includes new MAC features, such as energy consumption reduction, coexistence, and synchronization (Section 2.10).

### 3.0.8 Link setup

A single wireless link consists of two S1G WLAN prototypes, the S1G WLAN sender and the S1G WLAN receiver. In Fig. 3.4 the flow chart of the prototype using two prototypes is illustrated. It illustrates the data flow on outgoing and incoming paths. It starts with the data flow, initiated by the *virtual device* (TUN device). The source path contains the carrier sense, data framing, CRC, forward error correction (FEC) features and modulation. The sink path consists of the demodulator, the correlator, FEC, and CRC feature.

The following section gives details about the test site in which wireless links have been setup for performance tests.

## 3.1 Alternative testbeds and prototypes

There are few alternative solutions available, which have their advantages and disadvantages, namely:

1. National Instruments<sup>TM</sup>(NI) USRP-RIO [81]
2. Antcor S.A. 802.11 IP [82]

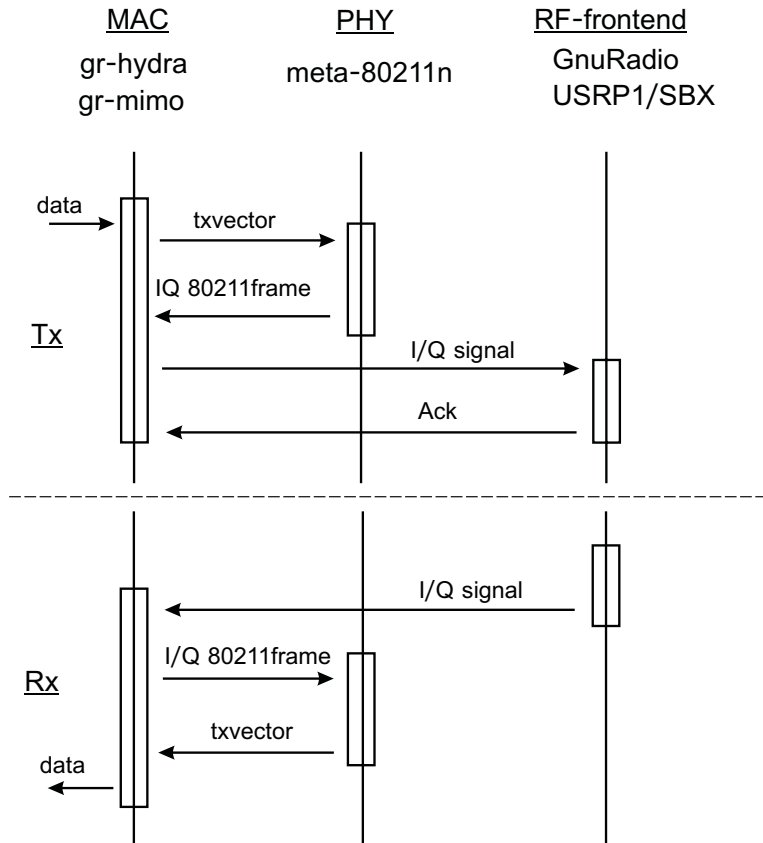


Figure 3.3 – S1G WLAN prototype SW module function call procedure.

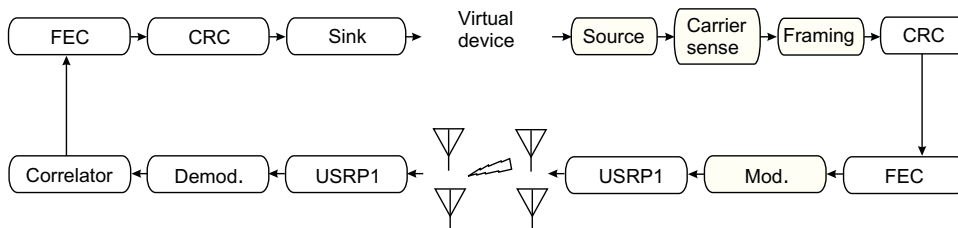


Figure 3.4 – Link setup and its relevant S1G WLAN prototype SW functions.

3. Epic Solutions (Maveriq™/Matchstiq™) [76]

Table 3.3 compares the proposed IEEE 802.11ah prototype with some alternative types. Some of the systems are still not available or require a significant overhead in software purchase; thus, are not candidates for the evaluation in this thesis.

System parameter	IEEE 802.11ah prototype (this thesis)	Antcor S.A. 802.11 IP [82]	Epiq Solutions [76]	NI USRP-RIO [81]
Platform	USRP 1, SBX (400 MHz-4.4 GHz)	FPGA, DSP	Maveriq	USRP-294x
Processor	USRP 1: Cyclone EP1C12Q240; SBX: ADF4350	n.a.	Spartan-6, Lz150T	Xilinx Kintex 7 FPGA
RF range	SBX: 440 MHz - 4.4 GHz	920 MHz band	100 MHz to 6 GHz	50 MHz to 6 GHz
RF accuracy	SBX: n.a.	n.a.	–	0.01 to 2.5 ppm
PHY	$f_c = 923$ MHz, $BW = 1$ MHz (C++, Python)	flexible	flexible	flexible
MAC	basic CSMA/CA (C++, Python)	n.a.	n.a.	n.a.
Scalability	high	medium	medium	medium
Throughput	low-high	medium-high	medium	high
Accuracy	low-medium	–	–	–
Price <sup>1</sup> [USD]	4.000	40.000	44.000 (incl. SDK)	24.000 (incl. SDK)

**Table 3.3** – Comparison of proposed IEEE 802.11ah WLAN prototype vs. alternative platforms. Alternative platforms have not been tested. Thus, the performance and accuracy is unknown. The price includes the required software development kit (SDK).

## 3.2 The test site

To test the performance of the sub-1 GHz WLAN prototype, a controlled environment<sup>2</sup> is required to avoid the emission of radiated energy from the non-certified

<sup>2</sup>A controlled indoor environment is the primary candidate to test non-certified wireless radio. To conduct measurements in wide area outdoor environments, one may acquire specific test frequencies, which were not available for this thesis. [83] contains a setup description for outdoor measurements.



prototype. Therefore, three potential candidates exist, the *anechoic chamber*, a *shielded tent*, and a *shielded room*.

In addition, wired cables could be used for initial testing of the prototype. However, this would have the disadvantage of limited multi-path effects. Hence, setting up the prototype in a controlled environment, e.g., in a shielded room, would allow testing of wireless multi-antenna systems. Line-of-sight (LOS) setups between a pair of prototypes, e.g., for single wireless link setup, would be easily possible. However, the predominance of a LOS component or high correlation between different paths because of the short distance between the WLANs, have been reported to have a negative impact on the performance gain of MIMO transmissions [84]. The following subsections provide more details about the test site environments.

### 3.2.1 Anechoic chamber

For testing the sub-1 GHz WLAN prototype, an *anechoic chamber* was used for initial sub-1 GHz WLAN multi-flow measurements. The main characteristic of an (ideal) anechoic chamber is that there are no reflections of radiated waves inside the chamber due to the mounted absorbing material at the chamber walls (Fig. 3.5).

Therefore, such chambers are useful to measure the radiation of large radar antennas or satellites due to the controlled environment with no levels of interference caused by ambient signals outside the anechoic chamber. For initial testing of non-certified wireless terminals such anechoic chambers may be useful. However, for measuring wireless terminals with multi-antennas, which are used in indoor and outdoor environments with dominant multipath characteristics, anechoic chambers provide a very different environment [84]. Further, anechoic chamber, shielded tent, and shielded room have the disadvantage of limited measuring distance and lower frequency usage due to the characteristic of the absorbers (anechoic chamber) or reflections (shielded room). By consequence, anechoic chambers are insufficient for testing multi-antenna MIMO systems.

### 3.2.2 Shielded tent

A *shielded tent* is an object that consists of a synthetic cloth with a metal mesh-type structure to avoid the emission of radiated waves from inside the tent to the outside (Fig. 3.6).

The shield tent has the dimension of 2 m<sup>3</sup>. A low skin depth of the mesh cloth is typical for shielded tents. Ideally - similar to a Faraday cage - no or less radiated wireless emission should be able to penetrate the tent. However, using a shielded tent has significant disadvantages:

1. *Shielding quality*: The shielding of the tent is inefficient because of the low skin depth ( $\leq 2$  mm) of the wall material. It was observed that the spectral energy of WLAN AP beacons from office WLANs can be detected in the inside location of the shielded tent. The reduced shielding quality would lead

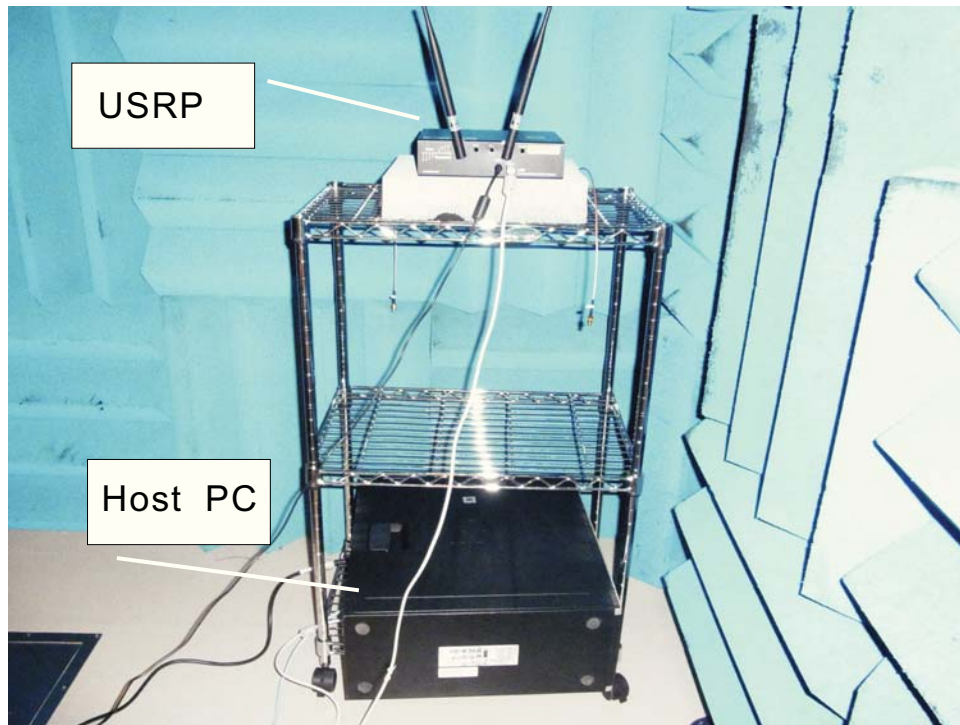


**Figure 3.5** – S1G WLAN prototype setup inside the anechoic chamber. The photograph shows the USRP 1 and the host PC.

to unwanted wireless interference of data transmissions outside the tent and also would have a negative impact on the measurement results taken inside the tent.

2. *Reduced handling:* Due to the limited size of the cavity, wireless terminal settings are very limited. In addition, modifications by humans during testing are difficult due to open/closing the tent manually.
3. *Material quality:* Shield tents are easy to damage, e.g., broken zipper, broken mesh. Further, shield tents do not provide any cooling facilities. By consequence, it is difficult to maintain a constant operating temperature inside a shielded tent.

By consequence, a shielded tent provides a very limited test environment for multi-node and multi-antenna settings, such as the proposed sub-1 GHz WLAN prototype. As an alternative to anechoic chambers and shielded tents, the advantages of a shielded room are given in the following.

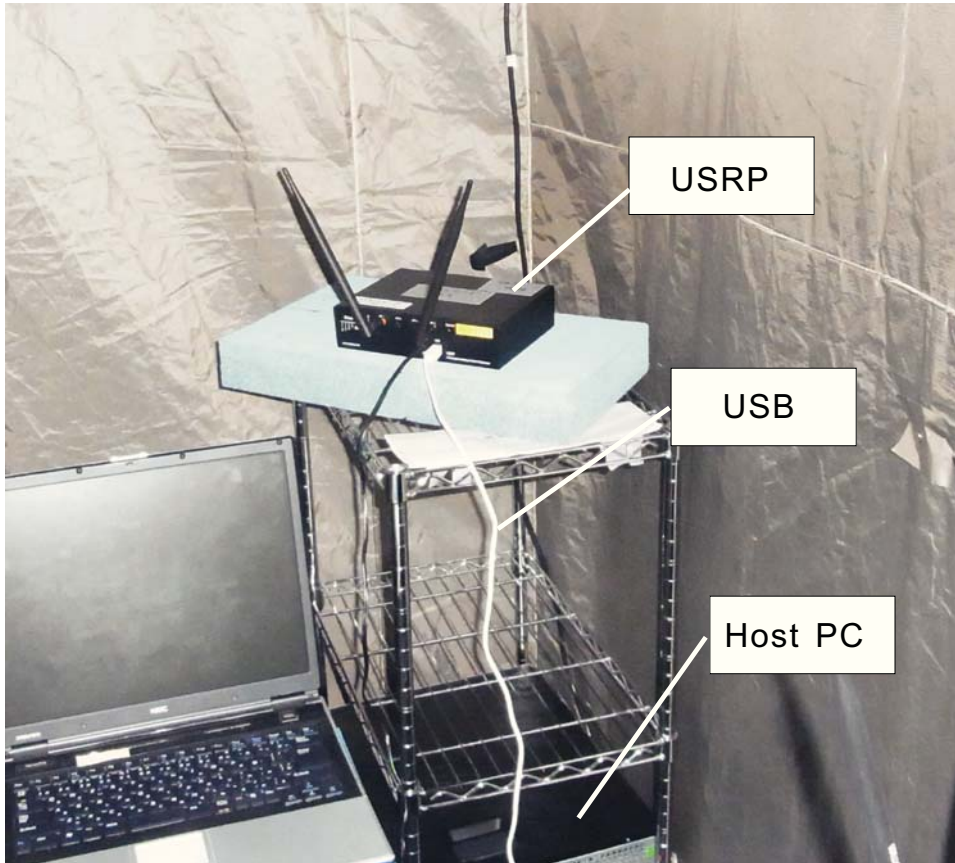


**Figure 3.6** – S1G WLAN prototype setup inside the shielded tent. The photograph shows the USRP 1, the USB connection, and the host PC.

### 3.2.3 Shielded room

A *shielded room* was used for the main part of the measurements, e.g., to evaluate various diversity gains of the sub-1 GHz WLAN prototype. The shielded room is a metal-box cavity of 4×5 m and 3 m height and provides a large skin depth of 10 cm. Typically, shielded rooms do not have any absorbers mounted on the walls (Fig. 3.7). The shielded room allows the measurements of various *equipment under test* (EUT), including *devices under test* (DUT) and *antennas under test* (AUT), which can be placed inside the shielded room. The radiation generated emission by the devices stays inside the cavity. The advantages of the shielded room are:

1. *Easy access*: The large dimension of the cavity makes it easier to manipulate wireless testbed settings, e.g., placing of the wireless nodes and variation of the

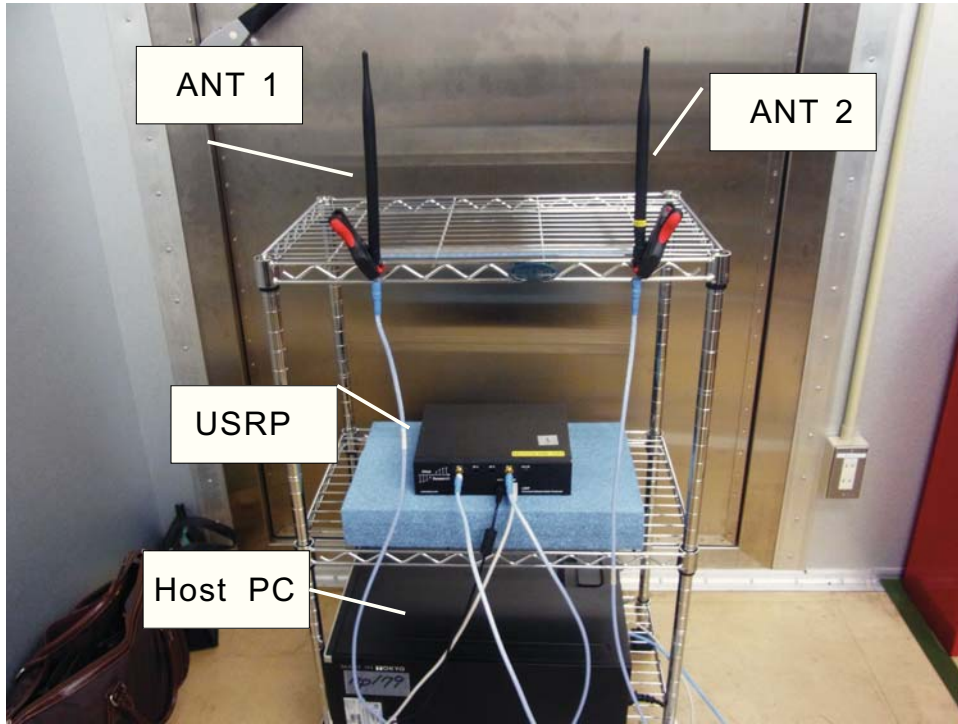


**Figure 3.7** – S1G prototype setup inside the shielded room. The photograph shows the USRP 1 and the host PC. In addition, it shows the two VERT 900 antennas separated at  $d = 30$  cm distance.

antenna distance, during tests. In addition, wireless tests can be controlled from the outside by using access tunnels.

2. *Test under multipath conditions:* The shielded room provides a reflective reference environment, which is more suitable for the testing of wireless terminals compared to anechoic chambers. The reflection of the metal walls provides a more suitable realistic multipath environment compared to the wireless propagation conditions inside an anechoic chamber. Thus, the shielded room is recommended for wireless multi-antenna measurements.

3. *Controlled channel conditions*<sup>1</sup>: Measurements conducted in the shielded room are likely to be constant due to the controlled condition of the static cavity. By consequence, the shielded room is somewhat similar to electromagnetic *reverberation chambers*<sup>2</sup>, which are often used for 3GPP LTE measurements, e.g., to create constant Rayleigh fading conditions [84].
4. *Test of non-certified devices*: The shielded room allows measurements of non-certified wireless equipment, which is otherwise not allowed to be tested in the free field.
5. *Cooling*: Shielded rooms provide air cooling functions and make the setup of large number of wireless terminals and PCs easy to maintain, e.g., constant environmental temperature.

By consequence, the use of the shielded room for testing wireless terminals with small antennas is a good compromise compared to anechoic chambers and reverberation chambers. However, the impact of the reflections on the communication among the wireless terminals due to the metal walls of the metal-box cavity remains unclear<sup>3</sup>. The presence of a large number of obstacles located inside the shielded room should provide sufficient scatter points (clusters), which provides a multipath rich environment, e.g., to measure multi-antenna diversity gains. It can be confirmed that the communication distances between the test nodes at the selected test site (anechoic chamber, shielded room) is sufficient<sup>4</sup> for the testing in the far-field modeled by [29, 83]

$$d_{test} \geq \frac{2(d_1 + d_2)^2}{\lambda}, \quad (3.1)$$

where  $d_1$  is the dimension of the equipment under test (EUT) in [m],  $d_2$  is the antenna dimension in [m], and  $\lambda$  as the test frequency wavelength [m]. With  $d_1 = 0.15$  m and  $d_2 = 0.4$  m (two  $\lambda/2$ -dipole antenna array) the minimum required test distance for the far-field becomes  $d_{test} = 1.89$  m. The actual distance among the WLAN sender and receiver node at the test site was 3 m. By consequence, mutual antenna coupling is negligible for all tests at this location.

---

<sup>1</sup>The wireless measurements have been conducted under controlled channel conditions. However, the measurements in the shielded room have indicated some effects of time-variant conditions, when using a wireless terminal - here the SDR - that consists of antennas, RF front-end, USRP, software and host PC. Marginal dynamics of the channel (Rayleigh channel model) may be amplified by any of these SDR components; thus, leading to the conclusion of time-variant transmission conditions even under stable environmental conditions.

<sup>2</sup>An introduction of reverberation chambers for testing of 3GPP wireless terminals, which use multi-antenna settings is given in [84].

<sup>3</sup>The fact that signal emission inside a shielded room injects fields of static modes, which would be somewhat similar to electromagnetic reverberation chambers, may impact the transmission characteristic of all wireless nodes located in a shielded room.

<sup>4</sup>The recommended distance for far-field testing is  $\geq 2\lambda$  [29].

### 3.3 Test site measurement configuration

To provide detailed information about the multi-node S1G WLAN measurements, test site measurement configurations in different environments are shown in the following.

#### 3.3.1 Setup A: Anechoic chamber with ground plane

The wireless measurements in this thesis have been conducted in an anechoic chamber and a shielded room, which enables the propagation of wireless signals in free space under controlled environmental conditions. The inner surfaces of the anechoic chamber are covered with pyramidal urethane foam, which absorbs any radio emissions inside the chamber (80-140 dB) [29]; thus, any radio emission of the device under test (DUT) to the outside of the chamber is avoided. Advantages of this facility is a limited measurement impact due to ambient interference, constant noise floor, minimal reflections of walls and constant environmental conditions (temperature, humidity). Disadvantages when using an anechoic chamber are the limitations of the distance between the wireless transmitters, which results in a LOS condition. In addition, the mitigation of reflections (so called clusters) results in highly correlated propagation paths, which only provide a limited path orthogonality for MIMO systems. As a result, a limited MIMO transmission performance is observed. The schematics of the anechoic chamber and shielded room are depicted in Fig. 3.8. The multi-node setup inside the anechoic chamber is shown in Fig. 3.9. The measurement setup for a single flow (1 flow) in the anechoic chamber is depicted in Fig. 3.10(a) and for multi-flows (2 flows) in Fig. 3.10(b).

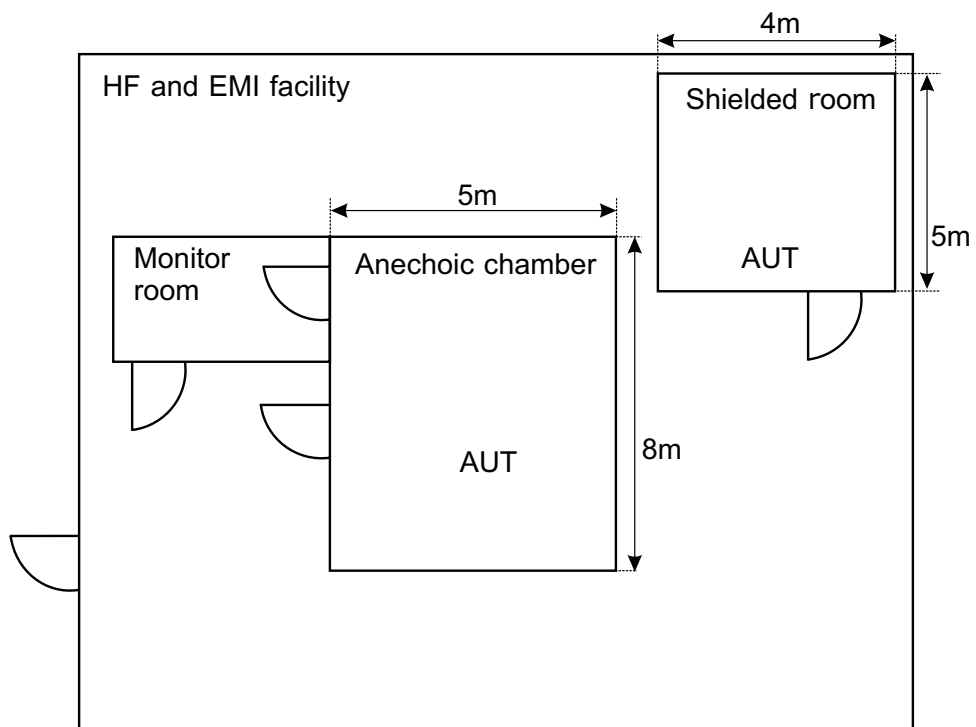


**Figure 3.8** – Schematic representation of the anechoic chamber and shielded room of the used HF and EMI measurement facility.



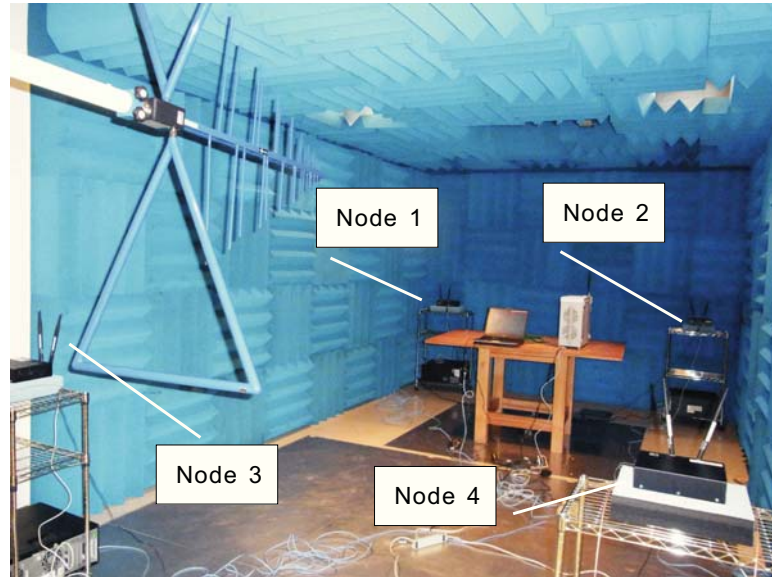


**Figure 3.9** – Multi-node S1G WLAN prototype setup inside the anechoic chamber. The picture indicates the 1 GHz measurement antenna attached (left side), which was removed during the wireless test to avoid wireless reflections in the anechoic chamber.

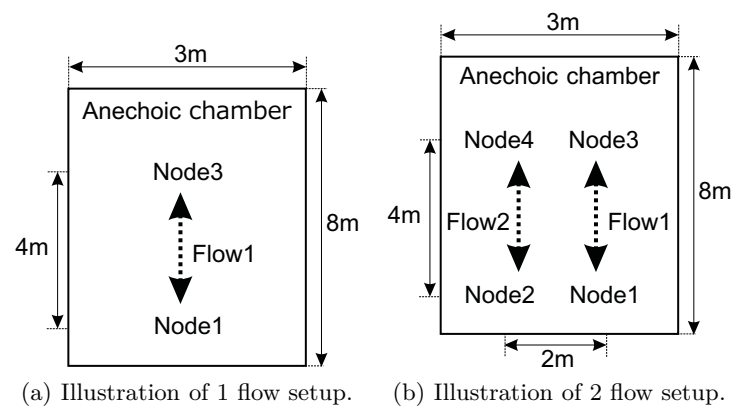


**Figure 3.10** – Illustration of S1G WLAN prototype setup in the anechoic chamber.



### 3.3.2 Setup B: Shielded room

The multi-node setup in the shielded room is shown in Fig. 3.11.

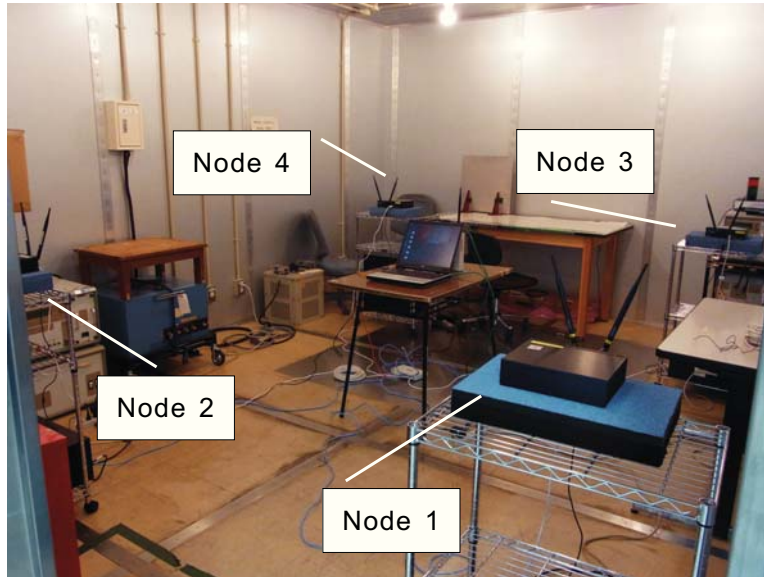


**Figure 3.11** – Multi-node S1G WLAN prototype setup inside the shielded room.

The measurement setup for single flow (1 flow) in the shielded room is depicted in Fig. 3.12(a) and for (multi-flows) 2 flows in Fig. 3.12(b).

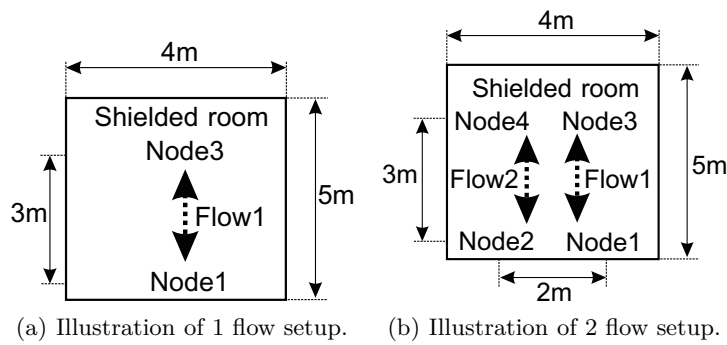


**Figure 3.12** – Illustration of S1G WLAN prototype setup in the shielded room.

### 3.3.3 Setup C: Shielded tent

The shielded tent was used for initial measurements of the S1G WLAN prototype. The physical dimensions of the shielded tent do only provide a limited test environment for multi-node measurements. Fig. 3.13 illustrates the initial setup in the shielded tent.

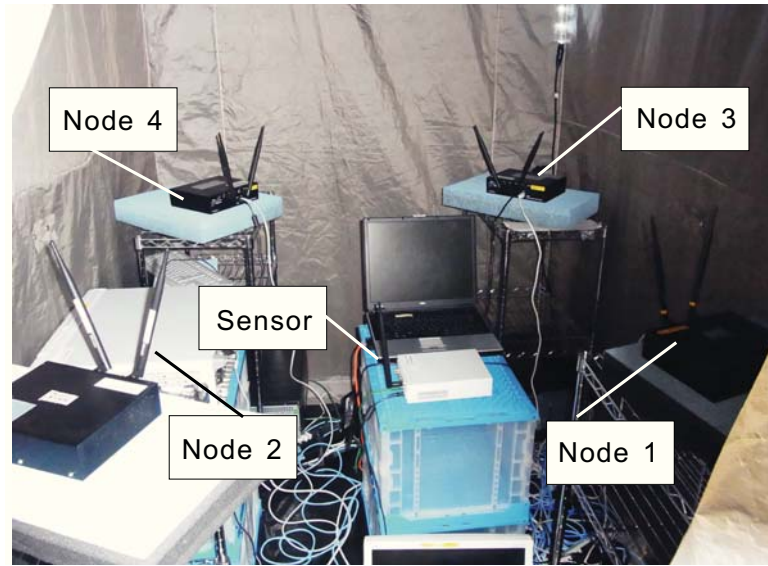


**Figure 3.13** – Multi-node S1G WLAN prototype setup inside the shielded tent.

The measurement setup for single flow (1 flow) in the shielded tent is depicted in Fig. 3.14(a) and for multi-flows (2 flows) in Fig. 3.14(b).

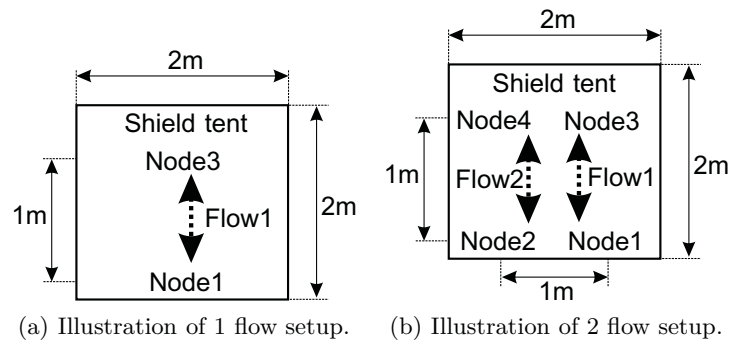


**Figure 3.14** – Illustration of S1G WLAN prototype setup in the shielded tent.

### 3.4 Other used equipment

In addition to the S1G WLAN prototype, extra devices have been used for testing wireless data transmissions. For conducting sub-1 GHz wireless coexistence measurements, selected WPAN devices have been used. To identify the spectrum characteristics of data signals, a spectrum analyzer was applied to the test setup. To study the spectrum characteristics in detail and to record the monitored data, e.g., batch mode evaluation, a supplementary S1G spectrum sensor has been developed in this thesis.

#### 3.4.1 Used 900 MHz & 2.4 GHz WPAN devices

To study wireless coexistence issues in the sub-1 GHz ISM-band, IEEE 802.15.4 sensor nodes have been selected, which have been part of the test scenarios. The selected WPAN devices allow to transmit short burst sensor data, e.g., 10 byte, in short distances. The results of the concurrent use of IEEE 802.11ah and IEEE 802.15.4 networks indicated that there is a demand for access control to reduce the number of packet collisions, which occur when wireless carrier sense levels - here WLAN and WPANs - are not synchronized, and as such lead to unstable system operations. A thorough evaluation of the assessment in real wireless networks is given in Chapter 6. Table 3.4 lists the WPAN devices, which have used throughout this thesis. The aim of using these WPAN devices is twofold. First, a setup scenario is developed, which consists of real-world hardware. This will give first-hand results on the hardware performance. Second, it will enable a discussion how to develop countermeasures against coexistence problems in the 900 MHz radio-band.

Hardware	Type	Modulation	Protocol	Remarks
UD-Stick	2.4 GHz	GFSK	IEEE 802.15.4	ZigBee™
UZ-Stick	2.4 GHz	GFSK	IEEE 802.15.4	ZigBee™
NEC-950	950 MHz	GFSK	proprietary	Echonet device
Satori	920 MHz	GFSK	IEEE 802.15.4	ZigBee™/Wi-SUN
TI 1120	950 MHz	GFSK	IEEE 802.15.4	ZigBee™

**Table 3.4** – List of available WPAN devices in this thesis.

#### 3.4.2 Spectrum analyzer

Measurements of basic spectrum characteristics in this thesis were conducted by using a spectrum analyzer. Spectrum measurements were conducted in the sub-1 GHz ISM-band to detect the presence of wireless signals. To measure wireless signals in the sub-1 GHz band, it is essential to understand the performance, and to identify potential coexistence problems through spectrum sensing and observation of sensed signals. Hence, it is required to have a spectrum analyzer to evaluate and

record the transmitted data signals, including data packets and acknowledgments (ACKs). A spectrum analyzer from Agilent<sup>TM</sup>, which operates from 3 kHz up to 3 GHz, has been applied to the test setup. A 900 MHz antenna was used when conducting the sub 1 GHz measurements [69]. A disadvantage is the practical recording of sensed data, e.g., for signal evaluation in batch mode. Therefore, as an alternative, a novel spectrum sensor has been developed in this thesis that is outlined in the following.

### 3.4.3 S1G spectral-time sensor (COTS-SDR)

There are no or little number of spectrum sensors at the market available that are useful to monitor the sub-1 GHz spectrum. None of these solutions offer a high data resolution. A high signal sampling performance is required to obtain a sufficient amount of data that reveals the details of the signal. Hence, the configuration of a novel spectrum sensor is proposed in this thesis. The proposed spectral-time sensor (STS) allows high sampling rates, which is efficient to monitor signals with high accuracy. Monitored signals can be easily recorded and stored for further evaluation, e.g., in batch mode. The USRP 2 is selected to realize a novel spectrum sensor, which represents a COTS-SDR solution. The USRP 2 is highly advantageous due to its higher sampling rate and A/D converter accuracy, compared to USRP 1 (Section 3.0.5). The COTS USRP 2 provides a single interface to a wide selection of daughterboards. The SBX daughterboard is a recommend choice because it enables the signal reception in the sub-1 GHz band. Software modifications have been created to extract the FFT from the recorded I/Q signals. The data resolution indicates a high accuracy and enables an efficient spectrum validation. Fig. 3.15 depicts the schematic of the spectral-time sensor.

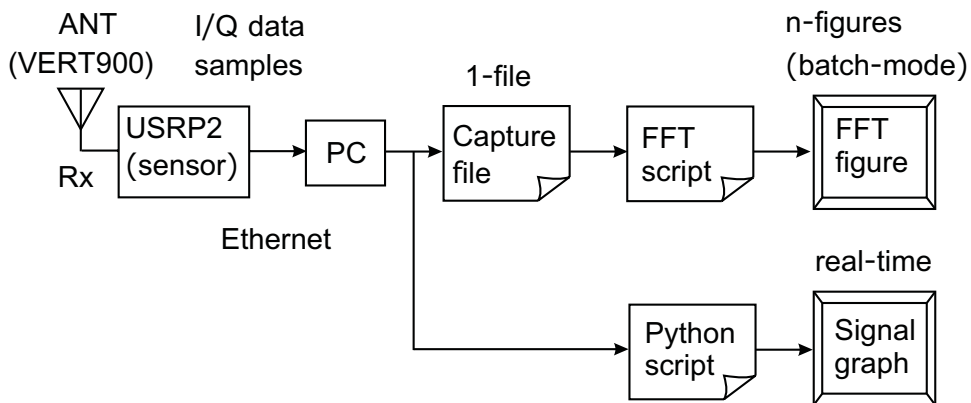


**Figure 3.15** – Schematic of the S1G spectral-time sensor, operating in the sub-1 GHz radio-band.

The USRP 2 has been used to sense the spectrum activities due to the higher sampling rate, compared to the USRP 1. Fig. 3.16 illustrates the USRP spectral-time sensor setup in the lab. It shows the USRP 2 RF front-end and the host PC, connected via Ethernet port.

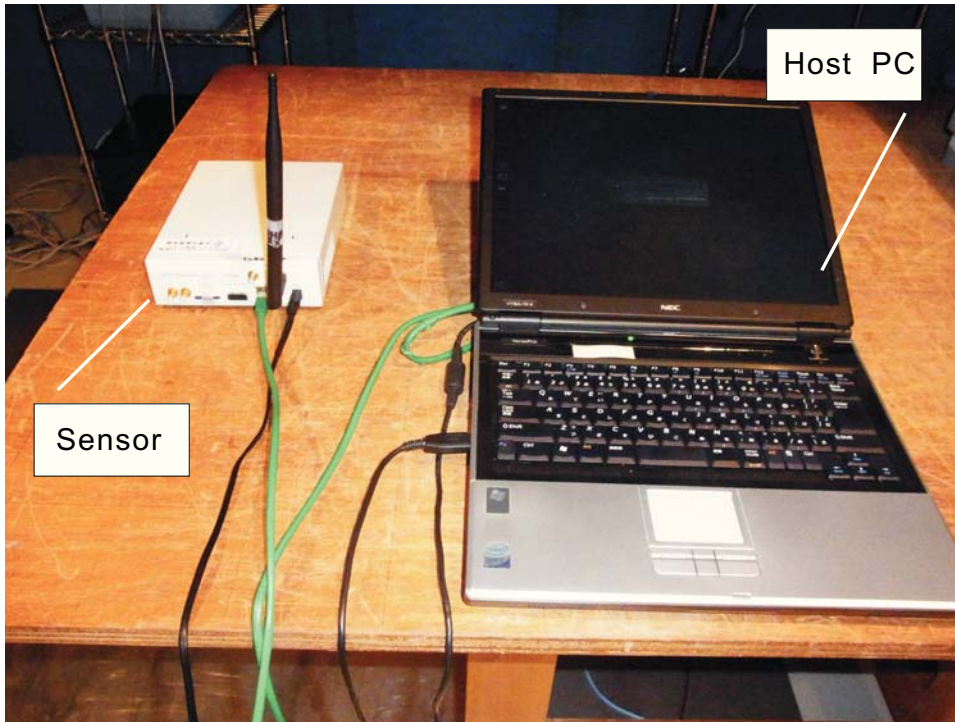


**Figure 3.16** – Photograph of the spectrum sensor configuration (USRP 2 and host PC).

### 3.5 Signal assessment

A single link S1G WLAN setup is used to obtain test signals and to record the transmission of WLAN data frames. Fig. 3.17 illustrates the 2-way communication setup. The setup consists of a sender side (Tx) and receiver side (Rx), which both use a host PC to run the software (Section 3.0.6) and two USRP 1 devices to transmit the wireless signal at  $f_c = 923$  MHz. RF-cables have been applied to connect the wireless interfaces of the two USRP 1 devices. In addition, an RF-splitter was used to redirect the signal to a spectrum analyzer. Simple ICMP messages (ping, 100 byte) were transmitted over the wireless link. The observed power density spectrum of the tested S1G prototype setup is shown in Fig. 3.18. It



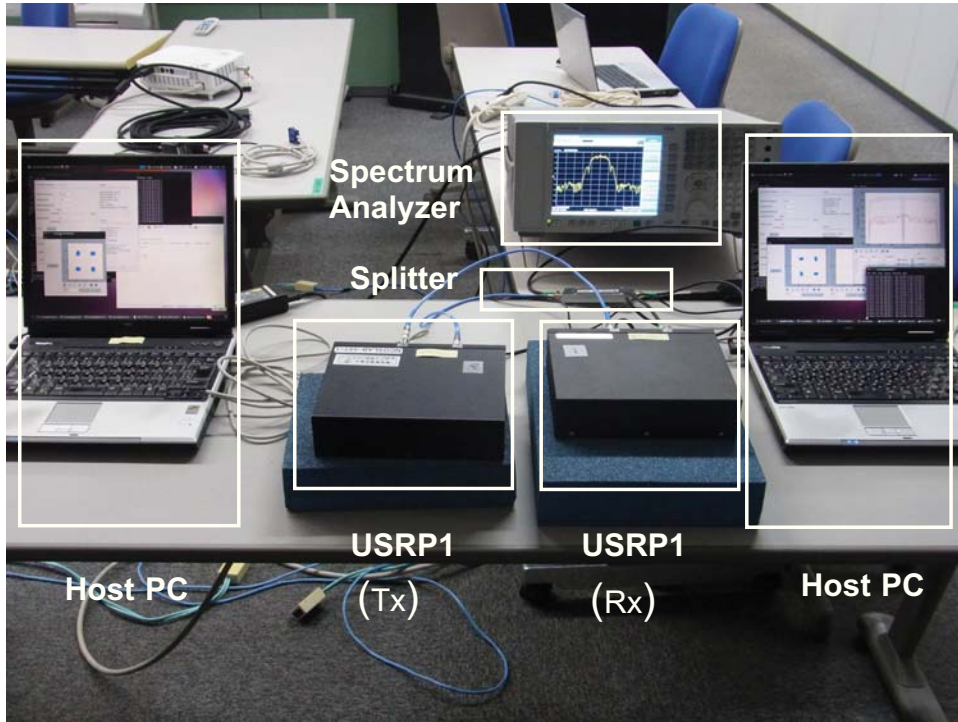


**Figure 3.17** – S1G WLAN prototype setup in the lab. The photograph shows the sender node (Tx) and the receiver node (Rx) and two USRP 1 devices [85].

can be clearly observed that the center of the signal is at  $f_c = 923$  MHz. Further, the observed signal bandwidth is  $BW = 1$  MHz. The received signal strength  $P_{rx}$  is 50 dB higher than the recorded noise floor. Symmetric side-lobes can be observed in the adjacent channel bands, which are caused by the non-optimal signal emission of the USRP 1. The recorded signal amplitude (real part) is presented in Fig. 3.19 over the monitored samples. It shows the *short training field* (STF) at the beginning of the signal, followed by the *long training field* (LTF) and the *signal field* (SIG). The signal continues with the payload (ICMP request message, 100 B). Next, the S1G WLAN signal was monitored in a free space environment. Again, the S1G spectrum sensor (Section 3.4.3) was used to monitor the spectrum activity. The monitored FFT signal is presented in Fig. 3.20. It shows the monitored FFT signal and the peak signal of the S1G WLAN prototype with  $f_c = 923$  MHz. A reduced signal level can be observed due to the free space loss of the received signal  $P_{rx}$ . The recorded S1G WLAN signal in Fig. 3.19 follows the PPDU frame format of the WLAN protocol, which is shown in Fig. 3.21. Next, images are presented that provide evidence of the measured S1G signals at  $f_c = 923$  MHz as part of a *visual*

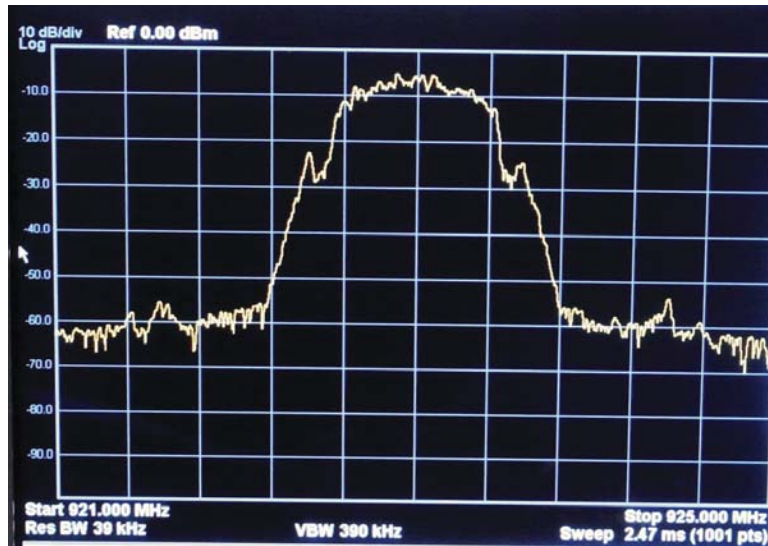


**Figure 3.18** – S1G power spectrum density screen shot at  $f_c = 923$  MHz. The figure shows the sensed power spectrum density of the prototype setup shown in Fig. 3.17.

*explanation* [86,87] of the measured signal quantities. The measurements have been conducted with the proposed S1G WLAN prototype [85]. The proposed spectral-time sensing enables the identification of *signal spillage* in the radio-band. This is beneficial to study wireless coexistence problems in detail (Chapter 6). Spectral-time observations are presented for two different MCS constellations, MCS 2 ( $N_{ss} = 1$ ) and MCS 2 ( $N_{ss} = 2$ ), each for ICMP and UDP traffic. Table 3.5 summarizes the relevant IEEE 802.11ah PHY parameters for 1 MHz. Table 3.6 summarizes the spectral-time sensing parameters. Fig. 3.22 illustrates the IEEE 802.11ah 1 MHz OFDM signal constellation with fixed pilot tones. Fig. 3.23 illustrates the IEEE 802.11ah 1 MHz OFDM signal constellation with traveled pilot tones.

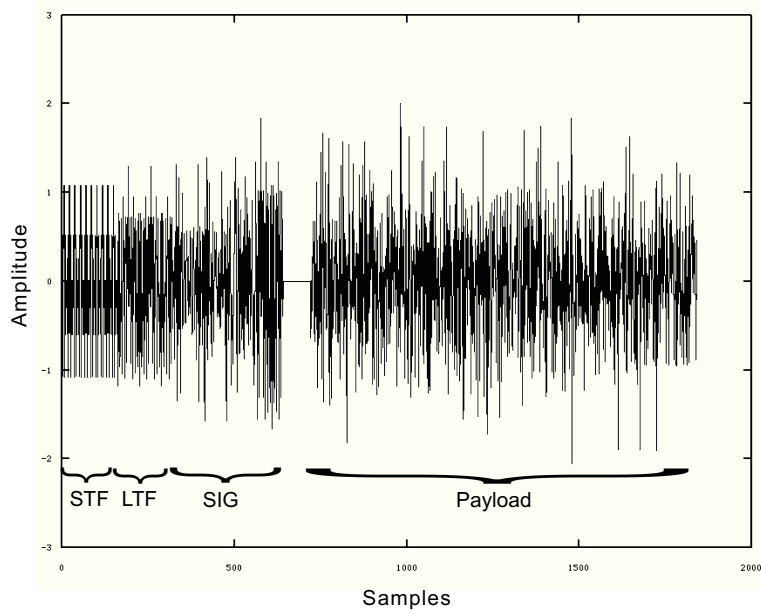


**Figure 3.19** – Real part of S1G WLAN prototype output signal. The illustration shows the STF, LTF, signal field, and payload.

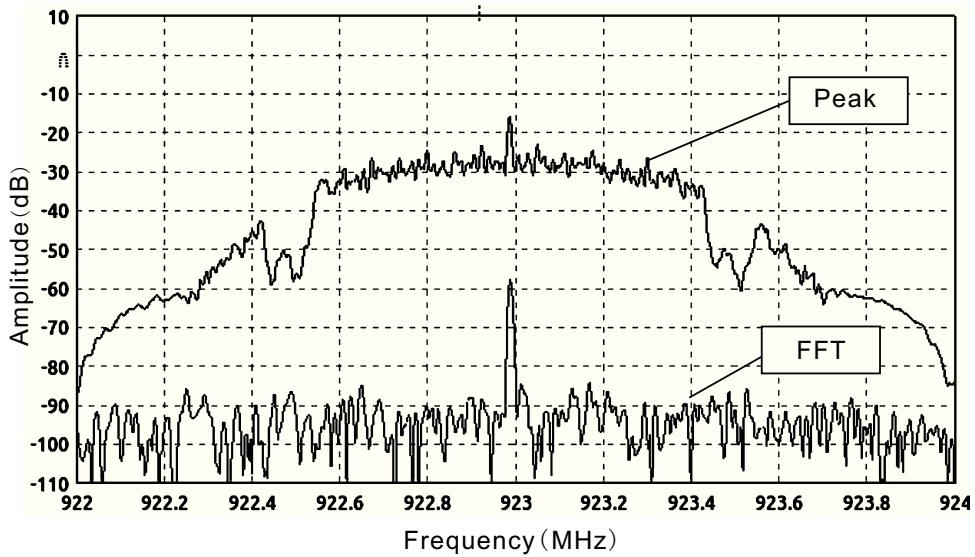
Parameter	Value
Bandwidth	1 MHz
OFDM symbol	40 $\mu$ s (long GI)
STF & LTF	4 $\times$ OFDM symbol = 160 $\mu$ s
Pilot tones (fix)	$k_{Pilot_{Fix}}^0; k_{Pilot_{Fix}}^1 = -7, 7$
Pilot tones (travel)	$k_{Pilot_{Travel}} = n \bmod N_{TP, BW}, N = TP, 1 MHz = 13$

**Table 3.5** – IEEE 802.11ah PHY parameters for 1 MHz operation.

Parameter	Value
Bin size	125 $\mu$ s
Sensing interval	5 MHz

**Table 3.6** – spectral-time sensing parameters.

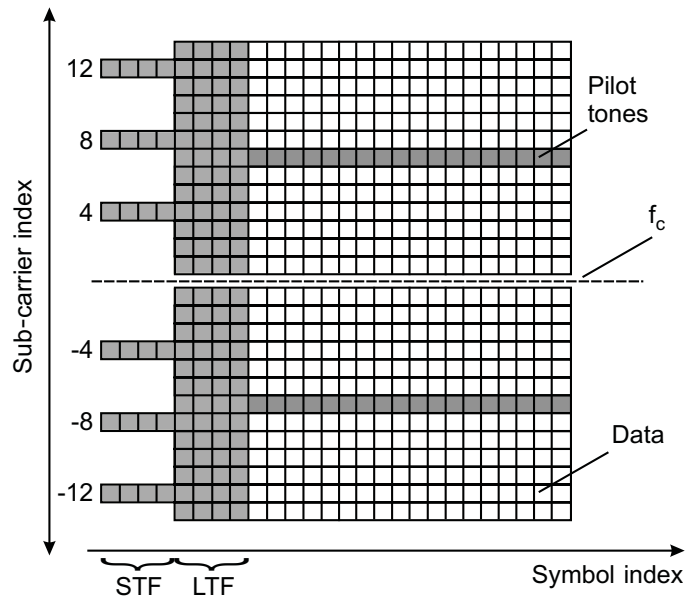




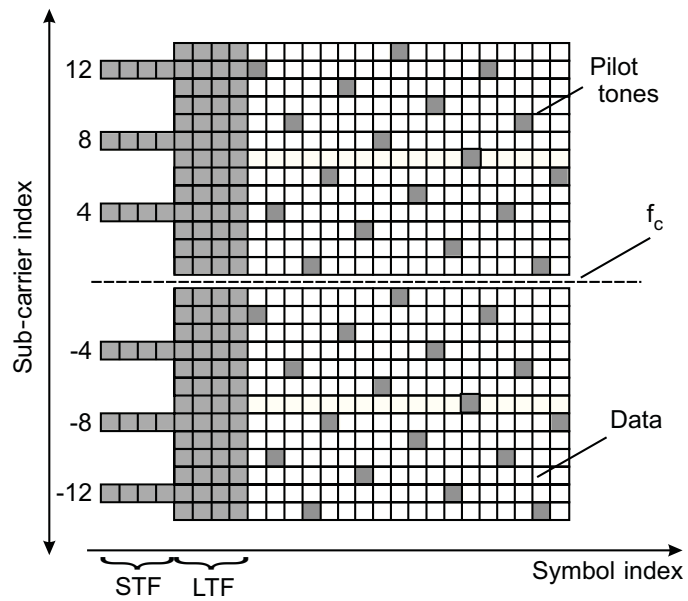
**Figure 3.20** – FFT signal of S1G WLAN prototype output signal, measured in free space,  $d = 1$  m measurement distance between sensor and signal source. The illustration shows the FFT signal and the peak signal,  $f_c = 923$  MHz,  $BW = 1$  MHz.

Preamble				Payload	
STF				LTF	
HT-SIG		LTF2		Meta	Data

**Figure 3.21** – Tx frame format of S1G WLAN prototype.

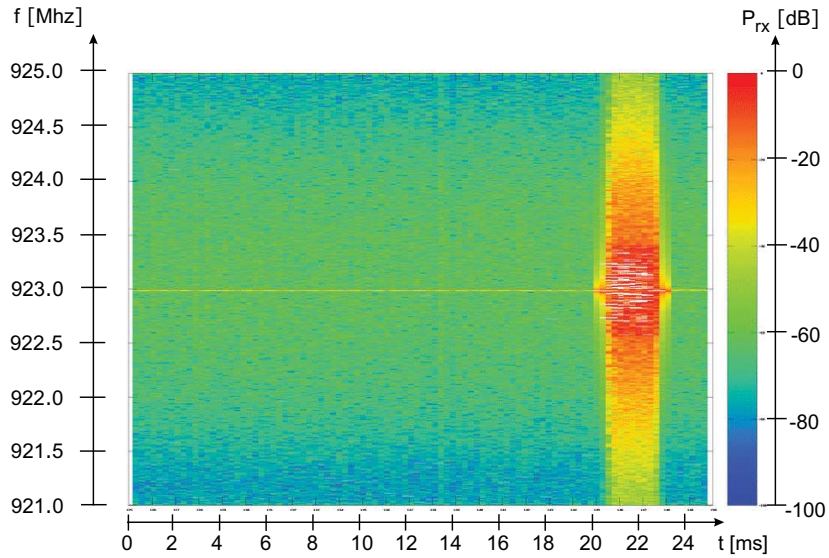


**Figure 3.22** – IEEE 802.11ah 1 MHz OFDM constellation (fixed pilots).



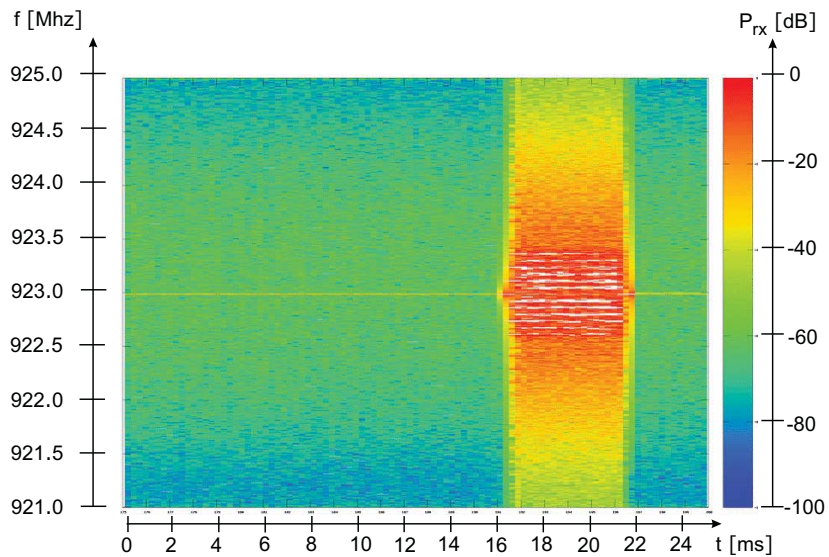
**Figure 3.23** – IEEE 802.11ah 1 MHz OFDM constellation (traveled pilots).

Fig. 3.24 shows the spectral-time observation of 100 B ICMP; MCS 2,  $N_{ss} = 1$ .



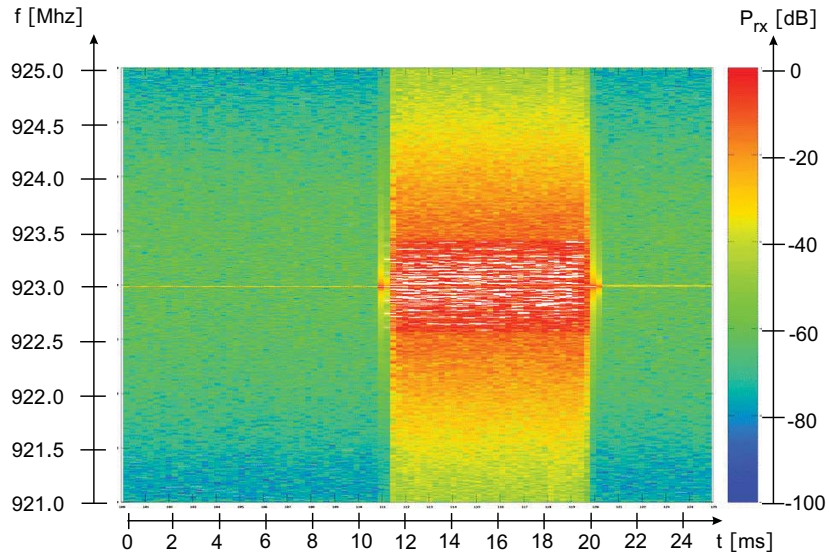
**Figure 3.24** – 100 B ICMP; MCS 2,  $N_{ss} = 1$ .

Fig. 3.25 shows the spectral-time observation of 400 B ICMP; MCS 2,  $N_{ss} = 1$ .



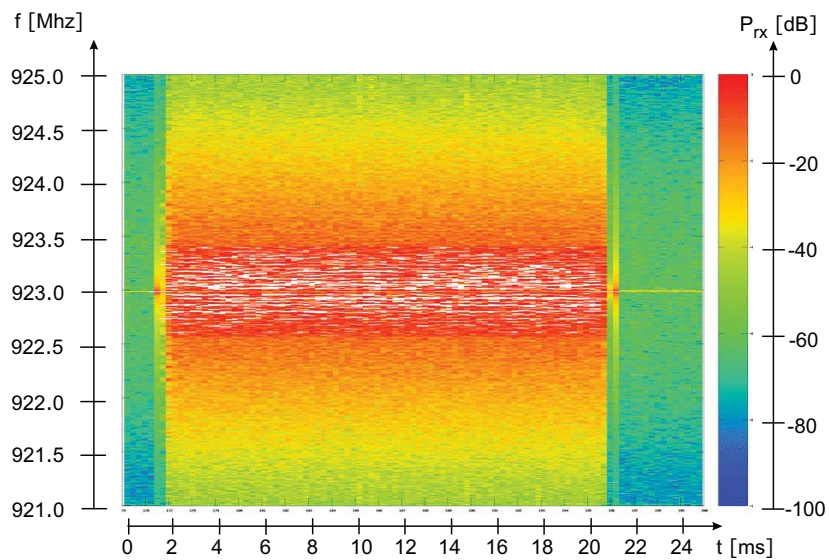
**Figure 3.25** – 400 B ICMP; MCS 2,  $N_{ss} = 1$ .

Fig. 3.26 shows the spectral-time observation of 800 B ICMP; MCS 2,  $N_{ss} = 1$ .



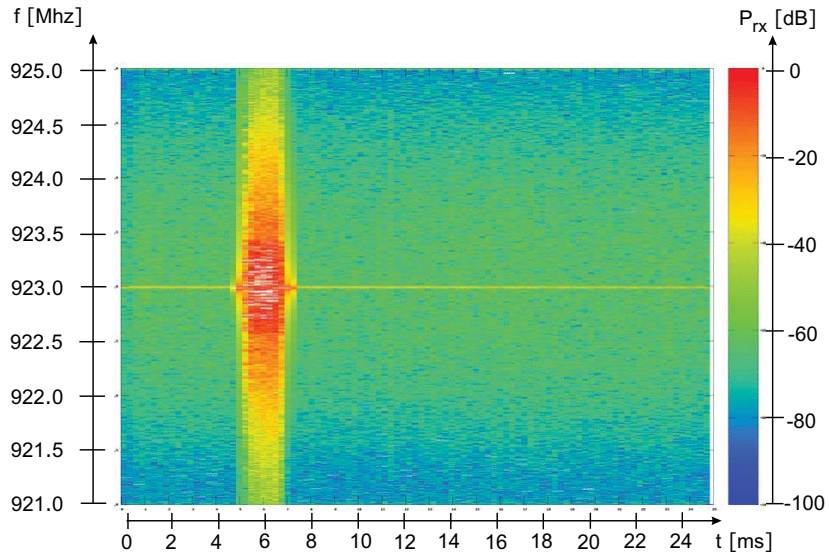
**Figure 3.26** – 800 B ICMP; MCS 2,  $N_{ss} = 1$ .

Fig. 3.27 shows the spectral-time observation of 1400 B ICMP; MCS 2,  $N_{ss} = 1$ .



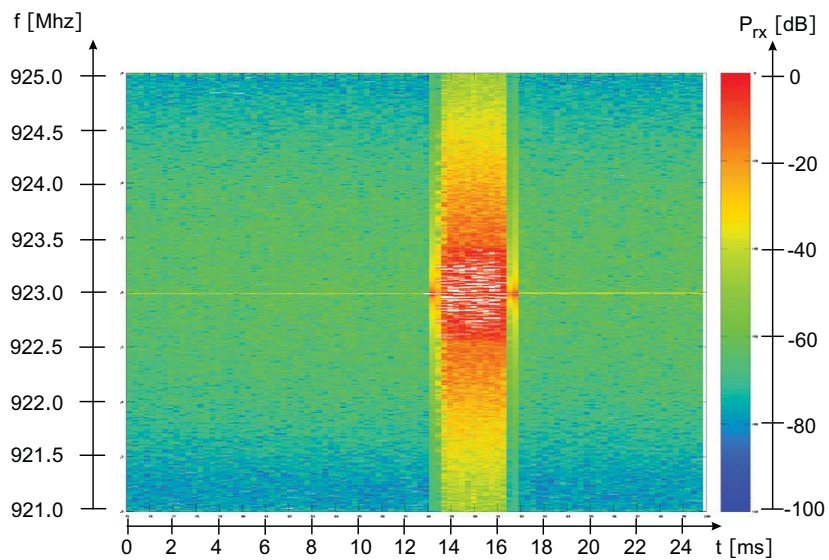
**Figure 3.27** – 1400 B ICMP; MCS 2,  $N_{ss} = 1$ .

Fig. 3.28 shows the spectral-time observation of 100 B ICMP; MCS 2,  $N_{ss} = 2$ .



**Figure 3.28** – 100 B ICMP; MCS 2,  $N_{ss} = 2$ .

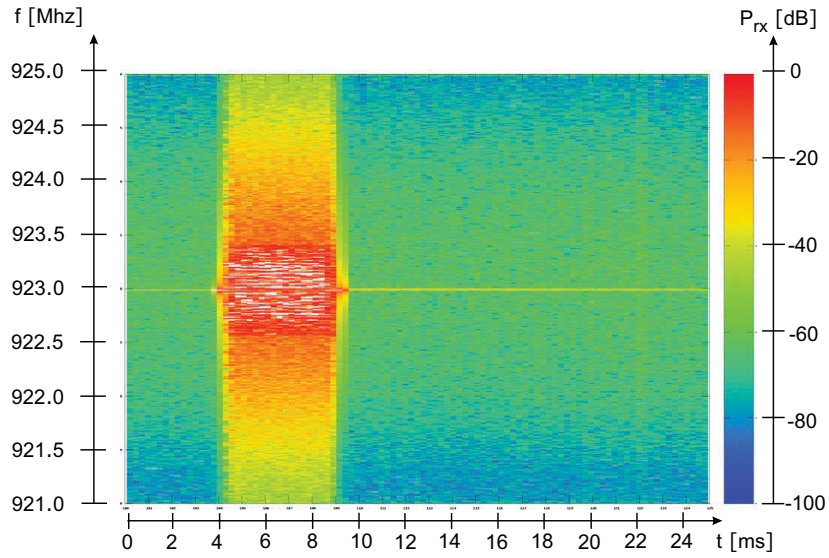
Fig. 3.29 shows the spectral-time observation of 400 B ICMP; MCS 2,  $N_{ss} = 2$ .



**Figure 3.29** – 400 B ICMP; MCS 2,  $N_{ss} = 2$ .

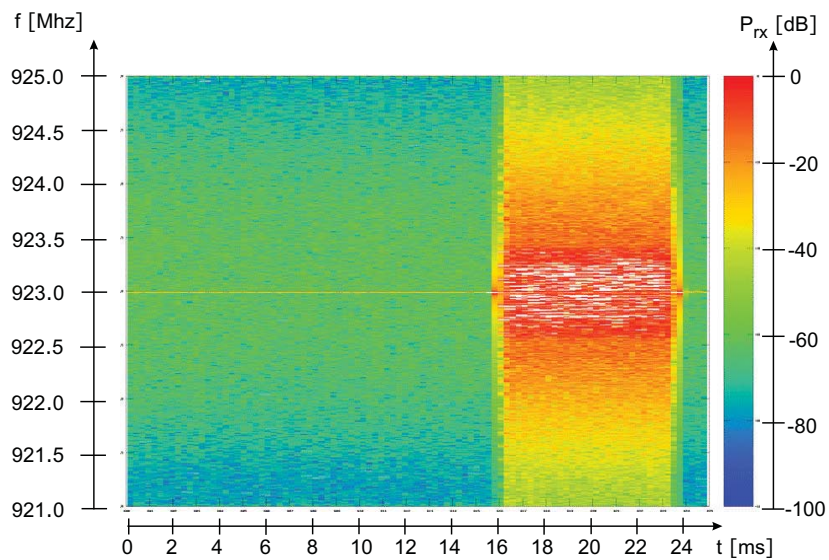


Fig. 3.30 shows the spectral-time observation of 800 B ICMP; MCS 2,  $N_{ss} = 2$ .



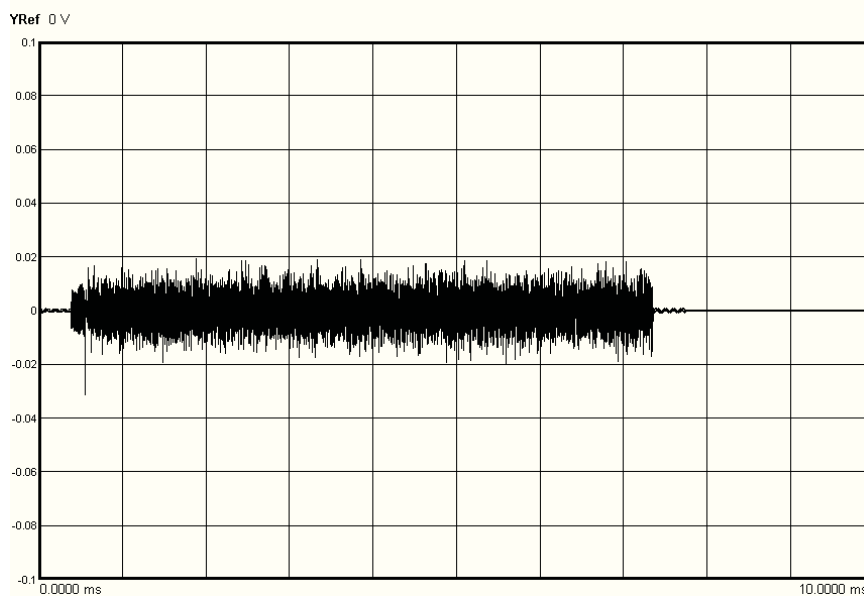
**Figure 3.30** – 800 B ICMP; MCS 2,  $N_{ss} = 2$ .

Fig. 3.31 shows the spectral-time observation of 1400 B ICMP; MCS 2,  $N_{ss} = 2$ .



**Figure 3.31** – 1400 B ICMP; MCS 2,  $N_{ss} = 2$ .

Fig. 3.32 shows the I/Q signal envelope observation (obtained with a spectrum analyzer) of 1400 byte ICMP data packet at MCS 2,  $N_{ss} = 2$  as a reference (same signal, same time duration).



**Figure 3.32** – I/Q signal envelope observation of 1400 byte ICMP data packet, MCS 2,  $N_{ss} = 2$ .

### 3.6 Bibliographical notes

Wireless prototypes have been widely proposed in the literature. These prototypes can be realized by designing a SDR-based system. SDR foundations and architectures are outlined in [88] and [89], which both give an overview on SDR fundamentals. However, both publications are missing the practical implementation (howto) on how to realize a SDR-based communication system. A first practical approach on SDR implementation can be found in [90], which includes computer simulations on cellular telecommunication systems and software radio communication systems. First practical use of SDR-based communication systems is discussed in [91]. It reports on various spectrum observations and spectrum utilization, including the 700-800 MHz radio-band in New Jersey, U.S. over an 18-hour period.

The use of multi-antenna MIMO systems are in the focus of numerous wireless research projects. A comprehensive overview of MIMO-OFDM related wireless prototypes and testbed setups is given in [31] and [34]. The result of the literature survey revealed significant research work regarding 2.4 GHz WLANs and LTE

systems at 1800 MHz. However, no significant work has been found for sub-1 GHz WLANs. Significant work on MIMO-OFDM in an open-source project was published by Mandke *et al.*, in [79] and [80].

The open source project *Hydra* provides a stable platform for WLAN protocols. In addition, USRP has been used for setting up wireless prototypes in some research projects, which is also supported by Hydra. By consequence, the combination of Hydra software and USRP hardware enables a cost-efficient up-to-date WLAN prototype development. The main difference between 2.4 GHz WLANs and WLANs at 900 MHz is the coverage range. In this thesis, wireless signal characteristics and transmission performance of sub-1 GHz WLANs are analyzed in these constrained areas, which has been unexplored in the literature.

Proposed solutions on a MAC reference architecture for IEEE 802.11n are proposed by Loeb *et al.*, in [92], with an enhancement resulting in an universal MAC architecture for homogeneous networks in [93]. The proposed MAC reference architecture is based on the *Click modular router* software that is also implemented in the IEEE 802.11ah prototype. Compared with *specification and description language* (SDL), unified modeling language (UML), and *GnuRadio*, the Click modular is most suitable for implementing an advanced MAC, considering the expressiveness, timing behavior and realization of state machines [94]. Run time overhead when using Click modular router was found to be moderate [94]. Graphical modeling aspects, which are helpful when modifying Click modular router modules are outlined in [94], which includes the representations of Click router elements.

Research on future MAC functions include full duplex wireless transmission [95] and self-interference cancellation in multi-antenna systems [96]. A Matlab<sup>TM</sup> IEEE 802.11ah reference code is given in [97]. Single I/Q output signals (Tx vectors) can be generated with the help of this reference code<sup>1</sup>. The waveform can be then further processed, e.g., to use it as an input signal for a waveform generator. The reference signal has exhibited helpful insight of the generated IEEE 802.11ah power spectrum density of 1 MHz and 2 MHz signals at 920 MHz using short and long preamble formats. Any interpretation ambiguity of the IEEE 802.11ah protocol amendment can be avoided and the spectrum compliance of the reference signal can be tested.

## 3.7 Discussion and summary

### 3.7.1 Discussions

One of the most relevant shortcoming of using an SDR-based S1G WLAN prototype is the limited system performance. It results in high delay for encoding and

---

<sup>1</sup>Note that the reference code does not provide any kind of IEEE 802.11ah Tx/Rx communication [97]; thus, a prototype is required to enable an over-the-air Tx/Rx communication based on the IEEE 802.11ah WLAN protocol.



decoding of wireless signals. It was observed that this delay - as result of the encoding/decoding SW module - was measured at 54 ms throughout all measurements and results in measured RTT, which is at 120 ms. The optimization of the RTT performance is out of the scope for this thesis. However, an optimized RTT would be beneficial, e.g., in outdoor long-range tests. The signal assessment has indicated significant side lobes of the emitted sub-1 GHz signal that was found to be caused by the characteristic of the USRP 1 RF performance.

The out-of-band (OOB) emissions cause interference to wireless systems that co-exist, e.g., RFID in adjacent channels. This is of importance because IEEE 801.11ah must coexist with short-range communication devices; thus, IEEE 802.11ah must not degrade the performance of other devices in near proximity. A careful control and sufficient suppression of OOB emissions is essential, similar to the problems of reconfigurable wireless systems such as IEEE 802.22 [68]. To mitigate the effects of OOB emissions practical filter approaches are beneficial to add to the modulation. OOB remedies include spectral subcarrier shaping and weighting, interference cancellation precoding schemes, and *elliptic* infinite impulse response (IIR) filter design to attenuate the OOB emissions [98]. The required suppression of OOB emissions which must follow the regulated signal power limitations are the real challenges for IEEE 802.11ah. A more granular power limitation, particularly in adjacent channels would be beneficial to avoid that IEEE 802.11ah becomes a *non-starter* in terms of commercial viability. A more flexible power limitation scheme would be needed, otherwise IEEE 802.11ah will end as a niche product.

Further improvement of the spectrum compliance should be in the scope for future work on sub-1 GHz WLANs. As a huge advantage, the SDR offers a large degree of flexibility. For instance, alternative frequencies can be easily applied, such as 433 MHz. Frequency agile systems, such as the proposed WLAN prototype, can be used to evaluate new modulation schemes. For instance, orthogonal frequency division multiple access (OFDMA) to utilize unused spectrum in the sub-1 GHz ISM radio-bands could be easily implemented to the proposed S1G WLAN prototype. However, wireless prototypes cannot reach the cutting-edge performance of chip-based Wi-Fi modules. In particular, the SDR-based IEEE 802.11ah WLAN prototype has shown throughput limitations, due to hardware/software bottlenecks. Thus, SDRs are beneficial to setup flexible wireless prototypes but they can rarely reach high throughput regimes.

### 3.7.2 Summary of the chapter

This chapter has outlined the fundamental design issues of the proposed IEEE 802.11ah WLAN prototype. The prototype has been implemented and realized as a 2-way wireless communication system that operates in the sub-1 GHz ISM-band. It utilizes advanced IEEE 802.11n features, including MIMO-OFDM modulation. An SDR-based WLAN has been created that consists of USRP 1, which allows the operation of two internal RF daughterboards, which enable a  $2 \times 2$  MIMO system. The challenges on designing the required software architecture were outlined. The

proposed software solution is a combination of GnuRadio and the software project Hydra. Software modifications have been outlined, which are required to enable a functional  $2 \times 2$  MIMO system that operates at  $f_c = 923$  MHz and  $BW = 1$  MHz.

It was found that more modifications on the PHY were required to enable an IEEE 802.11ah wireless communication over-the-air. Simple down-clocking does not provide the required information, e.g., how to scale OFDM parameters correctly, or how to define the OFDM data index parameters. These parameters need to be thoroughly provided by the IEEE 802.11ah WLAN protocol amendment.

Motivated by the aim to sense the spectrum activity in the sub-1 GHz radio-band, a novel S1G spectral-time sensor was proposed that operates at 900 MHz. The implemented S1G spectrum sensor allows accurate spectrum sensing of emitted wireless signals, e.g., from the S1G WLAN prototype. This enables a detailed packet collision assessment and the discussion of spectral coexistence characteristics in the 900 MHz radio-band.

Additionally, different test environments have been introduced to facilitate wireless tests with the *non-certified* S1G WLAN prototype. An anechoic chamber, a shielded tent, and a shielded room have been used for wireless tests and their advantages and disadvantages have been discussed.

Finally, the signal emission of the prototype has been evaluated. The signal characteristics have been presented including a discussion on the monitored power spectrum. It was observed that IEEE 802.11ah wireless signals are emitted at the correct frequency band at the desired carrier frequency. Further, spectral-time observations showed that the signal emission is indeed limited to 1 MHz channel bandwidth. A detailed observation of the power density spectrum relieved that minor sideband emissions need to be further mitigated, e.g., with appropriate filter settings. It can be concluded that the transmission of IEEE 802.11ah PHY/MAC frames was successfully accomplished, which comply with the IEEE 802.11ah protocol in major aspects.

In the following chapters the prototype is used for the test and assessment of S1G WLAN transmissions, including coverage enhancement, precoding improvement, MIMO transmissions and beamforming. Of particular interest is the coexistence among wireless personal area network devices operating at 900 MHz and the IEEE 802.11ah WLAN prototype.

## Chapter 4

# Coverage enhancement

The coverage boundaries and the coverage enhancement of a sub-1 GHz WLAN are examined in this chapter. The primary system characteristic of a narrow-band S1G WLAN is a significant increased outdoor coverage, compared to legacy indoor WLANs, such as IEEE 802.11b/g/n. In addition to an increased coverage, a single S1G WLAN AP must serve hundreds of remote STAs within a single S1G WLAN AP coverage range of  $r \leq 1$  km combined with a high transmission reliability. By consequence, S1G WLANs have to enable larger distances combined with a reduced signal outage probability, which would allow an efficient and robust one-hop reach topology over a large wireless distance.

Improving the wireless coverage of S1G WLANs is in the focus of this chapter. Fig. 4.1 illustrates the wireless coverage range of a single WLAN AP with several STAs within the wireless coverage area. One design constraint is that S1G WLANs have to support energy consumption reduction strategies, which do not allow the increase of sending power  $P_{tx}$  to increase the coverage. Hence, an alternative procedural method is required that would enable the increase of the link budget that minimizes the signal outage; thus, enhances the wireless coverage. In general, the improvements of a wireless system are either *reliability* oriented or *capacity* oriented. Improving the reliability of a wireless system is required when extended coverage is the primary goal. Outdoor wireless systems have to assure a minimum signal outage over a long distance  $d$  between AP and STA (Fig. 4.1).

This thesis proposes to improve existing multi-antenna diversity strategies to enable an increased received signal level at the receiver. Diversity strategies include spatial diversity (the use of multiple antennas) and code-diversity (precoding, beamforming) schemes. Diversity schemes, such as *selective transmission/selective combining* (ST/SC), *maximum ratio transmission/maximum ratio combining* (MRT/MRC), and *space time block codes* (STBC), allow raising the received wireless signal at the receiver by transmitting signal replicas [99].

In contrast, indoor wireless systems aim to provide high capacity links, e.g., to enable fast download applications. Hence, improving data rate is the primary goal

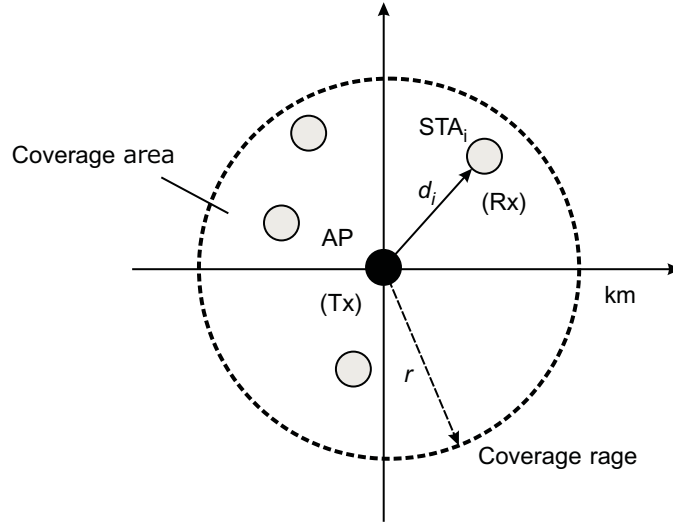


**Figure 4.1** – Illustration of wireless coverage range of WLAN AP.

of indoor WLANs, which can be achieved through multiplexing strategies<sup>1</sup>. The use of multiple-antennas allow two groups of operations, which are assigned in the PHY layer, which are:

1. *Transmit diversity*: Multiple antennas are used at the transceiver to explore spatial diversity, e.g., at the WLAN AP, to improve the downlink to the STA, e.g., increased coverage extension or robustness to mitigate instantaneous channel fading when the channel conditions are bad. Precoded data are sent to the receiver to reduce transmission errors. Data transmission reliability is the primary goal when using transmit diversity schemes, such as *precoding* or *beamforming*.
2. *Spatial multiplexing*: The objective of spatial multiplexing is to increase the data rate by utilizing multiple spatial streams while sending different data simultaneously. Large antenna spacing with low mutual antenna coupling is required to exploit the spatial diversity of uncorrelated wireless channels.

In this thesis, the increase of wireless coverage and transmission reliability of S1G WLANs is proposed by applying modified *precoding* schemes.

<sup>1</sup>Increasing the coherence bandwidth is the primary strategy, when higher data rates are required.

## 4.1 Precoding

In MIMO systems, closed-loop schemes<sup>1</sup> explore the downlink channel and then feedback the channel state information (CSI) back to the sender side, e.g., to optimize the *precoding*<sup>2</sup>. Fig. 4.2 illustrates a general linear precoder with bandwidth limited feedback channel and codebook selection.

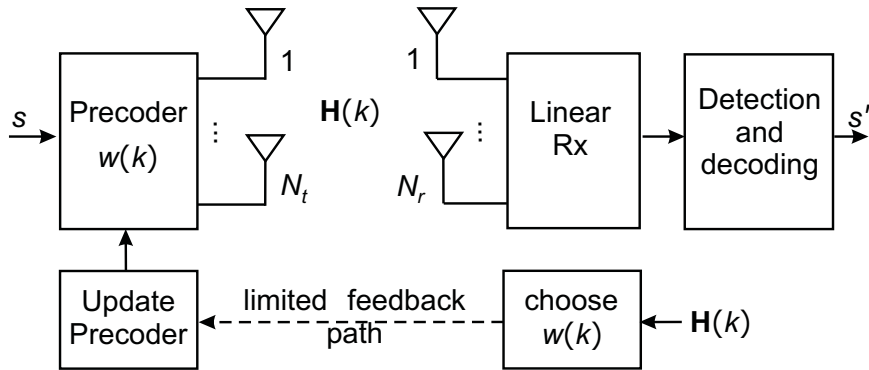


**Figure 4.2** – Illustration of a general linear precoder with limited feedback and codebook selection  $w(k) \in \mathbf{W}$ .

To further increase the transmission reliability, precoding schemes allow an optimized use of multi-antenna. Optimal precoding aims to maximize the received signal at the receiver side. To reduce the feedback overhead, codebook-based precoding is preferable, where only the code bits (index) corresponding to the codewords are sent as limited feedback to the sender. The performance loss of codebook-based precoding has been found as minimal compared to optimal precoding when transmit mode selection (SISO/MIMO) is applied [84]. In LTE systems, 3-bit precoding codebooks have been predefined when two transmit antennas are used [26].

Precoding<sup>3</sup> combined with limited feedback is widely used in MIMO communication systems. The precoding enables an increased signal strength at the receiver by emitting multiple data streams with different weighting factors at each antenna at the sender side. The received signal  $\mathbf{y}$  is given by

$$\mathbf{y} = \mathbf{H}\mathbf{W}\mathbf{s} + \mathbf{n}, \quad (4.1)$$

where  $\mathbf{W}$  is the precoding matrix,  $\mathbf{s}$  is the send data signal,  $\mathbf{n}$  is the channel noise vector, and  $\mathbf{H}$  is the complex Gaussian channel matrix  $N_t \times N_r$ . Further,  $\mathbf{H}$  can be separated as Kronecker spatial correlated Rician and Rayleigh channel, separated

<sup>1</sup>In open-loop systems different versions of a signal are transmitted on different spatial paths.

<sup>2</sup>Beamforming with large mutual antenna coupling is used in smart antennas (classical beamforming) [84].

<sup>3</sup>Precoding can be considered as a form of beamforming.

in line of sight (LOS) and non-line of sight (NLOS) components given by

$$\mathbf{H} = \sqrt{\frac{K}{1+K}} \mathbf{H}_{NLOS} + \sqrt{\frac{1}{1+K}} \mathbf{H}_{LOS}, \quad (4.2)$$

where  $\mathbf{H}_{NLOS}$  is given by [100]

$$\mathbf{H}_{NLOS} = [\mathbf{R}_{rx}]^{1/2} [\mathbf{H}_{iid}] [\mathbf{R}_{tx}]^{1/2}, \quad (4.3)$$

with  $\mathbf{R}_{rx}$  and  $\mathbf{R}_{tx}$  as the independent correlation matrices, the channel model factor  $K$ , and the random complex Gaussian variables with zero mean  $\mathbf{H}_{iid}$ . The precoding matrix  $\mathbf{W}$  is defined by the antenna constellation and is given by  $N_r \times N$  with  $M < \min(N_t, N_r)$ .

#### 4.1.1 Alamouti precoding

A simple *space time block coding* (STBC) is the *Alamouti* space time coding<sup>1</sup>. The matrix for encoding and transmitting sequence for two-branch antenna diversity scheme is given in Table 4.1.

**Table 4.1** – Alamouti transmission sequence [101].

	antenna 0	antenna 1
time $t$	$s_0$	$s_1$
time $t + T$	$-s_1$	$s_0^*$

For a  $2 \times 1$  antenna system, the combined signal, which is forwarded to the signal detector, e.g., the *maximum likelihood detector*, is given by

$$\begin{aligned} s_0 &= h_0^* r_0 + h_1 r_1^*, \\ s_1 &= h_1^* r_0 - h_0 r_1^*, \end{aligned} \quad (4.4)$$

where  $s_i$  is the transmit signal,  $h_i$  is the channel state, and  $r_i$  is the received signal.

For a  $2 \times 2$  antenna system, the combined signal is given by

$$\begin{aligned} s_0 &= h_0^* r_0 + h_1 r_1^* + h_2^* r_2 + h_3 r_3^*, \\ s_1 &= h_1^* r_0 - h_0 r_1^* + h_3^* r_2 - h_2 r_3^*. \end{aligned} \quad (4.5)$$

Fig. 4.3 illustrates the BER performance of  $2 \times 1$  and  $2 \times 2$  multi-antenna construction when the precoded Alamouti scheme was applied.

Next, the codeword generation and selection are described in detail.

<sup>1</sup>STBC for large antenna arrays require high computational power. However, this drawback diminishes with the continuing increase of CPU power in communication devices.

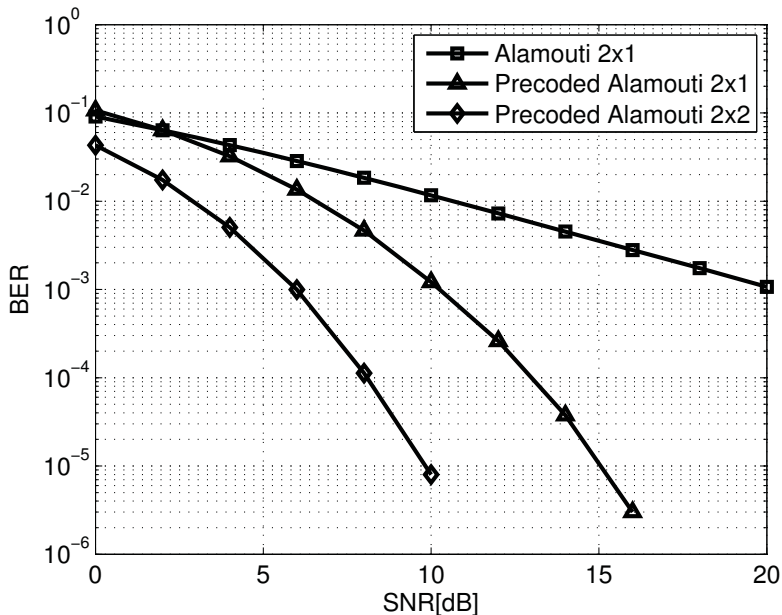


**Figure 4.3** – Comparison of precoding schemes for two and four antenna constellation, QPSK, 1000 packets, with the codebook from [102].

#### 4.1.2 Codeword generation

Precoding is a highly efficient solution when there is limited CSI information available at the sender, e.g., to minimize the feedback overhead. Precoding uses so called codebooks, which are pre-defined as a finite set. These codebook sets are kept in the memory storage of the sender and receiver. To optimize the precoding and to reduce the feedback overhead only codebook index information is exchanged between the sender and receiver instead of entire codebooks [103]. The elements in the codebook  $W_c$  are referred as *codewords*, such as

$$W_c^k = \{w_0^k, \dots, w_n^k\}. \quad (4.6)$$

To determine which codeword increases the link capacity of the current channel state, the transmitter selects the optimal codebook from the reported codebook constellation. The codeword selection is done by a selection algorithm which determines the optimal precoding by minimizing the chordal distance of  $w \in W_c$  for the input signal vector  $v$  given by

$$w = \underset{w \in W_c}{\operatorname{argmin}} d(v, \bar{w}) \quad (4.7)$$

Next, to minimize the mean squared error among selected codewords, the chordal distance  $d_c$  must be maximized. The selected codewords are applied by the sender to the transmitted signal increasing the robustness of the transmitted data over wireless channels. Under the assumption of limited feedback and minimum mean squared error criteria, the optimal precoder is designed by applying the *complex Grassmannian packaging* where the chordal distance between any two codewords  $\mathbf{W}_1$  and  $\mathbf{W}_2$  is maximized with [104]:

$$d_c(\mathbf{W}_1, \mathbf{W}_2) = \frac{1}{\sqrt{2}} \|\mathbf{W}_1 \mathbf{W}_1^* - \mathbf{W}_2 \mathbf{W}_2^*\|_W. \quad (4.8)$$

Fig. 4.4 illustrates the chordal distance of a Grassmannian manifold.

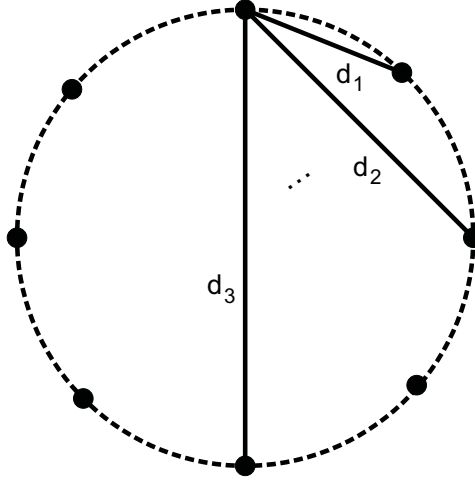


**Figure 4.4** – Illustration of the chordal distance  $d_c$  at different locations of an optimal quantization Grassmannian manifold  $G(m, n)$ .

The chordal distance between any two vectors  $\mathbf{u}$  and  $\mathbf{v}$  is approximated by

$$d_c(\mathbf{u}, \mathbf{v}) = \sqrt{1 - \frac{|\langle \mathbf{u}, \mathbf{v} \rangle|^2}{\|\mathbf{u}\|^2 \|\mathbf{v}\|^2}}, \quad (4.9)$$

with  $\langle \mathbf{u}, \mathbf{v} \rangle$  denotes the inner product and  $\|\mathbf{u}\|^2$  the Euclidean norm. Two linearly dependent vectors have the chordal distance zero, whereas two orthogonal vectors have the maximum chordal distance equal to 1. A codebook  $W^i$  is finite set of  $n$  vectors, called codewords  $w^n$  in which all the codewords maximize the minimum distance  $d$  between any two codewords in the entire vector set [103].



### 4.1.3 Codeword selection strategies

Precoding in MIMO systems requires pre-selected codewords which are optimized for robust wireless transmission over independent and identically distributed (iid) wireless channels. For instance, with the help of the *Grassmannian line packing* method, a maximum distance between any two codewords can be obtained [104]. In case of correlated channels, other codebook selections are more appropriate, e.g., which are optimized for short-range indoor communication. In outdoor locations, other codebooks are required, e.g., to provide robust communication over long-range wireless links. Such communication links suffer from channel dynamics with severe signal outages. By consequence, codebooks must be carefully selected and optimized for different communication environments and application scenarios.

Optimal error-correcting codes have a sequence set with a large chordal distance. Such codes are given by

$$\frac{2^{2m} - 2^m}{2}, \quad (4.10)$$

where the entire code length  $L$  is  $2^{2m}$  (with even index part). The *Gold* sequence, *Kasami* sequence, and *Kerdock* sequence are members of these error-correcting codes [105]. If the minimum distance is

$$2^{2m} - 2^m, \quad (4.11)$$

the entire code length  $L$  is  $2^{2m+1}$  (with odd index part); cf. [106].

## 4.2 Codebooks for coverage enhancement

Three different candidate codebooks have been evaluated to judge their precoding performance, the Grassmannian, the Kerdock and a modified Kerdock manifold. The modifications are proposed to achieve an increased wireless coverage range due to increase of the precoding gain, which is measured by an improved bit error performance (BER). The proposed S1G WLAN prototype utilizes the codewords, which are from a pre-defined codebook<sup>1</sup>.

The codewords are being used to describe the current channel state. It is efficient to transfer the codeword index instead of the entire codeword. Further, the prototype uses a *rotation* matrix [107, 108]. The limited feedback scheme is as follows:

1. At time  $\tau = 0$ , the precoder applies the SU-MIMO codeword  $w(k)$ .
2. For the following time instant  $\tau = 1, 2, \dots, T_{max}$ , the next codeword from the codebook  $W$  is chosen with  $w_\tau = w_i \cdot w_{\tau-1}$ , with  $w_i$  as an element of  $W$ .

---

<sup>1</sup>The IEEE 802.11ah draft reserves a 1-bit field for codebook information that can be selected to specify the codeword length [bit], for single user (SU) and  $N_c = 1$ , and for the quantized beamform angle feedback  $\Psi$  and  $\Phi$  [5].

The receiver reports the index of the precoding matrix  $w_i \in W$ . Sending the codeword index instead of the codeword is more bandwidth efficient.

3. To further increase the precoding efficiency, the precoder may use a codebook with rotating codewords  $w_r(k)$ .
4. At time instance  $T_{max} + 1$ , the precoding resets the codebook at  $\tau = 0$ .

### 4.2.1 Grassmannian codebook

In Section 4.1.3 it was argued that the Grassmannian manifold offers the optimal precoding for a multi-antenna system with i.i.d. channel model, in relation to maximize the distance among the codewords. However, there are two major drawbacks, which can be extracted from the Grassmannian manifold  $G(m, n)$  as follows:

1. The large number of codewords causes additional computational power overhead to the wireless system that is required to identify the codewords with the largest codeword distance.
2. The amount of feedback information that is considered when using Grassmannian manifolds is non-optimal, compared to the Kerdock manifold.

In this thesis, the Grassmannian manifold codebook is applied to the S1G WLAN prototype to evaluate the precoding performance of this codebook. The implemented codebook (2-bit) in the sub-1 GHz prototype is the Grassmannian and its codewords,  $\mathbf{w}_0^{gm}$   $\mathbf{w}_1^{gm}$ . The codewords  $\mathbf{w}_i^{gm}$  are given by [104, 106]

$$\begin{aligned} \mathbf{w}_0^{gm} &= \begin{bmatrix} -0.1612 - j0.7348 & -0.5135 - j0.4128 \\ -0.0787 - j0.3192 & -0.2506 + j0.9106 \end{bmatrix}, \\ \mathbf{w}_1^{gm} &= \begin{bmatrix} -0.2399 + j0.5985 & -0.7641 - j0.0212 \\ -0.9541 & 0.2996 \end{bmatrix}. \end{aligned} \quad (4.12)$$

### 4.2.2 Kerdock codebook

In [105] it is proposed to utilize *Kerdock Codes* for limited feedback precoded MIMO systems. Kerdock codebooks allow a simple codeword search with less requirements on the memory space [109]. The performance compared with Grassmannian is similar under Rayleigh channel conditions. If computational capabilities are reduced, the Kerdock codebook can be a powerful precoder in such systems. The advantages of the Kerdock manifold are:

1. Finite set of codewords that contains a reduced number of codewords that need to be stored in the wireless system, compared to the Grassmannian manifold.
2. Reduced amount of feedback information. With a reduced number of feedback information the same manifold as the Grassmannian can be offered.

For a  $2 \times 2$  transmit antenna system the Kerdock codeword  $\mathbf{w}_i^k$  constellation is given by

$$\mathbf{w}_0^k = \frac{1}{\sqrt{2}} \begin{bmatrix} 1 & 1 \\ 1 & -1 \end{bmatrix}, \mathbf{w}_1^k = \frac{1}{\sqrt{2}} \begin{bmatrix} 1 & 1 \\ j & -j \end{bmatrix}, \quad (4.13)$$

with the codebook basis  $\mathbf{w}_0$  and  $\mathbf{w}_1$ , with  $\mathbf{w}_0$  as the *scaled* Sylvester-Hadamard matrix [105]<sup>1</sup>.

### 4.2.3 Modified Kerdock codebook

The proposal is to combine the advantages of Grassmannian and Kerdock [106, 110]. A combination of large codeword distances such as the Grassmannian, and the efficient codeword set of the Kerdock manifold, lead to a modified Kerdock codebook. Two characteristics have been identified when combining Grassmannian and Kerdock. First, a significant increased BER performance can be observed. Second, the modified Kerdock requires a larger number of feedback information, similar to the Grassmannian. However, this drawback diminishes in communication systems, which already applied the Grassmannian manifold.

To increase the precoding performance, modifications on the Kerdock manifold are applied through experimental testing. The following modifications on the codewords  $\mathbf{w}_i^{km}$  have been identified to be most efficient in regard to increased BER performance:

$$\mathbf{w}_0^{km} = \frac{1}{\sqrt{2}} \begin{bmatrix} 1 & 1 \\ 1 & -1 \end{bmatrix}, \mathbf{w}_1^{km} = \frac{1}{\sqrt{2}} \begin{bmatrix} 1 & 1+j \\ 1+j & 1-j \end{bmatrix}. \quad (4.14)$$

Eq. 4.14 shows the codewords, which have been analyzed in a simulation study. Further, the modified Kerdock codebook has been applied to the sub-1 GHz prototype, in which the over-the-air transmission performance was evaluated.

## 4.3 Evaluation on precoding performance

Simulations on the codebook performance have been conducted for a  $2 \times 2$  Alamouti scheme (Section 4.1.1) and QAM modulation of the transmitted symbols. A slow fading, non-frequency selective channel model was applied to the simulation study. The symbols were transmitted under the assumption that the receiver has perfect knowledge of the channel state.

### 4.3.1 Grassmannian and Kerdock (simulation)

Fig. 4.5 illustrates the performance comparison between Grassmannian and proposed Kerdock precoding.

---

<sup>1</sup>The construction of the Kerdock codebooks for two and four transmit antenna constructions are presented in [105].

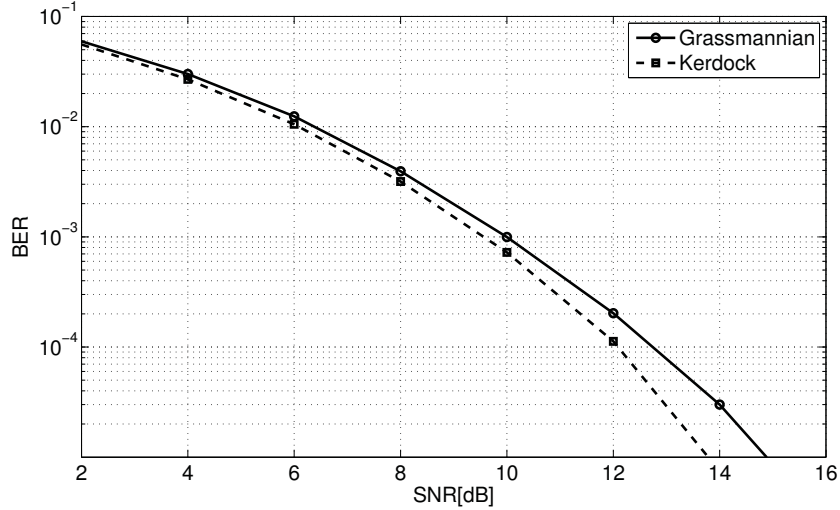


**Figure 4.5** – Illustration of performance comparison between Grassmannian (Eq. 4.12) and proposed Kerdock precoding (Eq. 4.13).

At  $\text{BER}=10^{-5}$  an increased gain ( $> 1$  dB) can be observed for Kerdock codebook with reduced computational overhead, compared to the Grassmannian codebook.

### 4.3.2 Modified Kerdock (simulation)

The BER performance results of the modified Kerdock codebook are illustrated in Fig. 4.6, Fig. 4.7, and Fig. 4.8, for different ICMP frame size, including 10 B, 100 B, and 1000 B frame size. The precoding performance of the modified Kerdock manifold is compared to the BER performance of the Grassmannian manifold.

When the Kerdock codebook is used, an increased gain ( $2 > \text{dB}$ ) can be observed in Fig.4.6 at error probability  $10^{-5}$  and for 10 B packet size. The precoding gain is significantly higher compared to the unmodified Kerdock manifold. A similar increased gain ( $> 2$  dB) can be observed in Fig.4.7 for an error probability of  $10^{-5}$  and an increased packet size of 100 B. The coding gain of the modified Kerdock manifold remains high even for larger frame sizes. Due to the larger packet size, an increased BER can be observed ( $> 2$  dB) compared to Fig. 4.6.

In Fig.4.8 an error probability  $10^{-5}$  and packet size 1000 B, a significant increased gain ( $> 4$  dB) over Grassmannian codebook can be observed when the modified Kerdock codebook is applied to the precoder. An increased of the precoding gain can be observed for larger packet lengths. Similar to the observations in Fig. 4.7, an increased BER can be observed ( $> 2$  dB) due to the increased packet size.

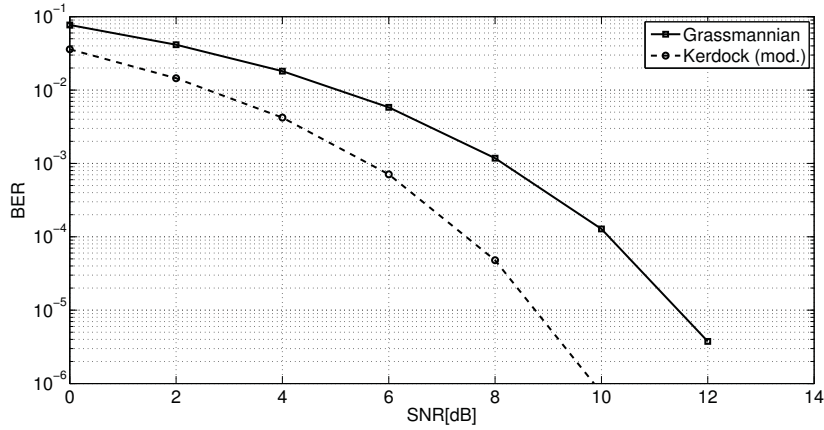


**Figure 4.6** – Precoding performance comparison of Grassmannian (Eq. 4.12) and modified Kerdock precoding (Eq. 4.14). Frame size = 10 B, ( $10^5$  simulated packets).

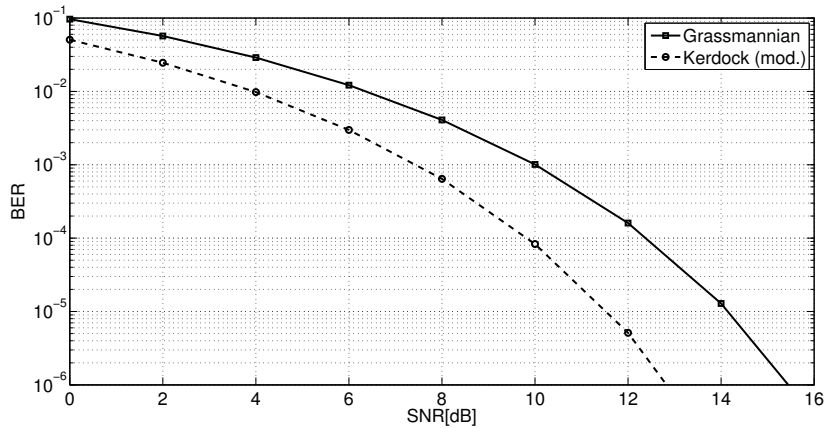


**Figure 4.7** – Precoding performance comparison of Grassmannian (Eq. 4.12) and modified Kerdock precoding (Eq. 4.14). Frame size = 100 B, ( $10^5$  simulated packets).

The observation is that the modified Kerdock manifold achieves additional precoding gain in the regime of 2 to 4 dB. Further, the precoding gain of the modified Kerdock manifold enables an improved BER performance for large data frames. However, due to the Kerdock codebook modifications, the modified codewords result in an increase of feedback information, which as been found as an identical amount

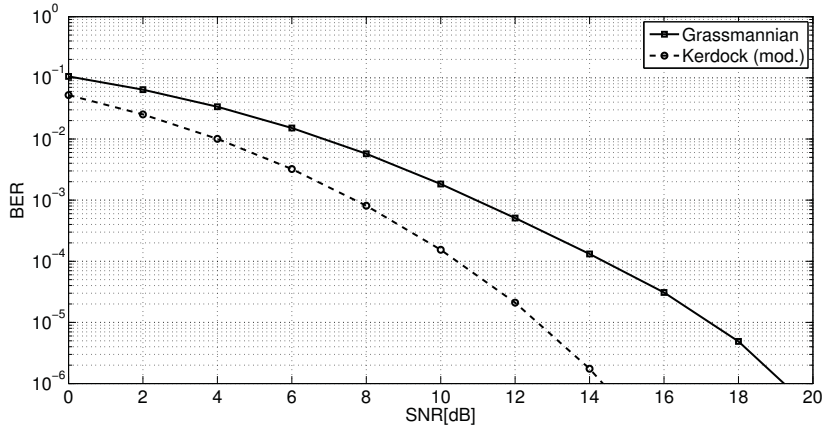


**Figure 4.8** – Precoding performance comparison of Grassmannian (Eq. 4.12) and modified Kerdock precoding (Eq. 4.14). frame size = 1000 B, ( $10^5$  simulated packets).

of feedback information as for the Grassmannian manifold. It can be concluded that the modified Kerdock manifold is highly efficient in utilizing the additional channel state information. The characteristics of the feedback information will be discussed in Section 4.4.

### 4.3.3 Experimental evaluation of modified codebooks

To conclude the 2-bit precoding performance evaluation, when using the proposed codebooks in Section 4.2, the precoding performance is measured, without loss of generality, by transmitting a single ICMP flow. The ICMP flow is a data flow that was configured with 100 B packet frame size, LOS, 1 m Tx-Rx distance,  $f_c = 923$  MHz, sending interval=0.3, MCS=2, beamform on, measurement located in a shielded tent.

The results of the precoding performance measurement that identifies the wireless transmission delay of the Grassmannian, Kerdock, and the modified Kerdock precoding are illustrated in Fig. 4.9. Each codebook has a different impact on the transceiver precoding performance that results in different transmission delay. It can be observed from Fig. 4.9 that the Grassmannian manifold causes an average delay that was measured at 142 ms, with a standard deviation of 32 ms. The Kerdock manifold causes a reduced average delay, which was measured at 138 ms and an reduced standard deviation of 26 ms. The modified Kerdock manifold causes a further decreased average delay, which was measured at 134 ms and an reduced standard deviation of 21 ms. The reduction of transmission delay allows a higher

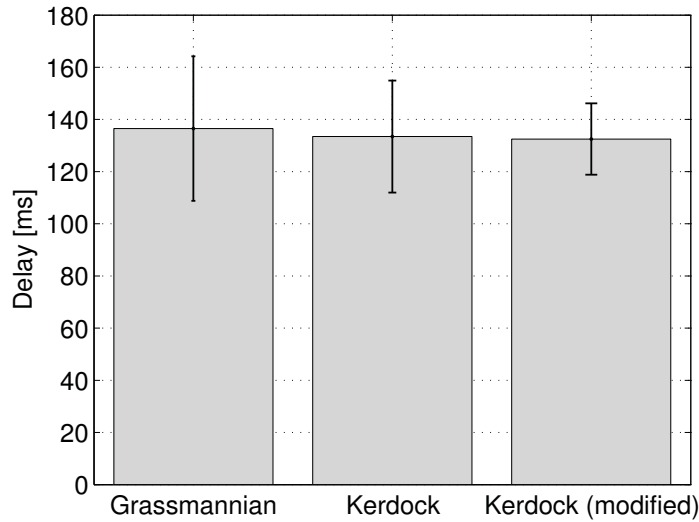


**Figure 4.9** – Illustration of measured delay performance comparison between Grassmannian, Kerdock, and modified Kerdock codebook. Frame size = 100 B ( $10^3$  ICMP packets sent).

data rate due to the increased system performance when the Kerdock and modified Kerdock manifold was applied to the precoder.

Next, the results of the measured SNR are shown in Fig. 4.10, when the Grassmannian, Kerdock, and the modified Kerdock manifold are applied to the S1G WLAN precoder.

The measured average SNR at the receiver side was at 21 dB when the Grassmannian manifold was applied with a standard deviation of 1.5 dB. When the Kerdock manifold was applied the measured average SNR was at 25 dB with a standard deviation of 10 dB. This is a significant increase of average SNR of 4 dB. In addition, the increase of the standard deviation also identifies higher SNR gains, which are up to 37 dB. The measured average SNR of the modified Kerdock manifold was at 26 dB and a standard deviation of 11 dB. The modified Kerdock manifold adds to the precoding gain, while the delay is reduced (Fig. 4.9). The increase of SNR significantly adds to the increase of the wireless coverage.

Then, the results of the average noise variance are shown in Fig. 4.11 when the Grassmannian, Kerdock, and the modified Kerdock manifold are applied to the precoder.

The average noise variance was at 36 dB with 12 dB standard deviation when the Grassmannian manifold was applied to the precoder. The average noise variance was at 32 dB with 17 dB standard deviation when the Kerdock manifold was

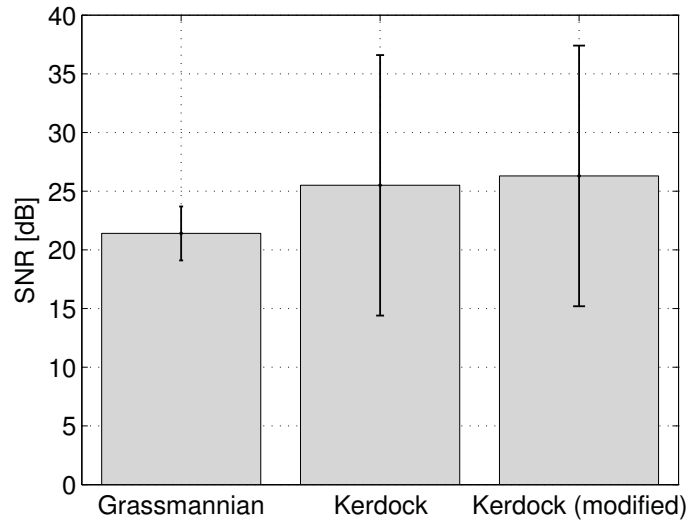


**Figure 4.10** – Illustration of measured SNR performance comparison between Grassmannian, Kerdock, and modified Kerdock codebook. Frame size = 100 B ( $10^3$  ICMP packets sent).

applied. The average noise variance was at 33 dB and 18 dB standard deviation when the modified Kerdock manifold was applied. It can be concluded that the Kerdock manifold and the modified Kerdock manifold significantly reduce the noise variance, which was measured at 4 dB. The modified Kerdock codebook increases the SNR performance at 4 dB compared to the Grassmannian manifold while reducing the average delay at 6 ms and noise variance at 4 dB. It can be concluded that performance gains are possible when modifying precoding schemes combined with improved system performance (delay, noise variance).

Finally, the modulation performance of Grassmannian precoding is shown in Fig. 4.12(a) and for modified Kerdock precoding in fig. 4.12(b). It can be observed that the received QPSK symbols have much lower variance when the modified Kerdock manifold is applied to the precoder compared to the Grassmannian manifold. A lower variance results in higher precoding gains of the transmitted symbols.

#### 4.4 Precoding performance evaluation of rotating codebooks

The S1G WLAN prototype precoder uses rotating codebooks in which codewords are executed in a pre-defined sequential order. A rotating codebook reduces the



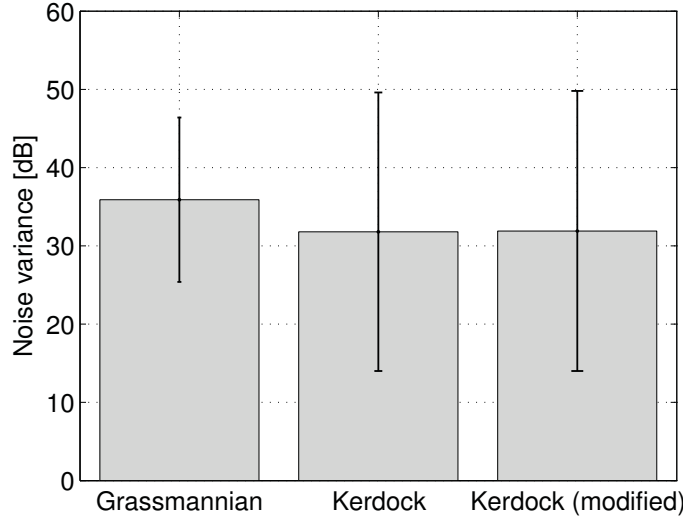
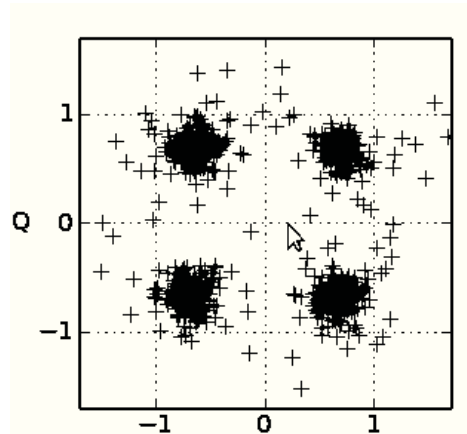


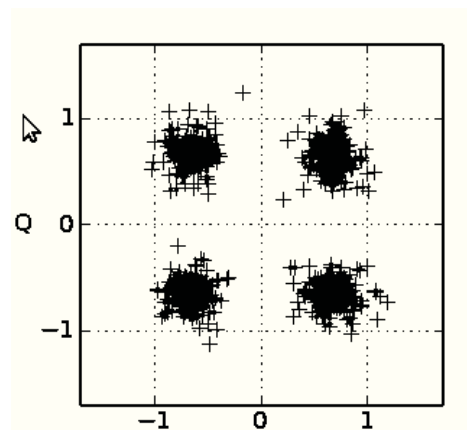
**Figure 4.11** – Illustration of measured noise variance comparison between Grassmannian, Kerdock, and modified Kerdock codebook. Frame size = 100 B ( $10^3$  ICMP packets sent).

signal overhead due to the a-priori knowledge of the cyclic codebook set. The codeword index, sent by the receiver to the transmitter as feedback information about the channel state, identifies the codeword at the sender side, which will be selected for data signal precoding. In the case of a  $2 \times 2$  MIMO setting, the S1G WLAN prototype utilizes four channel state parameter according to the channel matrix,  $h_{11}$ ,  $h_{12}$ ,  $h_{21}$ , and  $h_{22}$ . When the Grassmannian manifold is applied, the precoder utilizes all four channel matrix parameter.

In the case of a  $2 \times 2$  MIMO setting with Kerdock precoding, four channel state parameter are utilized, in which two parameters,  $h_{11}$  and  $h_{22}$ , contain the same channel information as  $h_{12}$  and  $h_{21}$ . Thus, the channel state is reported in a reduced channel state set, which improves the precoding process. In the case of a  $2 \times 2$  MIMO setting and modified Kerdock precoding, four channel state parameter are utilized,  $h_{11}$ ,  $h_{12}$ ,  $h_{21}$ , and  $h_{22}$ . The following figures illustrate the precoding performance of the sub-1 GHz prototype. Fig. 4.13 illustrates the measured rotation of the *perturbed* H-matrix at antenna distance  $d = 5$  cm and 200 B. The figure shows the four channel state parameter,  $h_{11}$ ,  $h_{12}$ ,  $h_{21}$ , and  $h_{22}$ . The figure also illustrates the monitored wireless channel dynamics, which occur as *perturbations* in all four channel state parameters.



(a) Original codebook (Grassmannian).

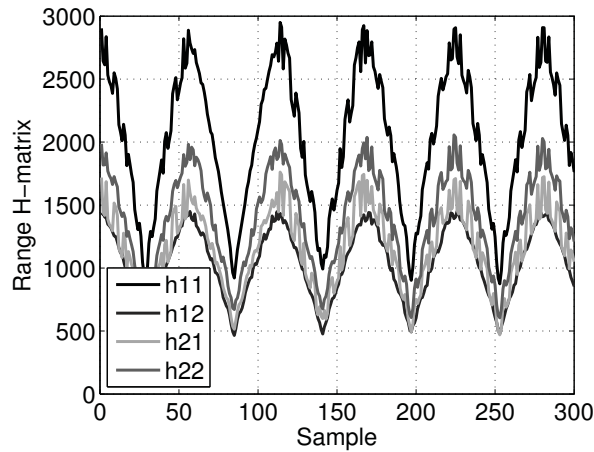


(b) Modified codebook (Kerdock).

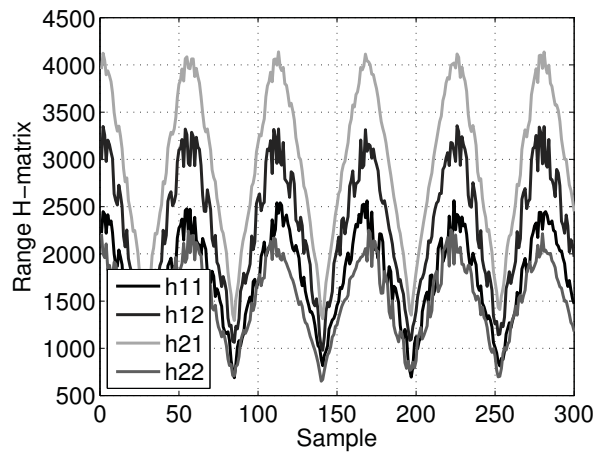
**Figure 4.12** – Comparison of QPSK I/Q scatter plot of Grassmannian and modified Kerdock manifold.

Next, the rotation matrix was monitored for an increased data frame size. Fig. 4.14 illustrates the rotation of the perturbed H-matrix at antenna distance  $d = 5$  cm and 400 B.

Then, the rotation matrix was monitored for an increased antenna distance. Fig. 4.15 illustrates the rotation of the perturbed H-matrix at antenna distance  $d = 20$  cm and 200 B.



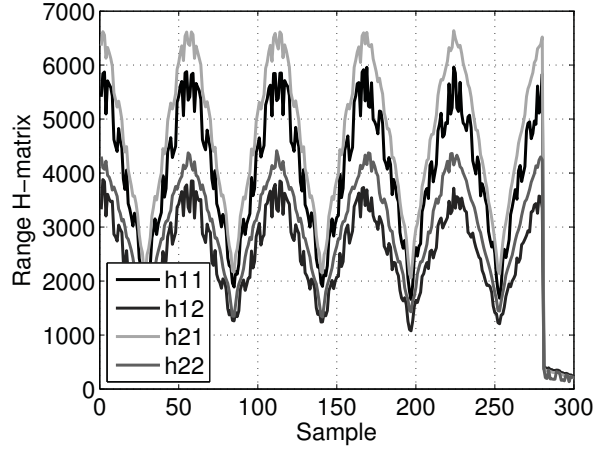
**Figure 4.13** – Rotation of the perturbed H-matrix at antenna distance  $d = 5$  cm and 200 B.



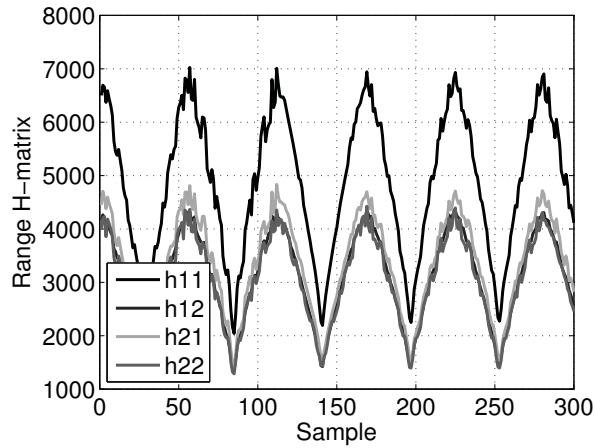
**Figure 4.14** – Rotation of the perturbed H-matrix at antenna distance  $d = 5$  cm and 400 B.

Next, the rotation matrix was monitored for an increased antenna distance and an increased data frame size. Fig. 4.16 illustrates the rotation of the perturbed H-matrix at antenna distance  $d = 20$  cm and 400 B.

To obtain the transmission performance of the the Kerdock manifold, the rotation matrix information was monitored for different signal attenuation settings to emulate variable communication distances. Fig. 4.17 illustrates the rotation of the



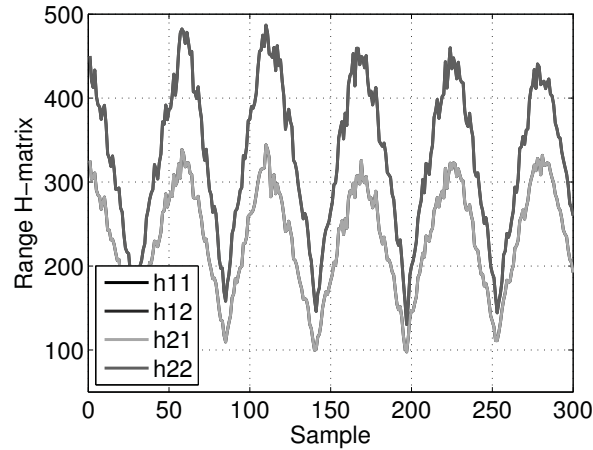
**Figure 4.15** – Rotation of the perturbed H-matrix at antenna distance  $d = 20$  cm and 200 B.



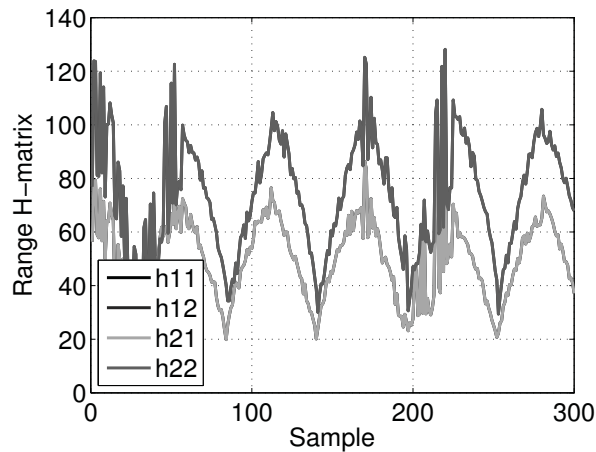
**Figure 4.16** – Rotation of the perturbed H-matrix at antenna distance  $d = 20$  cm and 400 B.

perturbed H-matrix at antenna distance  $d = 5$  cm and 400 B, 20 dB attenuation, at the sender side.

Next, the rotation matrix was analyzed for the Kerdock manifold for increased attenuation settings. Fig. 4.18 illustrates the rotation of the perturbed H-matrix at antenna distance  $d = 5$  cm and 400 B when 30 dB attenuation was applied at the sender side.

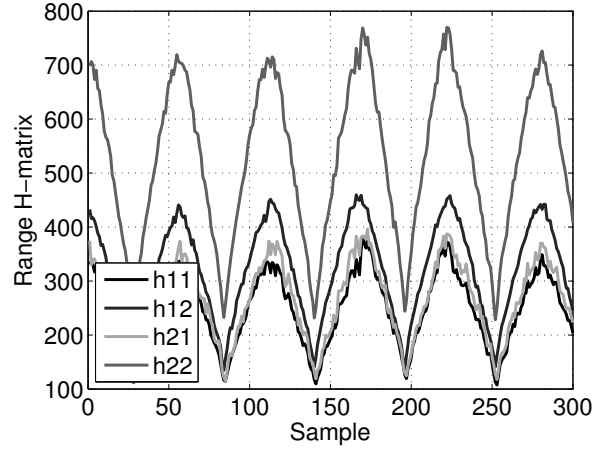


**Figure 4.17** – Rotation of the perturbed H-matrix using Kerdock precoder at antenna distance  $d = 5$  cm and 400 B, 20 dB attenuation, at the sender side.



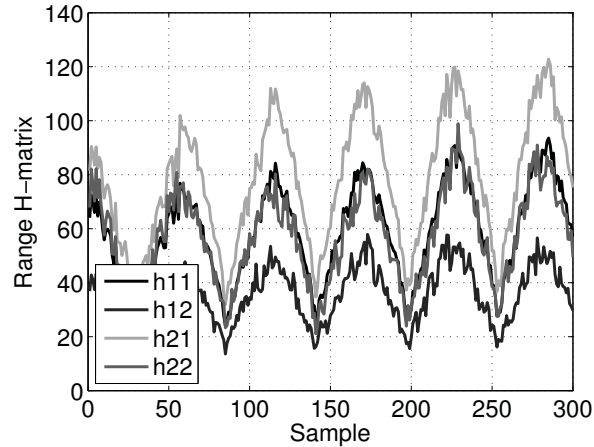
**Figure 4.18** – Rotation of the perturbed H-matrix using Kerdock precoder at antenna distance  $d = 5$  cm and 400 B, 30 dB attenuation, at the sender side.

Fig. 4.19 illustrates the rotation of the perturbed H-matrix at antenna distance  $d = 5$  cm and 400 B, when 20 dB attenuation was applied at the sender side for the modified Kerdock precoder.



**Figure 4.19** – Rotation of the perturbed H-matrix using modified Kerdock precoder at antenna distance  $d = 5$  cm and 400 B, 20 dB attenuation, at the sender side.

Next, the rotation matrix was monitored for the modified Kerdock manifold at higher signal attenuation. Fig. 4.20 illustrates the rotation of the perturbed H-matrix at antenna distance  $d = 5$  cm and 400 B, 30 dB attenuation at the sender side.



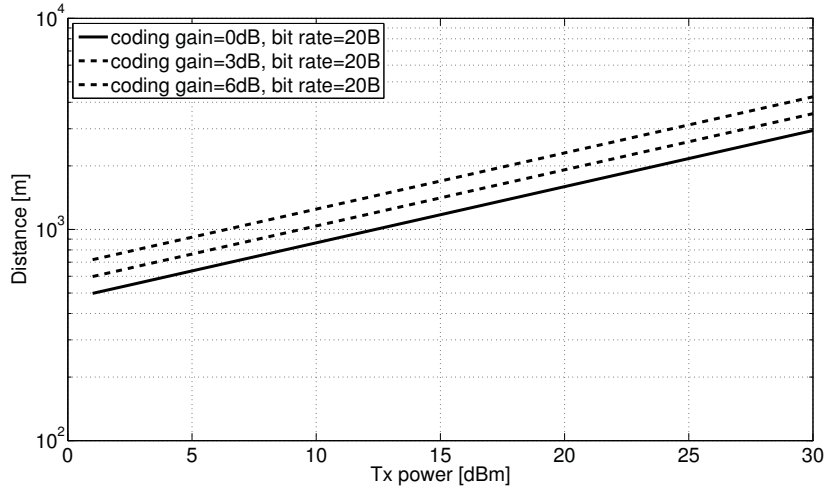
**Figure 4.20** – Rotation of the perturbed H-matrix using modified Kerdock precoder at antenna distance  $d = 5$  cm and 400 B, 30 dB attenuation, at the sender side.

Finally, statements on the coverage improvement are given. From the calculation of the link budget (LB) the coverage improvement can be estimated.

$$LB(dB) = P_{tx} + G_a + G_c - (n_v + n_f + \frac{Eb}{N_o} + l_i + l_f + 10 * \log_{10}(r_{bit} \cdot 1000)) \quad (4.15)$$

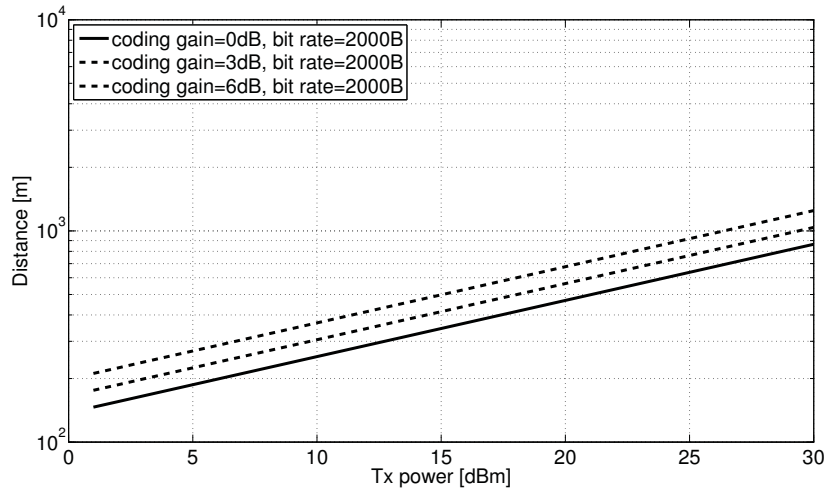
were  $P_{tx}$  is the sending power (0 to 30 dBm), antenna gain  $G_a$  (3 dB), coding gain  $G_c$  (0, 3, 6 dB), noise variance  $n_v$  (3 dB), noise figure  $n_f$  (8 dB), implementation loss  $l_i$  (1 dB), fading loss  $l_f$  (8 dB), and bit rate  $r_{bit}$  (20 B, 2000 B).

Fig. 4.21 illustrates the simulation results on tx power vs. distance (Tx-Rx) for different coding gains (0, 3, 6 dB) and bit rate = 20 B. Next, Fig. 4.22 illustrates the



**Figure 4.21** – Tx power vs. distance for different coding gains and bit rate (20 B).

simulation results on tx power vs. distance (Tx-Rx) for different coding gains (0, 3, 6 dB) and bit rate = 2000 B. Fig. 4.23 concludes the evaluation and illustrates the important relation of coverage range and number of wireless stations. In particular, by increasing the coverage range (e.g., higher precoding gain as proposed in this thesis) more wireless stations are within one-hop coverage of an S1G WLAN AP. This effect significantly minimizes the installation costs of a wireless infrastructure, because a reduced number of S1G WLAN APs would be needed. However, new challenges appear due to the *massive access* in high-density WLANs as described later in Section 7.1.



**Figure 4.22** – Tx power vs. distance for different coding gains and bit rate (2000 B).

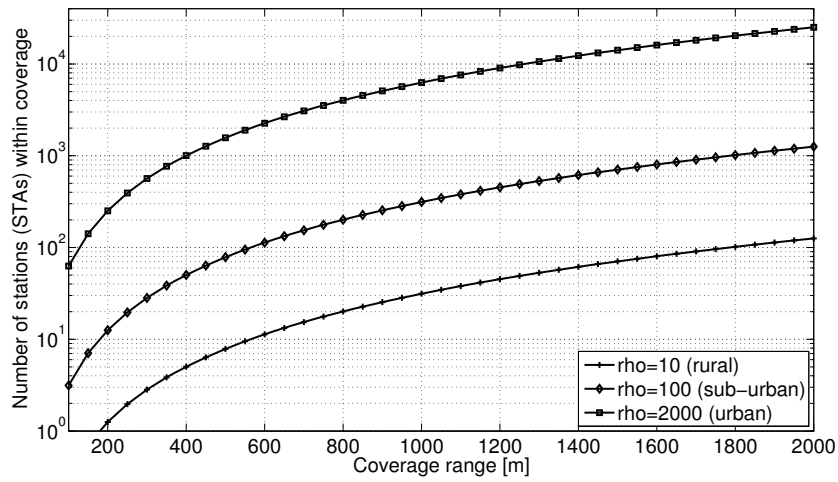


**Figure 4.23** – Coverage range vs. number of WLAN STAs and different network densities (rural, sub-urban, urban).



## 4.5 Experimental $2 \times 2$ beamform evaluation

The beam characteristics of different beamforming schemes are discussed in the following. Fig. 4.24 illustrates a beamform configuration in a wireless system. Fig. 4.24(a) illustrates the different beamform characteristics, for main beam directed to STA 1, but with increase of noise level at STA 2. In Fig. 4.24(b) the null beam is directed to the STA 2 to minimize the interference, but with reduced signal level at STA 1.

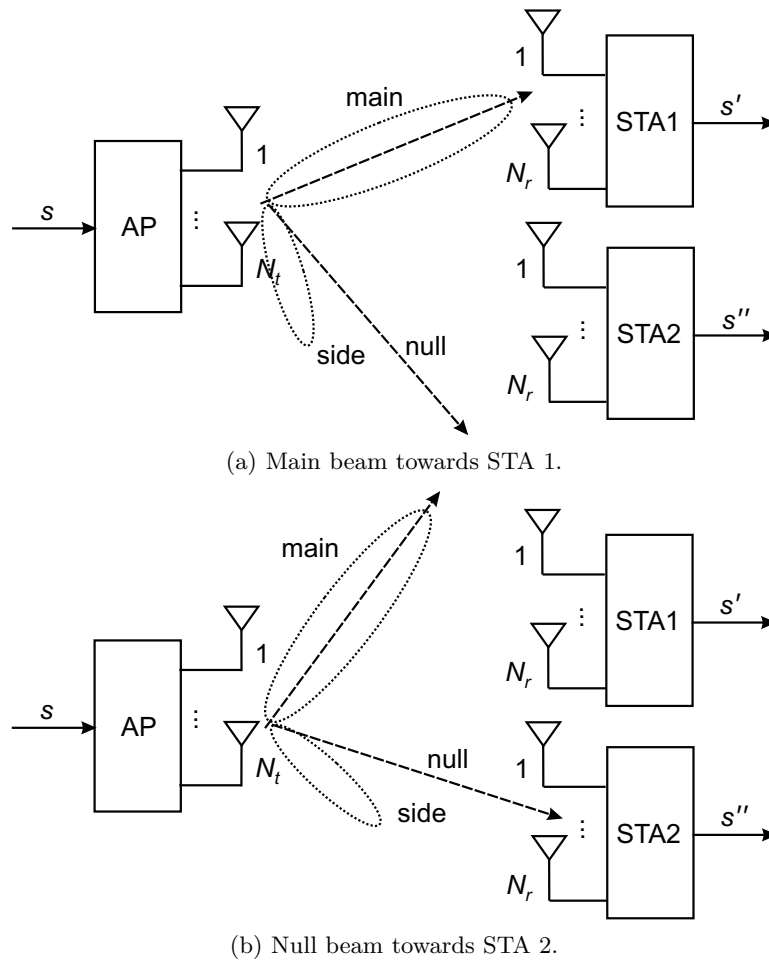
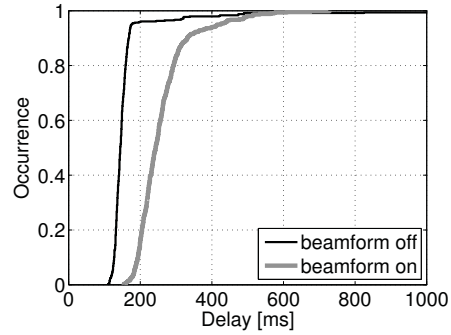


**Figure 4.24** – Illustration of beamforming configuration in a wireless system, with main beam, null beam and side lobe, directed to a single user in a multi-user scenario.

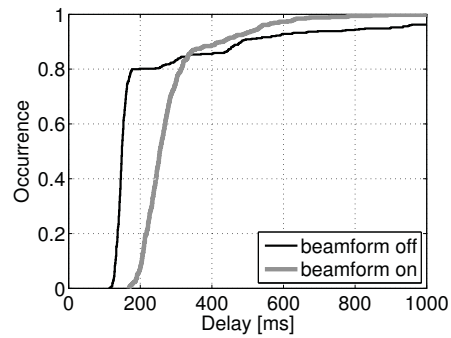
### 4.5.1 Multi-flow: 2-flow configuration

The transmission performance of 2 flows is discussed in the following. Eight scenarios have been evaluated, single flow performance of flow 1 (Fig. 4.25(a)) and flow 2 (Fig. 4.25(b)), and concurrent transmission of flow 1 and flow 2, in which each scenario has been evaluated with and without beamforming applied. A constant bit rate unicast flow is applied to measure the transmission statistics rather than a simple best-effort data flow.

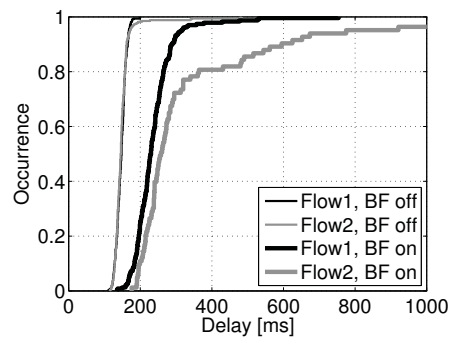
The measured transmission performance of single flows (flow 1 and flow 2) is shown in Fig. 4.25. In addition, the delay performance is shown, for concurrent transmission of flow 1 and flow 2 (Fig. 4.25(c)).



(a) Single flow 1 delay performance, beamform off/on.



(b) Single flow 2 delay performance, beamform off/on.



(c) Delay performance of concurrent transmission of flow 1 and flow 2, beamform off/on.

**Figure 4.25** – ECDF of beamform delay performance of single and concurrent transmission of flow 1 and flow 2, without and with beamforming applied.

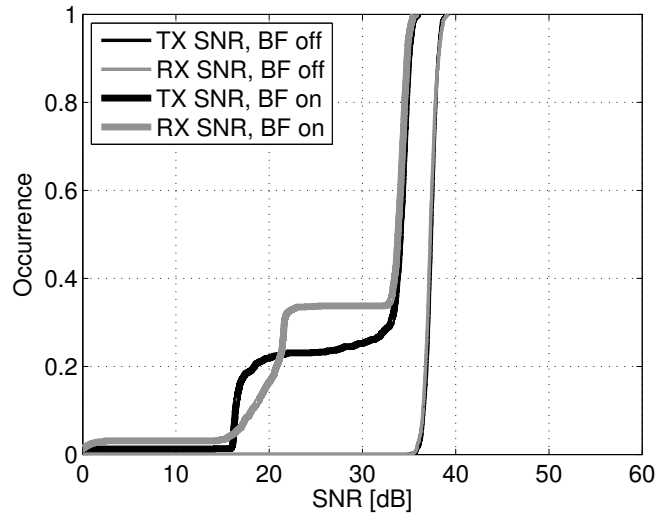
The figure shows the experimentally determined cumulative probability distribution function (ECDF) of single flows with and without beamforming applied. The mean delay of flow 1 when transmitting data without beamforming is at 180 ms. When beamforming is applied, the transmission delay increases at 22 ms. Fig. 4.25(b) shows similar results when flow 2 is transmitting data. The mean delay without beamforming is at 184 ms. When beamforming is applied, the delay increases to 222 ms. It can be concluded that the beamforming operation causes significant delay to the S1G WLAN prototype that is at  $> 40$  ms. Similar results are presented in Fig.4.25(c), which shows the transmission performance of concurrent flows. The figure illustrates that without beamforming the concurrent transmission causes a delay at 180 ms for flow 1 and flow2, respectively. When beamforming is applied, the delay increases at 210ms for flow 1 and 218ms for flow 2. It can be concluded that the delay increases when beamforming is applied for concurrent flows, which is in the same regime as for single flows when beamforming is applied.

The measured SNR and noise variance performance of flow 1 and flow 2 (single flows), with and without beamforming applied, is shown in Fig. 4.27.

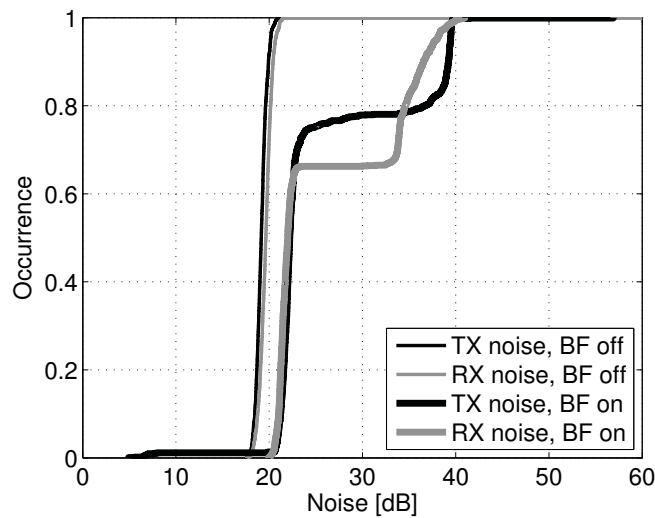
In Fig. 4.26(a), the measured mean SNR of flow 1 is at 37 dB without beamforming. With beamforming applied, the measured SNR of flow 1 is at 35 dB. The monitored mean SNR of flow 2 is at 31 dB without beamforming applied and 32 dB with beamforming applied. It can be concluded that the mean SNR reduces at 5 dB for flow 1 when beamforming is applied. Further, it can be concluded that the mean SNR is increased at 1 dB at the sender side and receiver side for flow 2 when beamforming is applied. The monitored mean noise variance of flow 1 is illustrated in Fig. 4.26(b), which is at 20 dB without beamforming applied and 22 dB with beamforming applied. The monitored mean noise variance of flow 2 (Fig. 4.27(b)) is at 30 dB at the sender side and 35 dB at the receiver side without beamforming applied. The mean noise variance when beamforming is applied is at 28 dB at the sender side and 35 dB at the receiver side. It can be concluded that the mean noise variance increase at 2 dB for flow 1 when beamforming is applied. Further, it can be concluded that the monitored mean noise variance at the sender side for flow 2 is reduced at 2 dB when beamforming is applied. It can be concluded that the monitored beamforming performance exhibits different observations for SNR and noise variance for flow 1 and flow 2.

The measured transmission performance of concurrent flows with and without beamforming applied is shown in Fig. 4.29.

In Fig. 4.29, the mean SNR of flow 1 is at 22 dB for the receiver and 35 dB for the sender without beamforming. The mean SNR for flow 2 is at 21 dB for the sender and 19 dB for the receiver. In Fig. 4.28(b), the mean SNR of flow 1 is at 22 dB for both, sender and receiver when beamforming is applied. For flow 2 receiver side the mean SNR is 20 dB and 22 dB for sender side. In Fig. 4.28(b) the mean noise variance is at 42 dB for flow 1 and flow 2. A difference in the mean noise value can be observed for flow 1 sender side, which is at 25 dB when no beamforming is applied. In Fig. 4.29(b) the mean noise variance of flow 1 is at 45 dB for sender



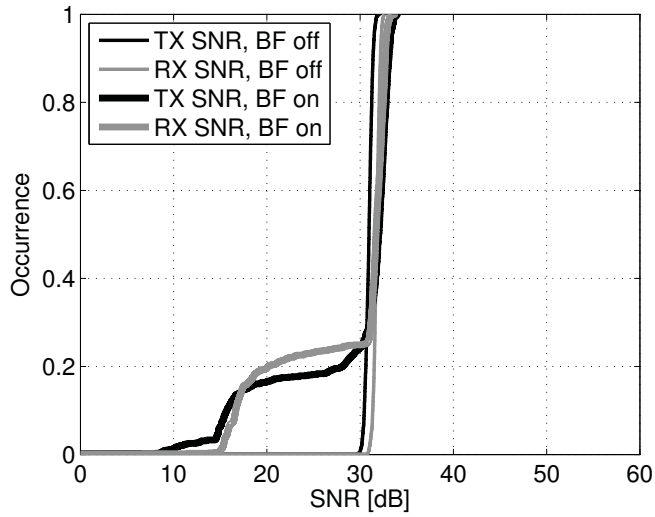
(a) Single flow 1 SNR performance, beamform off/on.



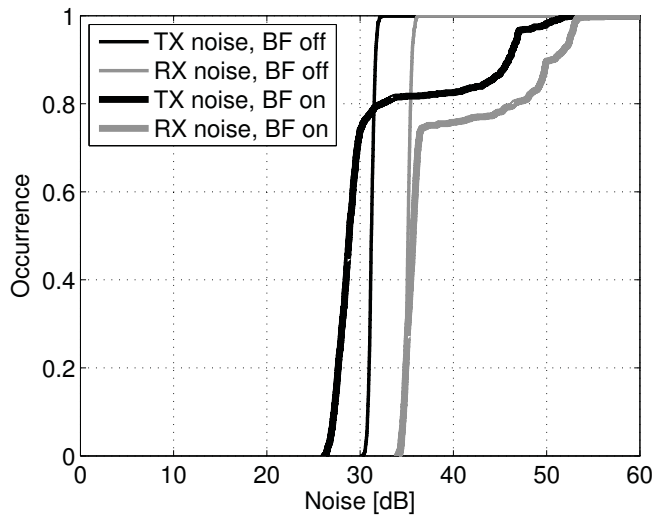
(b) Single flow 1 noise performance, beamform off/on.

**Figure 4.26** – ECDF of SNR and noise performance of flow 1 transmission without and with beamforming applied.

side and 42 dB for the receiver side when beamforming is applied. The mean noise variance of flow 2 is at 49 dB for for the sender side and 46 dB for the receiver side.



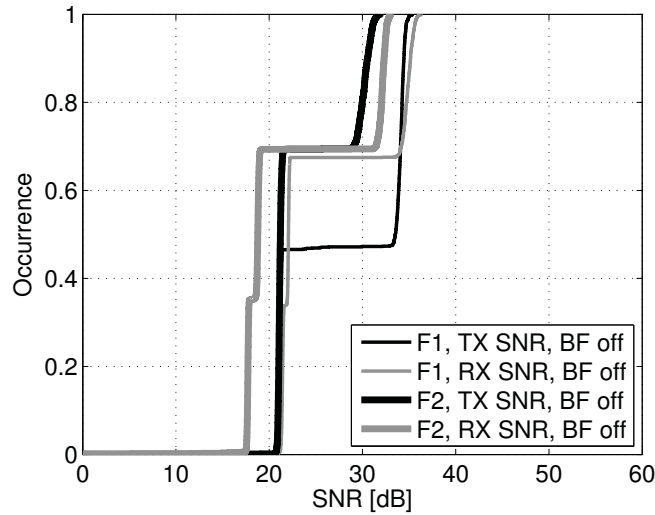
(a) Single flow 2 SNR performance, beamform off/on.



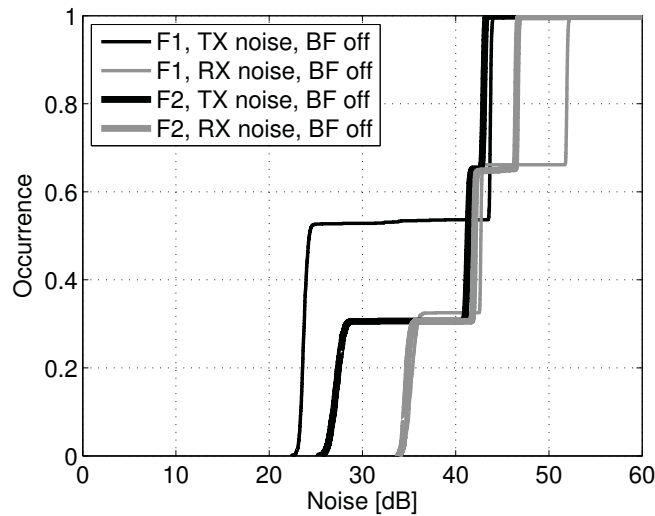
(b) Single flow 2 noise performance, beamform off/on.

**Figure 4.27** – ECDF of SNR and noise performance of flow 2 transmission without and with beamforming applied.

The measured throughput performance of single and concurrent flows, with and without beamforming applied, is shown in Fig. 4.31. In addition, the observed packet loss is added.



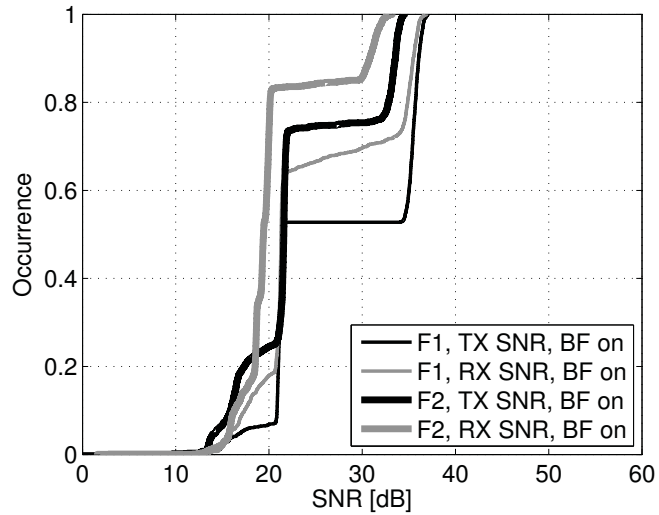
(a) Flow 1 and flow 2 SNR performance, beamform off.



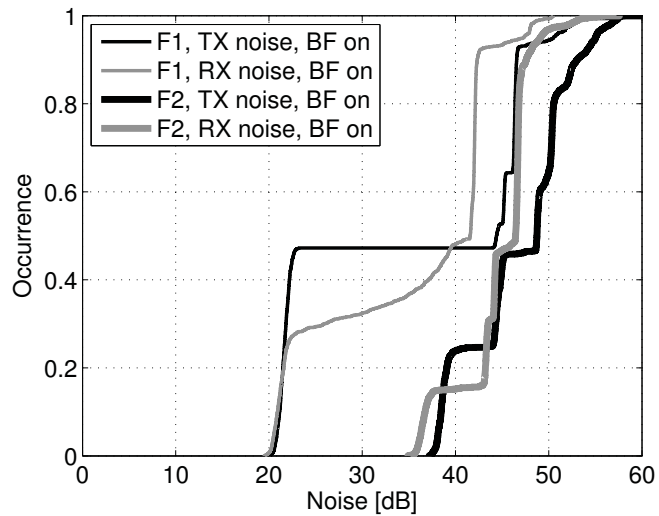
(b) Flow 1 and flow 2 noise performance, beamform off.

**Figure 4.28** – ECDF of SNR and noise performance of concurrent transmission of flow 1 and flow 2 without beamforming applied.

In Fig. 4.30(a) the throughput of single flow 1 and flow 2 with and without beamforming is presented. Without beamforming applied, the measured throughput



(a) Flow 1 and flow 2 SNR performance, beamform on.

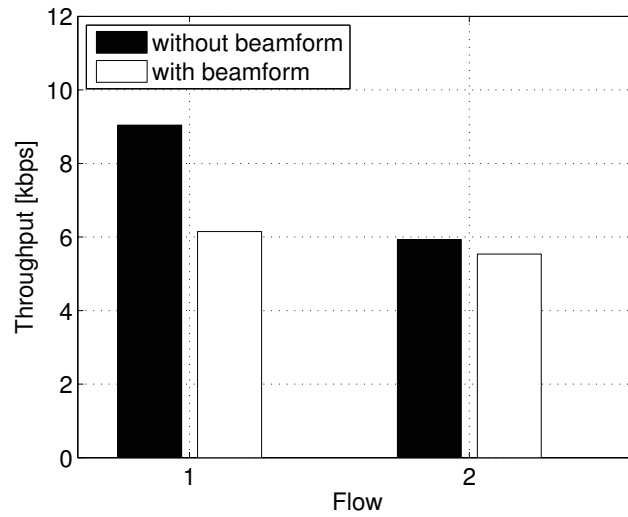


(b) Flow 1 and flow 2 noise performance, beamform on.

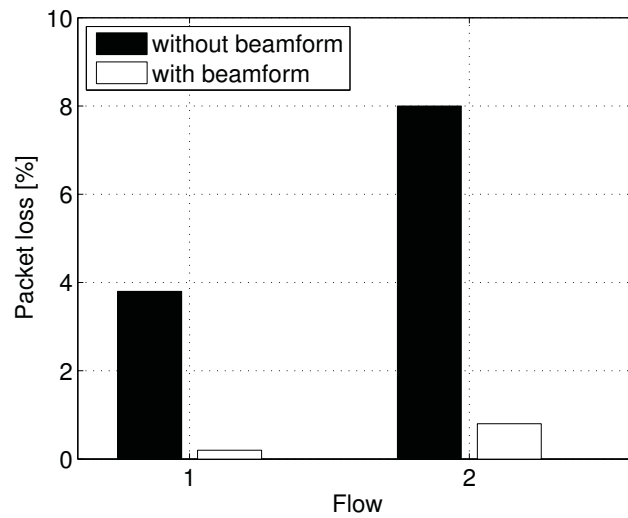
**Figure 4.29** – ECDF of SNR and noise performance of concurrent transmission of flow 1 and flow 2 with beamforming applied.

for flow 1 is at 9 kbps and 5.9 kbps for flow 2. With beamforming applied, the throughput of flow 1 is at 6.1 kbps and 5.7 kbps for flow 2. The packet loss for





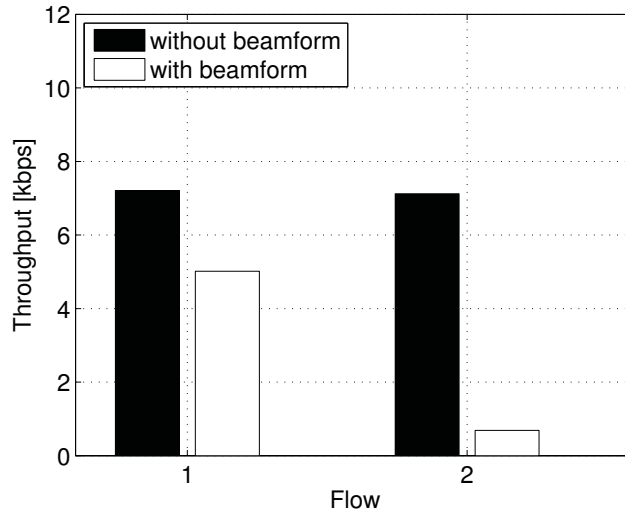
(a) Throughput performance of single flow 1 and single flow 2.



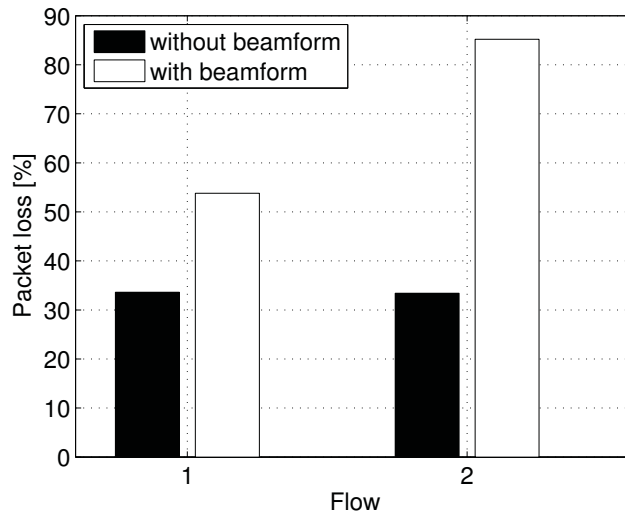
(b) Packet loss performance of single flow 1 and single flow 2.

**Figure 4.30** – Throughput and packet loss performance of single and concurrent transmission of flow 1 and flow 2, without and with beamforming applied.

single flow transmission is shown in Fig. 4.30(b). The measured packet loss for flow 1 is at 3.8% and 8% for flow 2 without beamforming applied. When beamforming



(a) Throughput performance of concurrent flow 1 and flow 2.



(b) Packet loss performance of concurrent flow 1 and flow 2.

**Figure 4.31** – Throughput and packet loss performance of single and concurrent transmission of flow 1 and flow 2, without and with beamforming applied.

is applied a significant drop in the packet loss can be observed, which is 0.2% for

flow 1 and 0.6 % for flow 2. The benefit of applying beamforming for single flows can be observed, which results in a significantly reduced packet loss ratio.

Next, the throughput for concurrent flows is shown in Fig. 4.31(a), where the measured throughput is at 7.2 kbps for flow 1 and flow 2 when no beamforming is applied. When beamforming is applied, the throughput for flow 1 is at 4.9 kbps and at 0.4 kbps for flow 2, which is a significant drop in throughput performance when beamforming is applied for concurrent flows. Finally, Fig. 4.31 illustrates the measured packet loss, which is at 33 % for flow 1 and flow 2 when no beamforming is applied. When beamforming is applied the packet loss increases up to 53 % for flow 1 and 85 % for flow 2. It can be concluded that tested beamforming has negative impact on the throughput and packet loss performance when concurrent flows are transmitted. However, the benefit of applying beamforming reduces for concurrent flows, compared to single flows.

Table 4.2 and Table 4.3 summarize the single flow and multi-flow measurement results, respectively.

**Table 4.2** – Summary of 2 flow measurement results, single flows. ICMP protocol,  $f_c = 923$  MHz, 2×2 MIMO-OFDM, MCS 10,  $d_{tx-rx} = 3$  m, 100 B packet size (header 28 B), sending rate= 0.3, location: Shielded room, path condition: LOS.

Parameter	Flow 1 single (BF off)	Flow 2 single (BF off)	Flow 1 single (BF on)	Flow 2 single (BF on)
RTT min [ms]	110.77	114.62	154.66	168.78
RTT avg. [ms]	170.231	248.23	259.72	286.68
RTT max [ms]	4388.271	2085.04	729.72	1062.84
RTT std. [ms]	236.814	282.25	75.54	110.84
# sent pkt.	500	500	500	500
# received pkt.	481	460	499	496
# lost pkt.	19	40	1	4
# duplications	5	44	19	21
Throughput [kbps]	9.041	5.929	6.147	5.553
Loss ratio [%]	3.80	8.00	0.20	0.80

**Table 4.3** – Summary of 2 flow measurement results, concurrent flows. ICMP protocol,  $f_c = 923$  MHz,  $2 \times 2$  MIMO-OFDM, MCS 10,  $d_{tx-rx} = 3$  m,  $d_{flow} = 2$  m, 100 B packet size (header 28 B), sending rate= 0.3, location: Shielded room, path condition: LOS.

Parameter	Flow 1 concurrent (BF off)	Flow 2 concurrent (BF off)	Flow 1 concurrent (BF on)	Flow 2 concurrent (BF on)
RTT min [ms]	111.51	115.83	111.51	176.41
RTT avg. [ms]	147.41	149.63	147.41	343.65
RTT max [ms]	200.49	484.49	200.49	1599.80
RTT std. [ms]	13.80	33.11	13.80	241.87
# sent pkt.	500	500	500	500
# received pkt.	332	333	231	74
# lost pkt.	168	167	269	426
# duplications	0	1	4	9
Throughput [kbps]	7.206	7.121	5.014	0.689
Loss ratio [%]	33.60	33.40	53.80	85.20

## 4.6 SISO and MIMO single flow performance

The single flow performance has been tested by using the S1G WLAN prototype. Fig. 4.32 shows the delay for SISO ICMP performance at different MCS rates, including MCS 0, MCS 1, MCS 2, MCS 4, MCS 4 and for different data packet sizes, including 100 B, 200 B, 400 B, 800 B, and 1400 B. The delay reduces with the increased data packet sizes (Fig. 4.32) due to the reduced signal overhead (reduced number of acknowledgment (ACK) frames) when larger packets are transmitted.

Fig. 4.33 illustrates the delay for MIMO ICMP performance at different MCS rates, including MCS 0, MCS 1, MCS 2, MCS 4, MCS 4 and for different data packet sizes, including 100 B, 200 B, 400 B, 800 B, and 1400 B.

Similar, to the SISO transmission, the delay reduces with the increased data packet sizes (Fig. 4.33) due to the reduced signal overhead (reduced number of ACK frames) when larger packets are transmitted.

Fig. 4.34(a) illustrates the SISO performance when ICMP traffic is transmitted. The benefit of using larger MCS rates can be observed, which results in higher throughput. For MCS 2 and packet size 1400 B the throughput is at 112 kbps. Fig. 4.34(b) illustrates the SISO performance when UDP traffic is transmitted. The benefit of using larger MCS rates can be observed, which results in higher throughput. For MCS 2 and packet size 1400 B the throughput is at 110 kbps.

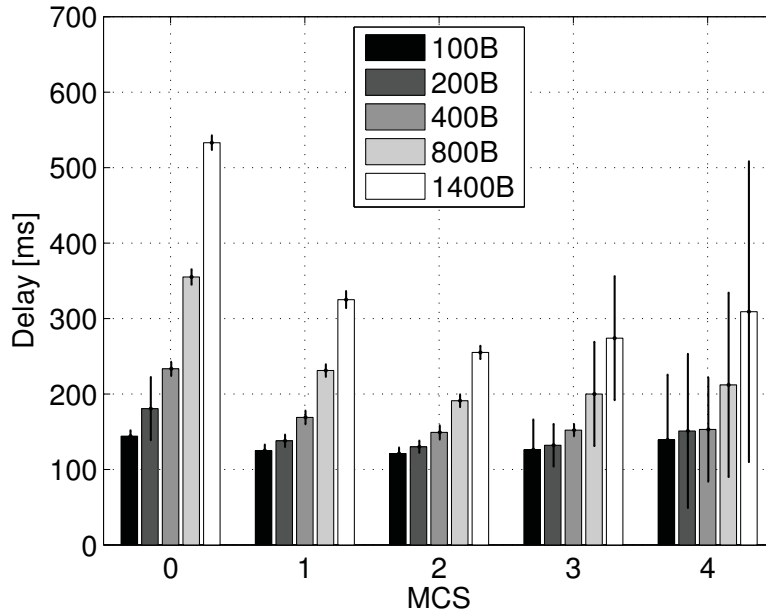
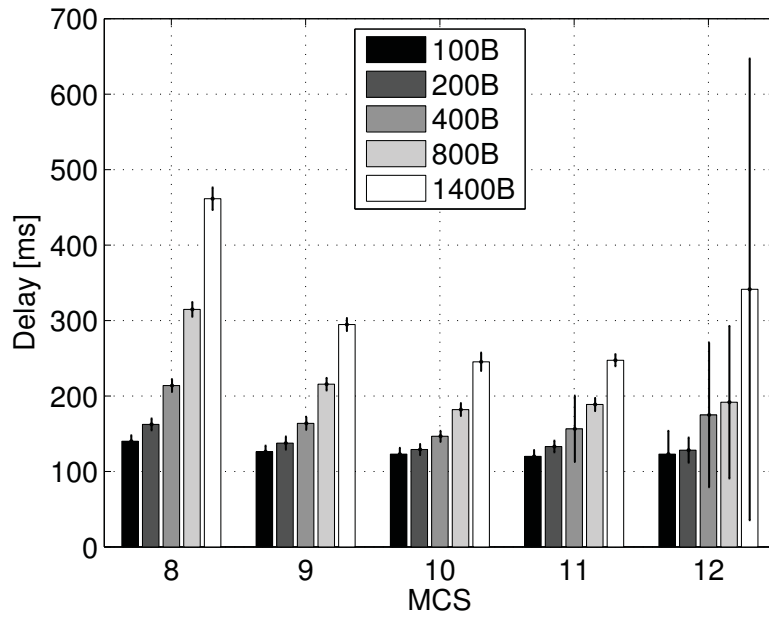


Figure 4.32 – Delay and standard deviation for SISO ICMP measurement.

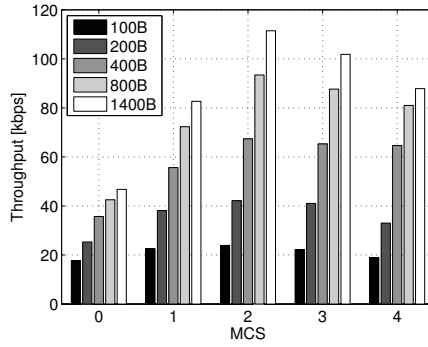
However, with increased MCS rate the throughput drops significantly, which is at 40 kbps for MCS 4 and 1400 B. Higher MCS rates have not been measured due to transmission errors when using higher MCS rates with the S1G WLAN prototype. The cause is the increased PHY operation time due to signal equalization and decoding operations, which increase with higher MCS rates. Fig. 4.34(c) illustrates the SISO performance when TCP traffic is transmitted. Due to the characteristic of TCP traffic (two-way handshake and slow start operation) a reduced throughput performance is observed compared to ICMP and UDP traffic. However, the monitored traffic is at 81 kbps for MCS 2 and 1400 B packet size, which demonstrates the practicability of the S1G WLAN prototype for all kind of traffic scenarios, including ICMP, UDP, and TCP.

Fig. 4.35(a) illustrates the MIMO throughput performance of ICMP transmissions. An increased MCS results in higher data rates, which is at 118 kbps for MCS 10 and MCS 11. The benefit of using MIMO can be observed when comparing the SISO ICMP throughput performance (Fig. 4.34(a)). Fig. 4.35(b) illustrates the MIMO UDP transmission performance, which is at 110 kbps for MCS 9, MCS 10, and MCS 11. The benefit of using MIMO to increase the throughput can be observed, compared to SISO UDP transmission performance (Fig. 4.34(b)).

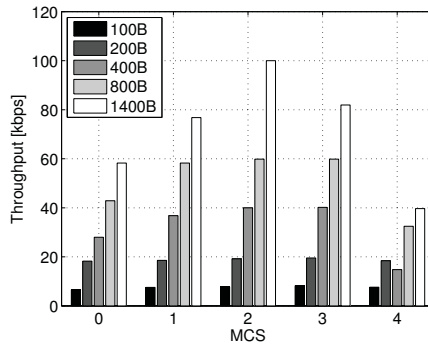


**Figure 4.33** – Delay and standard deviation for MIMO ICMP measurement.

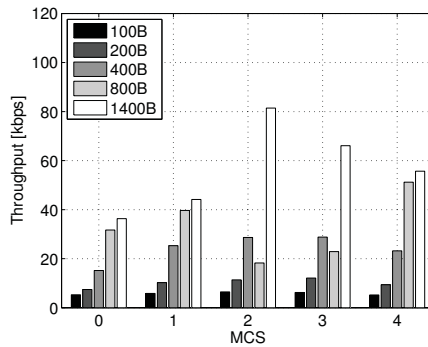
Finally, Fig. 4.35(c) shows the MIMO TCP performance with 84 kbps for MCS 10 and 1400 B. The MIMO TCP transmission performance demonstrates the feasibility of the S1G WLAN prototype.



(a) SISO ICMP throughput performance.

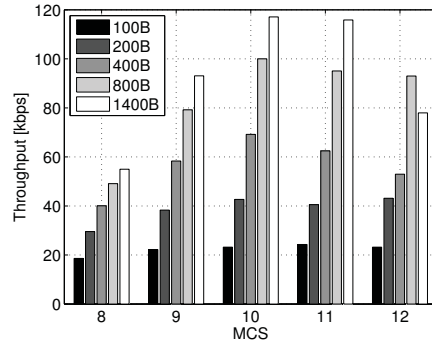


(b) SISO UDP throughput performance.

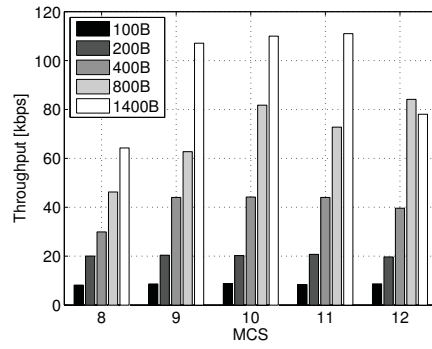


(c) SISO TCP throughput performance.

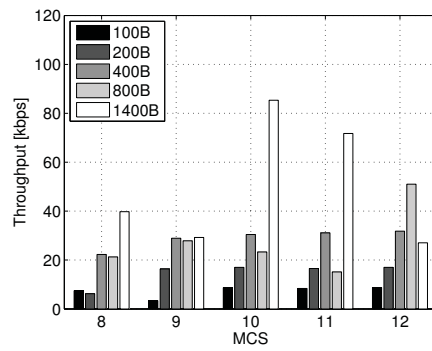
**Figure 4.34** – Measured SISO ICMP, UDP, and TCP throughput performance.



(a) MIMO ICMP throughput performance.



(b) MIMO UDP throughput performance.



(c) MIMO TCP throughput performance.

**Figure 4.35** – Measured MIMO ICMP, UDP, and TCP throughput performance.



## 4.7 Bibliographical notes

In [111], the use of Grassmannian subspace prediction schemes is motivated. A problem is the outdated information of a delayed channel feedback. It is argued that some of the proposed that is called Grassmannian subspace schemes highly depend on the channel propagation model. Hence, a CSI tracking scheme is proposed Grassmannian subspace predictive coding (GSPC), which mitigates the negative effect of delayed feedback [111, 112]. In [113], empirical results on beamforming in MISO systems are discussed. A comprehensive comparison of different codebooks, including *maximum Welch bound equality* (MWBE), WiMAX, *equal gain bipolar* (EGB), and tripolar codebooks was conducted and the complexity of each of the codebooks was shown. Further, the authors used the Jakes path loss model for their experiments. A codebook-based beamforming demonstrated improvements with a reduced complexity for an implementation in WiMAX for two and four antenna constellations.

Codebooks for precoding in LTE are defined in [114]. LTE classifies the precoding in transmission on a single antenna port, for spatial multiplexing, and transmit diversity. Further, precoding is defined two modes, one mode, which defines the precoding without supporting cyclic delay diversity (CDD) and a second mode that supports large CDD, which enhances the precoding by specifying additional support vectors for cyclic delay calculation. To further increase the throughput over large distance a full-duplex MIMO support is proposed. Fukumoto *et al.*, [115] proposed a MIMO FD wireless architecture for IEEE 802.11a, which achieved 80% higher throughput in MIMO networks compared to conventional WLAN protocols. The transmission performance in MIMO systems is greatly influenced by the selected precoding technique. The authors in [116] compared the precoding improvements of channel inversion (CI) and block diagonalization (BD) precoding schemes under realistic channel conditions. It was demonstrated that the BD precoding scheme outperforms the CI precoding, which was simulated for very high throughput (VHT) wireless local area networks (WLAN) IEEE 802.11ac multi-user (MU) multiple input multiple output (MIMO) that use orthogonal frequency division multiplexing (OFDM). The authors in [117] analyzed the transmission performance of implicit and explicit channel state information (CSI) methods, which have been specified in IEEE 802.11ac in which a compressed beamforming report based on singular value decomposition (SVD) is assumed. The comparison included overhead and packet error rate (PER) performance measures. It was demonstrated that explicit feedback requires a high precision feedback mode, which incurs larger transmission overhead. If accurate calibration is available, using implicit feedback would allow to further reduce the signaling overhead. A hybrid CSI transmission scheme was proposed that would allow improved calibration updates with without incurring additional overhead.

In general, precoding can be classified in linear and non-linear schemes. The authors in [118] refer to linear precoding in MIMO-OFDM based on deterministic CSI information at the transmitter (CSIT). It was demonstrated that spreading the CSI

information over a group of OFDM subcarriers instead of a per subcarrier-basis, would utilize all the diversity a wireless channel can provide; thus, increasing the transmission performance. Codebooks include the unitary space vector quantization (USVQ) [119], Grassmannian and LTE-A R10 discrete Fourier Transform (DFT) codebook [114], whereas the USVQ can adapt more faster to channel dynamics and shows a higher precoding performance than Grassmannian or DFT codebooks [103]. The IEEE 802.16e codebook has demonstrated increased performance in uncorrelated wireless channels, whereas DFT codebooks are more suitable for correlated channels [120].

Performance analysis of non-linear precoding schemes are reported in [121]. Non-linear precoding schemes, such as dirty paper coding, have been found as an alternative to linear precoding schemes, exploiting channels state information to achieve higher channel capacity. However, due to the high complexity of non-linear precoding schemes, such schemes are not considered in WLAN protocols. Next, when precoding is executed at the transmitter, complex multiplication between the data stream and the codebook requires increased computing power, which is analyzed by the authors in [103]. The impact on the codeword computation and the use of hardware resources are considered thoroughly. A basic binary shift rather than a binary-to-binary operation is examined to execute the multiplication and division of codeword and data signal processing. Codebook performance in millimeter-wave broadband WLANs has been reported by Liang *et al.*, in [122] discussing the challenges on codebook selection strategies and channel capacity improvements in WLANs.

Performance improvement of mixed rotating coding schemes have been reported in [123], including the Grassmannian, Kerdock, DFT, Sloane manifolds. However, the authors only reported on their findings regarding the mixed rotation precoder performance in particular. The reported gains at BER= $10^{-3}$  were only at 1.8 dB and 2.3 dB when using rotating precoding and mixed rotating precoding scheme, respectively. An advanced LTE beamforming concept is outlined in [124] in which wireless base stations collaborate among each other to adjust their beams to mitigate the inter-cell interference. Null-beams and directed beams are optimized so that only target nodes receive the directed beam, whereas other surrounding nodes receive null-beams; thus, reducing the interference level significantly.

Further, the concept of transmitting *companion PMIs* is presented in [124], in which the receiver feedback multiple PMIs to the BS to provide a set of optimal PMIs, based on transmitted channel state information. The BS selects the PMI, which creates the minimum inter-cell interference. In addition, the *worst companion PMI* are reported to the BS to avoid the selection of PMIs, which would otherwise increase the interference for a particular channel state. However, the additional PMI information is only feasible if the backhaul link offers sufficient transmission bandwidth, e.g, in high data rate systems [124].

## 4.8 Discussion and summary

### 4.8.1 Discussions

Obtaining additional gains by applying precoding schemes in multi-antenna systems is a straightforward method to improve the transmission performance. However, precoding gains seem to be affected by the entire WLAN. When using the sub-1 GHz WLAN prototype, the reported gains were challenging to obtain. For instance, the observed average SNR when using Kerdock manifold was higher compared to Grassmannian manifold, which would increase the wireless range of a single WLAN AP. However, the SNR variance also increased, which would lead to an increased probability of signal outages. Further, packet duplications have been observed during the measurements when using Kerdock codebooks, which would lead to the assumption that the sub-1 GHz WLAN prototype system performance need further improvement to enable the high precoding gains. Potential solutions would include:

1. Change of the USRP 1 to USRP 2 or higher models, e.g., USRP 300 or USRP 310. The newer USRP models provide improved FGPA calculation performance and allow channel bandwidth up to 160 MHz.
2. Change of GnuRadio software to improve the FPGA design. However, this would be time-intensive and would require the USRP 1 FPGA hardware design description.

Next, the precoding performance in the free field needs to be investigated for sub-1 GHz WLANs. In particular, long-range distances combined with hundreds of STAs associated with a single AP, including downlink and uplink scenarios, would have impact on the precoding performance. Thus, it is recommended to conduct outdoor measurements to verify the proposed precoding modifications. This would require the use of test frequencies in the free field, when using uncertified wireless equipment.

### 4.8.2 Summary of the chapter

The relevance of using precoding schemes in sub-1 GHz WLANs and their contributions to the wireless coverage have been evaluated in this chapter. Sub-1 GHz WLANs aim to cover up to 1 km wireless coverage range in outdoor deployment scenarios. The received signal strength at the receiver needs to be high enough to minimize signal outages so that a reliable long-range communication is feasible. In addition, larger range is envisioned and therefore an increased link budget is required. Increasing the wireless coverage by increasing the transmit power  $P_{tx}$  is not possible because of the limitations of the regulatory requirements and due to the character of a sensor device, which requires low power emission to reduce the energy consumption. The goal in this chapter was the coverage enhancement

in IEEE 802.11ah WLANs and multi-antenna precoding schemes have been examined to achieve this goal. In particular, the precoding has been found as a potential candidate to further increase the coverage, which results in an increased link budget.

Enhanced precoding schemes have been evaluated, including the Grassmannian manifold and the Kerdock manifold. The Grassmannian manifold provides an optimal precoding codebook, which supports the selection of optimal codewords with a reduced CSI feedback overhead. The maximum distance among the selected codeword allows optimal precoding. Codeword search functions require additional overhead for Grassmannian.

As an alternative to the Grassmannian manifold, the Kerdock manifold was proposed. The Kerdock manifold offers a limited codeword set, which is beneficial to reduce the storage capacity in the transmitter. In addition, the amount of CSI feedback can be further reduced, which requires less feedback overhead.

In addition, modifications on the Kerdock precoding codebook have been proposed, which further result in significant diversity gains. A diversity gain is claimed in the range of 2 dB to 3 dB when the proposed codebook modifications are applied. This means that precoding opens a field of innovative coding schemes which can result in significant transmit power improvements, e.g., to reduce communication so called gray-zones.

Diversity gains have been evaluated through an simulation study. In addition, the Grassmannian and the Kerdock codebooks have been implemented into the sub-1 GHz WLAN prototype and have been tested and analyzed. System evaluation included the simulation of precoding gains over uncorrelated Rayleigh fading channels. In addition, experiments were carried out, in which the precoding performance was evaluated under real conditions, including correlated Rician fading channels. Both, the simulation study as well as the experimental evaluation study have demonstrated significant increase of precoding gains; thus, the coverage range of S1G WLANs can be increased to support a higher number of associated WLAN STAs. New problems occur, such as massive access in high density WLANs, which are discussed in Chapter 7.

The proposed precoding modifications are capable of providing substantial gains which enable much larger outdoor coverage. The modified Kerdock codebook is a powerful precoding scheme that enables reliable links to mitigate transmission errors. This is from importance, e.g., to reduce the energy consumption due to less retransmissions. Finally, it was demonstrated that the proposed scheme has a low complexity and as such are easy to implement and to adapt in future long-range wireless communication networks, such as the IEEE 802.11ah WLAN protocol amendment.

## Chapter 5

# Energy consumption reduction

To utilize IEEE 802.11ah-based devices as so called Wi-Fi sensors the implemented Wi-Fi protocol features must support energy consumption reduction schemes. Wireless sensor networks are predicted to be deployed in a massive scale to serve utility companies with outdoor measurement data, including meter information, network state information, and environmental conditions. Wireless sensor networks belong to the information and communication technology (ICT) sector which already represents 2% of the carbon emission worldwide, with a contribution of 0.2% from wireless access technologies, which is equal to the emission to the carbon emission of all airplanes worldwide [125]. Thus, the sensor network's entire energy consumption reduction is a compelling necessity to be capable of meeting the demand of reducing the carbon footprint as well as to prolong the battery lifetime of deployed sensor nodes in a range of 10-20 years. Compared to the statement in [125], which stated that energy efficiency decreases monotonically with the throughput, the result of this chapter is that energy efficiency per bit is optimal for high modulation order that results in high throughput due to excellent wireless link quality.

A general trade-off formula between spectrum efficiency and energy efficiency is given in [125–127] which is

$$\eta_{\mu} = \eta_{\nu} (N_0 (2^{\eta_{\nu}} - 1))^{-1}, \quad (5.1)$$

where  $N_0$  is the spectral density of the noise power at the receiver and  $\eta_{\mu}$  and  $\eta_{\nu}$  as the spectrum efficiency and energy efficiency, respectively. However, if the link quality decreases (low SNR), the energy efficiency further reduces due to reduced number of transmitted bits. Thus, a general approach should be to avoid high order modulation schemes when the link quality becomes bad. Moreover, if the theoretical energy efficiency can be optimized for bad wireless links but real-world antenna RF chains remains powered on, e.g., due to default settings of Wi-Fi modules, no energy

consumption has been reduced as a consequence. Hence, this chapter motivates how to power off RF antenna chains that would result in a more power-efficient but low-complex system solution.

## 5.1 Energy consumption reduction strategies

In this chapter the energy consumption of a multi-antenna Wi-Fi module is in the research focus. Wi-Fi based sensor nodes need to reduce their energy consumption to compete with energy-efficient WPAN modules. In addition, high data rate modulation schemes as well as multi-antenna MIMO techniques, which are utilized in S1G WLANs based on the IEEE 802.11ah WLAN protocol, require a significant amount of energy. The idea is to design new adaptive controlling schemes that would enable the reduction of energy consumption in S1G multi-antenna WLANs. IEEE 802.11n Wi-Fi modules have been already shipped in large numbers. These Wi-Fi modules are used in this study as the evaluation basis for energy consumption in current Wi-Fi modules (IEEE 802.11ah Wi-Fi modules are not available yet). The idea is to analyze the energy consumption of IEEE 802.11n Wi-Fi modules as a basis for comparison. Further, an analytical model is developed to approximate the energy consumption of Wi-Fi modules. It was observed that the amount of energy consumption of a Wi-Fi module is mainly affected by the static power consumption of active MIMO radio frequency (RF) chains (dynamic power consumption is negligible). The proposed energy reduction strategy is based on a simple RF chain control to reduce the static power consumption. The RF chain control has been implemented and evaluated in a WLAN AP prototype. A significant reduction of 43% energy consumption is claimed for multi-antenna WLANs, including the IEEE 802.11ah WLAN protocol.

## 5.2 Problem formulation

It is essential to identify the energy consumption in WLAN APs to propose an optimal energy consumption reduction strategy. The energy consumption during the so called *sleep mode* of a commercial Wi-Fi module is measured with 100 mW, whereas in *idle mode* the energy consumption is at 820 mW while waiting to receive data [128]. Energy consumption is relevant for the entire WLAN, including the WLAN AP and STA. Whereas many energy saving schemes for WLAN STAs have been proposed, e.g., to prolong the battery lifetime of mobile STAs, the energy consumption of WLAN APs has been attracted some research recently. In this study, the energy consumption of the WLAN AP is in the research focus. Energy consumption reduction strategies for WLAN APs are divided into two states. One state is the active state when the AP is active, while transmitting or receiving data frames. The other state is when the AP is idle while waiting for ingress/egress data traffic. In addition, other states are defined, such as sleep state, in which the

AP deactivates some of its unused powered modules, such as LAN ports [129]. In addition to energy saving schemes in idle or sleep state, energy consumption can be further reduced during the WLAN AP active state, where there is a significant amount of energy consumption that could be minimized while the Wi-Fi module of the WLAN AP is transmitting or receiving data frames. The energy consumption in active state (transmitting or receiving data) when using different data rate modulation schemes does not vary significantly [128]. In addition, changing the channel bandwidth does not change the energy consumption either. Further, the transmit power  $P_{tx}$  has been found as not significant contributor to total WLAN AP energy consumption<sup>1</sup>. Remarkably, using multiple spatial streams in a multi-antenna WLANs, consumes about 53% more energy compared to a single stream. Measurement studies have demonstrated that each RF-chain adds 330 mW to the total energy consumption of the Wi-Fi module. By consequence, reducing the number of active RF-chains would allow a significant energy reduction of the entire Wi-Fi module.

### 5.3 Proposal: Selective multi-antenna RFCC

An energy-saving estimation scheme is proposed, in combination with a selection scheme for multi-antenna RF-chain switch control. Switching off a particular RF-chain would deactivate the use of the selected antenna, which would otherwise require the powering of the related RF-chain. In case that a single antenna would be sufficient for data transmission only the related RF-chain will be powered on. Other RF-chains remain powered off to reduce energy consumption of the Wi-Fi module. In case that multiple-antenna are efficient to use, e.g., for high-speed data transmissions, the required RF-chains will be powered on to enable the transmission or reception of the associated antennas.

The proposal is a simple switching algorithm that would adopt to the channel or link state dynamics, i.e., if link conditions are sufficient for single or multiple antenna transmissions. Enhanced RF-chain switching schemes could include other relevant network parameters, such as data arrival rates. Further, an analytical model has been developed, which allows to judge the energy consumption of a multi-antenna based Wi-Fi module. The model is based on the energy consumption in WPANs and has been modified during this study to make it applicable to MIMO based WLANs. A real-world implementation was carried out in which an energy efficient WLAN AP prototype was assembled<sup>2</sup>. Using a WLAN AP prototype enables the evaluation of the actual energy consumption and to compare the results with the analytical energy consumption model.

---

<sup>1</sup>Only 10% energy reduction gain is obtained when  $P_{tx}$  is reduced at 97%.

<sup>2</sup>The energy efficient WLAN AP prototype was designed as a so called radio-on-demand (ROD) system [129].

### 5.3.1 RF chain control energy consumption reduction

As outlined above, there is a huge amount of energy consumption reduction potential in WLAN APs while sending/receiving data. In the active mode, the multiple antenna RF-chains consume significant amount of energy. Thus, a simple but yet efficient proposal is to switch on/off multiple RF chains to further reduce the energy consumption. Monitoring link layer parameters, such as RSSI, can be used to control the adaptive switching of RF chains. The result is that inefficient energy consumption of multiple chains can be avoided, e.g., due to wireless link performance that would be otherwise inefficient for wireless data transmission, such as fast signal fading. The proposed RF-chain selection control scheme has three states, an active state with 2-chains active, an active state with 1-chain active, and a sleep state. A legacy WLAN AP would have only have one active state for transmitting and receiving data and an idle state. Fig. 5.1 depicts the state diagram of the proposed RF-chain switch control scheme.

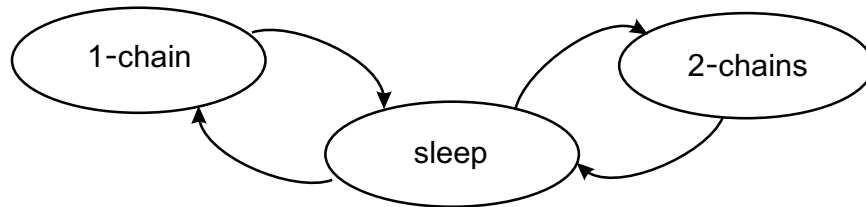


**Figure 5.1** – State diagram of the proposed RF-chain switch control scheme.

It has been confirmed that energy consumption can be saved up to 43% [130]<sup>1</sup>. In completion to the proposed energy reduction scheme, an analytical model is required to estimate the amount of energy, which can be saved. The model is helpful to judge the efficiency of the proposed energy consumption reduction scheme that is outlined in the following section.

### 5.3.2 Multi-antenna energy consumption model

The principal problem to design a Wi-Fi energy consumption model is that the energy consumption and transmission rate is not uniform. In addition, the WLAN performance depends on the dynamics of the wireless link conditions. Thus, the proposed model considers energy consumption that follows the effect of the transmission rate. An energy consumption estimation model for wireless sensor networks is the basis for the proposed Wi-Fi energy consumption estimation model. In [131], an energy consumption estimation model for WSNs was presented. The model considers a generic wireless transmitter and receiver. By multiplying the energy consumption of each transmitted data block the energy consumption can be estimated by the fraction of time for the block that was used [130]. In addition, new model

<sup>1</sup>A cooperative energy consumption reduction scheme has been proposed in [129].



parameters have been introduced to construct a model that is capable to estimate the total amount of energy consumption of a single Wi-Fi module. By consequence, the number of spatial streams (SS) has been added to estimate the RF-chain energy consumption as an additional model parameter, capable to consider the energy consumption of PHY/MAC processing on per bit bases. Eq. 5.2 describes the proposed energy consumption model that has been extended for WLANs, in particular for IEEE 802.11n based WLANs for different modulation schemes.  $E_N$  is the high-speed WLAN energy consumption per bit,  $N_{ss}$  is the number of chains (spatial streams) used,  $P_A$  and  $P_D$  describe the amount of energy consumption for the analog and digital components of the Wi-Fi module, respectively.  $T_{on}$  incorporates the active transmission time, whereas  $T_{tr}$  is the state transition time, and  $R_{mcs}$  describes the selected MCS index.

$$E_N = \frac{P_D}{R_{MCS}} + N_{ss} \left\{ \frac{(P_A T_{on} + 2P_{syn} T_{tr})}{L} + P_B \right\}. \quad (5.2)$$

The energy consumption for the entire transmission path is modeled by Eq. 5.3, where  $G_c$  defines the convolution coding gain of the modeled WLAN.  $N_f$  is the noise factor of the receiver, and  $\sigma^2$  is the spectral density of AWGN.  $P_B$  is given by

$$P_B = (1 + \alpha) \frac{4}{3G_c} N_f \sigma^2 \frac{(2^b - 1)}{b} \ln \left\{ \frac{4 \left(1 - 2^{-\frac{b}{2}}\right)}{b P_b} G_1 d^k M_l \right\}. \quad (5.3)$$

Eq. 5.4 makes the model simple and easy to apply, by adding the number of bits per m-QAM symbol, where  $b$  is given by

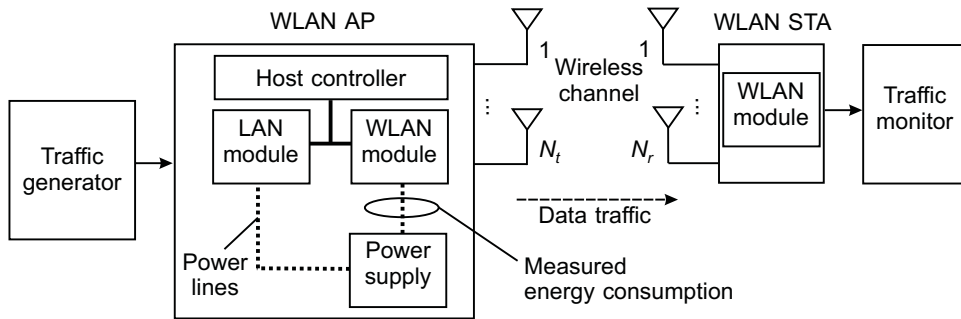
$$b = \frac{L}{B T_{on}}. \quad (5.4)$$

### 5.3.3 Analysis of the proposed RFCC scheme

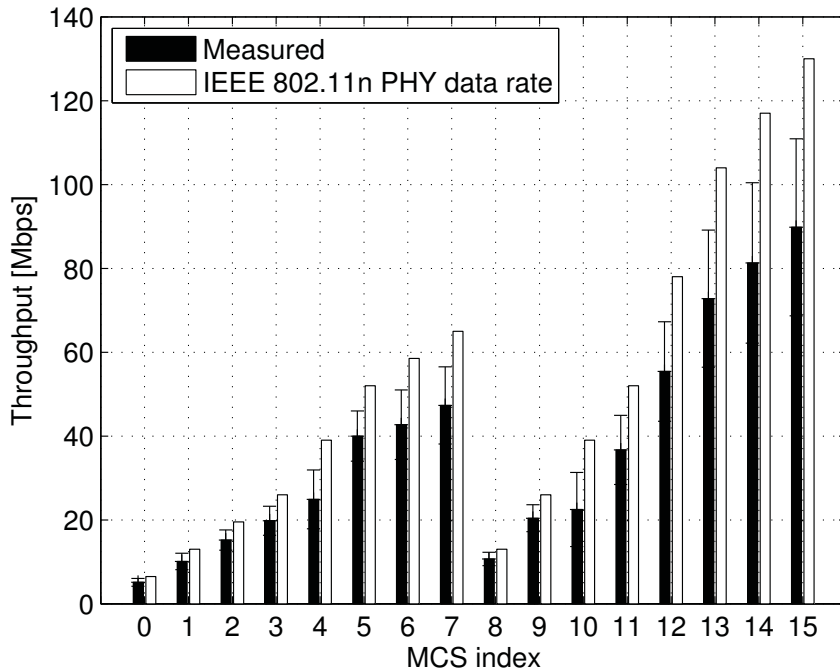
The RFCC scheme has been fully implemented as a new software module as part of the WLAN driver of an IEEE 802.11n Atheros<sup>TM</sup> based WLAN AP prototype. Fig. 5.2 illustrates the energy consumption measurement setup.

The RFCC implementation enables the verification of the chain control scheme under realistic conditions. Further, with the help of the measured system parameters, the proposed energy consumption model is verified. In Fig. 5.3, the IEEE 802.11n theoretical PHY data rate and the measured data rate of an IEEE 802.11n Wi-Fi module is illustrated. Increasing the MCS index changes the modulation rate from BPSK to 64 QAM with the highest data rate for a single spatial stream (MCS0-7). The use of two spatial streams increases the available PHY data rate (MCS8-15) as illustrated in the figure.

Fig. 5.4 depicts the modeled (Eq. 5.2, Eq. 5.3) and the measured energy consumption of the same IEEE 802.11n Wi-Fi module per bit [nW/bit]. It can be ob-

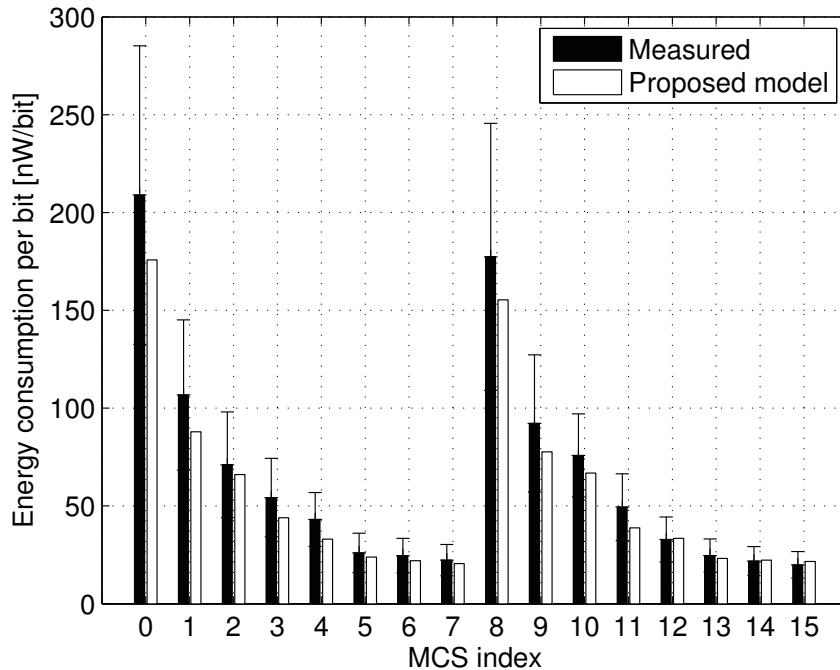


**Figure 5.2** – Energy consumption measurement setup (one-way directed traffic load).



**Figure 5.3** – Comparison of IEEE 802.11n theoretical PHY data rate and measured data rate of the tested IEEE 802.11n Wi-Fi module.

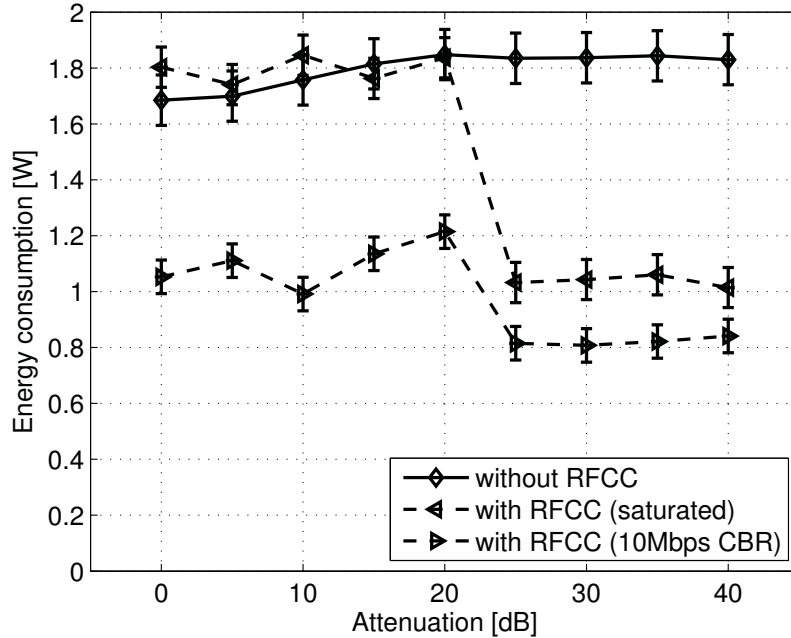
served that the measured energy consumption of the evaluated IEEE 802.11n Wi-Fi module can be predicted with the energy consumption model (Eq. 5.2, Eq. 5.3) with high accuracy. The energy consumption per bit reduces due to the energy supply



**Figure 5.4** – Results of the analytical energy consumption model verified with experimental data from the tested IEEE 802.11n Wi-Fi module.

of two RF-chains, which remains constant at 1.8 W and the increase of sent data packets. In Fig. 5.5 the measured energy consumption with and without RFCC is compared.

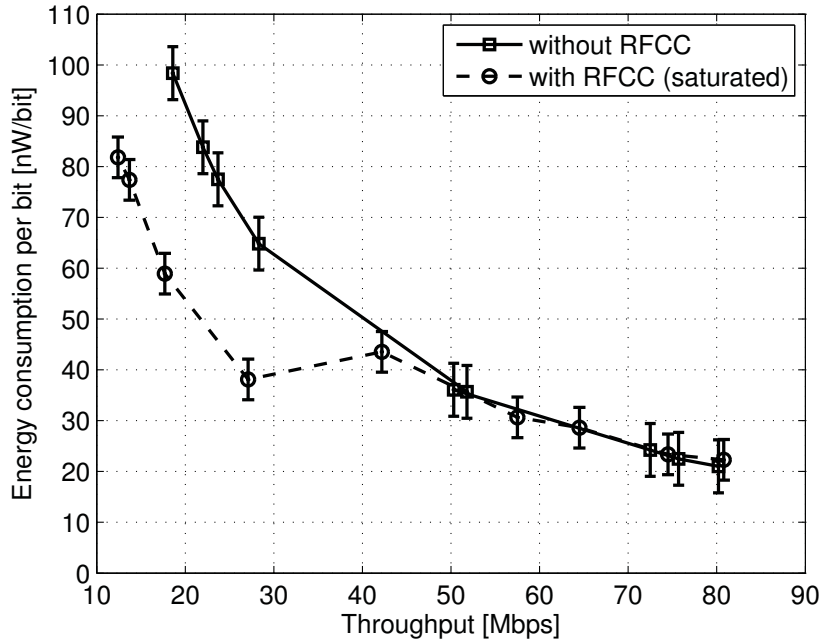
The following observations can be made. First, without using RFCC, the energy consumption is constant over a wide range of wireless link attenuation. This means even when the wireless link condition is poor, e.g., due to fast channel fading, a steady energy consumption is the result, which is observed at 1.8 W. In contrast, when the RFCC scheme is applied, the energy consumption of the tested IEEE 802.11n Wi-Fi module changes when the attenuation is higher than 20 dB, which emulates a poor wireless link performance. In particular, the energy consumption reduces from 1.8 W down to 1 W, which is a reduction of 43 % (saturated traffic). To verify the effectiveness of the RFCC scheme under dynamic traffic conditions, a different traffic model was evaluated. A low data rate arrival was selected with 10 Mbps and constant bit rate (CBR). It can be clearly observed in Fig. 5.5 that for small data traffic the IEEE 802.11n Wi-Fi module reduces its energy consumption significantly, from 1.0 W to 0.8 W.



**Figure 5.5** – Comparison of measured energy consumption with and without RFCC and different data traffic types.

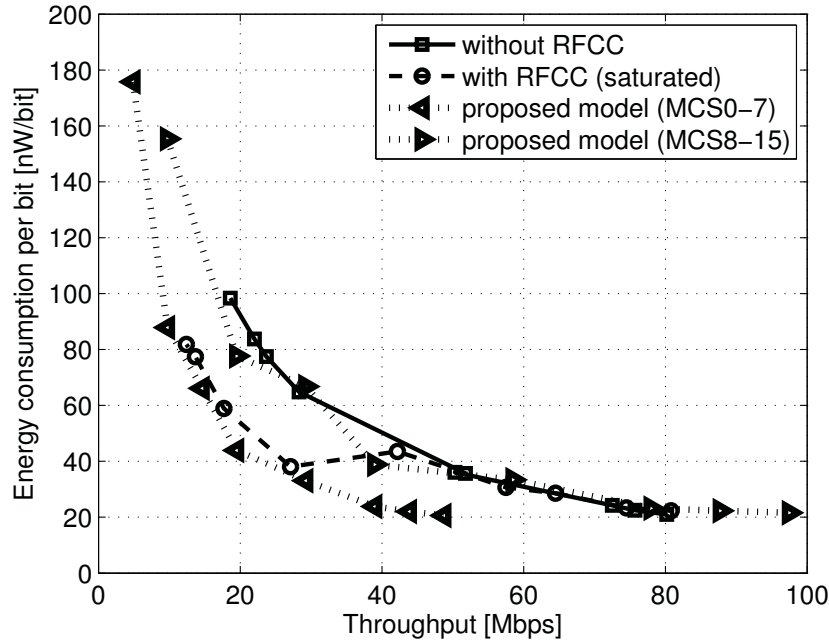
Finally, the measured energy consumption with and without RFCC vs. throughput is depicted in Fig. 5.6. It can be observed from the figure that in the low data rate regime (10-40 Mbps), the energy consumption without using RFCC is at 100 nW/bit and monotonically decreases with the increase of transmitted data packets, down to 20 nW/bit at 80 Mbps. In contrast, when the RFCC scheme is applied, the energy consumption in the low data rate regime is significantly reduced with 20 nW/bit until the high data rate regime (40-80 Mbps) is approached. A significant amount of energy consumption can be avoided by switching off multiple RF-chains in the IEEE 802.11n Wi-Fi module, i.e., in the WLAN driver software. Only one single RF-chain is used to transmit data in the low data rate regime, e.g., when the wireless link condition is poor, e.g., fast channel fading. The use of a single RF-chain in a MIMO system is somewhat similar to the *spatial modulation* presented in [125]. A comparison of the RFCC scheme and the spatial modulation scheme is part of the discussion at the end of this chapter.

Fig. 5.7 illustrates the measured energy consumption with and without RFCC vs. throughput. In addition, it is shown that the performance of the proposed energy consumption model (Eq. 5.2, Eq. 5.3) predicts the measured energy consumption with high accuracy.



**Figure 5.6** – Comparison of measured energy consumption with and without RFCC vs. throughput.

Two important observations related to the energy consumption can be made. First, the energy consumption model correctly predicts the characteristic when the RFCC scheme is applied for the low data rate regime (MCS 0-7). Second, the energy consumption model correctly predicts the characteristics of the high data-rate regime (MCS 8-15). It can be concluded that the model predicts the energy consumption with high accuracy compared with the measured data of both data rate regimes, including the energy consumption in the low data rate regime (MCS 0-7) as well as the high data rate regime (MCS 8-15). Under poor wireless link conditions, the RFCC switches to single antenna (SISO) transmission, which results in the lower energy consumption of the Wi-Fi module at 1.2 W, compared to case when the Wi-Fi module uses two RF-chains (MIMO), which consumes 2.0 W. Compared to the automatic rate control (ARQ), where MCS (single and multiple streams included) rates changes due to the transmission performance, the proposed RFCC scheme enables that the Wi-Fi module changes the state of the RF-chain to reduce the energy consumption. Finally, it is claimed that the proposed RFCC scheme reduces the total energy consumption in an IEEE 802.11n Wi-Fi module by 43% in case when the wireless link performs poorly, e.g., fast channel fading. By consequence,



**Figure 5.7** – Comparison of RFCC scheme and verification of the proposed energy consumption model.

other MIMO-OFDM WLANs, including IEEE 802.11ah, would also benefit from the reduced energy consumption when the RFCC scheme is applied.

## 5.4 Bibliographical notes

Transmitting data in short bursts at a high data rate modulation while increasing the duration of energy-saving idle or sleep sequences is one way of achieving high energy efficiency. However high data rate modulation schemes in combination with multi-antenna MIMO transmission schemes can lead to a significant amount of energy consumption in a Wi-Fi module and may not lead to energy efficiency improvements [128].

Further, when transmitting short data packets in an ideal environment it was observed that the use of a single antenna is most energy efficient [128]. The authors in [132] proposed an adaptive transmission rate control scheme for IEEE 802.11n. In addition to legacy auto rate control methods, the proposed scheme enhances the robustness of the communication by adding functions specific to IEEE 802.11n,

including the number of spatial streams, frame aggregation, and dynamic channel bandwidth allocation from 20 to 40 MHz. However, the proposed rate control scheme was not motivated by the demand of energy consumption reduction and as such the proposed scheme does not improve the energy efficiency of the Wi-Fi module. An energy management scheme for MIMO wireless terminals was proposed in [133]. The authors proposed a mechanism that supports the selection of transmitter antennas and RF chains, which could adaptively enabled or disabled to reduce the energy consumption of the Wi-Fi module. However, the energy efficiency of the entire Wi-Fi module was not evaluated thoroughly and information of the RF-chains remained unclear, e.g., if wireless channel conditions changes. Energy consumption reduction strategies for WLANs in idle state have been proposed in [129]. The proposed ROD was implemented using 2.4 GHz Wi-Fi hardware.

As a next step it was proposed to implement ROD functions in IEEE 802.15.4g/e sensor nodes. Furthermore, IEEE 802.11ah is a candidate for implementing ROD functions, e.g., to further optimize the energy consumption and to avoid inefficient use of energy, e.g., during idle state. In addition, cooperative schemes and sleep algorithms can further improve the energy consumption as outlined in [129]. Energy saving mechanisms are also discussed in the 3GPP for radio access network (RAN) equipment [134]. EnOcean [135] started to produce battery-less wireless sensors that harvest electricity through mechanical means (piezo, thermal). SIGFOX [136] proposes multi-kilometer ( $\leq 40$  km) wireless networks in the ISM band. The wireless system proposed by SIGFOX covers large areas in Europe at low data rate ( $\leq 1$  kbps) and low costs<sup>1</sup>.

Energy implications of being always connected are reported in [137], revealing that permanent internet connectivity of IoT devices lead to higher energy consumption; thus, diminish the positive effect of energy monitoring applications. Antenna selection schemes have been recently discussed. In particular, it has been reported that the selection of transmit antennas is beneficial in spatial modulation systems to improve the symbol error rate (SER) performance. A comparison of Euclidean distance optimized antenna selection (EDAS) and capacity optimized antenna selection (COAS) was reported in [138]. An improved significant SNR was reported, which outperform conventional multi-antenna MIMO systems with lower computational complexity.

## 5.5 Discussion and summary

### 5.5.1 Discussions

Enabling energy saving technology in S1G WLANs is not only about energy saving and cost reduction, but also adding new value to the new WLAN. It is essential to S1G WLANs that the energy consumption can be significantly reduced to compete with deployed WPAN systems. However, the energy consumption of S1G WLANs

---

<sup>1</sup>Modem costs  $\leq 1$  USD; annual subscription cost per device  $\leq 3$  USD.

is unknown due to the non-existing and certified IEEE 802.11ah Wi-Fi hardware. Thus, the analysis of the energy consumption of IEEE 802.11ah Wi-Fi modules can only be approximated, which would be in the same regime similar to the tested IEEE 802.11n Wi-Fi hardware. Alternatively, the testing of a single IEEE 802.11n Wi-Fi module was proposed. The tested IEEE 802.11n Wi-Fi module offers modulation schemes and multi-antenna use similar to IEEE 802.11ah. The implementation of the energy consumption reduction scheme in an IEEE 802.11n WLAN AP prototype has proven that the proposed RFCC scheme is a promising solution, which enables the saving of a significant amount of energy. By consequence, the amount of energy consumption can be reduced for IEEE 802.11ah in a similar regime. In addition, IEEE 802.11ah offers new MAC functions which would further benefit from the proposed RFCC scheme. For instance, IEEE 802.11ah long-range transmission schemes, such as the repetition mode (MCS 10), could benefit from a dynamic RF-chain switch to maximize the wireless coverage range.

Currently, there is a strong demand to reduce the energy consumption in other wireless communication systems, including cellular base stations. Therefore, the demand for energy consumption reduction schemes in WLAN APs is evident. In particular, the wide spread of countless numbers of WLAN APs in offices is a good example. A significant energy conservation potential can be observed in these WLAN deployments. Radio-on-demand (ROD) proposes to switch on/off a WLAN AP during the passive state. This is somewhat challenging due to the fact that the WLAN AP should always be accessible for WLAN STAs. However, this has been changed with the maintenance mode in IEEE 802.11v, where WLAN APs can be off-line for a certain time period, announced to the associated WLAN STAs. The proposed energy conservation mechanism only affects the active state, so there is no need to modify the IEEE 802.11 WLAN protocol. The proposed mechanism can be implemented as a simple enhancement to the WLAN driver, which have been proven to be accurate in an ROD WLAN AP [130]. A combination of low-complex Tx antenna selection schemes [138] and the proposed RFCC is beneficial to improve both transmission performance and energy efficiency. In particular, the combined scheme would be beneficial for both, the S1G WLAN AP and the STAs. Note that the proposal includes the Tx and Rx side.

Finally, the RFCC scheme is compared with the so called *spatial modulation* scheme. In [125] the authors argue that spatial modulation consists of a single RF-chain that powers a single antenna that is frequently changed within an antenna array. The use of a single RF-chain in a MIMO system reduces the static energy consumption to a minimum. Further, the spatial modulation by using different antennas adds additional information that relates to the antenna that is used for the transmission of the modulated signal (increase in channel capacity compared to SISO). A main drawback is the limitation of the spatial modulation channel capacity that cannot utilize the MIMO gains of multiple antennas. The data rate of spatial modulation is sub-optimal. Fast antenna switching, synchronization, and training are critical to spatial modulation. In contrast, the proposed RFCC is a simple but efficient 3-state model in which a single RF-chain is powered on if the



wireless link condition is bad (the RFCC approach can be understood as a sub-set of a full-MIMO system in which each antenna has its own RF-chain). If the wireless transmission over multiple antennas is inefficient the RFCC scheme switches to a single antenna (robust single-stream MCS rates). In contrast to legacy Wi-Fi systems where all RF-chains remain powered on, the RFCC scheme has only a single RF-chain powered on (single stream MCS). At this stage RFCC does not switch among the antennas such as in spatial modulation. In fact, switching among antennas would further deteriorate the throughput because some antenna may be associated with bad channel conditions. If the wireless link condition improves, RFCC switches to MIMO and uses multi-antenna which achieves high data rates. Although all RF chains are powered on when MIMO is activated, the high data rate increases the energy efficiency. It can be concluded that RFCC and spatial modulation can be combined to achieve increased data rate, e.g., by powering on additional RF-chains. Further, a combination of RFCC, spatial modulation and codebook selection may further improve the coverage range in Wi-Fi sensor networks.

### 5.5.2 Summary of the chapter

Future IEEE 802.11ah-based WLANs have to ensure a significant reduction of energy consumption of Wi-Fi hardware to succeed in the wireless market. In contrast to legacy WLANs, WPANs have already demonstrated a successful realization of efficient energy conservation strategies to prolong the battery lifetime of WPAN sensor nodes. S1G WLANs will need to enable similar energy consumption reduction strategies, e.g., to realize battery lifetimes of  $\geq 10$  years. In this chapter, a reduction of energy consumption was proposed for multi-antenna WLANs. Multi-antennas are used in S1G WLANs, which have shown a significant energy reduction potential. It is the aim of this proposal to mitigate any unnecessary energy consumption during the active communication state of a WLAN AP. If a simple SISO communication is preferable in contrast to MIMO, e.g., due to inefficient channel conditions, the proposed method will select active RF-chains to reduce the energy consumption of unused RF-chains in the Wi-Fi module.

Currently, no IEEE 802.11ah Wi-Fi module is available, e.g., to evaluate precisely the energy consumption of such Wi-Fi modules. To overcome this problem, it was proposed to study the energy consumption of a single IEEE 802.11n Wi-Fi module. This Wi-Fi module was evaluated and the energy consumption was reported for a  $2 \times 2$  MIMO-OFDM system. A significant amount of energy is consumed by the RF-chains in a multi-antenna system, even when the wireless channel performs poorly. It was proposed to reduce the number of RF-chains under poor wireless channel conditions. The proposed RF-chain control (RFCC) reduces the number of active RF-chains when the wireless link performs poorly, e.g., low SNR, retransmissions.

The RFCC was implemented and evaluated in a WLAN AP prototype. The evaluation results have shown a significant energy reduction at 43%. Additionally, a novel analytical Wi-Fi energy consumption model was developed to verify the

evaluation results. The proposed model allows the estimation of energy per bit and for different modulation schemes (MCS index). The evaluation has demonstrated that the model can be used to estimate the energy consumption with high accuracy. By consequence, the model can be applied to other WLAN protocols, including the future IEEE 802.11ah WLAN protocol. In particular, the energy consumption model can be used to predict the energy consumption of IEEE 802.11ah modules with high accuracy.

## Chapter 6

# Wireless coexistence

This chapter is focused on the coexistence problems in S1G WLANs and WPANs. The challenge of wireless *coexistence*<sup>1</sup> in the sub-1 GHz ISM-band<sup>2</sup> results in similar assumptions and remedies as for the coexistence problems in other ISM-bands, e.g., in the 2.4 GHz ISM-band. The media access is contention oriented, which can result in highly congested links with large number of packet collisions. However, a main difference is the presence of other wireless passive communication systems in some regulatory domains, such as a highly dense deployment of radio frequency identification (RFID) devices, which can result in congested wireless channels. It requires careful consideration of the presence of passive systems and how to protect these narrow-band systems from concurrent wireless transmissions on the same spectrum due to the limited system resources of RFIDs, e.g., buffer size and battery lifetime.

Coexistence is mainly referred as a description of how at least two independent systems - here wireless systems - can work in stable regimes, i.e., without unwanted system behaviors. For instance, wireless systems, such as WLAN and WPANs in the 2.4 GHz ISM-band have exhibited significant instabilities when both systems coexist, i.e., same or neighbor wireless channels. Although these systems should coexist without interfering each other, indeed wireless data transmission performance has indicated severe performance limits due to the *unslotted*<sup>3</sup> media access.

---

<sup>1</sup>Coexistence in the licensed band, e.g., LTE, is less interfered due to the use of a centralized media access synchronization scheme. In this thesis, the coexistence problems and potential solutions are described for the unlicensed ISM-band only.

<sup>2</sup>In this thesis, the 915 - 928 MHz radio-band is in the focus of the spectrum observations, considering the Japanese regulatory ARIB STD T-108 [20].

<sup>3</sup>Slotted media access can be found in *centralized* cellular systems, such as TDM. Legacy WLANs and WPANs use an unslotted, *distributed* media access reservation scheme. However, CSMA and polling allow the indication of a wireless transmission; thus, may indicate the media access for a certain time period.

As for sub-1 GHz wireless systems, some regulators<sup>1</sup> allow wireless communication in sub-1 GHz ISM-band without defining details of the used modulation scheme. Other wireless system parameters may be defined for certified wireless access, such as carrier frequency  $f_c$ , channel bandwidth  $BW$ , maximum sending power  $P_{tx}$ , antenna gain  $G_a$ , duty-cycle<sup>2</sup>, spectrum mask. Sub-1 GHz device manufacturers are not restricted to implement their own communication protocols and radio modulation schemes. In addition, media access schemes may be defined, such as *listen before talk* (LBT). Although media access may be only granted to *certified* communication devices, coexist problems may occur among wireless devices from different vendors and communication systems.

## 6.1 Interference in S1G ISM radio-bands

Coexisting problems may result in unwanted data packet loss due to retransmissions, e.g., occurred by collisions with concurrently sent data traffic. In addition, unsolved packet retransmissions may drain the battery; thus, significantly reduces the battery lifetime. A reliable wireless communication link is essential in energy efficient wireless sensor networks, such as S1G WLANs and WPANs. Thus, retransmissions due to interference problems, such as packet collisions, have to be mitigated. It is essential to detect packet collisions to optimize the wireless transmission so that sending power can be saved and battery lifetime can be prolonged. Under unstable conditions, such as many packet collisions, communication should backoff for a certain time period, and to trigger network remedies, as discussed in the following. In this chapter, opportunities and challenges in wireless sensor networks are reported. Proposals and guidelines are outlined to enable the deployment of next generation wireless sensor networks. It includes a practical perspective on the configuration aspects of S1G WPANs and WLANs. In particular, the detection of packet collision is from relevance to reduce the energy consumption in wireless sensor networks.

### 6.1.1 S1G WLAN to WPAN coexistence

The sub-1 GHz ISM radio-band allows the concurrent transmission of wireless signals emitted from different wireless systems on the same spectrum. Similar to the coexistence problems of WLAN and WPAN devices in the 2.4 GHz ISM radio-band, identical coexistence symptoms are found in the sub-1 GHz band. Differences are that the sub-1 GHz narrow-bands allow a large number orthogonal channels; thus, increasing the number of potential overlaying wireless networks. However, significant coexistence problems still exist within the disjoint channels and would have a

<sup>1</sup>Here regulators are refereed to state governments, official license holders, etc.

<sup>2</sup>Duty-cycle describes the time period in which a wireless communication device uses actively the wireless media for data transmission. For instance, a 10% duty-cycle per hour results in 360 s use of the wireless media. After using its 10% of its duty-cycle the device may need to wait for further transmission until the next cycle, e.g., next hour.

severe impact of the WLAN and WPAN based sensor devices in the sub-1 GHz ISM radio-band. Yuan *et al.*, [139] discussed the problems of adapting CCA thresholds in IEEE 802.15.4 wireless sensor networks in the presence of IEEE 802.11 transmissions operating on the same spectrum. The authors argued that in the presence of heavy traffic load of IEEE 802.11b/g transmissions, IEEE 802.15.4 suffer from a significantly reduced channel access probability due to the asynchronous sending power among WLANs and WPANs. Results were obtained through simulation studies. It is remarkably that the authors reported the mitigation of inhibition loss<sup>1</sup> by changing the CCA threshold in IEEE 802.15.4. However, the authors stated that packet loss due to packet collisions among IEEE 802.11b/g and IEEE 802.15.4 could not be reduced.

Woehrle *et al.*, [141] reported on the link characteristics in the 868 MHz ISM-band and the link properties of IEEE 802.15.4 WSNs. This radio-band has been found noise-free. However, a dense deployment of 100 nodes result in large variations in the performance characteristics, which have to be considered when a reliable routing protocol must be designed. Multi-path and the presence of humans adding to the dynamics of wireless channels in the 868 MHz radio-band.

Fig. 6.1 illustrates the coexistence problems in the sub-1 GHz ISM radio-band. In particular, the Japanese 920 MHz radio-band is limited by the LTE systems and requires that S1G systems do not interfere with LTE uplink transmissions (890 - 915 MHz). Within the S1G radio-band, other wireless systems are allowed to transmit radio signals according to ARIB STD-T 108 [20]. The wireless systems include passive RFIDs, proprietary sensor devices, and certified Wi-SUN devices.

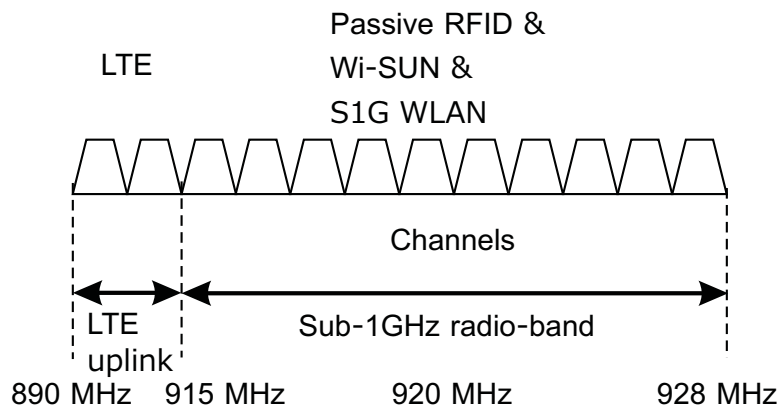


**Figure 6.1** – Coexistence problems in the sub-1 GHz ISM radio-band.

<sup>1</sup>Inhibition loss is classified as channel access failure due to increased number of retransmissions [139, 140].

### 6.1.2 S1G WLAN to UHF-RFID coexistence

Ultra-high frequency radio frequency identification, or so called UHF-RFID (at the 920 MHz radio-band), are widely spread and used in many applications. The UHF-RFID contains an UHF-RFID reader unit and an UHF-RFID tag. Well-known applications are medical items, carton boxes, libraries, farming, and logistics. Usually a hand-reader device is used to obtain the RFID data. RFID reader also implemented in cellular phones and smart phones. Passive RFID tags are certified for 10 mW, 250 mW, and 1 W. Active RFID tag systems are specified for 1 mW and 10 mW.

From strong interest is the coexistence of passive RFIDs and S1G WLANs. This is particularly true for Japan, where a widespread deployment of RFID in the 920 MHz is in the focus of potential coexistence problems when S1G WLAN devices will be shipped in the near future. Passive RFIDs are deployed in logistics and shopping centers. Hence, the presence of RFIDs must be considered and the coexistence with S1G systems must be carefully planned. Initially, RFID systems consist of cheap and easy to deploy passive devices with a very short wireless range ( $\leq 1$  m). Usually an emitted signal is reflected by the RFID tag and received by a data collector (RFID reader). Active RFIDs allow additional data storage, including authentication and execution of data mining procedures [142].

One solution for the coexistence of RFID and S1G WLANs can be obtained from the observation of the coexistence issues among WPANs and WLANs. RFIDs have similar bandwidth characteristics as for WPANs and Wi-SUN devices. The channel bandwidth is at 200 kHz compared to S1G WLANs with 1 MHz. Similar packet collision detection and classification schemes can be applied to RFIDs to mitigate unwanted inter-system interference. Further, in some locations, where a dense deployment of RFID is present, a proposed solution may consider a centralized coexistence mechanism. The idea is similar to the utilization of TV white space for WLANs, in which a centralized data base (DB) may contain all relevant devices. In the case of a dense number of RFIDs, a DB may store all RFIDs, which need to be protected against S1G WLANs. The DB will notify S1G WLANs about the channels that can be used. For instance lower spectrum bands can be reserved for RFID only, whereas higher spectrum bands can be used by S1G WLAN data transmission. Fig. 6.2 depicts the proposed sub-1 GHz radio-band sharing option between passive RFIDs (lower radio-band) and S1G WLANs (higher radio-band).

However, requirements on the duty cycle are different. In particular, RFIDs have characteristic short burst data, but require robust and error-free transmissions to avoid retransmissions that would otherwise result in rapid battery power depletion.

## 6.2 Packet collisions and collision patterns

To report on the observed interference problems in the sub-1 GHz radio-band, the proposed spectral-time sensing (STS) method was applied. For the STS, USRP 2

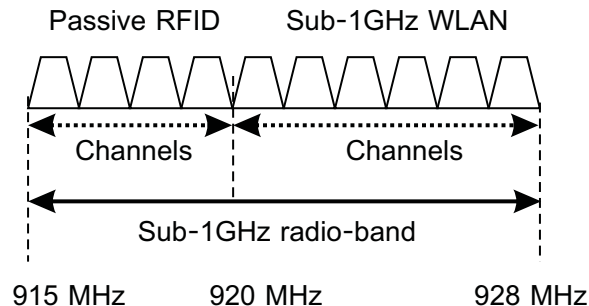


**Figure 6.2** – Proposed sub-1 GHz radio-band sharing between passive RFIDs (lower radio-band) and S1G WLANs (higher radio-band).

was utilized, which allows a high resolution spectral sensing over time. The results have been converted in batch-mode (off-line). Basic classification of interference in WLANs can be found in [143]. In addition to Sheth [143], the study focuses on new interference mitigation strategies that utilize MIMO functions. Rate adaptation schemes, such as WLAN *auto rate fallback* (ARF), may exacerbate the packet loss due to longer transmission time (*airtime*) of the sent packet [143]. Further, it is important to judge the channel characteristics for proposing coexistence schemes and interference mitigation strategies. Following the (*channel reciprocity principle*) the interference assumptions (MIMO channel) are valid for both, downlink and uplink as stated in [144]. When applying the reciprocity principle the downlink channel can be estimated from the uplink channel from transmissions at the same frequency region. For a MIMO link between terminal A and terminal B the wireless channel conditions for uplink  $\mathbf{H}_{AB}(f)$  and downlink  $\mathbf{H}_{BA}(f)$  are given by [144, 145]

$$\mathbf{H}_{AB}(f) = \mathbf{H}_{BA}(f) \quad (6.1)$$

## 6.3 WLAN/WPAN coexistence in the S1G ISM-band

### 6.3.1 Spectrum characteristic of S1G WLAN signal

The utilization of an SDR-based IEEE 802.11ah prototype has the advantage that further system insight can be obtained. The SDR platform allows the sending and receiving of wireless traffic, which are somewhat in compliance to the IEEE 802.11ah draft specifications. In addition, the SDR platform allows the monitoring of spectrum events by modifying the SDR setup. The proposed spectrum sensor (Section 3.4.3) allows the record of spectrum events in the 900 MHz radio-band. In particular, the IEEE 802.11ah WLAN prototype uses the carrier frequency  $f_c = 923$  MHz. Data transmissions can be monitored, such as ICMP messages, including

data and ACK frames. Fig. 6.3 illustrates the spectrum characteristics of a WLAN-DATA packet.

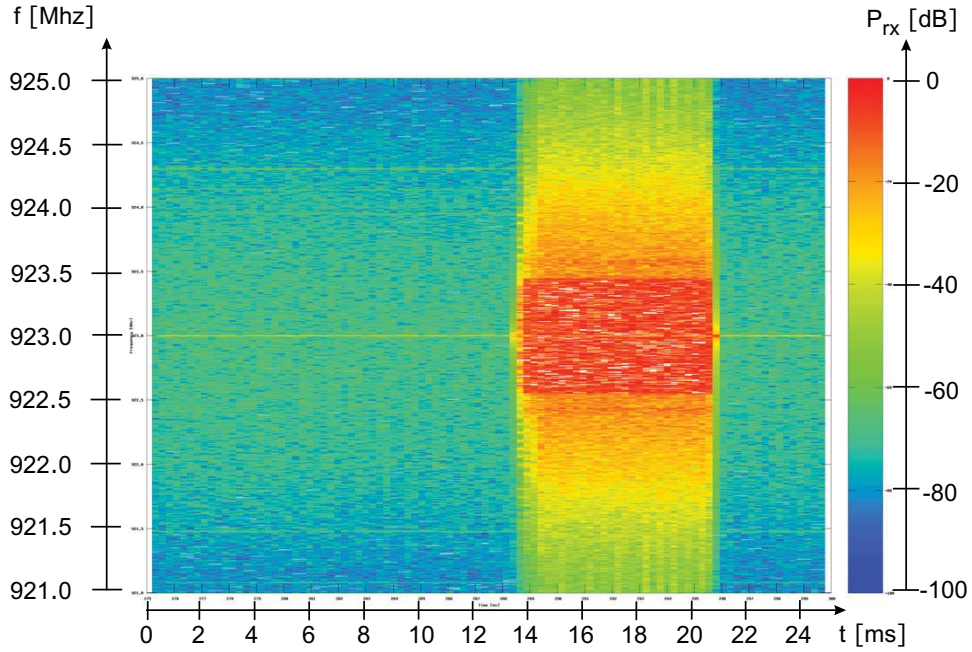


**Figure 6.3** – 923 MHz WLAN-DATA packet (sub-1 GHz prototype) spectrum characteristic.

It was found that this kind of new spectrum information has significant advantages. Spectrum analyzer can only report for short time events. In addition, low resolution and memory capacity are typical characteristics of a spectrum analyzer. Moreover, spectrum analyzer tools are very costly and provide only a limited function of modifying or manipulating data information. In contrast, the proposed spectral-time sensor provides high resolution spectrum information at low implementation costs as demonstrated in Fig. 6.3. The snapshot of the spectrum event demonstrate the received energy of a single IEEE 802.11ah WLAN data packet (800 B, MCS 4,  $N_{ss} = 1$ ) with the carrier frequency  $f_c = 923$  MHz in a time period of 6 ms (the snapshot reports about the time duration of 25 ms). In addition, the power density can be observed in Fig. 6.3. The coherence bandwidth ( $\pm 3$  dB) is between 922.5 and 923.5 MHz with residual power between 921 and 925 MHz.

### 6.3.2 Spectrum characteristic of S1G WPAN-DATA signal

To evaluate the spectral coexistence characteristics of a WLAN signal in presence of a WPAN signal, two WPAN devices were configured to operate on the same



spectrum at  $f_c = 923$  MHz. As WPAN devices, the Texas Instruments modes CC1123 were configured to transmit with  $BW = 200$  kHz. As a traffic flow, a continuous data sending rate was selected with packet size of 50 B. To evaluate on the spectrum characteristics of a WPAN signal the same method as described in Section 6.3.1 was applied. Fig. 6.4 illustrates the spectrum characteristics of a WPAN-DATA frame.

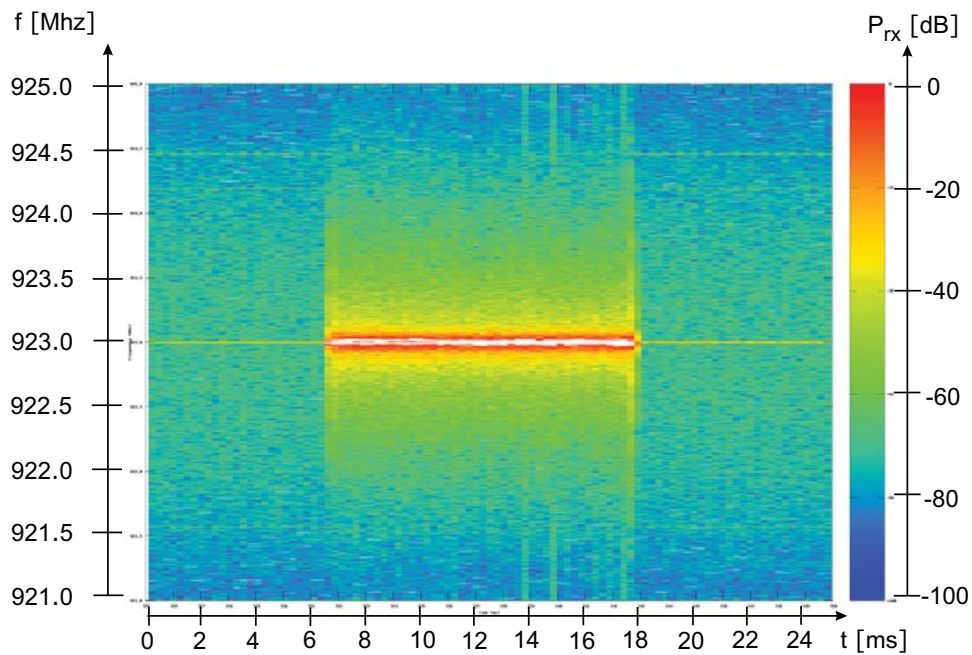


Figure 6.4 – 923 MHz WPAN-DATA frame (Ti) spectrum characteristic.

The figure demonstrates the received WPAN signal by the spectral-time sensor in a time duration of 10 ms. The coherence bandwidth ( $\pm 3$  dB) is in a range of 922.9 to 923.1 MHz. The entire residual power can be observed in a range of 921.5 to 924.5 MHz. The following observations are extracted from the figure when comparing WLAN (Fig. 6.3) and WPAN (Fig. 6.4) signals:

1. The WLAN signal appears in a shorter time frame than the WPAN signal. Here the WPAN signal was selected at a low bit rate; thus, the transmission results in a longer *airtime*. This has the effect that WLAN and other wireless systems will backoff from transmission until the WPAN signal transmission ends. Lower average transmission rate is the result when WPANs sent at low bit rates, e.g., to support reliable transmission among WPAN nodes.
2. The WPAN signal indicates a significant concentration of the sending power within the coherence bandwidth that is  $P_{tx} = 20$  mW compared to the WLAN

signal with  $P_{tx} = 1\text{ mW}$ . Although the sending power of the WPAN signal is significantly larger compared to the WLAN signal, the emitted power is only concentrated in a narrow-band of 200 kHz. The spectral observations reveal the significant asymmetry of the spectral power density distribution among WLAN and WPAN signals. This observation is of importance when optimal energy detection (ED) schemes need to be developed. The WPAN signal is more robust and harder to detect for WLANs (energy detection function in WLANs) due to its narrow-band characteristic.

3. The WLAN signal indicates a much larger residual power emission, which affects the neighbor channels. Thus, coexisting schemes based on channel planning have to consider this effect. Wider channel distances may be required to avoid adjacent-channel interference (ACI).

In the following observed data packet collisions are reported.

### 6.3.3 WLAN-DATA to WPAN-DATA collision pattern

To evaluate on the coexistence between WLANs and WPANs operating on the same spectrum, two wireless systems were configured, a WLAN (the IEEE 802.11ah WLAN prototype consisting of AP and STA) and a WPAN (consisting of 2 WPAN nodes, TI 1123). Without any modifications on the PHY and MAC parameters, both systems sent a continuous data transmission, WLAN at 800 B and WPAN at 50 B. To evaluate on the spectrum characteristics of the WPAN and WLAN signals, the same method as described in Section 6.3.1 was applied. Interestingly, interference has been found for different transmission patterns among WLAN and WPAN. First, a packet collision is reported that starts with the WPAN DATA frame that is interfered by a WLAN DATA frame. Note that the effect of the collision was also reported as CRC-errors in the TI module. The location of CRC-errors in a data frame pointed to the packet collision in the same way as it was observed with the help of the spectral-time sensor (when the WPAN data frame was interfered at the beginning, only the first data were reported to be incorrect. When the WPAN data frame was interfered at the end of the data frame, only the last data have been reported to be incorrect). This is an important observation, because it can simplify the collision detection scheme when external sensors are proposed to be used, e.g., to detect such packet collisions (the CRC information may sufficient enough, e.g., to dynamically adapt WLAN protocol parameters, such as inter-frame spacing). Fig. 6.5 exhibit the observed collision pattern of a WPAN-DATA to WLAN-DATA collision, after emitting the WPAN signal.

Next, an observed collision has been found that starts with the WLAN data packet that is interfered by the WPAN packet. It was observed that the packet collisions occurred at any location during the transmission.

Fig. 6.6 depicts the collision pattern of a WLAN-DATA to WPAN-DATA collision, after emitting the WLAN signal.

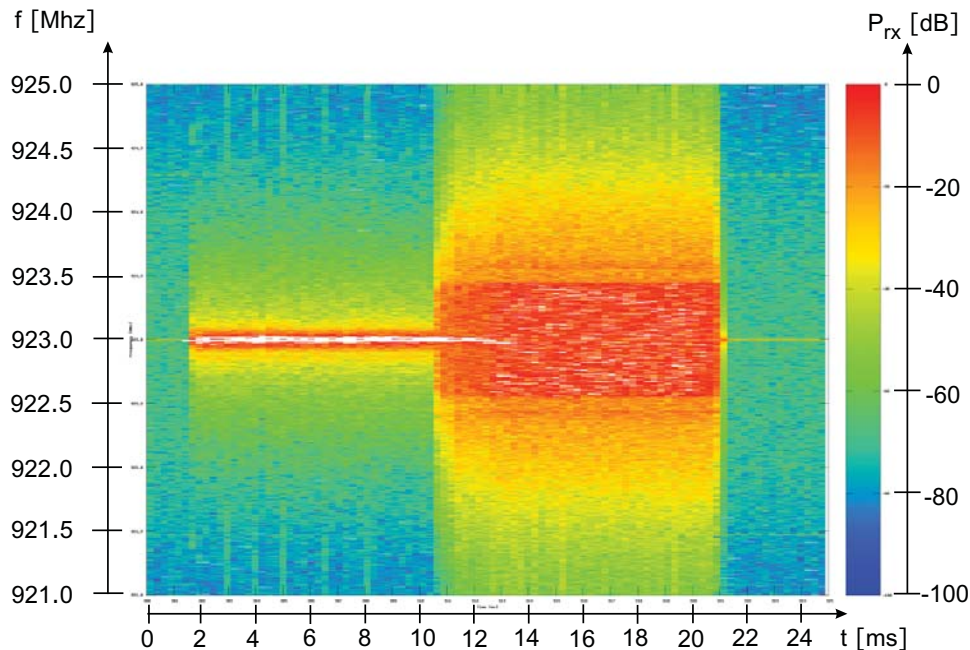


**Figure 6.5** – Spectrum characteristic of WPAN-DATA to WLAN-DATA collision.

Note that the CSMA/CA of the IEEE 802.11ah WLAN prototype was only in a state, which provide a simple media access scheme. However, it is stated that the WPAN module was an COTS product, which would be considered to be able to operate with a functioning LBT operation. However, this spectrum observation demonstrate that the media access control is inefficient. In addition, the media access of the WPAN module seems to be more aggressive, e.g., to maintain data rate even in the presence of other wireless systems (selfish-node).

#### 6.3.4 WPAN-DATA to WLAN-ACK frame collision pattern

The result of the WLAN to WPAN coexistence observation has demonstrated a significant number of collisions between WLAN-ACK frames and WPAN-DATA frames. This is classified in the following as *WPAN-DATA to WLAN-ACK* collision pattern. This collision pattern has importance to the S1G WLAN transmission. It will result in unwanted retransmissions of the WLAN-DATA packet due to the missing WLAN-ACK and the timeout sequence in which the WLAN-ACK would otherwise appear at the destination node. WPAN-DATA to WLAN-ACK collision easily occur due to the narrow-band energy characteristic of the WPAN-DATA, which can be easily overheard by the surrounding WLAN STAs. Thus, it is essential

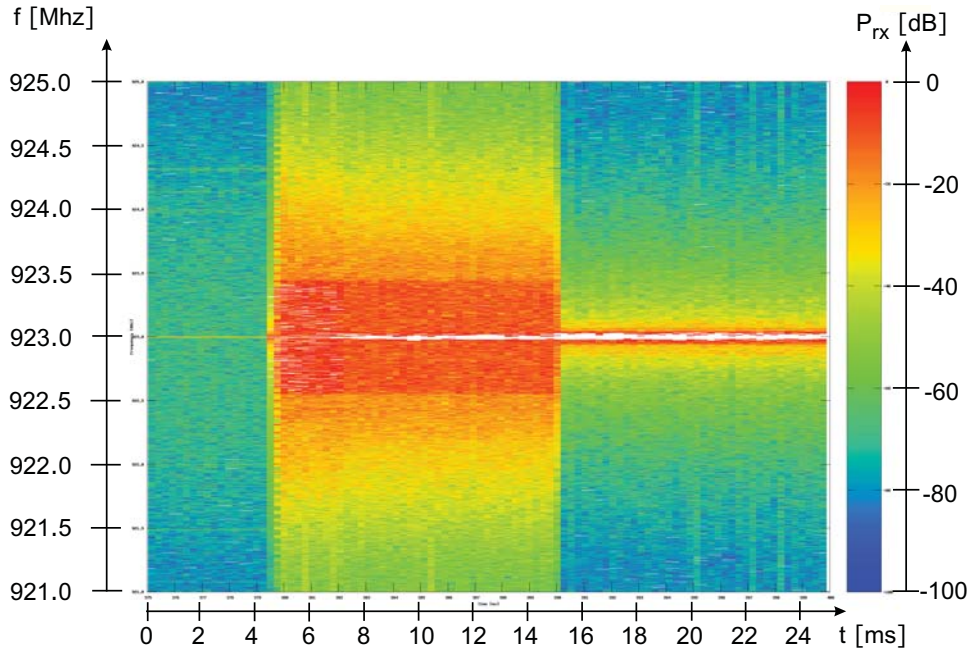


**Figure 6.6** – Spectrum characteristic of WLAN-DATA to WPAN-DATA collision.

to examine WPAN-DATA to WLAN-ACK collision patterns to mitigate the number of WLAN-DATA retransmissions. Fig. 6.7 illustrates the observed collision pattern of a WPAN-DATA to WLAN-ACK collision in the sub-1 GHz radio-band.

### 6.3.5 Observed collision patterns

The observed spectral collision patterns using so called spectral-time sensing (STS) method has indicated various collision patterns among WLAN and WPAN packets in the sub-1 GHz radio-band. Fig. 6.8 summarizes the statistical evaluation occurrence between sub-1 GHz WLAN prototype and 920 MHz WPAN Ti module (transmitted packets and retry count). To evaluate the performance of the carrier sense detection of the IEEE 802.11ah WLAN prototype, the carrier sense threshold was modified (0.05 to 0.75). 1000 packets (100 B) were submitted as constant ICMP data packet flow. Fig. 6.8 exhibits that a significant large number of retry counts (retry count = 1) occurred when WPAN was concurrently transmitting. The number of retries monotonously decreases with the observed retransmission count value, starting from 2 and ends with 7 retries as shown in Fig. 6.9. After 7 retries

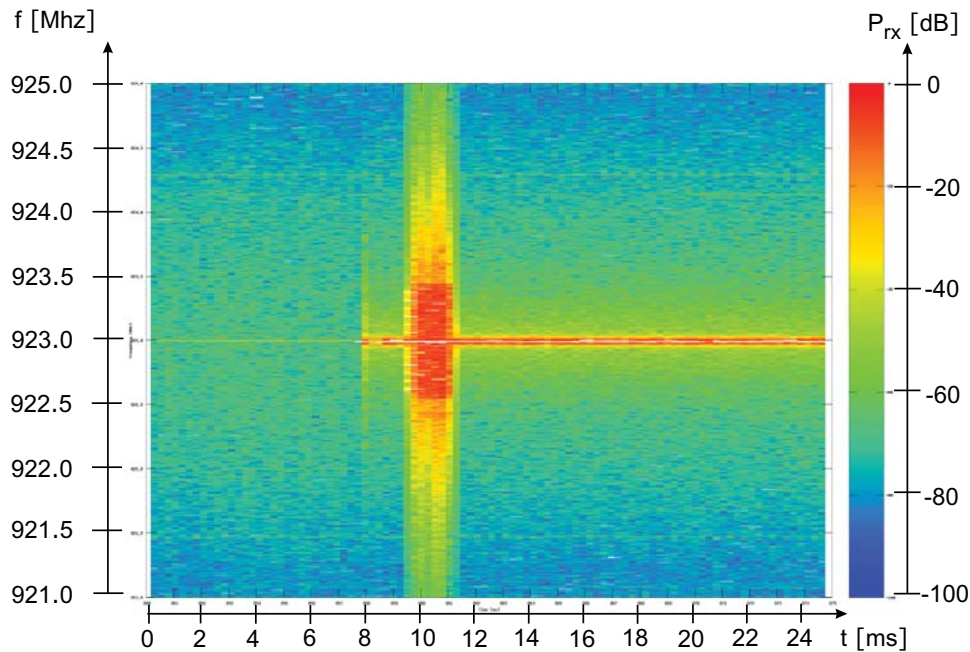


**Figure 6.7** – Spectrum characteristic of WPAN-DATA to WLAN-ACK collision in the sub-1 GHz radio-band.

WLAN packets were discarded. Two aspects are important. First, the retry count needs to be small to avoid any retransmissions of data packets to prolong the battery lifetime. Second, discarded packets need to be minimal to avoid data loss. The threshold at 0.5 gives the best trade-off of reduced transmission and minimal packet loss (discarded packets).

Fig. 6.9 summarizes the statistical evaluation occurrence between sub-1 GHz WLAN prototype and 920 MHz WPAN Ti module (retry count only).

### 6.3.6 Packet collision and collision detection

An energy-based signal detection scheme is proposed to report on transmitted WLAN and WPAN data frames. It uses the envelope of received wireless signals to identify potential signal features, such as detected packet collisions. In the following it is proposed to utilize the observed packet collisions of S1G WLAN and WPAN packets. The observed packet collisions are used to realize so called *spectral templates*. Spectral templates use time vs. spectral density (spectral power) to *classify* a particular event, such as WLAN-DATA to WPAN collision. Fig. 6.10 depicts the proposed packet collision classification.

Fig. 6.11 depicts the proposed packet collision classification of WLAN-ACK.



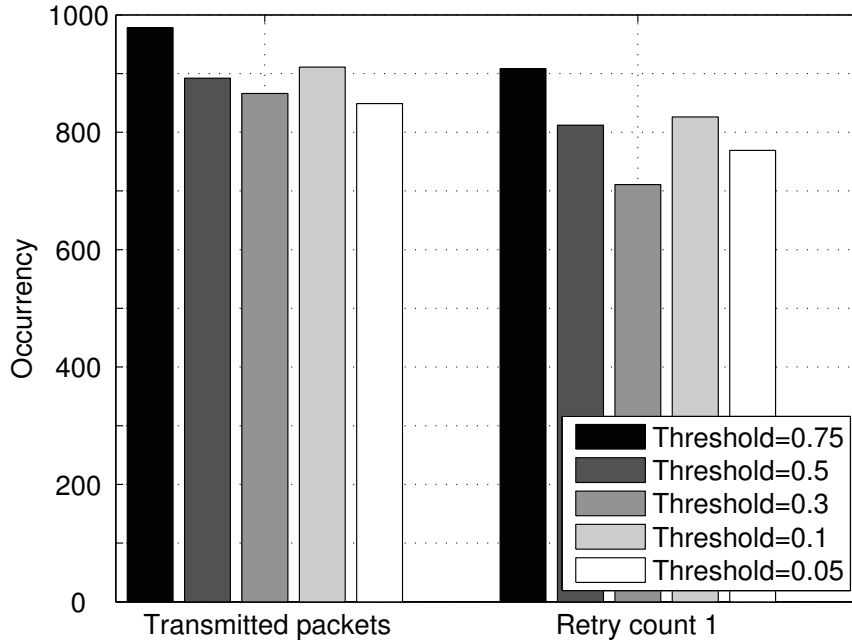


**Figure 6.8** – Statistical evaluation of collision occurrence between sub-1 GHz WLAN prototype and 920 MHz WPAN Ti module (transmitted packets and retry count).

Collision classification considers the detection of:

1. Data frames collisions (WLAN-DATA, WPAN-DATA) =  $DATA_{err}$ .
2. ACK frames collisions (WLAN-ACK, WPAN-DATA) =  $ACK_{err}$ .

The occurrence of data signals is classified in:

1. Correct signal reception.
2. Incorrect signal reception ( $DATA_{err}$  or  $AKC_{err}$ ).

Incorrect reception may be corrected by FEC algorithm, which does not result in packet loss. To classify the collisions, the so called fingerprinting method can be applied. Packet collision patterns are monitored and classified as finger prints and stored in a data base [146]. In an on-line phase the classification can be executed. In addition a dynamic confidence can be calculated, which announce the accuracy of the detected collisions [147, 148].

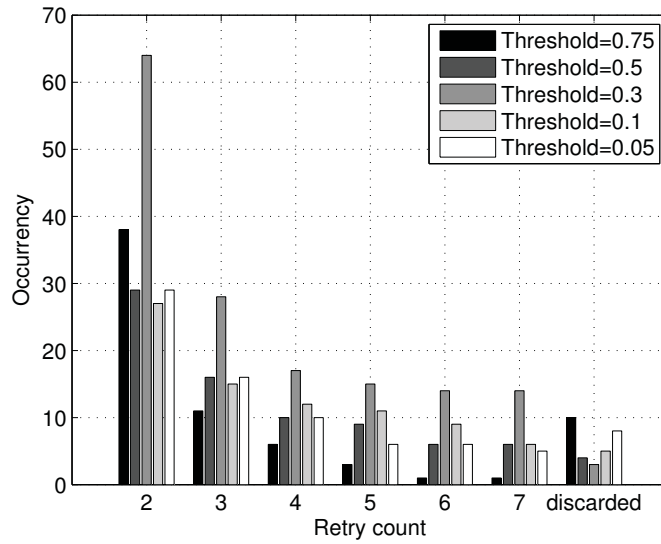


**Figure 6.9** – Statistical evaluation of collision occurrence between sub-1 GHz WLAN prototype and 920 MHz WPAN Ti module (retry count only).

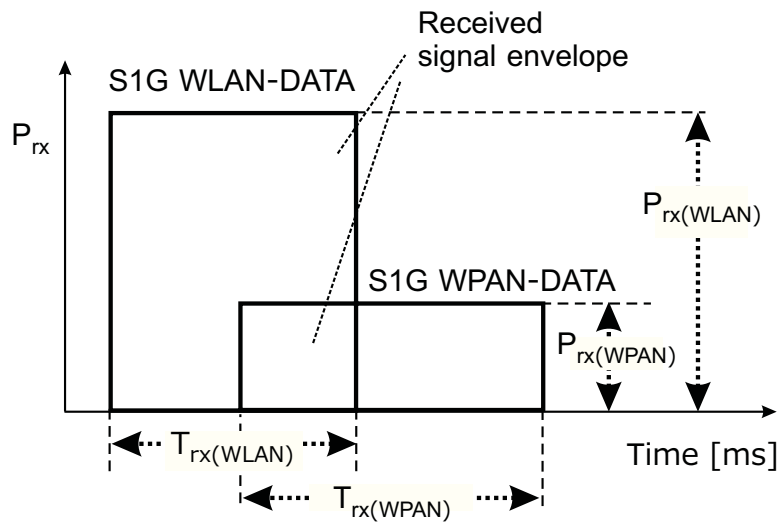


**Figure 6.10** – Proposed packet collision classification of WLAN-DATA (spectral template).

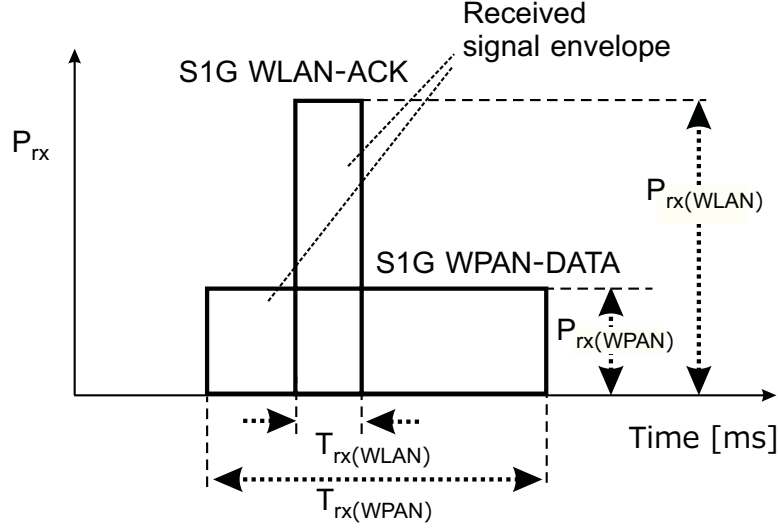


**Figure 6.11** – Proposed packet collision classification of WLAN-ACK (spectral template).

The proposed scheme can be applied in addition to common signal detection schemes, such as energy detection, CCA and AGC. The proposed scheme could significantly reduce the collision among WLANs and WPANs in the sub-1 GHz ISM radio-band. As a result of the reduced collision a higher throughput can be achieved for both systems, WLAN and WPANs. Further, unwanted data packet retransmissions can be considerably mitigated. To further evaluate the signal characteristic of the observed collisions, the received energy in relation to the bit rate is analyzed with [149]

$$\frac{RS_{WLAN1}}{BR_{WLAN1}} = \frac{RS_{WLAN2}}{BR_{WLAN2}} \quad (6.2a)$$

where  $RS_{WLAN1}$  and  $RS_{WLAN2}$  are the received signal energy [dBm] for WLANs at different data rates.  $BR_{WLAN1}$  and  $BR_{WLAN2}$  are the bit rates [kbps] of WLANs at different data rates. With

$$RS_{WLAN1} = RS_{WLAN2} + 10 \log_{10} \left( \frac{BR_{WLAN1}}{BR_{WLAN2}} \right) \quad (6.2b)$$

the WLAN signal power can be calculated.

The same model applies for WPANs given by

$$\frac{RS_{WPAN1}}{BR_{WPAN1}} = \frac{RS_{WPAN2}}{BR_{WPAN2}}, \quad (6.3a)$$



where  $RS_{WPAN1}$  and  $RS_{WPAN2}$  are the received signal energy [dBm] for WPANs at different data rates.  $BR_{WPAN1}$  and  $BR_{WPAN2}$  are the bit rates [kbps] of WPANs at different data rates. With

$$RS_{WPAN1} = RS_{WPAN2} + 10 \log_{10} \left( \frac{BR_{WPAN1}}{BR_{WPAN2}} \right) \quad (6.3b)$$

the WPAN signal power can be calculated.

## 6.4 Proposed coexistence mitigation strategies

The coexistence of WLANs and WPANs, which operates in the same spectrum, results in the reduction of media access opportunities due to spectral activities and due to interference of concurrent wireless transmissions in which two wireless signals collide. Some collisions may be handled by forward error correction (FER) schemes. Other collisions may result in CRC-errors, which cannot be corrected by the receiver. These interference problems are severe because of the retransmission operation of wireless transmitter, e.g., due to loss of successful transmissions (missing ACK). The retransmission of data frames result in dramatic depletion of battery power and as such have to be solved accordingly. Some simple remedies for these types of data frame collision problems are proper channel planning that can include intelligent channel switching, rate adaptation, advanced error coding or other schemes, such as beamforming (null-beam towards neighbors, distributed MAC and sensing). Fig. 6.12 illustrates interference mitigation strategies (remedies).

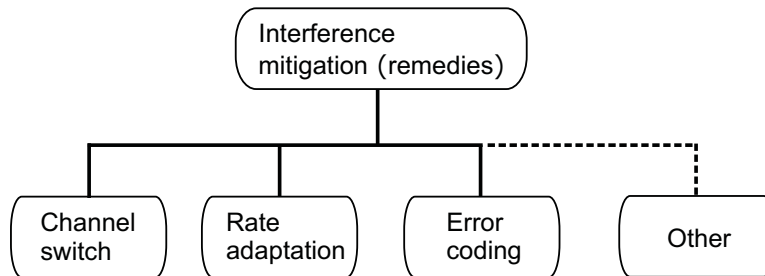


**Figure 6.12** – Interference mitigation strategies (remedies).

A promising way towards solving the collision of wireless signals (DATA frame, ACK frame), is the use of external spectral-time sensing in combination with an adaptive MAC. Combining the results of the spectral-time sensing and the report from the CRC-error or packet loss from the transceiver is proposed to be incorporated as a new packet collision detection scheme. Results of the packet collisions can be used for the detection as:

1. Packet collision detection as a result of a particular device, e.g., the sensing device.
2. Packet collisions detection as a result of network observation. This information is helpful to judge the size of the network and potential collisions. The media access can be organized in a way with reduced slot-times when the network density is high.
3. Network performance anomaly detection, and to trigger remedies, such as different media access time (airtime), or modulation rates.
4. Packet collision detection and to backoff from current transmission. This can be beneficial, when battery lifetime need to be protected. Thus, a combination of spectral-time sensing and battery status enables more energy efficient communication.
5. The starting collision of a collision between S1G WLANs and WPANs packets is uniformly distributed. This is somewhat similar as reported for IEEE 802.11a WLAN packets in [150].

In the following detailed proposals are listed, which aim to work as remedies (single or combined) to mitigate wireless interference and to enable coexistence among WLAN and WPAN in the sub-1 GHz radio-band.

#### 6.4.1 Cognitive radio architecture

The development of new functions and architectures for wireless communication systems make it difficult to adapt legacy systems in an easy and simple way. In particular, cognitive radio (CR) systems are a promising way to combine wireless systems with enhanced or new functions, such as spectrum sensing and energy efficiency. The proposed solution is to utilize and to implement an architecture that allows simple way to enhance wireless systems. The implementation of the IEEE 1900.6 interfaces for Cognitive Radio and other Advanced Radio Systems is the proposed solution.

Cognitive Radio concepts are available for different wireless systems, e.g., WLAN in the TV White Space (TVWS) or building blocks for cellular access in TVWS, e.g., IEEE P1900.4. The implemented cognitive controls include spectrum sensing, power (energy) awareness and network control. Applications of this technology include interference mitigation, white space data base and management and public safety. ISM-band cognitive radio technology is useful for urban environments and rural wireless network deployment. Fig. 6.13 illustrates interference mitigation strategies (remedies).

Cognitive Radio may be useful for ISM bands at 2.4/5GHz but also for operations at Sub 1GHz. In particular, the utilization of cognitive features for Sub 1GHz to solve coexistence between WLAN and WPANs are promising.

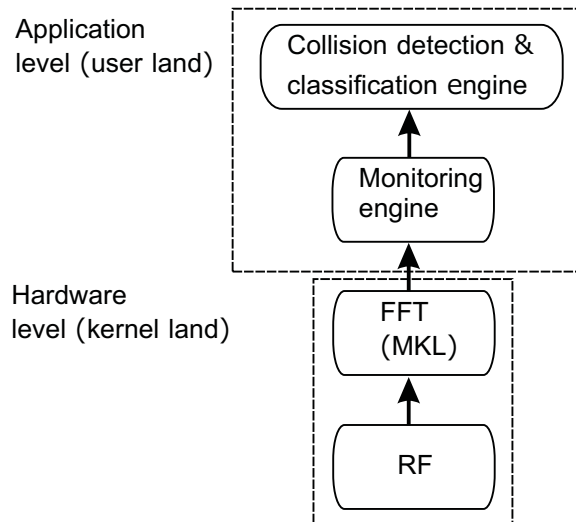


**Figure 6.13** – Intelligent sensing used by a cognitive radio system for WLAN and WPAN coexistence in sub-1 GHz.

#### 6.4.2 Proposal I: S1G collision detection unit (S1G-CDU)

The proposal is to build in a collision detection unit in a single WLAN AP. However this may only solve the collision forced by the WLAN. To mitigate the WPANs may also need to have a collision detection unit or collision detection engine. As an alternative a common collision detection interface (CDI) can be helpful. CDI can be used by WLANs and WPANs concurrently. The CDI can be on basis of the P1900.6 protocol. One aspect on the packet collision is the collision probability in MIMO-OFDM systems. IEEE 802.11ah utilizes multiple antennas (up to  $8 \times 4$  MIMO). Thus, the CDU has to consider the characteristics of MIMO packet collisions, MIMO packets exhibit different characteristics. This includes non-utilized LTF fields of a single antenna transmission. The signal outages may trigger WPANs to start packet transmissions with the result of packet collisions of WLAN data frames and WPAN data frames. Second, when beamforming is applied the signal characteristic may change and lead to packet collision. Beamforming may increase the signal at the destination with additional nulling at other stations. This may result in over-heard transmissions and triggers WPAN devices to start data transmissions. Again, packet collision in multi-antenna systems will occur.

Fig. 6.14 illustrates the use of a collision detection unit in sub-1 GHz.

In addition, a *detection probability table* can be computed, which can be utilized to determine the location  $P(i, j)$  of the interferer node  $I(m)$  in the coverage area  $c_{ij}(x, y)$  and is beneficial for range sensing devices. Murrioni *et al.*, [151] outlined the advantages of standardized interfaces and primitives for cognitive radio. Sensors,

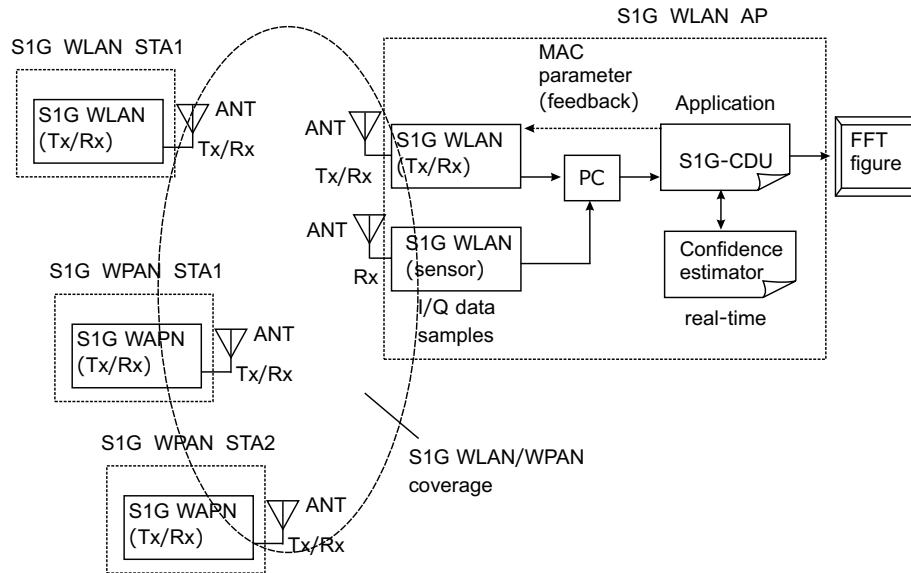


**Figure 6.14** – S1G collision detection unit in M2M networks (proposed embodiment).

cognitive engine, and data base are considered in the structure of a cognitive architecture. Dynamic spectrum access (DSA) is a promising method, which enables the spectrum sharing in time and space. It allows the optimal sharing of spectrum and the coexistence among various wireless systems, such as WLANs and WPANs. A cognitive radio (CR), which enables the spectrum sensing to detect spectrum events, such as packet collisions, is able to maximize the spectrum resources, while mitigating interference problems. In particular the distributed use of spectrum sensors and data bases in combination with cognitive engines (CE) is a promising way to realize these new wireless systems. To realize cognitive radios, the IEEE P1900.6 project within the IEEE DySPAN-SC started to standardize the interfaces and primitives among CE, sensors, and data bases. The advantage of standardizing the interfaces is to enable a common platform structure rather than developing proprietary cognitive radio architectures, which allows the reuse of cognitive radio elements and sensors.

In the context of sub-1 GHz WLAN and WPAN deployment, the IEEE 1900.6 enables the simple setup of an intelligent radio platform that is enable of spectrum events by sensing the spectrum activity in a pre-defined spectrum [152]. Packet collisions are detected and are used, e.g., to reduce the sending rate or increasing the data rate, e.g., to mitigate transmission airtime or packet collisions. Spectrum sensing information is obtained from spectrum sensors (dumb or smart) [153]. A wide range of sensors and data base systems, which use IEEE 1900.6 interface could

successfully access the data base and sensors. Further, regulatory requirements can be easily applied in a IEEE 1900.6 communication platform. For instance, regulator may require that certain sub-1 GHz radio-bands are only used by RFID whereas other parts of the radio-bands can be freely shared, e.g., by IEEE 802.11ah. This would allow that coexistence can be established and system can be simply comply to these regulatory requirements.

Further amendments in regard to data base access in a distributed spectrum sensing scenario are defined in [154]. Whereas [151] is highly related on use cases, which include the detection of *spectrum holes* a new avenue is envisioned that would make WLANs and WPANs smarter by using spectrum sensing. In particular, the utilization of IEEE 1900.6 interfaces in WLAN and WPAN systems is proposed in this thesis. Fig. 6.15 the proposed use of IEEE 1900.6 in sub-1 GHz is illustrated.

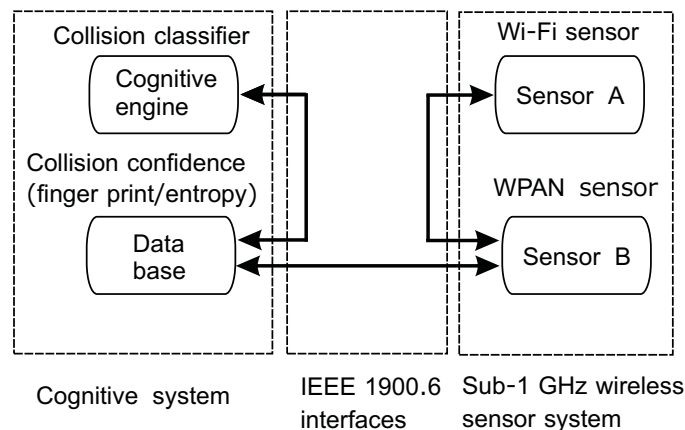


**Figure 6.15** – IEEE 1900.6 interfaces for spectrum sensing in sub-1 GHz (proposed embodiment).

### 6.4.3 Proposal II: Dynamic RAW (D-RAW)

The problem with the RAW is that the slot time is not specified in IEEE 802.11ah. The proposal is to utilize the detected collision occurrence (DCO) in WLAN/W-PAN. The proposed dynamic RAW (D-RAW) slot time computation utilizes the detected packet collision. The spectral-time sensing reports about collisions. In addition data transmission in adjacent channels can be reported. The result of the spectral-time sensing is reported to an RAW slot-time estimator. Thus, the most efficient slot-time can be computed for:

1. Presence of WLAN/WPAN collisions.
2. Number of WLAN STAs (low/medium/high dense deployment).

If a dense number of WLAN nodes is detected, the RAW slot-time is minimized to reduce the collision probability during a single slot. A trade-off algorithm is required to avoid that WLAN nodes suffer from non-granted media access (e.g., prioritization).

#### 6.4.4 Proposal III: Location-based clear channel access (LB-CCA)

In the presence of WPANs it is essential to protect passive WPAN devices from inter-system-interference. At certain locations a dense number of WPANs is observed, such as container terminals, shopping malls, and logistic centers. At these location it is beneficial to avoid unnecessary data packet transmissions in the sub-1 GHz radioband. Hence, a location-based clear channel access (LB-CCA) is proposed. This mechanism is implemented as a location-based detection feature. This is somewhat similar to radar-detection schemes in IEEE 802.11g in some countries, such as Japan. The location-data can be trained, similar to the location cognition proposal [146–148]. It can be also realized as a direct access on a location data base (DB).

#### 6.4.5 Proposal IV: Centralized clear channel access (C-CCA)

Future M2M APs will integrate multiple wireless systems, such as WLANs and WPANs. For instance, a novel M2M AP can be based on an S1G WLAN AP, which serves as access point for S1G Wi-Fi sensors. In addition, it may also serve multiple S1G WPAN sensors at a different wireless interface. In addition, the S1G M2M AP may utilize an S1G WLAN link as back-haul connection to provide wireless Internet or cloud access. A single S1G M2M cloud AP could simply control the media access among WLAN devices and WPAN devices. It is proposed that a centralized clear channel access (C-CCA) is executed in the S1G M2M AP and is beneficial to mitigate intra-system (WLAN to WLAN) and inter-system (WLAN to WPAN) interference and for temporal network deployment. A beaconing-frame is proposed that can be installed to the S1G M2M AP or gateway (GW). This beacon-frame, similar to the IEEE 802.11ah RAW, enables slotted access of WLAN devices, while transmitting WLAN packets on the back-haul link. Thus, the interference among the Wi-Fi sensor network and the WLAN back-haul network is mitigated. Fig. 6.16 illustrates the proposed media access in sub-1 GHz WPAN/WLANs.

### 6.5 Bibliographical notes

Packet collision detection schemes in particular for MIMO systems have been proposed by Nishimori *et al.*, [155,156]. The authors demonstrate that the throughput in wireless LANs can be significantly improved with the detection of the short preamble of IEEE 802.11g/a/n WLANs. In the short preamble, only a part of subcarriers contain data signals, whereas the remaining subcarriers remain unused,

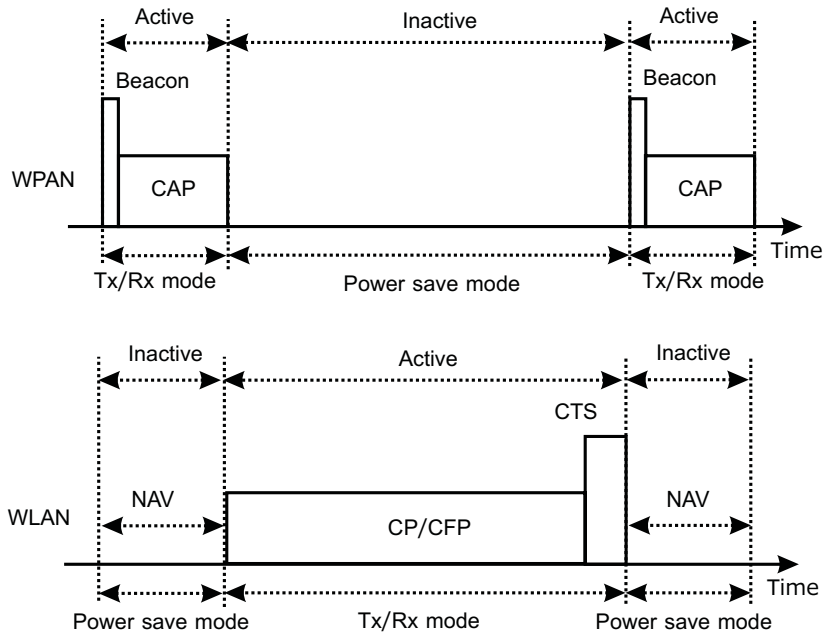


**Figure 6.16** – S1G WPAN/WLAN coexistence scheme (proposed media access).

which do not emit any signal energy. In case when the unused part of the sub-carriers exhibit a received signal (performing FFT), a packet collision is detected. Kim *et al.*, [157] proposed the identification of complex spectral patterns to conduct a *blind* estimation of transmitting wireless devices. The use of hidden Markov models (HMM) and neural networks were utilized to detect OFDM signals and its specific electromagnetic fingerprints from different WLAN devices, including IEEE 802.11a/g physical-layer frames. Scalia *et al.*, reported that vendors develop proprietary counter measures against interference due to market competition. In addition, proprietary schemes are yet unknown and only consider a specific interference problem, which may result in further (endless) modifications of proprietary counter measures in the future.

In [142], design challenges in energy-efficient MAC for wireless sensor networks are reported. The unique characteristic of WSNs is the limited power supply; thus, it makes the MAC design important to enable extended battery lifetimes. Node lifetime depends on how much energy can be conserved during communication<sup>1</sup>. It was reported that unnecessary transmissions (out of coverage, retransmissions) and longer listening periods are the ones that consume the highest amount of power.

<sup>1</sup>Modes of operation WSN mode, tx:32 mA, 95 mW; Rx: 18 mA, 55 mW; idle/sense: 8 mA, 25 mW; sleep: 20  $\mu$  A, 60  $\mu$  W [142].

Aman *et al.*, [150] report on their findings of collisions in OFDM IEEE 802.11a networks and propose to utilize an *error vector magnitude* (EVM) analysis to detect collisions. Similar to other researchers their focus is on packet loss detection, which is caused either by packet collisions or wireless channel dynamics (fading, shadowing, attenuation). Information about the packet loss cause is beneficial to enable *intelligent* decisions in the MAC layer<sup>1</sup>, e.g., either to backoff from transmissions in the case of collisions or to adjust the MCS rate due to channel dynamics, which could lead to gains up to 60% in throughput and reduces retransmissions up to 40% [150, 158]. Modeling the pdf, the presence of collisions result in the same mean, but a higher variance of the EVM is observed. A problem with this proposed method is that a threshold must be decided, which may be depend on a distinct hardware type. The authors propose that the threshold is located in the optima between the calculated pdf of *false positive* and *false negative*. This result in eight different thresholds for 16 QAM and 64 QAM at low and high SNR. A comparative study with [158] indicates that the proposed collision detection is robust over a large range of distance (5-30 m) between the interferer and the receiver. In addition, the proposed method only uses one decision metric (EVM), compared to [158] in which the decision metric consists of the three parameters (i) received signal strength, (ii) bit error rate and (iii) errors per symbol, which lead to higher decision complexity.

## 6.6 Discussion and summary

### 6.6.1 Discussions

A simple packet detection scheme based on energy detection can be a first choice. However, the narrow-band character of the WPAN signal makes the energy detection a challenging task. Other detection schemes may be a good alternative, including signal sensing and classification using so called filter-banks. Using these filter-banks, the classification of signals in WLAN and WPAN could be simple. To improve the confidence, the proposed confidence calculation schemes can be utilized. Further, if the filter bank scheme does not work, another alternative is simply by monitoring the CRC data. It has been observed that the location of the collision inside the packets has a strong relation on the CRC data. It can be observed that CRC errors at the beginning are similar with spectral-time observations, where CRC and spectral-time collisions are happen at the same location among the collided packets.

Further research is necessary. In particular, the research of mulit-antenna systems (MIMO-OFDM) and WPANs in the sub-1 GHz radio-band is proposed. This should include:

1. Mutli-antenna signal transmission and coexistence of WPANs.
2. Number of used antennas and its relevance for packet collisions.

---

<sup>1</sup>The MAC layer is unaware of the cause of transmission errors.



3. Beamforming (WLANs) and coexistence of WPANs.
4. Multi-antenna WLANs and multi-antenna WPANs.
5. Energy detection schemes for WLAN and WPAN coexistence.
6. Access strategies for WLAN and WPAN coexistence.

Most relevant are the reduction of unwanted packet retransmissions to save the battery lifetime of WPANs and WLAN devices. Other advanced signal detection include frequency-time wavelets, matched filter, cyclostationary feature detection, and higher-order statistical features. The advantages of a successful packet collision detection would be a further increase of wireless coverage in long-range networks by simply reducing the collision probability in wide-area wireless networks<sup>1</sup>. In addition, coexistence among WLANs and WPANs (including RFIDs) would be significantly reduced.

A problem with the collision detection method is the probability of false detection. If a packet collision occurred, but has not been reported a so called *false negative* decision is the result. In this case packet collisions are not reported and transmission results in continuous packet collisions. If packet collisions are reported but have not physically been occurred (*false positive*), wireless nodes may backoff from transmissions; thus, they miss the potential transmission opportunity, which results in reduced throughput performance. Again, a level of confidence can be added to the packet collision, which would be beneficial to predict the probability of packet collisions. Potential resources of false positive are other signal sources and internal WLAN card noise<sup>2</sup>.

It is well-known that a WLAN node (AP or STA) cannot listen to on-going transmissions while sending its own data. Thus, it makes the carrier sense multiple access with collision avoidance (CSMA/CA) a necessity [142]. However, this view may not hold upfront any longer in the context of a *cognitive* WLAN or WPAN. A simple proposal would be to enhance WLAN APs with additional WLAN interfaces, which are solely used for collision detection (CD). It would be beneficial to obtain data of collisions to change PHY and MAC parameter so that an S1G WLAN - that operates in a heterogeneous WLAN/WPAN infrastructure - can act and execute counter measures to mitigate packet collisions because of asynchronous energy-detection schemes among S1G WLANs and WPANs.

To further support the idea of using packet collision in heterogeneous wireless networks (WPANs/WLANs), a more efficient IEEE 802.11ah WLAN MAC can be

---

<sup>1</sup>The IEEE 802.11 High Efficiency WLAN (HEW) Study Group (now IEEE 802.11ax TG), started a new project to evaluate next generation WLANs that will consider larger number of APs, larger number of STAs, new/additional path loss models for outdoor deployment, full-duplex transmissions, and interference mitigation strategies [159].

<sup>2</sup>Some WLAN cards provide remedies to mitigate the effects of noise and interference, such as ambient noise immunity (ANI). However, it was reported that these counter measures have severe side effects in outdoor deployments on CCK and OFDM signal detection thresholds, when noise sensitivity parameters are not well adjusted [160].

developed that uses the information of failed transmissions. The collision detection can be used to enable a fair media access. So called *self-interference* strategies are useful to consider [96]. To increase the throughput over a large distance by factor 2, full duplex (FD) MAC mechanisms are proposed, similar to [95]. Packet collisions can be much simpler mitigated in a point coordinated network, where the WLAN AP manages the media access among the WLAN STAs. However, in heterogeneous networks the presence of multiple flows among WLAN STAs becomes more and more prominent. Thus, in a distributed wireless network where multiple flows compete for media access at same or adjacent wireless channels is much more challenging. Here, advanced distributed WLANs in combination with distributed sensing may enable a fair media access.

The coexistence evaluation has demonstrated significant similarities with the collision pattern and the reported CRC-errors from the wireless sensors (Ti-sensor) in the presence of wireless signals, which have been emitted by the IEEE 802.11ah WLAN prototype. As a result, the CRC-error characteristic can be utilized to identify the *location* of the collision, whether the packet was collided in the beginning, during the transmission, or at the end of the transmission. From this, further estimates can be obtained, such as the distance between the sender of each system, signal strength, or effectiveness of the carrier sense threshold.

### 6.6.2 Summary of the chapter

In this chapter, primary findings on the coexistence problems in the sub-1 GHz have been reported. As a main reason for the packet collision the CSMA/CA algorithm in the sub-1 GHz prototype was identified, which need further improvement on the packet detection and collision avoidance. However, the WPAN nodes are certified off-the-shelf products; thus, they are equipped with an pre-configured collision avoidance. However, the findings demonstrated that WPAN nodes interfere on-going data transmission of S1G WLANs; thus, leading to the conclusion that the collision avoidance and packet detection is insufficient for coexistence among WLANs and WPANs in the sub-1 GHz radio-band. More research on this topic need to be conducted to mitigate inter-system-interference. It was argued that reliable wireless communication links are essential for S1G WLANs and WPANs to avoid unwanted packet retransmissions. Packet retransmissions lead to rapid battery power depletion in wireless networks. Packet collisions are one aspect of inter-system interference, as well as for intra-system-interference (so called performance anomaly). It was shown that packet collisions are prominent in S1G WLANs and WPANs. It was demonstrated how to observe these packet collisions with spectral-time sensing. Further, packet collisions were classified for data packets (DATA) as well as for acknowledgments (ACKs).

## Chapter 7

# High-density media access

This chapter is focused on the media access in high-density S1G WLANs. The enhanced wireless communication range of S1G WLANs enables a high number of associated WLAN STAs. Firstly, the potential number of WLAN STAs is examined in this chapter for different environmental conditions and the negative aspects of management frame collisions are discussed. Secondly, a method is proposed, which enables the management of a large number of STAs in highly dense S1G WLANs. The proposal considers a physical network partitioning based on the orthogonal sectorization of a single WLAN AP coverage area. Finally, a new media access framework is proposed that utilizes the sectorization to realize a control-less wireless communication infrastructure that is required for massive IoT device deployments.

### 7.1 Problem formulation: Media access in highly dense WLANs

The number of potential WLAN STAs in IEEE 802.11ah networks, which can be associated with a single IEEE 802.11ah-based WLAN AP, is significantly higher compared to legacy WLANs, as such as in IEEE 802.11b/g networks. Whereas in IEEE 802.11b up to 10 WLAN STAs can be connected with a single IEEE 802.11b WLAN AP without significant performance loss, IEEE 802.11ah WLAN APs must support a much larger number of associated STAs. Hundreds or even thousands of potential Wi-Fi sensors can be associated with a single AP due to the wider coverage at  $f_c = 900$  MHz.

#### 7.1.1 Definition of massive access in WLANs

In the following a new definition is given that describes the circumstance of massive access in wireless networks. Massive access is defined in a wireless system, *as the*

highly frequent and concurrent access of wireless terminals due to a large number of users, which would result in unstable system behavior, e.g., by exceeding the system boundaries in legacy wireless communication systems; thus, system modifications are required to support the media access from a high number of users. Fig. 7.1 illustrates the stable region of a WLAN. The relevant system parameters are the pre-defined system boundaries, such as the maximum number of supported WLAN APs  $x'$  and the number of WLAN STAs  $y'$ . These parameters were identified, e.g., during the WLAN standardization process, use case discussion, specification framework definition, etc. [17]. If the number exceeds the system boundaries, the system becomes unstable; thus, resulting in unwanted severe communication failures, such as retransmissions or data loss.

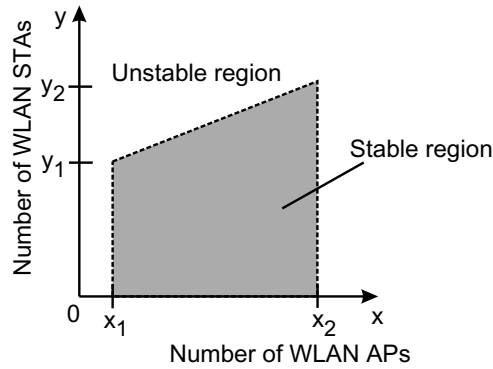


**Figure 7.1** – Stable region of a WLAN deployment.

Assumptions on the potential number of users in different networks are presented in the following. The number of WLAN STAs within WLAN AP coverage is given by

$$N_{sta} = \pi \left( \frac{r_{coverage}}{1000} \right)^2 \rho_{sta}, \quad (7.1)$$

with  $N_{sta}$  as the number of WLAN STAs,  $r_{coverage}$  as the wireless coverage range of a single WLAN AP (here an IEEE 802.11ah WLAN AP with 1 km coverage range), and  $\rho_{sta}$  as the WLAN STA density for different environments. A single IEEE 802.11ah WLAN AP with a wireless coverage range of 1 km is illustrated in Fig. 7.2.

The number of WLAN STAs as a function of WLAN AP coverage range and STA density for typical rural, sub-urban, and urban environments is illustrated in Fig. 7.3. The figure is useful to estimate the possible number of WLAN STAs for different regions. In rural areas the number of WLAN STAs does not increase significantly due to the low-density of terminals. However, in urban areas, due to the highly dense deployment of outdoor terminals, the number can reach up to thousands of WLAN STAs after 500 m.

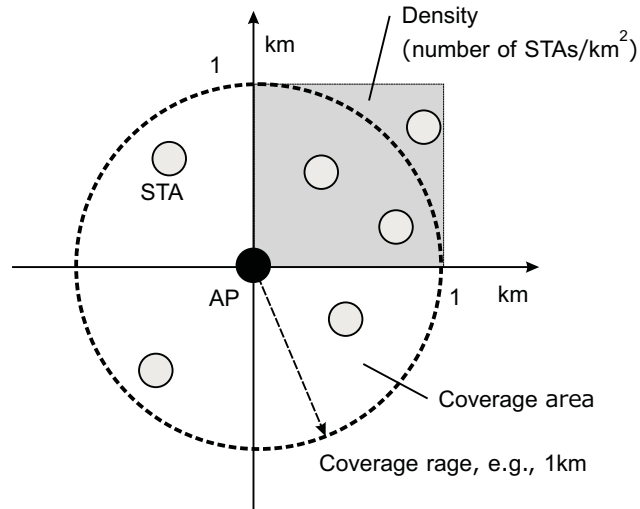


Figure 7.2 – Single WLAN AP with 1 km coverage range; cf. [161].

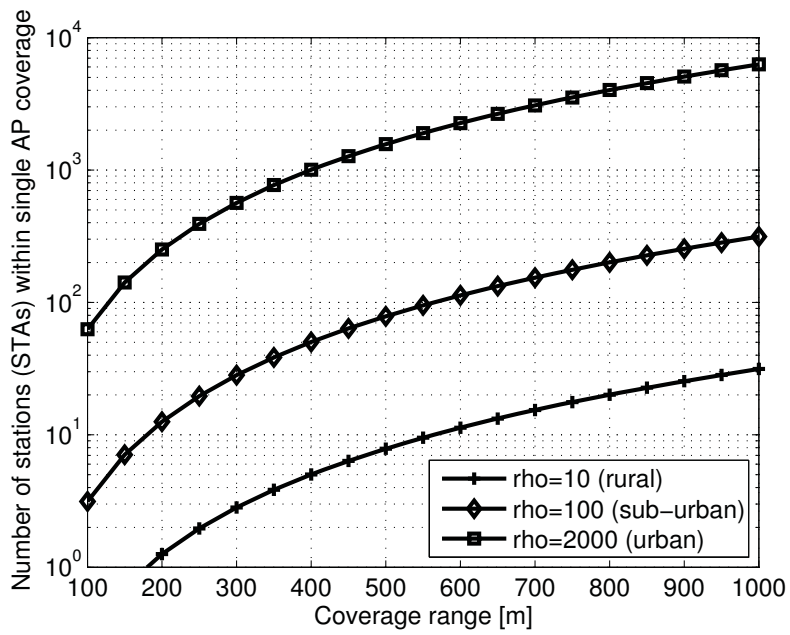
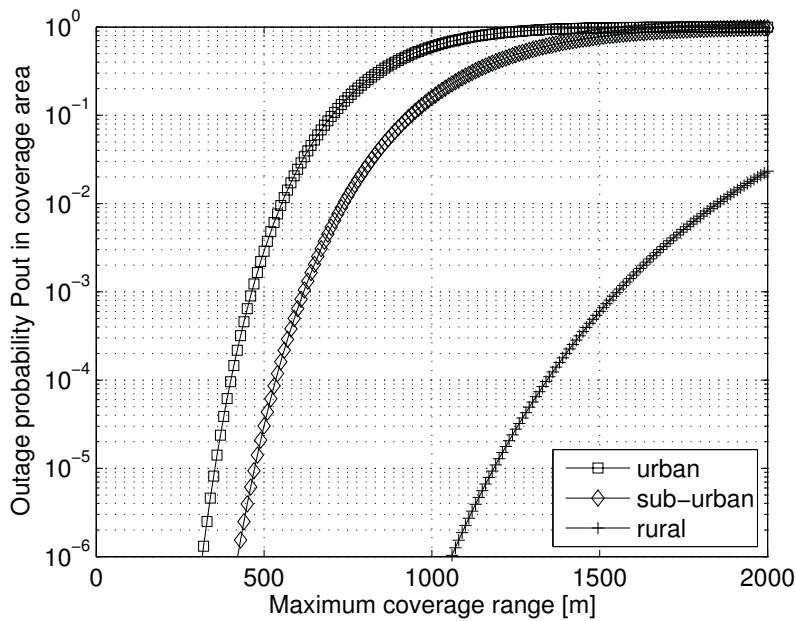


Figure 7.3 – Number of WLAN STAs as a function of WLAN AP coverage range and STA density.

To investigate the impact of a high-density deployment in real networks, the outage performance is examined to judge the wireless link characteristics of a wide coverage. Fig. 7.4 illustrates the outage probability for different path loss environments, including rural, sub-urban, and urban areas, with a typical shadowing parameter  $\sigma = 4$ , and receiver threshold  $rx_{thres} = -80$  dBm [2].



**Figure 7.4** – Outage probability for different path loss locations, including rural, sub-urban, and urban areas.  $\sigma = 4$ , receiver threshold  $rx_{thres} = -80$  dBm.

Fig. 7.4 illustrates the outage probability against the maximum coverage range. For low outage regions ( $P_{out} = 10^{-6}$ ) the maximum coverage range is very limited, reaching up to 300 m in urban areas. Thus, a large coverage range in urban areas may not hold. However, in sub-urban areas the coverage range increases; thus, the network performance can be easily negatively affected by high-density deployments.

Fig. 7.5 illustrates the outage probability for different path loss environments, including rural, sub-urban, and urban areas, with an increased shadowing parameter  $\sigma = 8$ , for the same receiver threshold  $rx_{thres} = -80$  dBm. For a larger amount of shadowing impact, Fig. 7.5 illustrates the outage probability against the maximum coverage range, showing that the coverage range further decreases in networks which suffer from larger channel dynamics.

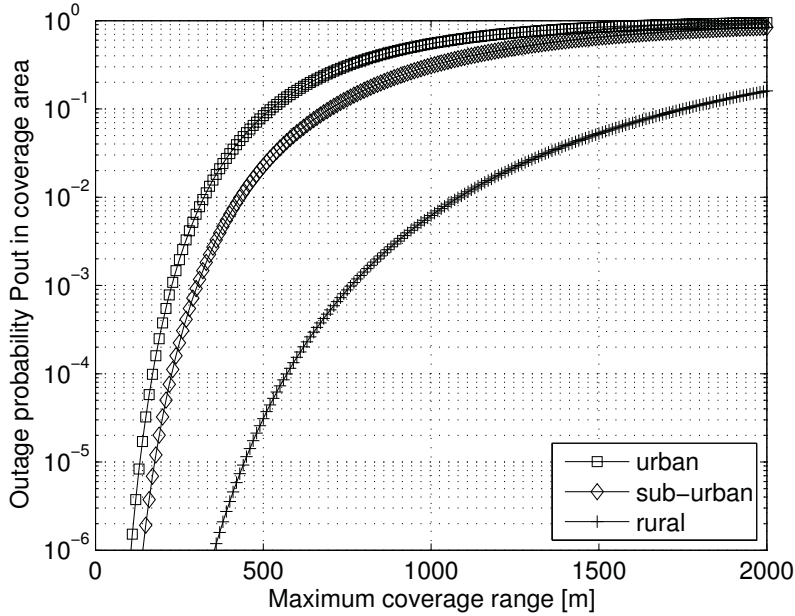


**Figure 7.5** – Outage probability for different path loss locations, including rural, sub-urban, and urban areas.  $\sigma = 8$ , receiver threshold  $rx_{thres} = -80$  dBm.

## 7.2 Proposal: Sector-based RTS/CTS media access scheme

### 7.2.1 Problem formulation

A single user in an intra-cell resource management is defined as an individual or group of wireless stations  $s_i$ . The basis for calculating the amount of WLAN users in high-density networks is given by the number of all WLAN STAs  $\rho_\gamma = \sum s_i$ , which are covered by the communication radius  $r_\gamma$  of a single WLAN AP $_\gamma$ . An increased outage probability due to link attenuation and shadowing (a thorough discussion on this topic is presented in [161]) causes a reduction of associated WLAN STAs. For a simple and effective modeling of the wireless access in high-density WLANs, a uniform distribution  $\vartheta$  per km<sup>2</sup> is sufficient for all WLAN STAs. For WLANs as defined in [5], with  $r_\gamma = 1000$  m and  $\vartheta = 2000$  the number of STAs within AP coverage  $r_\gamma$  reaches up to the significant large number of  $\rho_\gamma = 6283$  STAs when the well-known density function  $\pi(r/1000)\vartheta$  is applied [161]. This large number of WLAN STAs (which can be found in metropolitan areas) cannot be supported by any of the recent specified WLAN protocols. This high STA density requires

advanced media access support. Similar massive access scenarios of M2M clients in 3GPP networks, are reported in [162].

In case of long-range IEEE 802.11ah WLAN networks the number of WLAN STAs is three times larger compared to the defined number of supported WLAN STAs, which is 2007 [17].

The WLAN protocol specifies the number of supported WLAN STAs in the *address identifier* (AID). The AID value is an integer type value with a valid range from 1 to 2007 inclusive and is specified in the semantics of the service primitive in [17]. A closer look at the AID field indicates that the entire field length is 16 bits. For the AID only 14 least significant bits (LSB) are used and the 2 most significant bits (MSB) are set to 1. The assigned AID value is in the range 1-2007, whereas the numbers 2008-16383 are reserved (Table 7.1). Extensions to the AID field are required and have been proposed for the IEEE 802.11ah protocol amendment [5].

Bits 0-13	Bit 14	Bit 15	Usage
1-2007	1	1	AID in PS-Poll
2008-16383	1	1	reserved

**Table 7.1** – ID field encoding of AID from [17]

To mitigate the probability of data packet collisions in WLANs, the *carrier sense multiple access/collision avoidance* (CSMA/CA) media access scheme can be modified. Some WLAN operator enable the request to send (RTS)/ clear to send (CTS) access scheme function to reduce data collisions [163]. By adding the RTS/CTS access management procedure the problem of so called *hidden terminals* in WLANs can be mitigated. If RTS/CTS is activated, a WLAN STA broadcasts a single RTS frame to announce to other surrounding WLAN STAs that a data packet will be sent. If the recipient of the RTS frame is able to receive the RTS frame, it will issue a so called CTS frame to announce the start of the data transmission. This RTS/CTS handshake procedure will inform all surrounding nodes of the ongoing communication; thus, they will refrain from data transmission during the period. As a result, the probability of packet collisions is mitigated when RTS/CTS is used. This management scheme was developed on the assumption of supporting few WLAN STAs in a single network.

However, if the network density increases, the effectiveness of the RTS/CTS management scheme is not known. In particular, the RTS/CTS access scheme causes packet collisions, due to the high number of RTS frames which are emitted in high-density networks. As a result, no communication can be established when RTS frames cannot be received due to collided RTS frames among WLAN STAs.

In this section a modified RTS/CTS media access scheme is proposed, that aims to mitigate the collisions of RTS frames. In particular, the proposed RTS/CTS scheme reduces the collision probability by emitting RTS frames only in distinct network areas. The proposal utilizes the RTS/CTS access management scheme in combination with a novel sectorized media access scheme. The motivation of



sectorizing the wireless area is to avoid RTS collisions between neighbor sectors. In particular, RTS frames are only emitted in *orthogonal sectors* to mitigate the collision probability. The result is a significant reduction of RTS frame collisions.

### 7.2.2 Optimized media access scheme

An advanced RTS/CTS scheme is proposed based on a WLAN group assignment to schedule the emission RTS management frames. A group can be defined in different ways, a *logical group* defined by the *address identifier* (AID), a *physical group* defined from received WLAN AP beacons, and the combination of both. The idea is that the physical partitioning has advantages, such as utilizing a simple sectorized beamforming where beacons are sent to a specific sector, which is called *spatial orthogonal access*.

When applying the sector-based RTS frame transmission, the entire WLAN coverage of a single WLAN AP is divided into sectors in which the emission of RTS frames is organized in a way to mitigate the collision probability. Fig. 7.6 illustrates the entire coverage area of a single WLAN AP  $AP_\gamma$  which is divided into four sectors, with station  $s_{\gamma,j,i}$  in sector  $j$ .

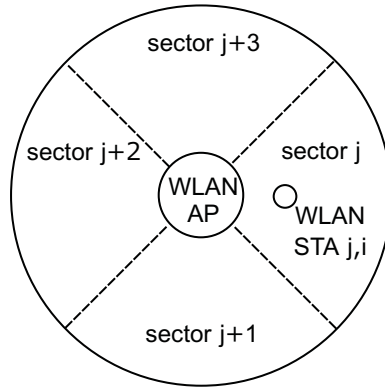


**Figure 7.6** – Illustration of the proposed sectorization scheme for RTS frame collision reduction.

The AP coverage of four sectors  $\Psi_j$  in which RTS frames from stations are emitted are separated by orthogonal sectors. For example,  $s_{\gamma,j,i}$ ,  $s_{\gamma,j+1,i}$ ,  $s_{\gamma,j+2,i}$ ,  $s_{\gamma,j+3,i}$  are distinct used to create an orthogonal network partition. Further, when the emission of RTS frames is organized time periods, such as  $t_{j,\delta}$ ,  $t_{j+2,\delta}$  in  $\Psi_j$ ,  $\Psi_{j+2}$  and  $t_{j+1,\delta+1}$ ,  $t_{j+3,\delta+1}$  in  $\Psi_{j+1}$ ,  $\Psi_{j+3}$ , RTS frame emissions are scheduled at distinct time slots. In combination with so called *time management frames* [17], which are used as tokens, the RTS emission is optimized. The tokens are sent by the WLAN AP to identify which WLAN STAs in which sectors are allowed to emit

RTS frames. Thus, the sectorized access scheme exploits the orthogonality of the entire WLAN AP coverage.

As an intra-system interference mitigation scheme, the orthogonal sectorization mitigates the collision probability of RTS frames by WLAN STAs in adjacent AP sectors. WLAN STAs are scheduled to emit RTS frames which are located in orthogonal sectors (non-adjacent AP sectors). Additionally, as an inter-system interference mitigation scheme, the orthogonal sectorization is beneficial to mitigate the collision probability between WLAN APs. The so called overlapping basic service set (OBSS) interference can be mitigated. Sectors from different WLAN APs can be organized in a fashion which minimizes the collision probability in an entire WLAN infrastructure. For instance, for  $AP_\gamma$ ,  $AP_{\gamma+1}$ ,  $AP_{\gamma+2}, \dots$ , each sector is colored by a finite color set. WLAN STAs in sectors with different colors are allowed to emit RTS frames; thus, reducing the collision probability among WLAN APs.

In Fig. 7.6 the beam of  $AP_\gamma$  encompasses a sector  $\Psi_{\gamma,j}$  with a group of STAs  $s_{\gamma,j,i}$ . With  $s_{\gamma,j,i}$  as the number of terminals in sector  $\Psi_{\gamma,j}$  the orthogonal sectorization scheme is modeled by

$$\sum_{\forall i \in \Psi_{\gamma,j}} s_{\gamma,j,i} \ll \sum_{\forall k \in AP_\gamma} s_{\gamma,k} \quad (7.2)$$

as the set of terminals  $s_{\gamma,j,i}$  in sector  $\Psi_j$ . At time  $T_{frame}$  the CSMA/CA media access is granted for  $s_{j,i}$  WLAN STAs in sector  $\Psi_j$  given by

$$\Delta T_{frame,j} = s_{i,T_{frame,j}}. \quad (7.3)$$

For WLAN backoff protocols a generic closed-loop model can be developed as presented in [164]. The saturated (asymptotic) throughput can be estimated with the model to discuss the performance gain of the WLAN AP sectorization. When  $n$  stations contend for channel access and each transmits with a probability  $\tau$ , the transmission probability per slot time  $P_{tr}$  is given by,

$$P_{tr} = 1 - [1 - \tau]^n. \quad (7.4)$$

when successfully transmitted, the probability  $P_s$  is given by

$$P_s = \frac{n\tau[1 - \tau]^{n-1}}{1 - [1 - \tau]^n}, \quad (7.5)$$

where  $\tau$  is the transmission probability of a single station given by

$$\tau = \frac{1}{n\sqrt{T_c/2}}, \quad (7.6)$$

with  $T_c$  as the sensed busy time during a collision. To calculate the normalized throughput  $S$ , which is useful to compare the backoff procedures, any successfully

data transmission during any chosen slot time when the channel is used contributes to the throughput modeled by [164]

$$S = \frac{P_s P_{tr} E[P]}{(1 - P_{tr} \cdot \sigma + P_{tr} P_s T_s + P_{tr} (1 - P_s) \cdot \eta)}, \quad (7.7)$$

with  $T_s$  as the sensed busy time of a successful data transmission,  $\eta$  as the residual frame collision coefficient, and  $\sigma$  as the duration of an empty time slot. The idea is to modify the legacy RTS/CTS access scheme to mitigate the collision probability of RTS frames. If RTS frame collision can be reduced, e.g., in high-density WLANs, an increase of the normalized throughput should be observed. The sectorization of the coverage area of the WLAN AP  $AP_\gamma$  with  $\Psi_j$  in combination with a synchronized time interval provides the desired framework for RTS frame collision reduction. The sector-based RTS scheme model is CSMA/CA-based (7.7) with a modified collision probability (7.3) as

$$\eta_{mod} = T_c \cdot P'_{c,\Delta}. \quad (7.8)$$

From [163], the collision probability of RTS frame  $P'_c$  is given by

$$P'_c = 1 - (1 - p_\eta)^{\nu(n-1)}, \quad (7.9)$$

where

$$p_\eta = 1 - \left(1 - \frac{1}{W_{avg}}\right)^{n-1}, \quad (7.10)$$

with  $W_{avg}$  as the average backoff window size and  $\nu$  as the *slot time* in  $\mu s$ .

The evaluation of the backoff performance considers five different window sizes 8, 64, 512, 1024, and 2048. The results are depicted in Fig. 7.7. It can be observed in Fig. 7.7 that an increased backoff window results in higher number of supported WLAN STAs. However, the omni-directional character of the legacy backoff scheme separates large network areas from the media access for a longer time-duration. By consequence, a sectorized media access scheme will show similar performance gains but with improved access probability for each user per sector (cf. the contention-free access per RAW time-slot, cf. Section 2.10.2). This is particularly true when a large number of Wi-Fi sensors want to access the spectrum at the same time slot. In the case of CSMA/CA, the WLAN STAs contend for access based on the random backoff procedure, which is equal for all WLAN STAs.

Two practical approaches exist to realize the sectorization, namely (i) physical sectorization by using sector antennas, and (ii) sectorization by exploiting beamforming features, e.g., such as down-link beamforming in IEEE 802.11n. Physical sectorization based on sector antennas has the advantage of a high reuse factor of sector optimization functions from cellular networks. However, the investment in sector antennas may not always be advantageous. Using beamforming by utilizing the available antenna arrays at WLAN APs enables a much higher degree of flexibility, e.g., in non-uniform distributed WLANs. A combination of beamforming and time-synchronization, by utilizing IEEE 802.11n time frames, allows that only

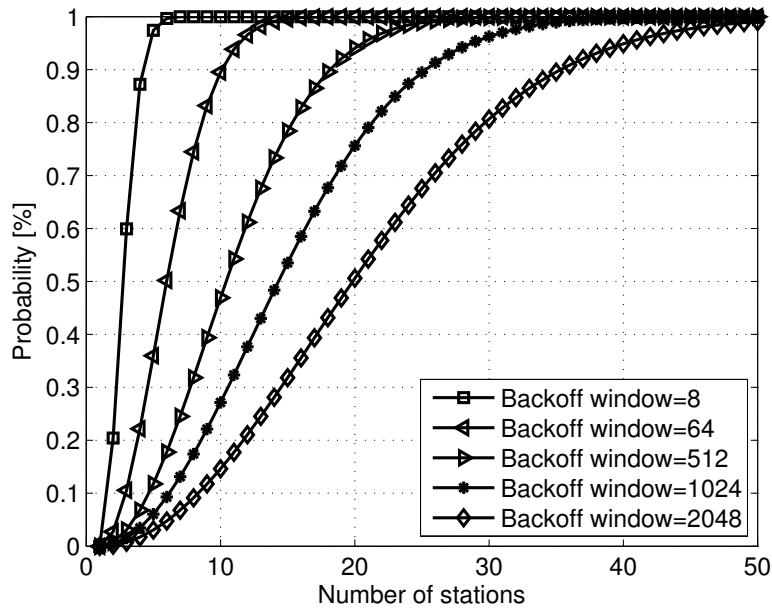


Figure 7.7 – CSMA/CA backoff performance for different window sizes.

WLAN STAs in a distinct network area will receive the sector information, e.g., to start the RTS/CTS handshake. The additional time frames enable the synchronization among the sectors and thus, increases the medium access accuracy.

The distance between adjacent WLAN AP sectors can be dynamically increased to further reduce the RTS frame collision probability, which provides a highly adaptive media access scheme and supports a large number of WLAN STAs with a high level of interference mitigation. To enable such orthogonal sectorization scheme an optional bit sequence in the IEEE 802.11ah protocol is proposed. The bit sequence is used to advertise the sectorization feature between WLAN AP and WLAN STAs.

To evaluate the performance of the proposed sectorization access scheme a simulation study is carried out. To emulate the narrow-band characteristic of IEEE 802.11ah WLANs, the IEEE 802.11 1.0 Mbps mode is selected, which provides a similar transmission characteristic compared to an IEEE 802.11ah WLAN operating at 1 MHz bandwidth ( $2 \times 2$  MIMO-OFDM). To follow the RTS/CTS model, a WLAN STA that receives a valid RTS frame refers to the so called *network access vector* (NAV) to decide if it can respond by sending the CTS frame. For simplicity, it is assumed that a STA is always ready to send; thus, the NAV counter is set to 0 (idle state). Table 7.2 lists the simulation parameters. To identify the dependency of the saturated throughput against the network density, a significant larger number of WLAN STAs is applied to the simulation study.

**Table 7.2** – List of simulation parameter used for model validation of the proposed sectorization schemes.

Parameter	Value [unit]
Data packet payload	200 bytes, 1023 bytes
MAC header (no QoS, no HT field)	272 bits
PHY preamble & header	128 bits
ACK frame & FCS	112 bits
RTS frame & FCS	160 bits
CTS frame & FCS	112 bits
Channel bit rate	1.0 Mbps
Propagation delay	$1\mu s$
Slot time	$50\mu s$
SIFS	$28\mu s$
DIFS (SIFS + 2 · Slot time)	$128\mu s$

### 7.2.3 Discussion of simulation results

The simulation results of saturated throughput performance are discussed. To identify the media access performance against the number of WLAN STAs, an increase in network density was evaluated. In Fig. 7.8 it can be observed that in the onset of the simulation study (1 to 10 WLAN STAs), the saturated throughput reaches a value of 0.8 while using CSMA/CA (the RTS/CTS scheme requires additional overhead, thus reduces the saturated throughput). If more than 10 STAs are within AP coverage, RTS/CTS significantly outperforms the CSMA/CA access scheme. The effectiveness of RTS/CTS can be clearly observed due to the mitigated collision probability when using RTS/CTS management frames. This result is consistent with the observations in [164].

Further, Fig. 7.8 reveals the circumstance that if more than 100 STAs are within coverage, the RTS/CTS throughput performance is reduced and a dramatic decrease of saturated throughput can be identified. What the graph should make clear is that RTS/CTS was not designed to support a large number of WLAN STAs in high-density networks. As a reason for the significant reduction in throughput performance, the negative impact of RTS frame collisions becomes prominent, which was observed in the simulation study. It can be concluded that the RTS/CTS access scheme is not suitable to manage the media access in high-density WLANs which consist of hundreds or thousands of WLAN STAs. In fact, neither CSMA/CA nor RTS/CTS support efficient media access that is required in high-density WLANs.

To study the effectiveness of the proposed orthogonal sectorized media access scheme, a simulation was carried out comparing the proposed scheme and the legacy RTS/CTS scheme in high-density WLANs. Firstly, Fig. 7.9 illustrates the limited media access support of RTS/CTS. Starting from 100 WLAN STAs, RTS/CTS shows a decline in network throughput performance, indicating that this media

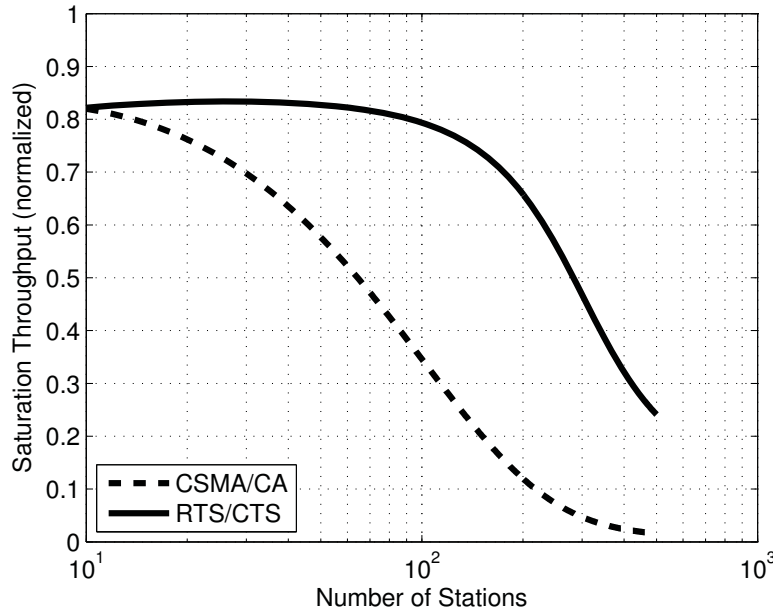


**Figure 7.8** – Throughput performance of highly dense WLANs (<500 STAs) comparing the CSMA/CA and the RTS/CTS medium access scheme.

access scheme is not suitable in high-density networks. The simulation study considers the evaluation of the impact of small (200B) and large data packet sizes (1023B) against the network density and the media access strategy. Large packets are present in networks with multi-media content transmissions, whereas small packets are observed in sensor networks. For both, small data packets and large data packets, the RTS/CTS access scheme shows throughput limitations for large number of WLAN STAs, starting from 100 WLAN STAs. Secondly, Fig. 7.9 illustrates the improved saturated throughput performance for large number of WLAN STAs when the proposed orthogonal sectorization is applied. The throughput is significantly constant over an increased number of WLAN STAs. In particular, up to five times increase in WLAN STAs is supported by the proposed scheme, before the proposed scheme shows a decline in throughput (due to transmission timeouts). Fig. 7.9 illustrates that the increased throughput holds for both, small data packets as well as for large data packets.

It can be concluded that the legacy CSMA/CA media access scheme and its enhanced RTS/CTS mechanism do not provide sufficient media access support for high-density WLANs. In contrast, the proposed orthogonal sectorized RTS/CTS enables the media access in high-density WLANs. Up to five times increase in network

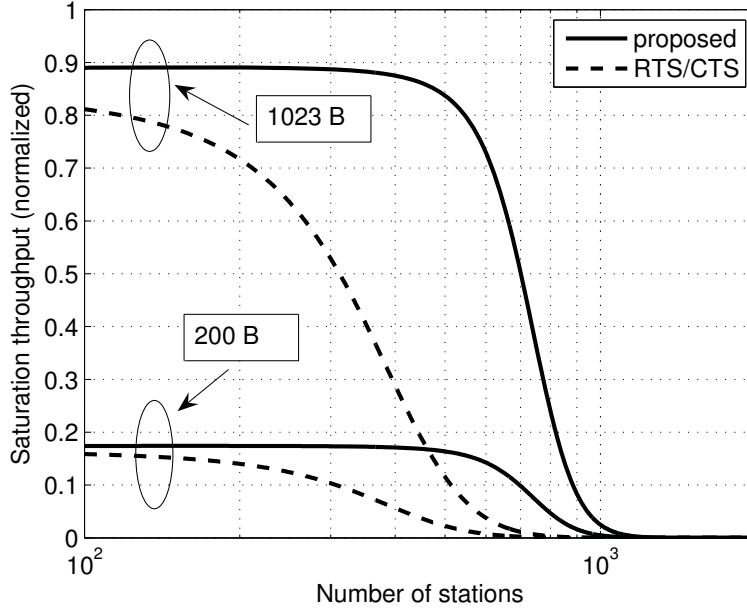


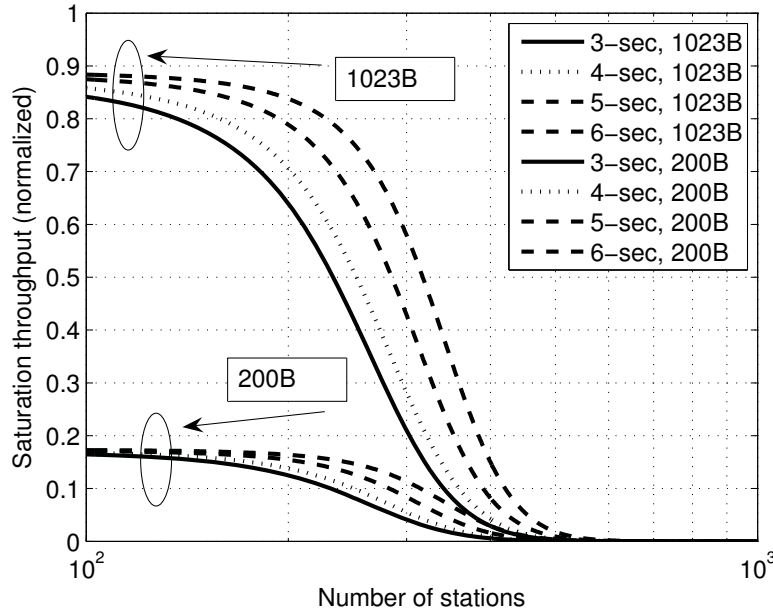
**Figure 7.9** – Throughput performance of RTS/CTS and sector-based RTS/CTS with frame collision probability  $P'_c = 0.01$  for packet size 200 B and 1023 B.

density is supported. The simulation study confirms the assumptions that a sectorization is beneficial in high-density WLANs, which is exploited by a synchronized RTS frame emission in orthogonal WLAN sectors.

Further, the results in Fig. 7.8 and Fig. 7.9 suggest that different access regimes exist depending on the network density. Clearly, there are three regimes in which each of the access scheme show some efficiency. Additionally, the boundaries of each regime are used to identify decision thresholds, such as:  $\chi = \sum s_{\gamma,i} \forall i$  as the sum of STAs associated with  $AP_{\gamma}$ ; (i) if  $\chi \geq 100$  STAs, the proposed scheme enables the reduction of RTS frame collisions, (ii) if the number of STAs is between  $\chi < 100$  and  $\chi \geq 10$ , RTS/CTS access scheme should be applied, (iii) whereas with  $\chi < 10$  STAs CSMA/CA should be used to minimize the management overhead.

The simulation study concludes with an evaluation of four different sector sizes to identify the impact on the number of sectors. In particular, the different sector sizes 3, 4, 5, and 6 sectors, are evaluated. Additionally, the number of potential retransmission is changed to observe the saturated throughput against the number of retransmissions. Fig. 7.10 shows the result when different sector sizes are used for retransmission threshold  $r_{thres} = 3$ . It can be observed from Fig. 7.10 that an

increase of the sector number enables a higher number of supported WLAN STAs. This is particularly true for both, small (200 B) and large data packets (1023 B).



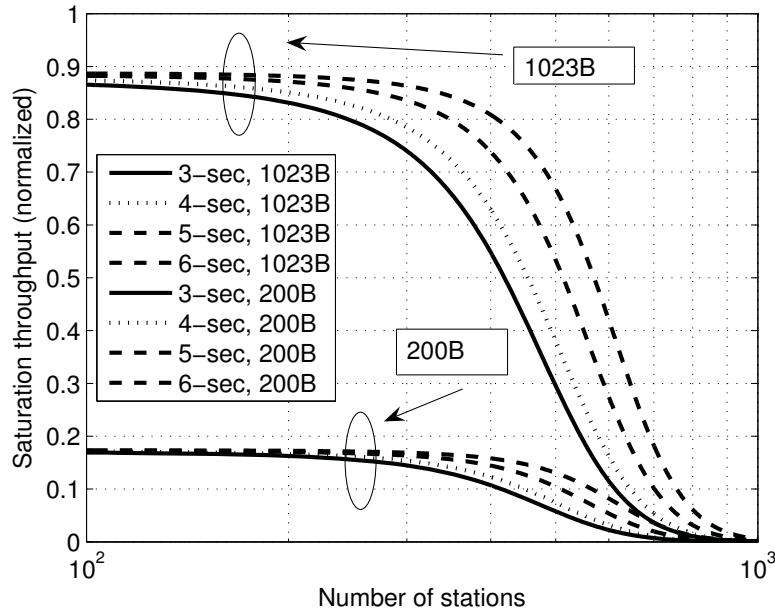
**Figure 7.10** – Impact of different sector sizes versus network throughput,  $r_{thres} = 3$ .

Fig. 7.11 shows the result for  $r_{thres} = 6$ . In case when the number of retransmissions is increased, a higher number of WLAN STAs is supported. Data packets are retransmitted over a longer period until they are discarded, e.g., reaching the retransmission limit. However, a larger number of WLAN sectors would require a careful synchronization mechanism, which must be provided, e.g., by an advanced radio resource management (Section 7.3).

### 7.3 Radio resource monitoring and management (RRMM) framework

In this section, the idea of an orthogonal sectorized media access is applied to an generic radio resource management framework in WLANs. The motivation is that both, the media access in high-density WLANs as well as an intelligent radio resource management will be beneficial for long-range WLAN outdoor deployments. High-density deployments of Wi-Fi sensors require a simple but efficient way of radio resource management to avoid maintenance overhead, which would otherwise





**Figure 7.11** – Impact of different sector sizes versus network throughput,  $r_{thres} = 6$ .

increase exponentially with the number of wireless nodes. If a massive deployment of WLAN sensors would require too much maintenance overhead, such networks would not be attractive to system operators, due to increased operational costs. Instead a simple but highly flexible management framework must be designed to enable the deployment of large-scale heterogeneous sensor networks.

Additionally, an intelligent radio resource management must enable the coexistence among WLANs and WPANs. Due to the fact that in near future a wide spread outdoor deployment of WPANs (IEEE 802.15.4) and WPANs (IEEE 802.11ah) in the S1G ISM-bands will appear, requires an intelligent radio resource management, e.g., to mitigate interference problems as presented in Chapter 6, Section 6.4. The fact that lower carrier frequencies reach wider coverage areas, increase the coexistence issues in mixed WPAN/WLAN networks. WPAN and WLAN devices will compete for the same spectrum resources but are not optimized for concurrent wireless access. An advanced radio resource management must take this into account and must offer potential solutions. In the following, a generic radio resource management is developed that provides some solutions to these challenges.

The motivation is to combine the media access management framework with advanced spectrum sensing features and cognitive radio functions as outlined in Section 6.4.1. Spectrum sensing features are essential in order to maintain reliable

and robust communication links over large distances in wide area sensor networks. For instance, packet collisions must be classified to identify problems in wireless carrier detection in WPANs and WLANs. Cognitive radio functions combined with spectrum sensors provide an appropriate method to accomplish these tasks. Frequent spectrum sensing must be applied to such radio resource management to act with low latency on any kind of packet collisions or transmission anomalies.

Additionally, large scale IoT and M2M outdoor deployments require simple and control-less/control-free system architectures to reduce the complexity of such networks. Otherwise, high-density outdoor deployments would be difficult to install due to the complexity of the access control of hundreds or thousands of wireless nodes. A control-free WLAN/WPAN management framework enables a distributed access management with a central point of coordination and to shift the network complexity away from the access network plane to the management plane. This would provide a more efficient access control of hundreds or thousands of IoT devices.

An advanced RRMM logically combines WPANs and WLANs on the management plane. The management plane coordinates the access infrastructure in WPANs and WLANs. Management data is forwarded to centralized decision entities in the RRMM. Additionally, reports on wireless transmission failures are collected and decisions are made to mitigate retransmissions. Spectrum sensor devices which are added to the access infrastructure, frequently reports spectrum measurement results by using common network interfaces. Cognitive decision engines classifies the spectrum sensing reports and reports performance anomalies to the RRMM management plane. Additionally, spectrum data are stored in an RRMM data base (DB). The coordination of spectrum access between WPANs and WLANs is executed by the RRMM.

The advantage of the proposed RRMM framework is the simple installation to enable a control-less or even control-free wireless system architecture, which is required in future high-density WLAN/WPAN outdoor deployments. The RRMM monitors and manages the actions, including sectorization, synchronization, antenna array switching, and interference mitigation. Sectorization and grouping are essential in regard of the access priority. As motivated in Section 7.2 the sectorization allows an efficient coordination of wireless terminals in a wide coverage area. The sectorization must follow an optimization scheme that enables reduced collision probability combined with low network latency. In addition, some wireless nodes require higher access priority, such as alarm nodes [165]. Such device become part of specific groups in the RRMM. Next, the synchronization of sleep and wake-up periods is managed by the RRMM to improve the energy efficiency in sensor networks [166]. A centralized RRMM framework must enable and support energy conservation strategies, such as sleep and wake-up cycles. Then, antenna array switching becomes an important part of an advanced RRMM framework [167]. There are different kinds of beamforming mechanism required to optimize the throughput per single user, including horizontal beamforming [168], vertical beamforming [169],

3D-beamforming [170], and pencil beamforming [171]. A centralized RRMM framework must coordinate and optimize the physical beam constellations among multi-antenna WLANs and WPANs to maintain a high network capacity. Finally, interference alignment is an integral part of an advanced RRMM to mitigate the coexistence problems and to increase the network throughput performance [172]. In addition, interference avoidance mechanisms must be supported by the RRMM [173]. A more detailed sequence description of the proposed RRMM framework, which enables a control-less WLAN/WPAN communication infrastructure, is presented in Table 7.3.

**Table 7.3** – Sequence description of the proposed RRMM framework to enable a control-less WLAN/WPAN communication infrastructure.

Proposed advanced RRMM framework
Step 1: Sectorization of WPANs and WLANs and access prioritization of wireless terminals, e.g., sensor data, alarm, status information;
Step 2: Establish time synchronization among wireless networks; e.g., to enable sleep modes (energy saving strategies);
Step 3: Coordinated beamforming in multi-antenna WLANs and WPANs;
Step 4: Interference mitigation and sensing of spectrum anomalies, such as packet collisions and transmission failures;
Step 5: Execute media access, monitor, and control, dynamically add remove wireless terminals (massive access support).

The advanced RRMM framework in Table 7.3 comprises the aspects of an intelligent sectorization (Section 7.2) with the sensing of spectrum activities (Section 6.4.1) to mitigate interference and coexistence problems while increasing the transmission performance in hybrid WPAN/WLAN systems. Such combined approach enables a simple coordination of hundreds or thousands of wireless terminals in a large-scale deployment. IoT and M2M access networks would benefit from this approach because less system overhead is required in the wireless access networks. Major parts of the control is shifted to the management plane of an advanced RRMM framework. In particular, hybrid IEEE 802.15.4 and IEEE 802.11ah access networks can be installed dynamically with reduced coexistence problems. A practical deployment of an advanced RRMM would bring further insight on which functions need to be addressed in particular. For instance, asynchronous carrier sense detection thresholds must be adjusted to increase the effectiveness of the proposed framework.

## 7.4 Bibliographical notes

Several standardization organization addresses the problems of managing wireless networks and device provisioning, such as the *Open Mobile Alliance* (OMA) [174] and the *Broadband Forum* (BBF) [175]. A combined cellular and WLAN broadband in-house infrastructure is presented in BBF MR-235. However, these specifications of indoor networks have a low level of applicability for wide area outdoor deployments, such as IEEE 802.11ah. Hierarchical network architectures for high-density access terminals are presented in OMA DM v2.0. As an upcoming alternative, OneM2M [176] specifies an access framework for massive M2M device deployments. This framework is suitable, e.g., for IEEE 802.11ah devices, which require a simple but efficient access infrastructure.

Several radio resource management architectures can be found in the literature. The authors in [177] outline management schemes based on bandwidth, tx power, antenna, and inter-cell access schemes. Further, in [178] practical resource management schemes in different wireless systems, including 3G, beyond 3G, and related business models are presented. Additionally, the 3GPP community is under way to propose solutions for the integration of massive M2M access in cellular networks [165, 179, 180]. However, these studies have a limited use for the coexistence problems of hybrid WPAN/WLAN systems. The transmission challenges, when a large number of WLAN nodes is present, have been evaluated in [181–187]. However, these studies consider a lower network density compared to the assumption in this thesis. However, a helpful definition of massive access missing in these studies. This thesis defines massive access in Section 7.1.1.

Studies in [184, 186, 187] do not give detailed information about the network density, relieving the circumstance that massive access scenarios are not in the main research focus. Typically, these studies consider a low density, e.g., 20 APs, as in [182], or single WLAN/STA communication, as in [183], and [185]. The study in [181] considers 50 WLAN nodes and argues that the collision probability increases in dense WLANs significantly. The authors in [188] evaluated a CSMA-type MAC protocol based random network, while further investigating on a specific scenario on geometry and propagation models. Here, the authors propose a circular sector for a specific path loss model, which they evaluated for different medium access probabilities and network densities. Radio resource management (RRM) in LTE is discussed in [189].

## 7.5 Discussion and summary

### 7.5.1 Discussions

IEEE 802.11ah provides multi-antenna support to exploit multi-path characteristics in wireless networks. The PHY model is optimized for outdoor long-range communication. Combined with beamforming, IEEE 802.11ah enables a highly

adaptive sectorization scheme. However, it is not well understood how a large number of WLAN STAs can be supported by single or multiple beams. The exchange of beamforming control data can be critical to the network performance, which is well-known problem in ESPAR antenna deployments [60].

Further, an important aspect is the utilization of multi-user MIMO (MU-MIMO) in WLAN-based sensor networks. IEEE 802.11ah offers such capability due to the mandatory multi-antenna support. However, the transmission performance and spectrum efficiency [bit/Hz/s/user] depends on the number of users. If the user density is low in a cell (or sector), the performance of single-user MIMO (SU-MIMO) is high compared to MU-MIMO. In the case when the density of users is increased, the space multiplexing performance is reduced for SU-MIMO. If the user density is high, MU-MIMO results in additional spectral efficiency; thus, highly dense wireless networks, such as IEEE 802.11ah, should utilize MU-MIMO to increase the spectral efficiency.

It is also envisioned that in the near future (2016-2020), the regulator will have the obligation<sup>1</sup> to coordinate the media access to mitigate the interference for wireless legacy devices, including passive RFIDs. A centralized wireless spectrum monitoring system, such as the proposed RRMM framework, would allow concurrent wireless media access among wireless systems in the same radio-band, prevent from illegal spectrum activities; thus, increases the reliability of these wireless communication systems, even in disaster events (disaster networks), such as tsunamis, earthquakes, or to support humans in dangerous and difficult-to-reach areas. For instance, a similar system could be added to current regulator obligations for 700 MHz cellular systems that is to be used to protect the licensed spectrum users from illegal spectrum operations by secondary users, as suggested by the Bangladesh Telecommunication Regulatory Commission (BTRC) [190].

### 7.5.2 Summary of the chapter

This chapter has outlined the considerable performance gain that can be achieved adopting orthogonal sectorization to mitigate RTS management frame collisions, proposing a synchronized RTS frame emission. The proposed sectorization access management scheme showed that up to five times more WLAN STAs can be supported with respect to high-density deployments. The results obtained in this chapter for radio resource management showed that at the MAC layer a significant gain can be achieved when the coverage area of wide area WLANs is logically divided into sectors. A key role plays an advanced RRMM framework that controls the sectorization in hybrid networks that comprises of WPAN and WLAN devices. Important aspects are the optimization of increased network throughput, while mitigating the collision probability and transmission latency in such hybrid WPAN/WLAN sensor networks.

---

<sup>1</sup>Most likely the regulator will reject to have the obligation to dynamically control the spectrum access. Instead, some third party may be responsible to manage the spectrum access, including temporal license, rewards and restrictions.

This chapter logically concludes the development of S1G WLANs and the deployment of long-range WLANs in large outdoor deployments. Chapter 4 motivated the need for coverage enhancements in S1G WLANs to enable a one-hop reach for a large number of WLAN STAs and a reliable long-range wireless link among the S1G WLAN AP and S1G WLAN STAs. Next, in Chapter 6 it was observed that severe packet collisions occur in hybrid WLAN and WPAN deployments. These deployment scenarios are envisioned in future smart cities and smart grids, e.g., for wireless monitoring of meter data. This chapter added a further component to this discussion, namely the impact of a significant larger number of WLAN STAs, which is the consequence of outdoor deployment of long-range WLANs. In addition to the coverage enhancements, as proposed in Chapter 4, this chapter adds to the problem of massive deployment of WLAN STAs. As a consequence, a proper radio resource management is required that focuses on network aspects, including coexistence, interference mitigation, coverage range and average throughput.

The proposed framework opens the avenue for further discussion. In particular, conducting outdoor measurements would be beneficial to obtain further insight of the characteristics of such deployment scenarios. A sector-based approach, as proposed in this chapter, is a promising way to mitigate packet collisions among signaling data, such as RTS frames. However, a centralized RRM scheme is required that also incorporates the presence of other wireless systems on the same spectrum, including WPANs and RFIDs.

## Chapter 8

# Conclusions

S1G WLANs appears to be a highly efficient wireless communication technology for short burst data traffic. In particular, IoT and M2M services will benefit from the new IEEE 802.11ah WLAN protocol amendment that utilizes the license-exempt 900 MHz ISM-band in various countries. It is predicted that IEEE 802.11ah WLANs will foster the use of WLAN technology in a large variety of wireless sensor networks. Therefore, this dissertation contributes a set of protocol enhancements that addresses the fundamental system challenges of S1G WLANs. These system challenges have been addressed from a plurality of perspectives, namely prototyping and over-the-air evaluation, coverage enhancement, energy consumption reduction, coexistence, and high-density media access. These five objectives are motivated by a thorough introduction of the sub-1 GHz research in this dissertation. The introduction started with the recapitulation of the petition issued by Google Inc. that called for an unrestricted access in the license-exempt S1G radio-band that will enable a plethora of new innovative wireless services in the near future [8]. Technological developments (the push) as well as new applications, markets and business opportunities (the pull) were discussed as part of the introduction. In essence, the use of the IEEE 802.11 WLAN protocol for sensor devices will result in a new wireless system in the near future, which is the *Wi-Fi sensor* device. Longer wireless coverage ranges, the need for energy consumption reduction, and high-density networks are the challenging tasks for WLANs operating on the 900 MHz ISM radio-band. The use of carrier frequencies in the ISM-band below 1 GHz for WLANs was the imperative for the majority of the evaluations. The proposed WLAN enhancements are unique because the target carrier frequency was in the 900 MHz spectrum. In parallel to this dissertation, the standardization work of the IEEE 802.11ah Task Group flourished and aims to amend the IEEE 802.11 WLAN protocol and add an additional operational spectrum at 900 MHz. Insights on the significant challenges and opportunities of the S1G WLANs have been analyzed. It is apparent that the S1G WLANs will provide a wider range of indoor and outdoor WLANs compared to today's WLANs that operate on the 2.4 GHz and 5 GHz spectrum. It is evident

that the IEEE 802.11ah based WLANs will cause to new communication challenges. The scenario of providing a large coverage area leads to interference challenges in highly dense S1G WLAN deployments. Therefore, the evaluation demonstrates that the IEEE 802.11ah suffers from potential coexistence problems, such as an increase of packet collisions. Remedies to mitigate the coexistence problems are imminent, and hence potential solutions were proposed. As one of the major contributions of this dissertation, an S1G WLAN prototype was constructed, which was very useful in conducting an over-the-air evaluation. In essence, no S1G WLAN devices were available during the time this dissertation was written, which would have been based on the IEEE 802.11ah ah WLAN protocol amendment. The first IEEE 802.11ah-based WLAN devices will be shipped in 2015/2016. Hence, the construction of a novel S1G WLAN prototype is important. This chapter is organized as follows. In Section 8.1, the recapitulation of the research objectives is presented by asking relevant questions related to prototyping, coverage enhancement, energy consumption reduction, coexistence, and high-density media access. The questions motivated the categorization of the five tasks in this dissertation. Next, in Section 8.2, a list of the five tasks is presented, which gives a summary of the research results. Finally, in Section 8.3, future research topics of S1G WLANs are identified. The chapter concludes with an epilogue in Section 8.4. Based on the results obtained from the analysis, simulation, and field measurements, the following conclusions are drawn.

## 8.1 Recapitulation of research objectives

The targeted research questions were categorized as follows:

1. *“How does a real-world S1G WLAN operate?”*: The transmission performance of WLANs at 2.4/5 GHz is well investigated. However, with the use of lower frequencies, new system challenges arise, including a limited channel bandwidth and MIMO-OFDM operation in narrow-bands. It is essential to have first-hand experiences with real-world hardware of S1G WLANs. Upper throughput performances should be known, e.g., to make realistic predictions of the network throughput characteristics. In this dissertation, an S1G WLAN hardware prototype was proposed. In particular, the design steps and the selection process for the relevant hardware components were discussed. Information was provided on which hardware was used and on which software extensions are essential to provide a helpful step-by-step description, e.g., to re-build the prototype, by other researchers. The main contribution of this thesis is a full functioning and highly flexible IEEE 802.11ah prototype. The prototype is highly useful to test PHY and MAC modifications and to conduct wireless measurements over-the-air. Up to now, there has been a lack of certified IEEE 802.11ah hardware. However, the proposed prototype is available and is simple to use, e.g., for wireless coexistence measurements.



2. *“What are the coverage boundaries of the S1G WLANs?”*: The S1G WLANs exploit the wider propagation of radio waves at the 900 MHz band. Thus, a two to three time wider coverage is the target for the S1G WLAN coverage. In particular, the IEEE 802.11ah WLAN amendment aims to enable a wireless coverage range up to 1 km at low data rates. The S1G WLANs exploit the multi-path propagation by using multiple-antennas. Hence, MIMO precoding becomes an important part of the design of long-range S1G WLANs. A longer range can be achieved, when precoding was modified so that the link budget is increased at 2 to 3 dB. The S1G ISM-bands exhibit significant limitations in the channel bandwidth. For instance, Japan only allows a 1 MHz channel bandwidth in the 915 to 930 MHz band. Applying the MIMO-OFDM technology in the limited channel bandwidth, e.g., for short data burst transmissions, is a new paradigm in wireless sensor communication. Thus, it is beneficial to obtain a thorough understanding of the performance of the MIMO-OFDM technology in narrow-bands, e.g., to estimate the upper transmission boundaries. This dissertation presents the very first insight in MIMO-OFDM S1G WLAN performance. Therefore, a thorough evaluation of a multi-flow D2D communication scenario was part of the discussion to identify the potential of interference mitigation and the type of precoding schemes that would be beneficial.
3. *“How to address the demand for an energy-efficient S1G WLAN?”*: Next, the energy consumption of an IEEE 802.11n WLAN module was evaluated because there was no IEEE 802.11ah WLAN module available yet. An adaptive RF chain control for a multi-antenna MIMO-OFDM was proposed. Energy was reduced to 50 % when switching occurred among the active multi-antenna RF-chains. It contained a thorough evaluation on the RF-chain control (RFCC) proposal. In addition, a helpful analytical model was proposed to verify the experimental results. A comparison of the analytical and experimental results exhibited identical characteristics. The validity of the proposed energy consumption model was confirmed.
4. *“What are the problems with coexistence in sub-1 GHz?”*: Similar to the coexistence of wireless systems at 2.4 GHz, e.g., among WLANs, Bluetooth™, ZigBee™, IEEE 802.11, and IEEE 802.15, a potential threat of coexistence problems was identified when utilizing S1G WLANs. Using the proposed S1G WLAN prototype, a first-hand study regarding coexistence problems among the WLAN and IEEE 802.15.4 WPAN was conducted to monitor the coexistence problems. Packet collisions of WLAN and WPAN frames were classified, and coexistence problems were identified.
5. *“How to maintain a high-density WLAN because of wider coverage?”*: A wider coverage range of the S1G WLAN allows more WLAN STAs to associate with a single WLAN AP. The high-density WLANs and the massive access of the WLAN STAs in S1G networks is a new challenge in future long-range

WLANs. Massive access scenarios in S1G WLANs are part of this evaluation. A sectorized RTS/CTS access scheme was proposed that enables the S1G WLAN to serve hundreds or thousands of WLAN STAs at one single WLAN AP concurrently.

In essence, the research objectives are categorized in the following tasks:

1. IEEE 802.11ah WLAN prototype and test site (Chapter 3).
2. Coverage enhancement (Chapter 4).
3. Energy consumption reduction strategies (Chapter 5).
4. Coexistence in the S1G ISM-band (Chapter 6).
5. High-density media access and radio resource monitoring and management (RRMM) framework (Chapter 7).

In the following sections, the contributions to each task are summarized.

## 8.2 Recapitulation of research contributions

In the following points, the research contributions of this dissertation are summarized:

1. IEEE 802.11ah WLAN prototype development and test site:  
 In this dissertation, a narrow-band S1G  $2 \times 2$  MIMO-OFDM WLAN was proposed. The WLAN prototype enables first-hand performance evaluations on the wireless signal characteristic, throughput boundaries and coexistence. In addition, the proposed WLAN protocol modifications were successfully evaluated in field measurements. These measurements included enhancements on the MIMO precoding. Other measurements included the D2D settings with two consecutive data flows. Next, a novel wireless sensor was developed to conduct spectral-time observations of packet collisions in the sub-1 GHz radio-band. The original contributions include extensive measurements using the proposed S1G WLAN prototype. The S1G prototype utilizes the 920 MHz carrier frequencies in the Japanese ISM-band. The channel bandwidth was set to 1 MHz. A narrow-band  $2 \times 2$  MIMO-OFDM WLAN was proposed that uses SDR components and software that allows a simple setup of a flexible WLAN. Modifications of the on-going IEEE 802.11ah WLAN standardization were implemented. Detailed signal characteristics were discussed and the upper throughput boundaries were identified at 100 kbps, which was found to be in the wireless transmission performance regime of the S1G WLAN prototype. The ICMP, UDP, and TCP transmissions were included in the performance evaluation. The use of the prototype and its results from the field measurements demonstrated the practicability of constructing a  $2 \times 2$  MIMO-OFDM system.

2. Coverage enhancement:

Apparently, the codebook design supported the wider coverage range of the S1G WLANs. In essence, the usefulness of the precoding modifications was beneficial. The use of the Grassmannian and Kerdock manifold contributed to an increased link budget. Additionally, modifications on the Kerdock manifold reached up to 3 dB and the link budget increased; thus, further enhancing the wireless coverage of an S1G WLAN. In addition, evidence was provided, which indicated that the multi-flow scenarios suffered from a significant drop in the transmission performance; thus, leaving the opportunity for optimization.

3. Energy consumption reduction strategies:

Contributions on reducing the energy consumption of a multi-antenna MIMO system were presented, which led to a reduction in the energy consumption of the WLAN AP during the active data frame transmission. Using a multiple-antenna MIMO system, the RF-chains were identified as the main contributor to the energy consumption of a WLAN module (here an IEEE 802.11n WLAN module was the evaluation target). By simply switching off the unused RF chains while sending a low data rate caused a significant energy consumption reduction of up to 40%. In addition, the energy consumption scheme was evaluated with a numerical model.

4. Coexistence in the S1G ISM-band:

The opportunity to provide large coverage enables new services and applications in the low-cost consumer market, including wide range sensing and metering applications. Coexistence challenges are presented, which appear when the WPAN and WLAN operate at the same carrier frequencies and send data packets concurrently. Spectrum measurements illustrate the serious packet collisions. This has motivated to classify the different collision patterns in this dissertation. It was found that the collision occurs for data frames as well as for management frames (ACK frames). The WLAN data frames and WPAN data frames are affected by the packet collisions. Packet detection threshold modifications exhibited a significant change in the observed number of packet collisions.

5. High-density media access:

To alleviate the interference among a large number of S1G WLAN STAs, a novel high-density media access has been in the research focus. The motivation was to operate an S1G WLAN in a large dense outdoor deployment. Packet collisions that occur, even when the RTS/CTS schemes were used required new media access solutions. The evaluation included hundreds of simulated WLAN nodes. It was found that the RTS frame collisions led to a significant performance loss in high data rate regimes. A basic coexistence framework for monitoring, controlling, and executing was evaluated.

### 8.3 Future research topics

S1G WLANs will open an avenue to completely new applications and services. New services will include long-range wireless metering and sensing, combined with simple data gathering, such as temperature and pressure as well as complex data gathering, such as biorhythm and surveillance. Potential use cases for S1G WLANs are:

1. Wireless energy distribution management system.
2. Digital grid.
3. Wireless software-defined networks (SDN).

S1G WLANs are a perfect choice for low and medium data rate applications. The cost-efficient, reduced energy consumption and simple deployment make S1G WLANs a strong candidate for licensed-except indoor and outdoor networks. Research on this particular topic would foster the on-going standardization activities, e.g., the coexistence between WLAN and WPAN devices that use the same wireless channels. Subsequent research topics include:

1. Coexistence among S1G WLAN and RFID systems.
2. Wi-Fi off-loading in S1G WLANs.
3. New applications of S1G WLANs, including unmanned autonomous vehicles (UAV), WSN-UAVs, disaster networks, robotics (mobile home robots), 3D-networks [191], and aerial relay stations [192].
4. Ultra-reliable wireless communication in hostile environments (nuclear plants, oil platforms).
5. Aerial surveillance (harbor security, logistics).
6. Proprietary IEEE 802.11ah WLAN protocol enhancements to enable ultra-reliability and ultra-security in tactical and commercial S1G WLANs.
7. Zero-energy WLANs based on the IEEE 802.11ah WLAN protocol and energy harvesting from the ambiance [193].
8. Wake-up and radio-on-demand (ROD) for the IEEE 802.11ah WLAN protocol [194].
9. Cognitive network management and resource virtualization in large-scale wireless long-range WLANs [195, 196].
10. Access network discovery and selection functions (ANDSF) [197].
11. Relaying and relay nodes in S1G WLANs [189].

12. Full-duplex (FD) wireless communication and spatial modulation in Wi-Fi sensor networks [95] and self-interference cancellation [96].
13. Mobility and drive tests in S1G WLANs.

An rising topic of interest with respect to link relaying is how to further optimize IEEE 802.11ah WLAN protocol to increase the energy efficiency of the IEEE 802.11ah-based *Wi-Fi sensors*.

## 8.4 Epilogue

WLANs offer a simple setup and are cost efficient; thus, WLANs can be seen as a *disruptive innovation*. However, can WLANs disrupt the wireless market domain? Will the cellular operators feel the *innovator's dilemma*? Indeed, Wi-Fi has already become a disruptor in the cellular market. The WLAN protocols are recognized as competitive solutions which standardizes at relevant carrier frequencies. Cellular operators recognize the presence of tremendous Wi-Fi success and are already engaging in discussions that the unlicensed band should be partly utilized by LTE<sup>1</sup>. However, the IEEE 802.11 Task Groups can find new opportunities and can finalize standardization projects within few years. They can utilize the available frequency resources (white space access, large bandwidth) and can contribute several standards simultaneously. Wi-Fi will evolve as a disruptive innovation in several wireless areas in the near future. Disruptive technology always comes out of nowhere and comes quickly so that it is a challenge to identify relevant market movements. A *disruption* of the IEEE 802.15 and ZigBee product lines and market shares by the IEEE 802.11ah WLAN protocol is possible. The future will tell whether the IEEE 802.11ah WLAN protocol had only a *singularity* effect in the wireless sensor market or it has become a strong competitor with a large market share leaving the IEEE 802.15.4 and ZigBee products behind.

---

<sup>1</sup>LTE Advanced in the unlicensed spectrum [198]. This can be also interpreted as a potential strategy against the disruptive character of Wi-Fi.



## Appendix A

# IEEE 802.11n, 802.11ac, 802.11ah PHY/MAC parameter list

Table A.1 and Table A.2 (continued) give a detailed comparison of IEEE 802.11ah<sup>1</sup>, IEEE 802.11n, and IEEE 802.11ac PHY/MAC parameters. The presented overview is of importance, e.g., to identify upper performance boundaries of the protocols or to implement a wireless prototype.

The *Greenfield Mode* can be selected to increase the efficiency of WLANs, e.g., to eliminate the support of legacy WLANs, i.e., IEEE 802.11a/b/g, to improve the efficiency. The *OBSS* feature allows the mitigation of interference with other wireless systems that operate in the same radio-band in near location.

---

<sup>1</sup>Under standardization development [199].

**Table A.1** – Comparison of the IEEE 802.11 protocol amendments IEEE 802.11n [18], IEEE 802.11ac [16], and IEEE 802.11ah [5].

<b>System parameters</b>	<b>IEEE 802.11n (20 MHz)</b>	<b>IEEE 802.11ac (20 MHz)</b>	<b>IEEE 802.11ah (1 MHz)</b>
Radio frequency [MHz]	2400-2497, 5150-5350, 5725-5825	5170-5330, 5490-5710, 5735-5835	917.5-923.5 (South Korea), 916.5-927.5 (Japan), 863-868 (Europe), 755-787 (China), 866-869 and 920-925 (Singapore), 902-928 (US)
Channel bandwidth [MHz]	20	20	1-16
Modulation type	BPSK, QPSK, 16QAM, 64QAM	BPSK, QPSK, 16QAM, 64QAM, 256QAM	BPSK, QPSK, 16QAM, 64QAM, 256QAM
Num of subcarriers/- data/pilot	56 /52 / 4	56 /52 / 4	26 / 24 /2
Pilot subcarrier	-21, -7, +7, +21	-21, -7, +7, +21	-7, +7
$N_{st}$ [Number of total OFDM subtones]	56	56	26
$N_{sd}$ [Number of complex data numbers per spatial stream per OFDM symbol]	52	52	24
$N_{sp}$ [Number of pilot values per OFDM symbol]	4	4	2
$N_{ss}$ [Number of spatial streams]	1-4	1-8	1
$N_{es}$ [Number of BCC encoders for the DATA field]	1-2	1	1
$N_{sts}$	1-4	–	1-4



**Table A.2** – Comparison of the IEEE 802.11 protocol amendments IEEE 802.11n [18], IEEE 802.11ac [16], and IEEE 802.11ah [5] (continued).

System parameters	IEEE 802.11n (20 MHz)	IEEE 802.11ac (20 MHz)	IEEE 802.11ah (1 MHz)
Num of FFT points	64	64	32
STF duration [ $\mu s$ ]	8	8	160
STF duration (double guard interval) [ $\mu s$ ]	–	–	40 (if 2 MHz)
LTF1 duration [ $\mu s$ ]	8	8	160
LTFS duration [ $\mu s$ ]	4 (Mixed), 8 (Greenfield)	4	40
SIG duration [ $\mu s$ ]	4	4	240
Guard interval duration [ $\mu s$ ]	0.8	0.8	8
Double guard interval duration [ $\mu s$ ]	1.6	1.6	16
Short guard interval duration [ $\mu s$ ]	0.4	0.4	4
Greenfield	(option)	(option)	n.a. only if 2 MHz
Data Rate [199]	600 Mbps (40 MHz, 4 SS)	6.933 Gbps (160 MHz, 8 SS)	17.7 Mbps (256 QAM, $N_{ss} = 4$ , short GI)



## Appendix B

# Standard contributions by the author

The following related standard contributions have been submitted by the author:

### IEEE 802.11ah TG standard contributions

1. Stefan Aust, “*Coexistence in 950 MHz-958 MHz in Japan*”, IEEE 802.11-10/1420r0/1/2/3, December 6, 2010.
2. Stefan Aust, “*Additional Use Cases for Sub-1 GHz license-exempt Frequency Bands*”, IEEE 802.11-10/1458r0, December 21, 2010.
3. Stefan Aust, Je-Hyung Song Dave Halasz, “*Proposed IEEE 802.11ah Use Cases*”, IEEE 802.11-11/0017r0/1/2/3/4/5, January 6, 2011.
4. Stefan Aust, “*AP Power Saving*”, IEEE 802.11-11/0046r0/1/2, January 14, 2011.
5. Stefan Aust, Jae-Hyung Song, Dave Halasz, “*Proposed TGah Use Cases SED*”, IEEE 802.11-11/0174r0, January 20, 2011.
6. Stefan Aust, “*TGah Use Cases Straw-polls*”, IEEE 802.11-11/0221r0, February 4, 2011.
7. Stefan Aust, “*TGah Use Case: AP Power Saving in Smart Grid*”, IEEE 802.11-11/0273r0, February 28, 2011.
8. Stefan Aust, “*TGah list of use case submissions*”, IEEE 802.11-11/0274r0/2, February 28, 2011.

9. Stefan Aust, “*TGah STA Analysis for Smart Grid Use Case*”, IEEE 802.11-11/0355r0, March 14, 2011.
10. Stefan Aust, Mitsuru Iwaoka, Shusaku Shimada, “*Japanese Channelization for 802.11ah*”, IEEE 802.11-11/1318r0, September 21, 2011.
11. Shusaku Shimada, Stefan Aust, Mitsuru Iwaoka, “*Proposed US Channelization for IEEE 802.11ah*”, IEEE 802.11-12/0092r0/1, January 16, 2012.
12. Shusaku Shimada, Stefan Aust, Kei Sakaguchi, Mitsuru Iwaoka, “*Time Freq. Measurement Mechanism & Procedure*”, IEEE 802.11-12/0872r0/1, July 16, 2012.
13. Shusaku Shimada, Stefan Aust, Mitsuru Iwaoka, Yusuke Asai, “*Spectrum access and Tx control for regulatory conformance*”, IEEE 802.11-12/0871r0/1, July 15, 2012.
14. Shusaku Shimada, Kei Sakaguchi, Ken Mori, Mitsuru Iwaoka, Stefan Aust, “*TSF Timer Frequency Management and Measurement Procedure (TFM2P)*”, IEEE 802.11-12/1250r0, October 31, 2012.
15. Shusaku Shimada, Kei Sakaguchi, Ken Mori, Mitsuru Iwaoka, Stefan Aust, “*TSF Timer Freq. Management and Measurement Procedure (TFM2P)*”, IEEE 802.11-12/1376r0, November 13, 2012.
16. Shusaku Shimada, Kei Sakaguchi, Fei Tong, Stefan Aust, Ken Mori, Mitsuru Iwaoka, “*Estimated battery life improvement by (TFM2P)*”, IEEE 802.11-12/1065r0/1/2, September 17, 2012.
17. Shusaku Shimada, Stefan Aust, “*Supplementary specifics of sensor use cases for defining the enhanced power saving feature*”, IEEE 802.11-13/0101r0, January 15, 2013.
18. Shusaku Shimada, Stefan Aust, Mitsuru Iwaoka, “*Utilization of Direct Link for Power Saving*”, IEEE 802.11-13/0325r0, March 19, 2013.

## IEEE 802.15.4s standard contributions

1. Stefan Aust, Shusaku Shimada, Mitsuru Iwaoka, Shouichi Kitazawa, “*Consideration of the 900 MHz ISM radio-band*”, IEEE 802.15-13-0153-00-0sru/0/1/2, March 19, 2013.
2. Shusaku Shimada, Shouichi Kitazawa, Stefan Aust, Mitsuru Iwaoka, “*SRU by radio resource measurement & management for enhanced reliability*”, IEEE 802.15-13-0132-02-0sru/0/1/2, March 20, 2013.

## IEEE DySPAN-SC P1900.6/P1900.6a WG standard contributions

1. Stefan Aust, “*P1900.6 New Topics*”, DCN 6-10-0017-00-000, May 20, 2010.
2. Stefan Aust, Darcy Swain, “*DA Extensions Merged*”, DCN 6-10-0029-00-0000, August 20, 2010.
3. Stefan Aust, Darcy Swain, “*DA Extensions Merged*”, DCN 6-10-0029-00-0000, August 20, 2010.
4. Stefan Aust, Darcy Swain, “*Proposed PAR on DA interface extensions*”, DCN 6-10-0034-00-0000, September 9, 2010.
5. Stefan Aust, “*P1900.6 comments on draft PAR*”, DCN 6-10-0040-01-0000, November 4, 2010.
6. Stefan Aust, “*Candidate Data Sources*”, DCN 6-10-0041-00-0000, November 5, 2010.
7. Stefan Aust, “*Candidate standard groups*”, DCN 6-10-0047-00-0000, December 9, 2010.
8. Stefan Aust, “*IETF PAWS BoF Discussion*”, DCN 6-11-0008-02-0000, February 16, 2011.
9. Stefan Aust, “*P1900.6a Usage Model - Green Cognitive Radio*”, DCN 6-11-0018-02-0000, May 5, 2011.
10. Stefan Aust, “*P1900.6a Usage Model - Green Cognitive Radio*”, DCN 6-11-0018-02-0000, May 5, 2011.
11. Stefan Aust, Bernd Bochow, “*P1900.6a: Guidelines for Contributions*”, DCN 6-11-0022-01-0000, June 20, 2011.
12. Stefan Aust, “*P1900.6a Functional Requirements - Green Cognitive Radio*”, DCN 6-11-0021-02-0000, September 9, 2011.
13. Stefan Aust, Masahito Iwai, Tetsuya Ito, “*P1900.6a: Enhanced Interface for Green Cognitive Radio*”, DCN 6-11-0056-01-0000, December 12, 2011.
14. Stefan Aust, Masahito Iwai, Tetsuya Ito, “*Proposed text contributions to P1900.6a Draft standard - Sect. 5 (The IEEE 1900.6 reference model), sect. 6 (Information description)*”, DCN 6-12-0012-01-0000, March 23, 2012.
15. Stefan Aust, Masahito Iwai, Tetsuya Ito, “*IEEE P1900.6a: Explanation of proposed text in DCN 6-12-12*”, DCN 6-12-0014-01-0000, March 23, 2012.



# Symbols

The following list contains the symbols that recur throughout this thesis. Mathematical quantities are listed for the ease of use.

$BW$	channel bandwidth
$C$	(Shannon) channel capacity
$c$	velocity of electromagnetic waves in free space ( $\frac{1}{\sqrt{\epsilon_0 \cdot \mu_0}} = 2.99792458 \cdot 10^8 \frac{m}{s}$ )
$d$	distance
$d_1$	EUT dimension (rounded)
$d_2$	AUT dimension (rounded)
$d_a$	antenna separation distance
$d_{BP}$	break point distance
$d_c$	chordal distance
$d_{test}$	distance between multiple EUTs, DUTs, AUTs at the test site
dB	decibel
dB <sub>i</sub>	decibel (isotropic)
dB <sub>m</sub>	decibel (milliwatt)
det	matrix determinant
$f_0$	center frequency
$f_1$	lower band frequency
$f_2$	upper band frequency
$f_c$	carrier frequency
$G_{rx}$	receiver antenna gain
$G_{tx}$	transmitter antenna gain
<b>H</b>	MIMO channel transmission matrix
$h(\tau)$	impulse response
$h_{rx}$	receiver antenna height
$h_{tx}$	transmitter antenna height
<b>I</b>	MIMO channel identity matrix
$i, n$	index
$k$	sampling rate
$\log_2(\cdot)$	base 2 logarithm
$\log_{10}(\cdot)$	base 10 logarithm

$N_0$	spectral density of the noise power
$N_c$	number of columns in a CSI matrix (determined by the $N_c$ index field of the MIMO control filed) [17]
$N_r$	number of rows in a CSI matrix (determined by the $N_r$ index field of the MIMO control filed) [17]
$N_{es}$	number of BCC encoders for the DATA field
$N_{rx}$	number of receive antennas
$N_{sd}$	number of complex data numbers per spatial stream per OFDM symbol
$N_{sp}$	number of pilot values per OFDM symbol
$N_{ss}$	number of spatial streams
$N_{st}$	number of total OFDM subtones
$N_{tx}$	number of transmit antennas
$r_{coverage}$	wireless coverage range (one-hop)
$rx_{thres}$	receiver threshold [dBm]
$S$	throughput (normalized)
$T_{RAW}$	RAW duration (IEEE 802.11ah)
$T_S$	time slot (IEEE 802.11ah RAW)
$T_{beacon}$	beacon time interval
$t$	time variable
$W$	Watt
$\mathbf{W}_k$	codebook
$w_i$	codeword
$\epsilon_0$	vacuum permittivity (electric constant), 8.854e-012 [F/m]
$\eta_\mu$	spectrum efficiency
$\eta_\nu$	energy efficiency
$\mu_0$	vacuum permeability (magnetic constant), 1.257e-006 [Vs/Am]
$\lambda$	wavelength
$\sigma^2$	variance
$\tau$	delay
$\in$	in
$(\cdot)^T$	transpose
$(\cdot)^H$	Hermitian transpose
$(\cdot)^*$	complex conjugate



# Abbreviations

3GPP	3rd generation partnership project
4G	fourth generation
AC	access category (EDCA)
ACI	adjacent channel interference
ACK	acknowledgment
ANDSF	access network discovery and selection function
ANI	ambient noise immunity
AP	access point
ARF	auto rate fallback
ARQ	automatic repeat request
API	application programming interface
AUT	antenna under test
AWGN	additional white Gaussian noise
BD	block diagonalization
BCC	binary convolutional coding
BER	bit error rate
bps	bits per second
BPSK	binary phase shift keying
BS	base station
BSS	basic service set (IEEE 802.11)
BTRC	Bangladesh telecommunication regulatory commission
CBR	constant bit rate
CC	computational complexity
CCA	clear channel assessment
C-CCA	centralized CCA (proposed)
CDF	cumulative distribution function
CDU	collision detection unit (proposed)
cf.	Latin: confer
CFP	contention free period
CF-Poll	contention free-poll
COTS	commercial off the shelf (general purpose HW)
CP	contention period

CPU	central processing unit
CRA	concentric ring array
CRC	cyclic redundancy check
CS	carrier sensing
CSI	channel state information
CSMA	carrier sense multiple access
CSMA/CA	carrier sense multiple access/collision avoidance
CSMA/CD	carrier sense multiple access/collision detection
CTS	clear to send
CW	contention window
D2D	device-to-device
DA	directional antenna
DCF	distributed coordination function
DCN	document counting number
DCTS	directional CTS
DFT	discrete Fourier transform
DIFS	DCF inter-frame spacing
DL	downlink
DNAV	directional NAV
DOA	direction of arrival
DPC	dirty paper coding
D-RAW	dynamic RAW (proposed)
DS	delay spread
DSSS	direct sequence spread spectrum
DTFT	discrete time Fourier transform
DUT	device under test
DySPAN-SC	dynamic spectrum access networks - standards committee
EBB	eigenvalue based beamforming
ECDF	experimentally determined CDF
EDCA	enhanced distributed channel access
EDCAF	enhanced distributed channel access function
EGB	equal gain bipolar (codebook)
EMI	electromagnetic interference
ERM	electromagnetic compatibility and radio spectrum matters
EIRP	equivalent isotropically radiated power
e.r.p.	effective radiated power
ESPAR	electrically-steerable parasitic array radiator
ETR	ETSI technical report
ETS	European telecommunication standard
ETSI	European telecommunications standards institute
EUT	equipment under test
EVM	error vector magnitude
FD	full duplex
FDD	frequency division duplex

FDMA	frequency division multiple access
FER	frame error ratio
FFT	fast Fourier transform
FHSS	frequency hopping spread spectrum
FIR	finite impulse response
FNBW	first null beam width
FSK	frequency shift keying
FTP	file transfer protocol
Gbps	gigabit per second
GHz	gigahertz
GW	gateway from/to fixed network
GMSK	Gaussian minimum shift keying
GSM-R	global system for mobile communications - railway
HC	hybrid coordinator
HCF	hybrid coordination function
HD	half duplex
HEMS	home energy management system
HEW	high efficiency WLAN
HF	high frequency
HPBW	half power beamwidth
HT	high throughput
HW	hardware
Hz	Hertz
ICI	inter carrier interference
ICMP	internet control message protocol
IDFT	inverse discrete Fourier transform
IEEE	institute of electrical and electronics engineers
IEICE	institute of electronics, information and communication engineers
IFFT	inverse FFT
IFS	inter-frame spacing
IG	interest group
i.i.d.	independent identically distributed
IoT	Internet of things
IP	Internet protocol
I/Q	in-phase/quadrature
ISM	industrial, scientific and medical
ISI	inter-symbol interference
ITU	international telecommunication union
ITU-T	ITU telecommunication standardization sector
L2	OSI-layer 2
L3	OSI-layer 3
LAN	local area network
LBT	listen before talk
LB-CCA	location-based CCA (proposed)

LDPC	low-density parity-check code
LMS	least mean square
LOS	line-of-sight
LS	least-squares
LTE	long term evolution
LTF	long training field
M2M	machine-to-machine
MAC	medium access control
Mbps	megabit per second
MCS	modulation and coding scheme
MHz	megahertz
MIMO	multiple-input multiple-output
MISO	multiple-input single-output
MKL	math kernel library (FFT, etc.)
MLME	MAC sublayer management entity
MMSE	(linear) minimum mean squared error
MoM	method of moments
MRC	maximum ratio combining
MRT	maximum ratio transmission
MS	mobile station
MSE	mean square error
MTC	machine type communications
MU	multi-user
MUI	multi-user interference
MU-MIMO	multi-user MIMO
MUSIC	multiple signal classification
MWBE	maximum welch bound equality (codebook)
NAV	network allocation vector
NDP	null data packet (channel sounding)
NLOS	non-line-of-sight
OBSS	overlapping basic service set
OCTS	omni-directional CTS
OFDM	orthogonal frequency division multiplexing
OLOS	obstructed LOS
OSTBC	orthogonal space-time block code
O-to-I	outdoor to indoor
PAN	personal area network
PBR	packet bit rate
PC	point coordinator (media access)
PCF	point coordination function
PDF	probability distribution function
PDP	power delay profile
PDU	protocol data unit
PER	packet error rate

PHY	physical layer
PIFS	PCF inter-frame spacing
PLCP	physical layer convergence procedure
PL	path loss
PLME	PHY sublayer management entity
PMI	precoding matrix index
PPDU	PLCP protocol data unit
PSD	power spectrum density
PSDU	PHY service data unit
PSMP	power-save multi-poll
QAM	quadrature amplitude modulation
OBSS	overlapped BSS
QPSK	quadrature phase shift keying
RAW	restricted access window (IEEE 802.11ah MAC)
RF	radio frequency
RFCC	RF chain control
RFID	radio frequency identification
RMa	rural macro
RMS	root mean square
RSSI	received signal strength indicator
RTS	request to send
RTT	round trip time
RX	(wireless) receiver
S1G	sub-1 GHz
S1G-CDU	sub-1 GHz collision detection unit (proposed)
SBA	switched beam antenna
SC	selective combining
SCM	spatial channel model
SCMA/CN	selective CSMA with cooperative nulling
SCME	spatial channel model extended
SEP	smart energy profile
SDMA	space division multiple access
SF	speed frame (IEEE 802.11ah)
SG	study group
SIFS	short inter-frame spacing
SIMO	single-input multiple-output
SINR	signal to interference plus noise ratio
SISO	single-input single-output
SMa	suburban macro
SNR	signal to noise ratio
SRU	spectrum resources usage (IEEE 802.15 SG SRU)
SS	spatial stream
SST	subchannel selective transmission (IEEE 802.11ah MAC)
STA	WLAN station

STBC	space time block code
STC	space time coding
STF	short training field
STS	spectral-time sensing
SUN	smart utility network
SVD	singular value decomposition
TBTT	target beacon transmission time
TCP	transmission control protocol
TDMA	time division multiple access
TG	task group
THP	Tomlinson-Harashima precoding
TWT	target wait time (IEEE 802.11ah MAC)
TX	(wireless) transmitter
TXOP	transmission opportunity
UCA	uniform circular array
UHD	USRP hardware driver
UHF	ultra-high frequency
ULA	uniform linear array
UDP	user datagram protocol
UL	uplink
UMa	urban macro
UMi	urban micro
URA	uniform rectangular array
USRP	universal software radio peripheral
VCO	voltage controlled oscillator
VSWR	voltage standing wave ratio
VP	vector perturbation
VSWR	voltage standing wave ratio
WAN	wide area network
WG	working group
Wi-Fi	wireless fidelity (in fact, it is not an acronym)
WIM1	WINNER channel model - phase I
WIM2	WINNER channel model - phase II
WINNER	wireless world initiative new radio
WLAN	wireless local area network
WPAN	wireless personal area network
ZF	zero forcing
ZP	zero padding

# Bibliography

- [1] K. Johansson, *Cost Efficient Provisioning of Wireless Access - Infrastructure Cost Modeling and Multi-Operator Resource Sharing*. PhD thesis, KTH Electrical Engineering, Sweden, 2005.
- [2] R. Porat, “Link Budget,” (DCN 11-11-0552-02-00ah-link-budget.xls), IEEE P802.11 Wireless LANs, April 2011.
- [3] E. Perahia and R. Stacey, *Next Generation Wireless LANs: 802.11n and 802.11ac, Second Edition*. Cambridge University Press, New York, 2013.
- [4] *IEEE 802.11ad: Draft Standard for Information Technology - Telecommunications and Information Exchange Between Systems - Local and Metropolitan Area Networks - Specific Requirements - Part 11: Wireless LAN Medium Access Control (MAC) and Physical Layer (PHY) Specifications - Amendment 3: Enhancements for Very High Throughput in the 60 GHz Band, P802.11ad<sup>TM</sup>/D9.0*. IEEE P802.11 Wireless LAN, July 2012.
- [5] *IEEE 802.11ah: Draft Standard for Information technology - Telecommunications and information exchange between systems Local and metropolitan area networks - Specific requirements, Part 11: Wireless LAN Medium Access Control (MAC) and Physical Layer (PHY) Specifications, Amendment 6: Sub 1 GHz License Exempt Operation, IEEE P802.11ah<sup>TM</sup>/D2.0*. IEEE P802.11 Wireless LAN, June 2014.
- [6] “IEEE P802.11 Task Group AH Meeting Update,” ([Online, last access: 9/30/14]. Available: [www.ieee802.org/11/Reports/tgah\\_update.htm](http://www.ieee802.org/11/Reports/tgah_update.htm)), Status of Project IEEE 802.11ah.
- [7] *IEEE 802.15.4: Wireless Medium Access Control (MAC) and Physical Layer (PHY) Specifications for Low-Rate Wireless Personal Area Networks (LR-WPANs)*. IEEE P802.15 Wireless Personal Area Networks, 2011.
- [8] A. Schlick and A. Sridhar, “Reply Comments of Google Inc. - In Support of Petitions for Reconsideration. In the Matter of Request by Progeny LMS, LLC for Waiver of Certain Multilateration Location and Monitoring Service Rules.

- Before the Federal Communications Commission, Washington, D.C. 20554,” Google Inc., Washington, U.S., WT Docket No. 11-49, pp. 1–10, August 2013.
- [9] S. Aust, R. Prasad, and I. Niemegeers, “IEEE 802.11ah: Advantages in Standards and further Challenges for Sub-1 GHz Wi-Fi,” IEEE International Conference on Communications (ICC '12), pp. 6885–6889, June 2012.
- [10] *IEEE 802.15.4g: Low-Rate Wireless Personal Area Networks (WPANs), Amendment 4: Physical Layer Specifications for Low Data Rate Wireless Smart Metering Utility Networks*. IEEE P802.15 Wireless Personal Area Networks, November 2011.
- [11] *IEEE 802.15.4e: Low-Rate Wireless Personal Area Networks (WPANs), (LR-WPANs) Amendment to the MAC sub-layer*. IEEE P802.15 Wireless Personal Area Networks, October 2011.
- [12] *IEEE 802.15.4k: Low-Rate Wireless Personal Area Networks (WPANs), Amendment 5: Physical Layer Specifications for Low Energy, Critical Infrastructure Monitoring Networks*. IEEE P802.15 Wireless Personal Area Networks, November 2012.
- [13] *Series Y: Global Information Infrastructure, Internet Protocol Aspects and Next-Generation Networks: Next Generation Networks - Frameworks and functional architecture models. Overview of the Internet of things, Recommendation ITU-T Y.2060*. Telecommunication Standardization Sector of ITU, ITU-T, June 2012.
- [14] N. Tajitsu, “NZ Telecom, Vodafone pick up rights to 700 MHz 4G spectrum,” Reuters, October 2013.
- [15] “Wi-Fi™ for the Smart Grid: Mature, Interoperable, Security-Protected Technology for Advanced Utility Management Communications,” Wi-Fi Alliance, 2009.
- [16] *IEEE 802.11ac: IEEE Standard for Information Technology - Telecommunications and Information Exchange Between Systems - Local and Metropolitan Area Networks - Specific Requirements - Part 11: Wireless LAN Medium Access Control (MAC) and Physical layer (PHY) Specifications - Amendment 4: Enhancements for Very High Throughput for Operation in Bands below 6 GHz, IEEE Std 802.11ac™-2013 (approved 11 December 2013)*. IEEE P802.11 Wireless LAN, December 2013.
- [17] *IEEE 802.11: IEEE Standard for Information Technology - Telecommunications and Information Exchange Between Systems - Local and Metropolitan Area Networks - Part 11: Wireless LAN Medium Access Control (MAC) and Physical Layer (PHY) Specifications, IEEE Std 802.11-2012*. IEEE P802.11 Wireless LAN, March 2012.



- [18] *IEEE 802.11n: IEEE Standard for Information Technology - Telecommunications and Information Exchange Between Systems - Local and Metropolitan Area Networks - Specific Requirements - Part 11: Wireless LAN Medium Access Control (MAC) and Physical Layer (PHY) Specifications - Amendment 5: Enhancements for Higher Throughput*. IEEE P802.11 Wireless LAN, October 2009.
- [19] P. Minyoung, "Specification Framework for TGah, DCN IEEE 802.11-11/1133r15," IEEE P802.11 Wireless LANs, 2013.
- [20] "920 MHz-Band Telemeter, Telecontrol and Data Transmission Radio Equipment for Specified Low Power Radio Station - English translation," Association of Radio Industries and Business (ARIB), ARIB STD-T108 Ver. 1.0, February 2012.
- [21] L. Barclay, *Propagation of Radiowaves - 2nd Edition*. The Institution of Electrical Engineers (IEE), 2003.
- [22] D. Parsons, *The Mobile Radio Propagation Channel*. Pentech Press limited, London, 1992.
- [23] S. Aust and T. Ito, "Sub-1 GHz Wireless LAN Propagation Path Loss Models for Urban Smart Grid Applications," Workshop on Computing, Networking and Communications (ICNC '12), pp. 123–127, February 2012.
- [24] N. Balakrishnan and V. Nevzorov, *A Primer on Statistical Distributions*. Wiley, 2003.
- [25] R. Porat, S. Young, and K. Doppler, "TGah Channel Model - Proposed Text," IEEE P802.11 Wireless LANs, IEEE 802.11-11/0968r3, pp. 1–6, March 2011.
- [26] "Evolved Universal Terrestrial Radio Access (E-UTRA): Further advancements for E-UTRA physical layer aspects (Release 9)," 3GPP, Technical Specification Group Radio Access Network, 3GPP TR 36.814 V9.0.0 (2010-03) Technical Report, March 2010.
- [27] "Statement on 870-876 MHz and 915-921 MHz - Update and Way Forward," Ofcom, June 2013.
- [28] *Electromagnetic compatibility and Radio spectrum Matters (ERM); Short Range Devices (SRD); Radio equipment to be used in the 25 MHz to 1000 MHz frequency range with power levels ranging up to 500 mW; Part 2: Harmonized EN covering essential requirements under article 3.2 of the R and TTE Directive*. European Telecommunications Standards Institute, final draft ETSI EN 300 220-2, V 2.3.1 (2009-12), December 2009.

- [29] *Electromagnetic compatibility and Radio spectrum Matters (ERM); Short Range Devices (SRD); Radio equipment to be used in the 25 MHz to 1000 MHz frequency range with power levels ranging up to 500 mW; Part 1: Technical characteristics and test methods.* European Telecommunications Standards Institute, final draft ETSI EN 300 220-1, V 2.4.1 (2012-01), January 2012.
- [30] “950 MHz-Band Telemeter, Telecontrol and Data Transmission Radio Equipment for Specified Low Power Radio Station - English translation,” Association of Radio Industries and Business (ARIB), ARIB STD-T96 Ver. 1.0, June 1999.
- [31] S. Aust, R. Prasad, and I. Niemegeers, “Performance Study of MIMO-OFDM Platform in Narrow-band Sub-1 GHz Wireless LANs,” (Tsukuba, Japan), The 9th International Workshop on Wireless Network Measurements and Experimentation (WiNMeE '13), in conjunction with the 12th International Symposium on Modeling and Optimization in Mobile, Ad Hoc, and Wireless Networks (WiOpt '13), pp. 89–94, May 2013.
- [32] C. Raghavendra and K. Sivalingam, *Wireless Sensor Networks*. Springer, 1st edition, 2004.
- [33] K. Mori, Y. Urabe, K. Takahashi, R. Yu Zhan, M. Sim, M. Umehira, S. Shimada, M. Iwaoka, and S. Aust, “Experimental results of indoor path loss in actual European houses,” (DCN 11-12/0244r0), IEEE P802.11 Wireless LANs, March 2012.
- [34] S. Aust, R. Prasad, and I. Niemegeers, “Analysis of the Performance Boundaries of Sub-1 GHz WLANs in the 920 MHz ISM-Band,” (Ilmenau, Germany), The 10th International Symposium on Wireless Communication Systems (ISWCS '13), pp. 866–870, August 2013.
- [35] G. Giannakis, Z. Liu, X. Ma, and S. Zhou, *Space-Time Coding for Broadband Wireless Communications*. Wiley, Canada, 2007.
- [36] M. Narandžić, C. Schneider, R. Thomä, T. Jämsä, P. Kyösti, and X. Zhao, “Comparison of SCM, SCME, and WINNER Channel Models,” IEEE 65th Vehicular Technology Conference (VTC '07-Spring), pp. 413–417, April 2007.
- [37] N. Fourikis, *Phased Array-based Systems and Applications*. Canada: Wiley, 1997.
- [38] T. Sarkar, M. Salazar-Palma, and E. Mokole, *Physics of Multiantenna Systems and Broadband Processing*. New Jersey: Wiley, 2008.
- [39] S. N. Makarov, *Antenna and EM Modeling with MATLAB<sup>TM</sup>*. New York: Wiley, 2002.

- [40] E. Warsitz, R. Haeb-Umbach, and D. Tran Vu, "Blind Adaptive Principal Eigenvector Beamforming for Acoustical Source Separation," In the Proceedings of the IEEE Interspeech 2007, pp. 1–4, August 2007.
- [41] E. Warsitz, *Mehrkanalige Sprachsignalverbesserung durch adaptive Lösung eines Eigenwertproblems im Frequenzbereich*. PhD thesis, Universität Paderborn, Germany, Fakultät für Elektrotechnik, Informatik und Mathematik, March 2009.
- [42] H. Liu, X. Cheng, Z. Zhou, and G. Wu, "Block Diagonalization Eigenvalue Based Beamforming Precoding Design for Downlink Capacity Improvement in Multiuser MIMO channel," International Conference on Wireless Communications and Signal Processing (WCSP '10), pp. 1–5, 2010.
- [43] A. Sibille, C. Oestges, and A. Zanella, *MIMO: From Theory to Implementation*. Elsevier, 2011.
- [44] R. Chen, J. Li, C. Li, and W. Liu, "Multi-user Multi-stream Vector Perturbation Precoding," Springer, Wireless Personal Communications, vol. 69, issue 1, pp. 335–345, April 2012.
- [45] R. Chen, C. Li, and X. Cai, "Low Complexity Multi-user Multi-stream Vector Perturbation with Quantized Channel Feedback," The 1st International Conference on Communications, Signal Processing, and their Applications (ICCSPA '13), pp. 1–5, February 2013.
- [46] D. Aronsson, G. Auer, S. Bittner, I. Cosovic, F. Danilo-Lemoine, D. Falconer, B. Hunt, M. Jiang, C.-T. Lam, A. Langowski, H. Liu, Y. Ma, M. Sabbaghian, F. Siddiqui, M. Sternad, T. Svensson, A. Tyrell, and K. Yu, "D2.3.3 -v1.00 - Link level procedures for the WINNER System," IST-4-027756 WINNER II, November 2007.
- [47] R. Porat, "Downclocking with adaptive sub-carriers for single user, multiple user, multiple access and/or MIMO wireless communication (Patent)," (Broadcom Corporation), EP 2515464 A2, October 2012.
- [48] H. Zhang, S. Vermani, and R. Porat, "11ah Data Transmission Flow," IEEE 802.11-11/1484r1, November 2011.
- [49] Y. Seok, H. Zhang, and R. Porat, "NDP sounding," IEEE 802.11-12/0617r0, May 2012.
- [50] H. Zhang, S. Srinivasa, and Y. Liu, "11ah Padding," IEEE 802.11-12/0818r0, July 2012.
- [51] "Liaison of Non-OFDM Use Cases from Wi-Fi Alliance™ to IEEE 802.11 Working Group," Wi-Fi Alliance™, ver. 4.0, pp. 1–9, July 2014.

- [52] R. de Vegt, "Potential Compromise for 802.11ah Use Case Document," IEEE 802, DCN 802.11/0457r0, March 2011.
- [53] K. Kobayashi and M. Nakagawa, "Spatially Divided Channel Scheme using Sectorized Antennas for CSMA/CA - "Directional CSMA/CA"," The 11th IEEE International Symposium on Personal, Indoor and Mobile Radio Communications (PIMRC '00), pp. 227–231, September 2000.
- [54] F. Babich, M. Comisso, M. D'Orlando, and L. Manià, "Performance Evaluation of Distributed Wireless Networks Using Smart Antennas in Low-Rank Channel," IEEE Transactions on Communications, vol. 55, no. 7, pp. 1344–1353, July 2007.
- [55] F. Babich and M. Comisso, "Throughput and Delay Analysis of 802.11-based Wireless Networks Using Smart and Directional Antennas," IEEE Transactions on Communications, vol. 57, no. 5, pp. 1413–1423, May 2009.
- [56] F. Babich, M. Comisso, and L. Manià, "Multi-Antenna Techniques for Wireless Mesh Networks in an Outdoor Environment," IEEE International Conference on Communications (ICC '07), pp. 4961–4966, June 2007.
- [57] F. Babich, M. Comisso, A. Dorni, F. Farisi, and L. Manià, "The Simulation of Smart Antennas in Network Simulator-2 Using MATLAB™," The 14th IEEE International Workshop on Computer Aided Modeling and Design of Communication Links and Networks (CAMAD '09), pp. 1–5, June 2009.
- [58] F. Babich, M. Comisso, A. Dorni, and M. Driusso, "Open Source Simulation of Smart Antenna Systems in Network Simulator-2 Using Octave," The 5th International Symposium on Wireless Pervasive Computing (ISWPC '10), pp. 51–56, 2010.
- [59] M. Comisso, *Beamforming Techniques for Wireless Communications in Low-rank Channels: Analytical Models and Synthesis Algorithms*. PhD thesis, Università degli studi di Trieste, Italy, March 2008.
- [60] R. Schlub, J. Lu, and T. Ohira, "Seven-element Ground Skirt Monopole ESPAR Antenna Design From a Genetic Algorithm and the Finite Element Method," IEEE Transactions on Antennas and Propagation, vol. 51, no. 11, pp. 3033–3039, November 2003.
- [61] S. Bandyopadhyay, S. Roy, and T. Ueda, *Enhancing the Performance of Ad Hoc Wireless Networks with Smart Antennas*. Auerbach Publications, 2006.
- [62] P. Shao, A. Matsumoto, S. Aust, T. Ito, and P. Davis, "A Collision Detection Method based on Power Sensing and Time-domain Signal Processing for Wireless LAN," The 11th IEEE International Symposium on Communications and Information Technologies (ISCIT '11), pp. 199–204, October 2011.

- [63] B. Zhou, S. Ma, and J. Xu, "Group-Wise Channel Sensing and Resource Pre-allocation for LTE D2D on ISM Band," *IEEE Wireless Communications and Networking Conference (WCNC '13): MAC*, pp. 118–122, 2013.
- [64] B. Zhou, H. Hu, S.-Q. Huang, and H.-H. Chen, "Intracluster Device-to-Device Relay Algorithm With Optimal Resource Utilization," *IEEE Transactions on Vehicular Technology*, vol. 62, no. 5, pp. 2315–2326, 2013.
- [65] T. Kim, S. Choudhury, Z.-Y. Jin, K. Doppler, and C. Ghosh, "Simultaneous Polling Mechanism for Low Power Sensor Network Using ZC Sequences," *The 23rd IEEE International Symposium on Personal, Indoor and Mobile Radio Communications (PIMRC '12)*, pp. 2024–2029, September 2012.
- [66] A. Hrovat, G. Kandus, and T. Javornik, "A Survey of Radio Propagation Modeling for Tunnels," *IEEE Communications Survey and Tutorials*, vol. 16, no. 2, second quarter, pp. 658–669, April 2014.
- [67] N. Lu and X. Shen, "Scaling Laws for Throughput Capacity and Delay in Wireless Networks - A Survey," *IEEE Communications Survey and Tutorials*, vol. 16, no. 2, second quarter, pp. 642–657, April 2014.
- [68] A. Flores, R. Guerra, E. Knightly, P. Ecclesine, and P. Santosh, "IEEE 802.11af: a standard for TV white space spectrum sharing," *IEEE Communications Magazine*, vol.: 51, issue: 10, pp. 92–100, October 2013.
- [69] "Ettus Research," ([Online, last access: 9/15/14]. Available: [www.ettus.com/](http://www.ettus.com/)), November 2012.
- [70] J. Corgan, "GnuRadio: The Free & Open Software Radio Ecosystem," ([Online, last access: 9/10/14]. Available: [gnuradio.org/redmine/projects/gnuradio/wiki](http://gnuradio.org/redmine/projects/gnuradio/wiki)), January 2013.
- [71] J. Mitola, "The software radio architecture," *IEEE Communications Magazine*, vol. 33, issue 5, pp. 26–38, May 1995.
- [72] R. Courtland, "Wi-Fi Radio Takes a Digital Turn," *IEEE Spectrum: The Magazine of Technology Insiders*, pp. 12–14, November 2012.
- [73] "Hi Performance Ubiquiti WLAN 900 MHz Radio," ([Online, last access: 9/10/14]. Available: [www.ubnt.com/xr9](http://www.ubnt.com/xr9)), Ubiquiti Networks, January 2013.
- [74] "Wideband Synthesizer with Integrated VCO: ADF4350, Rev. A," ([Online, last access: 9/15/14]. Available: [www.analog.com/static/imported-files/data\\_sheets/ADF4350.pdf](http://www.analog.com/static/imported-files/data_sheets/ADF4350.pdf)), Analog Devices, pp. 1–32, April 2011.

- [75] “RF Agile Transceiver, Data Sheet AD9361, Rev. D,” ([Online, last access: 9/15/14]. Available: [www.analog.com/static/imported-files/data\\_sheets/AD9361.pdf](http://www.analog.com/static/imported-files/data_sheets/AD9361.pdf)), Analog Devices, pp. 1–36, September 2013.
- [76] “Multichannel Reconfigurable RF Transceiver,” ([Online, last access: 9/10/14]. Available: [epiqsolutions.com/maveriq/maveriq\\_flyer.pdf](http://epiqsolutions.com/maveriq/maveriq_flyer.pdf)), Epiq Solutions, Maveriq, pp. 1–3, 2013.
- [77] “RF Frontend, SBX REV 3.0,” ([Online, last access: 9/15/14]. Available: [files.ettus.com/schematics/sbx/sbx.pdf](http://files.ettus.com/schematics/sbx/sbx.pdf)), Ettus Research, pp. 1–6, March 2011.
- [78] “XCVR Frontend, REV 1.0,” ([Online, last access: 9/15/14]. Available: [files.ettus.com/schematics/xcvr\\_dbs/xcvr2450.pdf](http://files.ettus.com/schematics/xcvr_dbs/xcvr2450.pdf)), Ettus Research, pp. 1–4, February 2008.
- [79] K. Mandke, S. Choi, G. Kim, R. Grant, R. Daniels, W. Kim, R. Heath Jr., and S. Nettles, “Early Results on Hydra: A Flexible MAC/PHY Multihop Testbed,” pp. 1896–1900, 65th IEEE Vehicular Technology Conference (VTC ’07-Spring), pp. 1896–1900, April 2007.
- [80] K. Mandke, R. Daniels, R. Heath Jr., and S. Nettles, “On the Challenges of Building a Multi-Antenna Software Defined Packet Radio,” Proceedings of the SDR Technical Conference and Product Exposition, pp. 1–6, October 2008.
- [81] “NI USRP RIO,” ([Online, last access: 9/15/14]. Available: [sine.ni.com/nips/cds/view/p/lang/en/nid/212174](http://sine.ni.com/nips/cds/view/p/lang/en/nid/212174)), National Instruments, August 2014.
- [82] “Antcor introduces first 802.11ah IP in the world,” ([Online, last access: 9/15/14]. Available: [www.antcor.com/](http://www.antcor.com/)), Antcor - Advanced Network Technologies (now: U-blox.com), August 2014.
- [83] *Electromagnetic compatibility and Radio spectrum Matters (ERM); Short Range Devices (SRD); Radio equipment to be used in the 25 MHz to 1000 MHz frequency range with power levels ranging up to 500 mW; Part 1: Technical characteristics and test methods*. ETSI, final draft ETSI EN 300 ww0-1, V2.4.1 (2012-01), January 2012.
- [84] B. Furth and S. Ahson, *Long Term Evolution: 3GPP LTE Radio and Cellular Technology*. CRC Press, Taylor & Francis Group, 2009.
- [85] S. Aust, R. Prasad, and I. Niemegeers, “Advances in Wireless M2M and IoT: Rapid SDR-prototyping of IEEE 802.11ah,” IEEE Local Computer Networks (LCN ’14), pp. 290–292, September 2014.

- [86] E. Tufte, *Visual Explanations: Images and Quantities, Evidence and Narrative*. Graphics Press LLC, 1997.
- [87] E. Tufte, *The Visual Display of Quantitative Information (second edition)*. Graphics Press LLC, 2001.
- [88] J. Mitola and Z. Zvonar, *Software radio technologies: selected readings*. IEEE, 3 Park Avenue, New York: IEEE Press marketing, 2001.
- [89] J. Bard and V. Kovarik, *Software defined radio: the software communications architecture*. Wiley Series in Software Radio, 2007.
- [90] R. Prasad and H. Harada, *Simulation and software radio for mobile communications*. Artech House, 2002.
- [91] B. Fette, *Cognitive radio technology*. Oxford, UK: Newnes, Elsevier, 2006.
- [92] H. Loeb and C. Sauer, "A Modular Reference Application for IEEE 802.11n Wireless LAN MACs," IEEE International Conference on Communications (ICC '09), pp. 1–5, June 2009.
- [93] H. Loeb, C. Liß, U. Rückert, and C. Sauer, "UMAC - A Universal MAC architecture for heterogeneous home networks," International Conference on Ultra Modern Telecommunications and Workshops (ICUMT '09), pp. 1–6, October 2009.
- [94] H. Loeb, *Application-driven Exploration of a Programmable Platform for Wireless LAN*. PhD thesis, Technische Fakultät der Universität Bielefeld, Germany, August 2011.
- [95] M. Khojastepour, K. Sundaresan, S. Rangarajan, X. Zhang, and S. Barghi, "The case for antenna cancellation for scalable full-duplex wireless communications," 10th ACM Workshop on Hot Topics in Networks, article no. 17, pp. 1–6, 2011.
- [96] N. Singh, D. Gunawardena, A. Proutiere, B. Radunović, H. Balan, and P. Key, "Efficient and Fair MAC for Wireless Networks with Self-interference Cancellation," International Symposium on Modeling and Optimization in Mobile, Ad Hoc and Wireless Networks (WiOpt '11), 2011.
- [97] E. Baik, S. Vermani, and B. Tian, "11ah Tx Reference Code," May 2014. IEEE 802.11ah TG, DCN IEEE 802.11-14/0631r02.
- [98] R. Grover, S. MacMullan, and M. Wyglinski, "Reconfigurable Wireless Platforms for Spectrally Agile Coexistence," IEEE International Symposium on Dynamic Spectrum Access Networks (DYSPAN '14), 458–466, April 2014.

- [99] L.-C. Wang, "Advances in coordinated multi-cell multi-user MIMO systems," tech. rep., Department of Electrical Engineering, National Chiao Tung University, Hsinchu, Taiwan. [Online, last access: 9/15/14]. Available: [www.ieee-globecom.org/2011/private](http://www.ieee-globecom.org/2011/private), December 2011.
- [100] I. Vermesan, A. Moldovan, T. Palade, and R. Colda, "On BER of STBC coded MIMO systems in different indoor environments," 18th International Conference on Microwave Radar and Wireless Communications (MIKON '10), pp. 1–4, 2010.
- [101] S. Alamouti, "A Simple Transmit Diversity Technique for Wireless Communications," *IEEE Journal on Selected Areas in Communications*, vol. 16, no. 8, pp. 1451–1458, October 1998.
- [102] Y. Cho, K. Jaekwon, W. Yang, and C. Kang, *MIMO-OFDM Wireless Communications with MATLAB<sup>TM</sup>*. John Wiley & Sons (Asia), 2010.
- [103] M. Yue, L. Lihua, J. Jin, and Y. Yucang, "An easy-to-implement dual codebook for multiuser MIMO systems," *IEEE Consumer Communications and Networking Conference (CCNC '13)*, pp. 709–712, 2013.
- [104] D. Love and R. Heath Jr., "Grassmannian Beamforming for Multiple-Input Multiple-Output Wireless Systems," *IEEE Transactions on Information Theory*, vol. 49, no. 10, pp. 2735–2747, October 2003.
- [105] T. Inoue and R. Heath Jr., "Kerdock Codes for Limited Feedback Precoded MIMO Systems," *Transactions on Signal Processing*, vol. 57, no. 9, pp. 3711–3716, September 2009.
- [106] S. Aust, R. Prasad, and I. Niemegeers, "Codebook Selection Strategies in Long-range Sub-1 GHz WLANs," ([Online, last access: 9/10/14]. Available: [www.sciencedirect.com/](http://www.sciencedirect.com/)), Elsevier, *Procedia Computer Science* (2014), vol. 32, pp. 133–140, DOI information: 10.1016/j.procs.2014.05.407, June 2014.
- [107] J. Roh and D. Bhaskar, "Efficient Feedback Methods for MIMO Channels Based on Parameterization," *IEEE Transactions on Wireless Communications*, vol. 6, no.1, pp. 282–292, January 2007.
- [108] B. Godana and T. Ekman, "Lineary Prediction of Time-Varying MIMO systems using Givens Rotations," *The 12th IEEE International Workshop on Signal Processing Advances in Wireless Communications (SPAWC '11)*, pp. 371–375, June 2011.
- [109] V. Prabhu, S. Karachontzitis, and D. Toumpakaris, "Performance Comparison of Limited Feedback Codebook-based Downlink Beamforming Schemes for Distributed Antenna Systems," *The 1st International Conference on Wireless Communication, Vehicular Technology, Information Theory and Aerospace*



- & Electronic Systems Technology (Wireless VITAE '09), pp. 171–176, May 2009.
- [110] S. Aust, R. Prasad, and I. Niemegeers, “Codebook Selection Strategies in Long-range Sub-1 GHz WLANs,” The 5th International Conference on Ambient Systems, Networks and Technologies (ANT '14), the 4th International Conference on Sustainable Energy Information Technology (SEIT '14Akshay Uttama,), June 2014.
- [111] D. Zhu, Y. Zhang, G. Wang, and M. Lei, “Grassmannian Subspace Prediction for Precoded Spatial Multiplexing MIMO with Delayed Feedback,” *IEEE Signal Processing Letters*, vol. 18, no. 10, pp. 555–558, October 2011.
- [112] D. Love, R. Heath Jr., V. Lau, D. Gesbert, B. Rao, and M. Andrews, “An Overview of Limited Feedback in Wireless Communication Systems,” *IEEE Journal on Selected Areas in Communications*, vol. 26, no. 8, pp. 1341–1365, October 2008.
- [113] M. Duarte, A. Sabharwal, C. Dick, and R. Rao, “Beamforming in MISO Systems: Empirical Results and EVM-based Analysis,” *IEEE Transactions on Wireless Communications*, vol. 9, no. 10, pp. 3214–3225, October 2010.
- [114] “Evolved Universal Terrestrial Radio Access (E-UTRA): Physical Channels and Modulation (Release 8),” 3GPP, Technical Specification Group Radio Access Network, 3GPP TS 36.211 V8.9.0 (2009-12) Technical Specification, March 2009.
- [115] M. Fukumoto and M. Bandai, “MIMO full-duplex wireless: Node architecture and medium access control protocol,” 7th International Conference on Mobile Computing and Ubiquitous Networking (ICMU '14), pp. 76–77, January 2014.
- [116] D. Nojima, L. Lanante Jr., Y. Nagao, M. Kurosaki, and H. Ochi, “Performance Evaluation for Multi-User MIMO IEEE 802.11ac Wireless LAN System,” 14th International Conference on Advanced Communication Technology (ICACT '12), pp. 804–808, 2012.
- [117] H. Lou, M. Ghosh, P. Xia, and R. Olesen, “A comparison of implicit and explicit channel feedback methods for MU-MIMO WLAN systems,” The 24rd IEEE International Symposium on Personal Indoor and Mobile Radio Communications (PIMRC '13), pp. 419–424, 2013.
- [118] F. Riera-Palou and G. Femenias, “Space-frequency linear precoding with optimal detection for MIMO-OFDM systems,” *IFIP Wireless Days 2010*, pp. 1–5, 2010.
- [119] W. Ping and L. Lihua, “Unitary Space Vector Quantization Codebook Design for Precoding MIMO system,” *IEICE Transactions on Communications*, vol. e91-b, no. 9, pp. 2917–2923, September 2008.

- [120] W. Lei, Z. Xiaofeng, Z. Yousi, and M. Shunliang, "Adaptive codebook for limited feedback MIMO system," IFIP International Conference on Wireless and Optical Communications Networks (WOCN '09), pp. 1–5, 2009.
- [121] L. Lanante Jr., M. Kurosaki, and H. Ochi, "Non-linear Precoding for Next Generation Multi-user MIMO Wireless LAN Systems," The 13th International Conference on Advanced Communication Technology (ICACT '11), pp. 1211–1216, 2011.
- [122] Z. Liang and Y. Ohashi, "Efficient Codebook-based MIMO beamforming for Millimeter-wave WLANs," The 23rd IEEE International Symposium on Personal Indoor and Mobile Radio Communications (PIMRC '12), pp. 1885–1889, 2012.
- [123] J. Julia and M. Meenakshi, *Performance Improvement in MIMO Systems Using Rotating Codebooks*. Advances in Intelligent Systems and Computing, vol. 176, Springer, pp. 489–496, 2012.
- [124] R. Hu and Y. Qian, *Heterogeneous Cellular Networks*. Wiley, 2013.
- [125] M. Di Renzo, H. Haas, A. Ghayeb, S. Sugiura, and L. Hanzo, "Spatial Modulation for Generalized MIMO: Challenges, Opportunities, and Implementation," *Proceedings of the IEEE*, vol. 102, no. 1, pp. 56–103, January 2014.
- [126] G. Li, Z. Xu, X. Xiong, C. Yang, S. Zhang, Y. Chen, and S. Xu, "Energy-efficient wireless communications: Tutorial, survey, and open issues," *IEEE Transactions of Wireless Communications*, vol. 18, no. 6, pp. 28–35, December 2011.
- [127] Y. Chen, S. Zhang, S. Xu, and G. Li, "Fundamental tradeoffs on green wireless networks," *IEEE Communication Magazine*, vol. 49, no. 6, pp. 30–37, June 2011.
- [128] D. Halperin, B. Greenstein, A. Sheth, and D. Wetherall, "Demystifying 802.11n power consumption," In the Proceedings of the International Conference on Power Aware Computing and Systems (HotPower '10), article no. 1, pp. 1–5, October 2010.
- [129] T. Tanaka, K. Abe, S. Aust, T. Ito, H. Yomo, and S. Sakata, "Automatic and Cooperative Sleep Control Strategies for Power-Saving in Radio-on-Demand WLANs," 5th IEEE Annual Green Technologies Conference (GreenTech '13), pp. 293–300, April 2013.
- [130] T. Tanaka, S. Aust, and T. Ito, "Enhanced Energy Consumption Reduction Schemes in Radio-On-Demand WLANs," The 24th IEEE Annual International Symposium on Personal, Indoor, and Mobile Radio Communications (PIMRC '13), pp. 2845–2849, September 2013.

- [131] S. Cui, A. Goldsmith, and A. Bahai, "Energy-constrained modulation optimization," *IEEE Transactions on Wireless Communications*, vol. 4, issue 5, pp. 2349–2360, September 2005.
- [132] I. Pefkianakis, Y. Hu, H. Wong, H. Yang, and S. Lu, "MIMO rate adaptation in 802.11n wireless networks," In the Proceedings of the International Conference on Mobile Computing and Networking (MobiCom '10), pp. 257–268, September 2010.
- [133] H. Yu, L. Zhong, and A. Sabharwal, "Power Management of MIMO Network Interfaces on Mobile Systems," *Transactions on Very Large Scale Integration (VLSI) Systems*, vol. 20, no. 7, pp. 1175–1186, July 2012.
- [134] "Telecommunication management; Energy Saving Management (ESM); Concepts and requirements (Release 10)," 3GPP, Technical Specification Group Services and System Aspects, 3GPP TS 32.551 V10.1.0 (2011-03) Technical Specification, March 2011.
- [135] A. Anders, *Energy for free: wireless technology without batteries*. EnOcean (White Paper), pp. 1–3, November 2006.
- [136] *SIGFOX: One network, a billion dreams: M2M and IoT redefined through cost effective and energy optimized connectivity*. SIGFOX (White Paper), pp. 1–17, January 2014.
- [137] "More data, less energy: Making network standby more efficient in billions of connected devices," tech. rep., International Energy Agency (IEA), [www.iea.org/etp/networkstandby](http://www.iea.org/etp/networkstandby), July 2014.
- [138] R. Rajashekar, K. Hari, and L. Hanzo, "Antenna Selection in Spatial Modulation Systems," *IEEE Communications Letters*, vol. 17, no. 3, pp. 521–524, March 2013.
- [139] W. Yuan, J. Linnartz, and I. Niemegeers, "Adaptive CCA for IEEE 802.15.4 Wireless Sensor Networks to Mitigate Interference," *IEEE Wireless Communications and Networking Conference (WCNC '10)*, pp. 1–5, April 2010.
- [140] W. Yuan, X. Wang, J. Linnartz, and I. Niemegeers, "Experimental Validation of a Coexistence Model of IEEE 802.15.4 and IEEE 802.11b/g Networks," In the Proceedings of the 4th International Symposium on Innovations and Real-time Applications of Distributed Sensor Networks (IRADSN '09), pp. 1–6, May 2009.
- [141] M. Woehrle and K. Langendoen, "868 MHz: A noiseless environment, but no free lunch for protocol design," *9th International Conference on Networked Sensing Systems (INSS '12)*, pp. 1–8, June 2012.

- [142] M. Ilyas and I. Mahgoup, *Handbook of Sensor Networks: Compact Wireless and Wired Sensing Systems*. CRC Press LLC, 2005.
- [143] A. Sheth, S. Nedeovski, R. Patra, S. Surana, E. Brewer, and L. Subramanian, "Packet Loss Characterization in Wi-Fi-based Long Distance Networks," IEEE International Conference on Computer Communications (INFOCOM '07), pp. 312–320, 2007.
- [144] P. Handayani and G. Hendranto, "Characterization of DOD and DOA correlation among converging indoor radio links by applying reciprocity principle," International Conference on ICT Convergence (ICTC '11), pp. 90–94, September 2011.
- [145] L. Aubert, B. Uguen, and F. Talom, "Deterministic simulation of MIMO-UWB transmission channel," *Comptes Rendus Physique*, vol. 7, issue 7, ScienceDirect, pp. 751–761, September 2006.
- [146] S. Aust, T. Ito, and P. Davis, "Seamless Indoor/Outdoor Location Cognition with Confidence in Wireless Systems," The 4th Workshop on User Mobility and Vehicular Networks (IEEE LCN ON-MOVE '10), pp. 653–657, October 2010.
- [147] S. Aust, T. Ito, and P. Davis, "Location Cognition for Wireless Systems: Classification with Confidence," The 3rd International ICST Conference on Mobile Wireless Middleware, Operating Systems, and Applications (Mobileware '10), June 2010.
- [148] S. Aust, T. Ito, and P. Davis, *Location Cognition for Wireless Systems: Classification with Confidence*. Mobile Wireless Middleware, Operating Systems, and Applications, Lecture Notes of the Institute for Computer Sciences, Social Informatics and Telecommunications Engineering (LNICST), vol. 48, pp. 144–157, 2010.
- [149] B. Tachigawa, *Smart-Sensor Wireless Network, Smart Meter, SUN and Zig-Bee Smart Energy (in Japanese)*. Liktelekom, 2013.
- [150] M. Aman, W. Chan, and B. Sikdar, "Collision Detection in IEEE 802.11 Networks by Error Vector Magnitude Analysis," Global Telecommunications Conference, Exhibition & Industry Forum (GLOBECOM '12), pp. 5440–5445, December 2012.
- [151] M. Murrioni, R. Prasad, P. Marques, B. Bochow, D. Nogueta, C. Sun, K. Moessner, and H. Harada, "IEEE 1900.6: Spectrum Sensing Interfaces and Data Structures for Dynamic Spectrum Access and Other Advanced Radio Communication Systems Standard: Technical Aspects and Future Outlook," IEEE Communications Magazine, pp. 118–127, December 2011.

- [152] *1900.6-2011 - IEEE Standard for Spectrum Sensing Interfaces and Data Structures for Dynamic Spectrum Access and other Advanced Radio Communication Systems*. IEEE-SA, pp. 1–168, April 2011.
- [153] D. Noguét, *Sensing Techniques for Cognitive Radio - State of the Art and Trends (White Paper)*. IEEE SCC41, April 2009.
- [154] *P1900.6a/D07, Nov 2013 - IEEE Approved Draft Standard for Spectrum Sensing Interfaces and Data Structures for Dynamic Spectrum Access and other Advanced Radio Communication Systems Amendment: Procedures, Protocols and Data Archive Enhanced Interfaces*. IEEE-SA, pp. 1–51, April 2014.
- [155] K. Nishimori, R. Kataoka, K. Hiraguri, and H. Makino, “Collision detection using MIMO transmission: proposal of interference detection method using short preamble signals,” IEICE technical report, cs, vol. 112, no. 309, pp. 77–82, November 2012.
- [156] K. Hiraguri, Y. Goto, T. Ogawa, H. Takase, K. Nishimori, and H. Makino, “Collision detection utilizing MIMO transmission: proposal of access control method for collision detection,” IEICE technical report, cs, vol. 112, no. 309, pp. 71–76, November 2012.
- [157] K. Kim, C. Spooner, I. Akbar, and J. Reed, “Specific Emitter Identification for Cognitive Radio with Application to IEEE 802.11,” Global Telecommunications Conference, Exhibition & Industry Forum (GLOBECOM '08), pp. 1–5, 2008.
- [158] S. Rayanchu, A. Mishra, D. Agrawal, S. Saha, and S. Benerjee, “Diagnosing Wireless Packet Losses in 802.11: Separating Collision from Weak Signal,” IEEE INFOCOM, April 2008.
- [159] “Status of IEEE 802.11 HEW Study Group,” ([Online, last access: 9/15/14]. Available: [www.ieee802.org/11/Reports/hew\\_update.htm](http://www.ieee802.org/11/Reports/hew_update.htm)), IEEE P802.11 - High Efficiency WLAN STUDY GROUP - MEETING UPDATE, June 2013.
- [160] L. Scalia, I. Tinnirello, and D. Giustiniano, “Side Effects of Ambient Noise Immunity Techniques on Outdoor IEEE 802.11 Deployments,” Global Telecommunications Conference, Exhibition & Industry Forum (GLOBECOM '08), pp. 1–6, December 2008.
- [161] S. Aust and T. Ito, “Sub-1 GHz Wireless LAN Deployment Scenarios and Design Implications in Rural Areas,” IEEE Global Communications Conference, Exhibition & Industry Forum (GLOBECOM '11) Workshop on Rural Communications-Technologies, Applications, Strategies and Policies (Rural-Comm '11), pp. 1045–1049, December 2011.

- [162] S. Lien, C. K.C., and Y. Lin, "Toward Ubiquitous Massive Access in 3GPP Machine-to-Machine Communications," *IEEE Communications Magazine*, pp. 66–74, April 2011.
- [163] K. Shih, W. Liao, C. H.C., and C. Chou, "On avoiding RTS collisions for IEEE 802.11-based wireless ad hoc networks," *Elsevier - Computer Communications*, pp. 69–77, 2009.
- [164] G. Bianchi, "Performance Analysis of the IEEE 802.11 Distributed Coordination Function," *IEEE Journal on Selected Areas in Communications*, vol. 18, no. 3, pp. 535–547, March 2000.
- [165] C.-Y. Tu, C.-Y. Ho, and C. Huang, "Energy-Efficient Algorithms and Evaluations for Massive Access Management in Cellular Based Machine To Machine Communications," *IEEE Vehicular Technology Conference (VTC '11-Fall)*, San Francisco, California, USA, pp. 1–5, September 2011.
- [166] G. Bacci, L. Sanguinetti, M. Luise, and H. Poor, "Improving the Energy Efficiency of Contention-based Synchronization of (O)FDMA Networks," *50th Annual Allerton Conference on Communication, Control, and Computing*, pp. 225–232, October 2012.
- [167] J. Lee, S. Hong, W. Kim, J. An, and M. Park, "A Switched Array Antenna Module for Millimeter-Wave Wireless Communications," *Global Symposium on Millimeter Waves (GSMM '08)*, pp. 161–163, April 2008.
- [168] R. Gabriel and K. Steinhauser, "Active Antennas for MIMO and Beamforming Operation," *International Workshop on Antenna Technology (iWAT 2013)*, pp. 394–397, March 2013.
- [169] P. Chaipanya, P. Uthansakul, and M. Uthansakul, "Reduction of Inter-cell Interference using Vertical Beamforming Scheme for Fractional Frequency Reuse Technique," *In the Proceedings of 2011 Asia-Pacific Microwave Conference (APMC '11)*, pp. 1614–1617, December 2011.
- [170] J. Koppenborg, H. Halbauer, S. Saur, and C. Hoek, "3D Beamforming Trials with an Active Antenna Array," *The International ITG Workshop on Smart Antennas (WSA '12)*, pp. 110–114, March 2012.
- [171] L. Yang, L. Liwan, P. Weifeng, C. Yanqin, and F. Zhenghe, "Switching Antenna Array Group by Group for Pencil Beam Forming," *The 2nd International Conference on Microwave and Millimeter Wave Technology (ICMMT '00)*, pp. 269–273, September 2000.
- [172] H. Al-Shatri, R. Ganesan, A. Klein, and T. Weber, "Perfect versus imperfect interference alignment using multiple MIMO relays," *International Symposium on Wireless Communication Systems (ISWCS '12)*, pp. 676–680, August 2012.

- [173] C. Jiang, Y. Shi, Y. Hou, W. Lou, S. Kompella, and S. Midkiff, "Squeezing the Most Out of Interference: An Optimization Framework for Joint Interference Exploitation and Avoidance," IEEE International Conference on Computer Communications (INFOCOM '12), pp. 424–432, March 2012.
- [174] [Online, last access: 9/30/14]. Available: [www.openmobilealliance.org](http://www.openmobilealliance.org): Open Mobile Alliance, May 2013.
- [175] "Considerations in Broadband Architecture Moving to FMC, issue: 1," The Broadband Forum, BBF Marketing Report, April 2011.
- [176] [Online, last access: 9/30/14]. Available: [www.onem2m.org](http://www.onem2m.org): oneM2M, May 2013.
- [177] B. Lee, D. Park, and H. Seo, *Wireless communications resource management*. Singapore: John Wiley & Sons, 2009.
- [178] S. Kyriazakos and G. Karetsos, *Practical radio resource management in wireless systems*. Artech House, 2004.
- [179] C. Ho and C.-Y. Huang, "Energy-Saving Massive Access Control and Resource Allocation Schemes for M2M Communications in OFDMA Cellular Networks," IEEE Wireless Communications Letters, vol. 1, no. 3, pp. 209–212, June 2012.
- [180] S.-Y. Lien and K.-C. Chen, "Massive Access Management for QoS Guarantees in 3GPP Machine-to-Machine Communications," IEEE Communications Letters, vol. 15, no. 3, pp. 311–313, March 2011.
- [181] H. Ma and S. Roy, "Contention Window and Transmission Opportunity Adaptation for Dense IEEE 802.11 WLAN based on Loss Differentiation," IEEE Conference on Communications (ICC '08), Beijing, China, pp. 2556–2560, May 2008.
- [182] K. Prasann, A. Niteshkumar, D. Kaushal, and V. Agarwal, "DTDS: Dynamic Traffic Diversion Scheme for High Dense 802.11 WLAN," The International Conference on Computing Sciences (ICCS '12), Phagwara, India, pp. 168–171, September 2012.
- [183] Q. Hou and L. Gao, "The Simulation of WLAN Outdoor Coverage in Hot Spot Area for Wireless Digital City," The 7th International Wireless Communications, Networking and Mobile Computing (WiCOM 2011), Wuhan, China, pp. 1–4, September 2011.
- [184] M. Driberg, F.-C. Zheng, R. Ahmad, and M. Fitch, "Impact of interference on throughput in dense WLANs with multiple APs," The 20th International Symposium on Personal, Indoor and Mobile Radio Communications (PIMRC '09), Tokyo, Japan, pp. 752–756, September 2009.

- [185] H. Ma, S. Roy, and J. Zhu, "PHY/MAC adaptation approaches for dense wireless LAN MESH," The 3rd International Conference on Communication Systems Software and Middleware and Workshops 2008, Bangalore, India, pp. 204–207, January 2008.
- [186] M. Driberg, F.-C. Zheng, R. Ahmad, and S. Olafsson, "An Improved Distributed Dynamic Channel Assignment Scheme for Dense WLANs," The 6th International Conference on Information, Communications & Signal Processing, Singapore, pp. 1–5, December 2007.
- [187] H. Luo and N. Shankaranarayanan, "A distributed dynamic channel allocation technique for throughput improvement in a dense WLAN environment," IEEE International Conference on Acoustics, Speech, and Signal Processing (ICASSP '04), pp. 345–348, May 2004.
- [188] G. Pastor, I. Mora-Jiménez, A. Caamaño, and R. Jäntti, "Medium Access Probability in Uniform Networks with General Propagation Models," The 10th International Symposium on Wireless Communication Systems (ISWCS '13), pp. 856–860, May 2013.
- [189] S. Sesia, I. Toufik, and M. Baker, *LTE - The UMTS Long Term Evolution: From Theory to Practice (second edition)*. Wiley, 2011.
- [190] M. Islam, *Auction for 700 MHz band by 2016*. [Online, last access: 9/10/14]. Available: [www.dhakatribune.com](http://www.dhakatribune.com): Dhaka Tribune, April 2014.
- [191] N. Ahmed, S. Kanhere, and S. Jha, "Link characterization for aerial wireless sensor networks," 2011 IEEE GLOBECOM Workshops, Wireless Networking for Unmanned Autonomous Vehicles, December 2011.
- [192] S. Rohde and C. Wietfeld, "Interference Aware Positioning of Aerial Relays for Cell Overload and Outage Compensation," IEEE Vehicular Technology Conference (VTC Fall '12), pp. 1–5, 2012.
- [193] R. Prasad, S. Devasenapathy, V. Rao, and J. Vazifehdan, "Reincarnation in the Ambiance: Devices and Networks with Energy Harvesting," IEEE Communications Surveys and Tutorials, vol. 16, no. 1, first quarter 2014, January 2014.
- [194] T. Abe, T. Morie, K. Satou, D. Nomasaki, S. Nakamura, Y. Horiuchi, and K. Imamura, "An Ultra-Low-Power 2-step Wake-Up Receiver for IEEE 802.15.4g Wireless Sensor Networks," Symposia on VLSI Technology and Circuits, pp. 68–69, June 2014.
- [195] A. Galis, H. Abramowicz, M. Brunner, D. Raz-Tehnon, P. Chemouil, J. Butler, C. Polychronopoulos, S. Clayman, H. de Meer, T. Coupaye, A. Pras, K. Sabnani, P. Massonet, and S. Naqvi, "Management and Service-aware



- Networking Architectures (MANA) for Future Internet. Position Paper: System Functions, Capabilities and Requirements,” 4th International Conference Communications and Networking in China (ChinaCOM '09), pp. 1–13, August 2009.
- [196] M. Chiosi, D. Clarke, P. Willis, and A. Reid, “Network Functions Virtualisation: An Introduction, Benefits, Enablers, Challenges and Call for Action,” Network Functions Virtualisation - Introductory White Paper, Issue 1, October 2012.
- [197] *Access Network Discovery and Selection Function (ANDSF) Management Object (MO) (Release 12)*. 3GPP TS 24.312 V12.4.0 (2014-03) Technical Specification: 3GPP, Technical Specification Group Core Network and Terminals, March 2014.
- [198] *Extending the benefits of LTE Advanced to unlicensed spectrum*. Qualcomm, April 2014.
- [199] “Wireless Communications Standards,” tech. rep., Rohde & Schwarz GmbH & Co. KG, 2013.



# Publications by the author

This dissertation is based on the following published publications. Additionally, paper contributions, which are yet under submission at the time of printing this dissertation, are also disclosed. Table B.3 provides an overview of the relations between publications and chapters of this dissertation.

## Journal and magazine publications

- J.1** S. Aust, R.V. Prasad, and I.G.M.M. Niemegeers, “*Codebook Selection Strategies in Long-range Sub-1 GHz WLANs*,” Elsevier, *Procedia Computer Science* (2014), DOI information: 10.1016/j.procs.2014.05.407, vol. 32, pp. 133-140, June 2014.

## Peer-reviewed conference/workshop publications

- C.1** S. Aust, and T. Ito, “*Sub-1 GHz Wireless LAN Deployment Scenarios and Design Implications in Rural Areas*,” IEEE Global Communications Conference, Exhibition & Industry Forum (GLOBECON ’11): 1st Workshop on Rural Communications - Technologies, Applications, Strategies and Policies (RuralComm ’11), Houston, Texas, USA, pp. 1045-1049, Dec. 5-9, 2011.
- C.2** S. Aust, and T. Ito, “*Sub-1 GHz Wireless LAN Propagation Path Loss Models for Urban Smart Grid Applications*,” International Conference on Computing, Networking and Communications (ICNC ’12): 1st Workshop on Computing, Networking and Communications, Maui, Hawaii, USA, pp. 123-127, Jan. 30 - Feb. 2, 2012.
- C.3** S. Aust, R.V. Prasad, and I.G.M.M. Niemegeers, “*IEEE 802.11ah: Advantages in Standards and Further Challenges for Sub-1 GHz Wi-Fi*,” IEEE International Conference on Communications (ICC ’12): First Workshop on Telecommunications: from Research to Standards, Ottawa, Canada, pp. 6885-6889, June 10-11, 2012.

- C.4** S. Aust, R.V. Prasad, and I.G.M.M. Niemegeers, “*Performance Evaluation of Sub-1 GHz Wireless Sensor Networks for the Smart Grid*,” 37th IEEE Local Computer Networks Conference (LCN '12), Clearwater, Florida, USA, pp. 292-295, Oct. 22-25, 2012.
- C.5** T. Tanaka, K. Abe, S. Aust, H. Yomo, S. Sakata, T. Ito, “*Automatic and Cooperative Sleep Control Strategies for Power-saving in Radio-On-Demand WLANs*,” 5th IEEE Annual Green Technologies Conference (GreenTech '13), Denver, Colorado, USA, pp. 293-300, April 4-5, 2013.
- C.6** S. Aust, R.V. Prasad, and I.G.M.M. Niemegeers, “*Performance Study of MIMO-OFDM Platform in Narrow-band Sub-1 GHz Wireless LANs*,” 11th International Symposium on Modeling and Optimization in Mobile, Ad Hoc, and Wireless Networks (WiOpt '13): 8th International Workshop on Wireless Network Measurements (WinMee '13), Tsukuba Center for Institutes, Tsukuba Science City, Japan, pp. 89-94, May 13-17, 2013.
- C.7** S. Aust, R.V. Prasad, and I.G.M.M. Niemegeers, “*Analysis of the Performance Boundaries of Sub-1 GHz WLANs in the 920 MHz ISM-Band*,” the 10th International Symposium on Wireless Communication Systems (ISWCS '13), Ilmenau, Germany, pp. 1-5, Aug. 27-30, 2013.
- C.8** T. Tanaka, S. Aust, and T. Ito, “*Enhanced Energy Consumption Reduction Schemes in Radio-On-Demand WLANs*,” 24th IEEE International Symposium on Personal, Indoor and Mobile Radio Communications (PIMRC '13): Mobile and Wireless Networks, London, UK, pp. 2830-2834, Sep. 8-11, 2013.
- C.9** S. Aust, R.V. Prasad, and I.G.M.M. Niemegeers, “*A Framework for Massive Access and Radio Resource Management in Sub-1 GHz WLANs*,” the 38th IEEE Conference on Local Computer Networks (LCN '13): 2nd IEEE International Workshop on Global Trends in Smart Cities (goSMART '13), Sydney, pp. 93-99, Australia, Oct. 21-24, 2013.
- C.10** S. Aust, R.V. Prasad, and I.G.M.M. Niemegeers, “*Codebook Selection Strategies in Long-range Sub-1 GHz WLANs*,” the 5th International Conference on Ambient Systems, Networks and Technologies (ANT '14), the 4th International Conference on Sustainable Energy Information Technology (SEIT '14), pp. 133-140, June 2-6, 2014.
- C.11** S. Aust, R.V. Prasad, and I.G.M.M. Niemegeers, “*Sector-based RTS/CTS Access Scheme for High Density WLAN Sensor Networks*,” the 3rd International Workshop on Trends in Global Smart Cities, in conjunction with the 39th IEEE Local Computer Networks (LCN '14), Edmonton, Canada, pp. 697-701, Sept. 8-11, 2014.

## Demo submissions

Accepted peer-reviewed demo abstract:

- D.1** S. Aust, R.V. Prasad, and I.G.M.M. Niemegeers, “*Advances in Wireless M2M and IoT: Rapid SDR-prototyping of IEEE 802.11ah*,” the 39th IEEE Local Computer Networks (LCN ’14), Edmonton, Canada, pp. 1-3, Sept. 8-11, 2014. Demo abstract.

Table B.3 lists all published contributions related to this thesis. Contributions to Chapter 2 are divided into PHY and MAC related topics.

Type	Ch.1	Ch.2 (PHY)	Ch.2 (MAC)	Ch.3	Ch.4	Ch.5	Ch.6	Ch.7
J1	–	●	○	●	●	–	–	–
C1	●	●	–	–	–	–	–	–
C2	○	●	–	–	–	–	–	–
C3	●	●	○	–	–	○	–	–
C4	○	●	○	●	–	–	–	–
C5	–	●	●	○	–	●	–	–
C6	–	●	●	●	–	–	–	–
C7	–	●	●	●	–	–	–	–
C8	–	●	○	●	–	●	–	–
C9	–	–	●	–	–	○	○	●
C10	–	●	●	●	●	–	–	–
C11	–	○	●	–	○	–	●	●
D1	–	●	○	●	○	–	○	–

**Table B.3** – Overview of the relation between chapters of the thesis and the list of publications by the author.

Legend: ● = Major contribution, ○ = Minor contribution,

(J) = Journal/letter submission, (C) = Conference/workshop submission,

(B) = Book/chapter submission, (D) = Demo submission.

## Related publications (under submission)

Publications that are under submission (not yet accepted) are:

- J.1** S. Aust, R.V. Prasad, and I.G.M.M. Niemegeers, “*Outdoor Long-range WLANs: A Lesson for IEEE 802.11ah*,” IEEE Communications Survey and Tutorials. Journal paper, first round of review accomplished, under revision, July/September 2014.

- J.2** S. Aust, R.V. Prasad, and I.G.M.M. Niemegeers, “*Analysis of Wireless Coexistence in mixed Sub-1 GHz WLAN/WPAN Systems*,” IEICE Communications Express (IEICE ComEX). Journal letter, submitted, September 2014.

## Other related publications (published prior to the thesis)

The following publications were published prior to the thesis:

- C.1** S. Aust, T. Ito, P. Davis, “*Location Cognition for Wireless Systems: Classification with Confidence*,” the 3rd International ICST Conference on Mobile Wireless Middleware, Operating Systems, and Applications (Mobilware '10), Chicago, USA, pp. 1-8, June 30 - July 2, 2010.
- B.1** S. Aust, T. Ito, P. Davis, “*Location Cognition for Wireless Systems: Classification with Confidence*,” Mobile Wireless Middleware, Operating Systems, and Applications (Mobilware '10), Lecture Notes of the Institute for Computer Sciences, Social Informatics and Telecommunications Engineering (LNICST), ISBN 978-3-642-17757-6, vol. 48, 2010, pp. 144-157, 2010.
- C.2** S. Aust, T. Ito, P. Davis, “*Seamless Indoor/Outdoor Location Cognition with Confidence in Wireless Systems*,” in the Proceedings of the 35th IEEE Conference on Local Computer Networks (LCN '10), the 4th Workshop on User Mobility and Vehicular Networks (onMove '10), Denver, Colorado, USA, pp. 653-657, Oct. 10-14, 2010.
- J.1** S. Aust, P. Davis, A. Yamaguchi, S. Obana, “*Enhanced Link-Status Detection for High Speed Link Aggregation in Cognitive Radio Networks*,” IEICE Transactions on Fundamentals of Electronics, Communications and Computer Sciences, vol. E91-A, issue 7, pp. 1609-1615, July 2008.

# Acknowledgments

First and foremost, I am deeply indebted to Prof. Dr. Ignas G.G.M. Niemegeers, TU Delft, for promoting my dissertation and supporting my work on sub-1 GHz WLANs at the TU Delft. The immense impact of the fast development of wireless M2M, IoT, and smart spaces has given me the insight that the work on sub-1 GHz has some profound importance for the wireless community. I would like to thank my adviser, Dr. R. Venkatesha Prasad, TU Delft. His willingness to support my work and his guidance throughout my research has allowed me to improve my research skills. I greatly thank him for giving me this opportunity and to invite me into the research family at WMC, TU Delft. I really enjoyed to be a part of the team. I also would like to thank the members of my committee. I greatly appreciate their time and suggestions to this dissertation. Your input during the review of this dissertation is highly appreciated! Within the WMC Lab and the Embedded Software Group at TU Delft, I owe many thanks to both students and staff. Specially, I thank Vijay Rao, MSc. for his personal support during my stay at TU Delft and the discussions on energy conservation related topics in wireless systems. I thank Huaizhou Shi, MSc. for the discussion on IEEE 802.22 and cognitive radio. I thank Kishor Chandra, MSc. for his hints on using Latex. I must express my appreciation to the many co-workers at NEC Communication Systems (NCOS), Ltd. in Tamagawa, Kawasaki, Japan who have helped me with their input and suggestions how to design a wireless prototype. I have to thank my NCOS Laboratory managers for their support through my studies on the new research domain of sub-1 GHz WLANs. I thank NCOS for the financial support for my business trips to numerous IEEE 802 standard meetings and international conferences. I am also thankful for NCOS financial support to purchase the SDR hardware, which I used to conduct most of the experiments in this dissertation. I am profoundly grateful of my NCOS sub-1 GHz team and their support during the journey of building up a software based narrow-band multi-antenna WLANs. I also owe many thanks the wireless team at NCOS for the joint research work on cognitive radio. Furthermore, I thank the members of the Radio-On-Demand (ROD) team at NCOS for the collaboration in the field of energy conservation schemes in wireless communication systems. Finally, I thank my family for their support while I was writing on my dissertation.





# Curriculum vitae

Stefan Herbert Aust was born in Delmenhorst, Germany, on March 28th, 1971. He finished the primary and high school educations in his hometown in 1992, followed by one year of military duty. Stefan started his tertiary education in 1993 at the University of Bremen and he graduated with the Diplom Ingenieur (Dipl.-Ing.) degree in information technology in 2001. From 2001 he was with ComNets, University of Bremen, Prof. rer. nat. C. Görg, until 2005, where he was responsible as a research associate for the contributions to the BMBF research project IPonAir. His research contributions were centered on Mobile IP, ad-hoc networks, and policy-based handover. From 2005 to 2008, Stefan was with Advanced Telecommunication Research Institute (ATR) International, Kyoto, Japan. He was in charge of wireless testbeds to emulate handovers in WLANs and IP-based packet switching. Since April 2008, Stefan is with NEC Communication Systems, Kawasaki, Japan. He has been promoted to the R&D manager position in April 2013. He is engaged in research on license-exempt wireless communication systems, energy-efficient radio-on-demand WLANs, and cognitive radio. During his research he successfully contributed to the IEEE DySPAN 1900.6, IEEE 802.15.4s, and IEEE 802.11ah TG. He was appointed as the IEEE 802.11ah use case ad-hoc chair. Since April 2013 he is the group leader of the NCOS sub-1 GHz project. In 2011, Stefan started his research work under the supervision of Prof. Dr. I.G.M.M. Niemegeers at the Wireless and Mobile Communications (WMC) group, faculty of Electrical Engineering, Mathematics and Computer Science (EEMCS), Delft University of Technology, the Netherlands. He is the recipient of the following awards:

1. IEEE standards award for outstanding contributions and development of IEEE 1900.6<sup>TM</sup>-2011: IEEE standard for spectrum sensing interfaces and data structures for dynamic spectrum access and other advanced radio systems.
2. The NEC Carrier Network Business Unit (CNBU) standardization awards 2011: fresh player award.

He has been the co-chair of the IEEE Local Computer Networks (LCN) *goSMART* workshop since 2012. He is member of the IEEE and IEICE. Stefan is married and has a son who is five years old.